Julian Alexander Amani

A novel approach of immittance-spectra analysis and how it resolves a decade-old deviation of the Frenkel-Poole model

Utilising process-specific physical models to find the electrical equivalent circuit representing the underlying physics in immittance spectroscopy

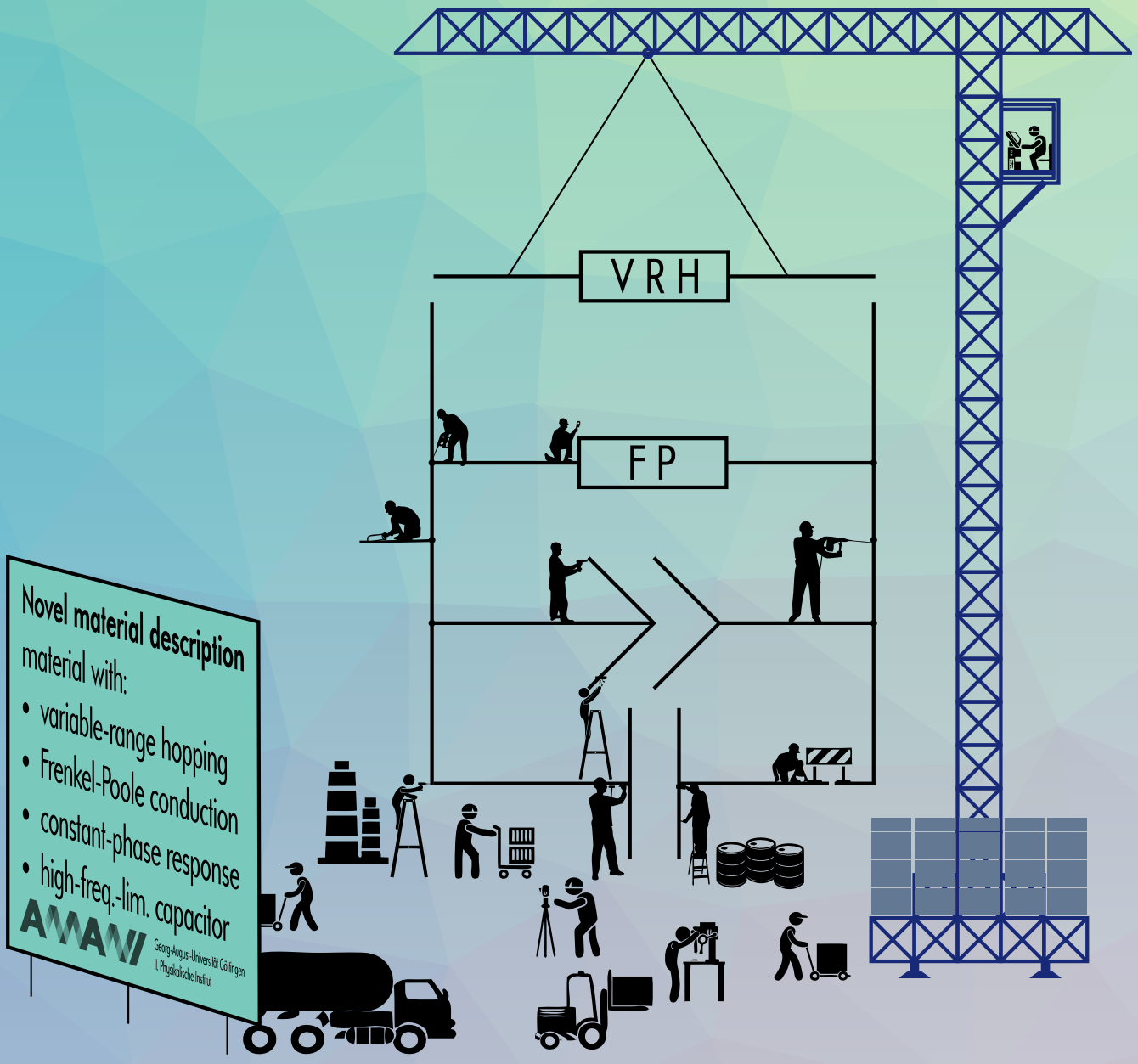

A novel approach of immittance-spectra analysis and how it resolves a decade-old deviation of the Frenkel-Poole model

Utilising process-specific physical models to find the electrical equivalent circuit representing the underlying physics in immittance spectroscopy

Dissertation

zur Erlangung des mathematisch-naturwissenschaftlichen Doktorgrades

'Doctor rerum naturalium'

der Georg-August-Universität Göttingen

---

im Promotionsprogramm ProPhys

der Georg-August University School of Science (GAUSS)

vorgelegt von

Julian Alexander Amani

aus Göttingen

Göttingen, 2016

Betreuungsausschuss

Professor Dr. Hans Hofsäss – II. Physikalisches Institut – Universität Göttingen

Professor Dr. Michael Seibt – VI. Physikalisches Institut – Universität Göttingen

Dr. Ulrich Vetter – II. Physikalisches Institut – Universität Göttingen

Mitglieder der Prüfungskommission

Referent: Professor Dr. Hans Hofsäss – II. Physikalisches Institut – Universität Göttingen

Korreferent: Professor Dr. Michael Seibt – VI. Physikalisches Institut – Universität Göttingen

2. Korreferent: Professor Dr. Ørjan G. Martinsen – Electronics Research – University of Oslo

Weitere Mitglieder der Prüfungskommission

Professor Dr. Wolfram Kollatschny – Institut für Astrophysik – Universität Göttingen

Professor Dr. Hans-Ulrich Krebs – Institut für Materialphysik – Universität Göttingen

Professor Dr. Vasily Moshnyaga – I. Physikalisches Institut – Universität Göttingen

Professor Dr. Andreas Tilgner – Institut für Geophysik – Universität Göttingen

Tag der mündlichen Prüfung:

Contents

1 Introduction

1.1 About this work

Immittance[1] spectroscopy is a well-established and versatile method with a broad range of applications in a wide variety of different fields and subjects, ranging from science to industrial solutions [3]. Specific examples of its application are given in section 1.2.1.

Although immittance spectroscopy is widely applied, commonly used strategies of analysing its measured data do not exhaust its full potential: On the one hand, the rarely used [119], but at least in some situations physically correct, process-independent Poisson-Nernst-Planck models[2] might describe *any* combination of processes by falling back onto *effective parameters* which, without any indication, do not necessary represent any actual underlying physical property of the system under investigation. On the other hand, the most common form of analysis is by electrical equivalent circuits (EECs). These are mere analogues which 'are almost always assigned without regard to the physics of the system' [110]. Due to this fact, their problem with circuit ambiguity in general (compare Figure 1.1) and the type of parameters which are obtained, EECs almost never represent the underlying physics and their parameters are likely irrelevant and incomparable between different experiments.

While analogues 'may produce plots that are impressive in their fit to the experimental data, they do little to advance the science' [110]. By introducing the dependence on external parameters in Maxwell's extension of Ampère's law, an EEC for a homogeneous piece of material is derived that allows replacing idealised lumped components, like resistors and capacitors, by process-specific physical models dependent on external parameters. Utilising these models for measurements over a range of external parameters in combination with global fits, that do extract relevant physical parameters (e. g. acceptor concentrations or bulk permittivities) describing all varied external conditions simultaneously instead of resistances and capacitances *per condition*, allows identifying as well as understanding the underlying physical processes whilst extracting physically relevant parameters comparable between different experiments and more easily verifiable as reasonable in comparison to resistances and capacitances. Voltage-dependent immittance spectra, as utilised in this work, include the full information of a conventional

[1] Immittance, at first a coinage by Bode [11] to generalise the equivalent representations of impedance and admittance, was later further extended into a universal designation for any equivalent representation of impedance, explicitly including those not influenced by dimensions: e. g. admittance, complex permittivity, complex conductivity or modulus [113]. Since this work exclusively deals with *electrical* immittance spectroscopy, the prefix 'electrical' is generally omitted, for any type of immittance.

[2] This designation has its usual meaning in the context of immittance spectroscopy as given in reference [119] and explained in section 5.1.

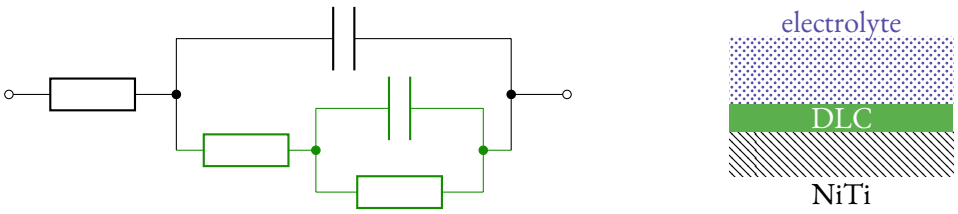

(a) Circuit for DLC on NiTi alloy in electrolyte by Chu [109]

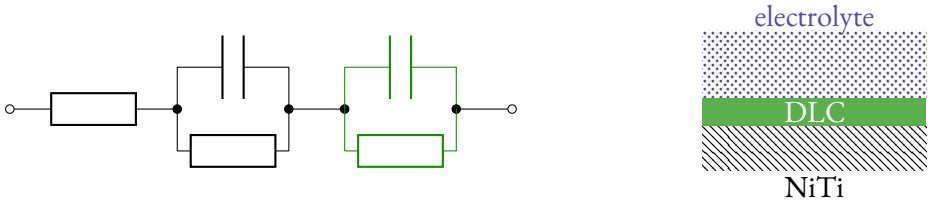

(b) Circuit for DLC on NiTi alloy in electrolyte by Sui *et al.* [174]

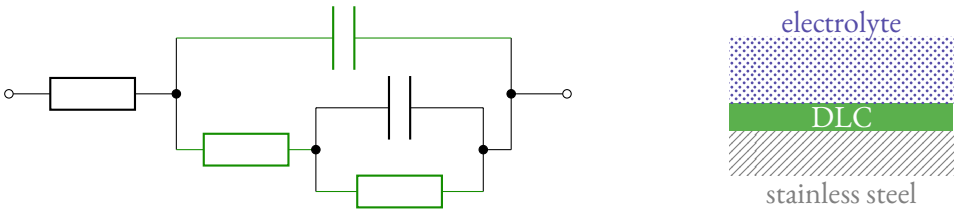

(c) Circuit for DLC on stainless steel in electrolyte by Maguire *et al.* [123]

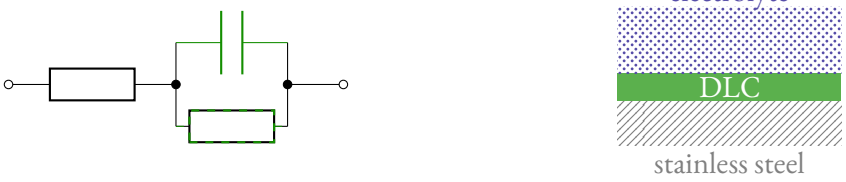

(d) Circuit for DLC on stainless steel in electrolyte by Liu *et al.* [103]

Figure 1.1: The challenges of circuit ambiguity using the example of diamond-like carbon: Diverse variants to represent the DLC in an EEC, used to fit measured immittance spectra, are used. Subfigures (a)-(d) show four exemplary representatives, where the components that should according to the corresponding authors be associated with diamond-like carbon (DLC) coating are coloured in green. In circuit (d) the parallel resistor is partially attributed to the DLC. Since in conventional EECs the fit parameters are resistances and capacitances (inductances rarely play a role within the typical frequency range of immittance spectroscopy), comparison of the results of different works is rarely possible. Further, some arrangements of components may ignore the underlying physics and, as a result, the different components are not exclusively representing the suggested pieces but are rather a combination of different pieces of the system. As a result, (accidental) usage of a circuit not representing the underlying physics may lead to misinterpretations.

current-voltage measurement. Additionally, they include the capacitive properties of the system. Consequently, even without introducing the presented novel approach of analysis, different serial pieces of the system[3] can principally be separated by their distinct capacitive bypass. As a result, the current-voltage behaviour of each separate piece can be extracted *individually*. Bulk and electrode processes or the influence of high-resistive contacts are inherently separable and can be analysed individually without involving unconfirmed resistance models representing parasitic contributions around the actual piece of interest in the experiment. The introduction of process-specific physical models with dependence on external parameters is, of course, not limited to the resistive part. Successfully fitting a serial piece simultaneously including external-parameter dependent models for both, resistive and capacitive part, can be seen as strong indication that the respective piece was correctly identified and, hence, its major underlying processes adequately understood. Furthermore, this is a convenient approach to study the compatibility of the involved dielectric and electric models at simultaneously obtained, hence self-consistent, data for the immittance of a serial piece. The approach becomes especially fruitful if both models share mutual parameters that may, consequently, be combined to single constants in the global fit. Although dielectric and electric behaviour is measured jointly, the processes responsible for each contribution can be quite different. Therefore, values of shared parameters obtained in such a way, that is furthermore not influenced by serial parasitic resistances and can due to the self-weighting effect of the models by their dependence on external parameters also include data from transition regions, may be considered more reliable as compared to those extracted solely on the basis of conventional current-voltage analysis. As a result, in the analysis of heterostructures with a thin film of tetrahedral-amorphous carbon (ta-C) on different crystalline p-type silicon substrates performed in this work, as many mutual parameters as possible were fitted jointly. Next to a joined acceptor concentration that could describe both voltage-dependent models for the resistance as well as for the capacitance of a depletion layer forming in p-type silicon, fit parameters could also be combined for the bulk properties of the thin film.

Latter could be used to verify a correction (suggested in this work) in the calculation of the superimposed field from the externally applied potential difference within the physical basis of the Frenkel-Poole model (i. e. without the need of introducing any more recent physical concepts like quantum mechanics or more elaborate local environments), that unexpectedly resolves an over 50 year old [80, 163] quantitative deviation of the Frenkel-Poole model (a semi-classical conduction model based on the process of introducing charges into the conductive band[4] by field-assisted thermal excitation from charged traps [46]). Through many enhancements of the Frenkel-Poole model over the years (contributions by different researchers are reviewed in section 5.6.1), especially a three-dimensional description of the local potential landscape first introduced by Jon-

[3] In this work, the word 'piece' designates a distinct unit of a potentially larger system, i. e. consisting of multiple pieces. The word 'part' is used to reference a subgroup of elements in a circuit, often the representation of a certain piece in the circuit.

[4] The term 'conductive band' is used troughout this work as a generalisation that shall indicate that it can be the conduction band in an n-type material, the valence band in a p-type material and, further for both cases, it can be the corresponding mobility edge if the material is disordered.

scher [80], a consistent description for small fields could be derived that resolved one of two major [144] quantitative differences between experimental data and the description of the model. The up to now [163] remaining deviation of an, in comparison to the predicted barrier-lowering coefficient, too shallow slope extracted from experimental data, could in this work be explained by using the, within the concept of classical electrodynamics required, internal field (i. e. the field inside a polarisable material) for the linear superimposed field in the local potential landscape around the trap, instead of the external field. That such a simple correction, which does not resolve any of the many remaining fundamental limits of the Frenkel-Poole model (discussed in section 5.6.2), especially concerning the description of the local potential landscape, could eliminate the one remaining quantitative deviation of the Frenkel-Poole model may at first seem surprising. However, a first attempt in understanding why the basic description might be sufficient is given in section 5.6.4. Verifying this hypothesis is a unique opportunity to test the capabilities of voltage-dependent immittance spectroscopy in a context where usually conventional current-voltage analysis is applied. Especially in this case, where the presence of permittivities (which are basically *the* fundamental dielectric property) within the resistive part is in question, the unification of fit parameters mutually shared between resistive and capacitive models, which is an integral part of the proposed novel approach of analysing immittance spectra using process-specific physical models dependent on external parameters, can unfold its full potential. Since it is found that a model, correctly calculating the internal field, with a connection of the permittivity can describe the system equally well as a model where both parameters can be chosen freely (in fact, in the free case, the fitting routine even chooses comparable values for the permittivity in resistive and capacitive part) this is a strong indication that the correction proposed in this work was indeed the missing feature of the Frenkel-Poole model that resolves the deviation between experimentally obtained and predicted barrier-lowering coefficients. Since it is actually quite surprising that such a simple correction *within the concept* of the Frenkel-Poole model could actually be responsible, instead of introducing more elaborate physical concepts or refinements around the crude assumption of the local potential landscape, this work also re-examines the structure of defects in undoped covalently bound semiconductors that may potentially represent those trap centres in the Frenkel-Poole theory. The central potential of such traps is indeed highly oriented and neither spherically symmetric nor at all well described by a Coulomb potential. Furthermore, the central part of such potentials is indeed sensitively dependent on the distinct material. In fact, the Frenkel-Poole conduction is observed for a *substantial range of materials*, with essentially only one similarity: a low mobility. Already this empirical finding suggests that a feature which is very different for all of these materials, namely the core potential of structural defects, should either not be a dominant property in the process or it should be an attribute of the model which is varied accordingly with the different specimens. The answer to the question why such a 'simple' model might describe the situation correctly is assumed to lie within the simplicity of the model itself. The Frenkel-Poole model is restricted to sufficiently high temperatures at which a significant amount of charge carriers can be thermally excited over relatively high barriers (e. g. in comparison to doping-levels in silicon). The relevant maximum of the barrier for the charges must be sufficiently

distant from the immobile oppositely charged trap centre that their respective interaction can be described by a Coulomb potential with the bulk permittivity of the surrounding medium. From the calculation of binding energies for deep level traps, which besides also gives the potential landscape of these traps, it is known that the binding energy, which is a parameter in the Frenkel-Poole model, is dominated by the core potential. However, any defect that is charged when empty (structural defects, e. g. dangling bonds, can fall into that category) has also an, usually assumed Coulombic, outer part of the potential. This outer potential was found by Grimmeiss and Skarstam [55] to show a hydrogenic characteristic and dominate the properties of excited states for deep centres.

The Frenkel-Poole conduction is obviously dominant in a regime (of voltage and temperature) where the thermal excitation over the barrier is sufficiently prominent to significantly exceed the contributions of any other current-transport process. Exactly then, the dominant contribution is by those charge carriers that have enough energy to overcome the final, that is the outer, barrier by the Coulombic interaction. The measurement in that regime only perceives those charges which fulfil these requirements (i. e. the high enough thermal energy) and since the charges overcome the barrier thermally, a process for which only the highest point of the barrier is decisive, the knowledge of the core potential may be restricted to the binding energy, which is a parameter in the Frenkel-Poole model. In summary, the Frenkel-Poole model is observed in a region where its assumptions, though very crude, are representing exactly the remaining relevant properties. The discrepancy in the barrier-lowering coefficient can be explained by an omitted factor in its calculation. Interestingly, Poole already explains in a footnote of his publication [149, third footnote on p. 128] that he omitted this factor since he is only interested in a qualitative description and it seems to have been forgotten ever since.

1.2 A broader perspective - general impact of this work on the field of immittance spectroscopy

1.2.1 Applications of immittance spectroscopy

One of the most obvious applications of immittance spectroscopy is in (electrical [17] or acoustical[5]) engineering, where it is an especially important tool to characterise any form of signal transmission: not only from cables or air but also more complex devices, explicitly including attenuators and amplifiers. Immittance spectroscopy is also commonly applied to characterise batteries and related materials [70, p. 430]. Its application ranges from battery health tests in workshops [20, 181] to understand the underlying physics in completely new types of batteries, e. g. all-solid-state thin-film microbatteries [98]. For the latter its unique properties that allowing, non-invasively and non-destructively, to obtain *in situ* information on degradation mechanisms and possible bottlenecks in the electrochemical reactions are of primary importance [69]. In a context where chemical reactions are involved, the measurement is referred to as electrochemical immittance (or impedance) spectroscopy (or EIS). It has been used in this field from the end of the 19th century onwards [110] and is still a standard method to determine corrosion properties [124, pp. 463-505] or chemical reaction rates in general [99, pp. 1-3]. For the former, the possibility of investigating the specimens in very different environments is of great benefit. The corrosion of a material or coating over time may be tested in the actual environment of interest itself. For example, to predict the *in vivo* ageing behaviour of metallic implant medical devices more realistically and especially include the often neglected influence of proteins and amino-acids on the corrosion of Ti-6Al-4V, a titanium alloy typically used for implants and prosthesis, the impedance of a specimen may be measured while corroding in different solutions, including blood [152]. The work of Shih *et al.* [165], also mentioned in the publication of Pound, measures the corrosion even *in vivo*. Although they did not use impedance spectroscopy (their measurement was electrostatic), the technique could in principle have been applied. In commercially available cardiac pacemakers, built-in time-dependent impedance measurement is used within human bodies [133]. The application of immittance spectroscopy in the investigation of biological samples is almost as old as the method itself (confer [56, pp. 411-418]). In comparison to competing measurement methods, immittance spectroscopy may often be more cost efficient and less time-consuming. For example, immittance spectroscopy may be used as 'a quick and easy alternative to the expensive and slow study of skin biopsies by microscopy' for an early detection of diabetes-related changes in the human skin [102]. Though this method has been used in biology or medicine already for a long time, the number of potential applications in this field is steadily increasing, especially those gathering properties towards smaller structures. The review by K'Owino and Sadik on applications in the fields of 'rapid biomolecular screening' and 'cell culture monitoring' already mentions label and mediator-free strategies for rapid screening of biocompatible surfaces, monitoring pathogenic bacteria, as well as the analysis of heterogeneous systems, like biological cells and tissues [92]. Even the detection of base pair mismatches in the DNA sequence, e. g.

of Hepatitis B virus, Tay-Sachs disease or *Microcystis spp*, is possible [92]. Through different adsorption and desorption rates antigens binding on antibodies present in human diseases, e. g. human mammary tumours may be detected; as may be pathogens, like the Hepatitis B virus or small amount of drugs and toxins (limit of detection around $10\,\mathrm{nmol\,l^{-1}}$). Furthermore, immittance spectroscopy allows the real-time monitoring of cell spreading as well as real-time detection and quantification of microbes, e. g. *Listeria innocua*, which enables monitoring the condition of food products like milk.

Further applications in material [153] and semiconductor physics [138] as well as geology [155] are possible.

1.2.2 Impact of this work on immittance-spectra analysis in other fields

All the above mentioned areas face similar challenges, as mentioned in the beginning of the introduction. The referenced examples still use EECs and in consequence have to deal with all resulting drawbacks, especially circuit ambiguity. Since different arrangements of circuit components are equally likely, depending on the chosen structure, the extracted relevant parameters (e. g. the concentration of a toxin) do not necessarily represent the actual value. In the end, in every application the resistances and capacitances should be converted into meaningful parameters.

The application of the presented approach is possible directly for at least every solid part that is described in an EEC. If, for example, the electrodes are coated with a material exhibiting Frenkel-Poole conduction, its description should, hence, include the model accordingly. In order to do that, it is important to know which component(s) of a circuit represent which piece of the system. At least for resistors or capacitors, that should be converted to the relevant parameters, a one-to-one assignment between components and underlying processes is necessary.

Unlike in the case of a solid state system investigated here, in these very different biologic fields, models for conduction or polarisation processes are typically not available. The presented approach might, hence, not directly be applied. However, the basic concept of the novel approach, the introduction of process-specific physical models dependent on external parameters may still be beneficial. Though the use of different conditions is expected to be more restricted than for inanimate, inorganic systems, it might still be possible to trigger some reactions within the system. If for example, the generation of ions at the cell membrane is dependent on some stimulus or some concentration of a species that may be introduced, this dependence might be directly included in the describing circuit. The above mentioned biological scenarios are possibly preferentially described by spatially-extended simulations. Also in those, the explained concept may be included by using condition-dependent models for specific relevant properties, e. g. the number of ions at a membrane may still be calculated dependent on some concentration of a certain protein instead of simply fitting its value for each protein concentration separately.

Although, again, indirectly, the concept of this work may be successfully applied to inorganic electrochemical impedance spectroscopy. Possibly the best lumped-component descriptions of an electrochemical system, like a battery, are given by the specific solutions of Poisson-Nernst-Planck models. Although these models can lead to misleading paramet-

ers, if some processes or ionic species where omitted. As described in more detail in section 5.1.2, the basic concept of the novel approach, the introduction of process-specific physical models dependent on external parameters, can be combined with lumped Poisson-Nernst-Planck models. In this case the process-specific physical models are not included as circuit components, but to replace the fit values independent of external parameters, like the dissociation of the local species. As those parameters become external-parameter-dependent functions, global fitting of immittance spectra for different conditions, including automatic local weighting of parameters due to their specific regions of importance, becomes possible and the probability accidental description with effective parameters is reduced.

1.3 The exemplary experimental application

As already indicated above, this work focuses primarily on the development of a novel method to analyse experimentally obtained immittance spectra by using process-specific physical models dependent on external parameters. Ultimately, this allows the extraction of process-specific parameters which are inherently linked to a physical meaning (e. g. an acceptor concentration or a barrier height, instead of a resistance or a capacitance) and can, hence, be better compared between experiments. Furthermore, the introduction of models with dependence on external parameters eliminates circuit ambiguity which, as can be seen in Figure 1.1, also improves the comparability between different experiments. Moreover, the regions of importance for the respective processes are automatically weight by the parameter-dependence of the models. Additionally, external-parameter dependence enhances the association of circuit components with distinct pieces of the system under investigation and reduces the absorption of deviations, e. g. by an incomplete model on one piece, into the fit parameters of another piece. Finally, if the same underlying physical properties are present in different models for the same piece they may be shared and, consequently, fitted jointly, even between capacitive and resistive properties.

The application of this novel approach on samples with ta-C films on p-type silicon substrates, with different doping concentration, is only an example. However, as explained below, a carefully chosen one.

The analysis of depletion layers in silicon, usually in form of capacitance-voltage measurements, is probably one of the most common applications of immittance spectroscopy in semiconductor physics. In comparison to many other systems investigated by immittance spectroscopy, which often rely on empiric models, depletion layers are relatively well-investigated and -understood phenomena which have theory-based models [138][176, pp. 245-297]. The latter is not only true for the capacitance of a depletion layer, but also for its resistance-voltage characteristic, i. e. its static current-voltage relation [176, pp. , 245-286]. As already explained, the novel approach in this work is based on introducing physical models dependent on external parameters. In the case of the depletion layer, both resistive and capacitive properties are dependent on the external parameter voltage and both models are based on microscopic assumptions (which is what is meant in this work by physical model dependent on external parameters). Voltage-dependent immittance spectra, as those obtained in this work, not only contain the capacitance-voltage information, but also the full resistance-voltage characteristic. Furthermore, the higher number of frequencies in the approach introduced in this work as compared to conventional capacitance-voltage analysis (often only one high- and one low-frequency measurement are performed [138, pp. 321-333, 388-389]) allows distinguishing and potentially identifying different serial parts in the system. This allows identifying potential parasitic contributions and, as also utilised in this work for the thin film, the introduction of separate descriptions for each serial piece of the complete system. For the depletion layer in silicon, well-known literature values exist for most model parameters (see section 2.4.1 for the sources of the literature constants for the depletion-layer model used in this work). The remaining parameters, which are determined by the fit, affect both, resistive

and capacitive properties. This enables evaluating yet another consequence of the novel approach: the simultaneous fit of parameters shared between the resistive and capacitive model. As a result of all above points, the presence of a silicon depletion layer in the experimental example system is a unique opportunity to compare the capabilities of the novel approach presented in this work with well-established conventional methods of analysing depletion layers. Interestingly, conventional capacitance-voltage analysis usually does not utilise the resistive information contained in the immittance measurement [138, pp.pp. 321-333, 388-389]. Although works often present resistive as well as capacitive analysis of the same system, the results are usually obtained in different set-ups (e. g. confer [18] and [49]). Consequently, the separately obtained measurement data is usually also independently analysed and only at the end both results are compared. As explained above, the novel approach presented in this work combinedly fits shared parameters and uses the voltage-dependent immittance spectra which contain both, the complete resistive and capacitive, information. Since a single measurement with the same set-up is utilised, to extract both kinds of data, resistive and capacitive information may be expected to be more likely consistent as compared to a case with two distinct set-ups. The well-established conventional methods of analysis for depletion layers in silicon and their relatively well understood properties make them a suited candidate for a comparison between the conventional capacitance-voltage analysis and the approach presented in this work. This comparison, shown in section 4.1.2.1, suggests that the extracted parameters between both methods of analysis are in agreement.

In this work, not solely the depletion layer in silicon alone is investigated, but a complete metal/insulator/semiconductor (MIS) structure, where the thin-film material ta-C acts as fairly leaky insulator material.[5] The analysis of a complete MIS structure is especially valuable, firstly, since this is a very common and often analysed system in the semiconductor industry and, secondly, since the novel approach presented in this work can bring its full potential to bear for systems consisting of multiple serial pieces. While for the depletion layer in silicon both, capacitive and resistive, properties are dependent on voltage, the bulk-capacitance of the amorphous thin film material, with solely one atom species consequently connected by non-polar bonds, is not expected to be dependent on it. The resistance, on the other hand, is known to exhibit Frenkel-Poole conduction (e. g. confer to the voltage and often also temperature-dependent current-voltage analysis of [38], [168, 91][6], [90], [53], [132] and in particular Ronning *et al.* [156], Hofsäss [68] and Brötzmann *et al.* [15] who used the identical set-up for the synthesis of the ta-C film) which is again a process dependent on voltage. For this specific model a quantitative discrepancy between the experimentally obtained and theoretically predicted barrier-lowering coefficient exists. According to the Frenkel-Poole theory (see [46]

[5] This material system was designated MASS for metal/amorphous semiconductor/semiconductor by Brötzmann *et al.* [14, 15].

[6] In these two latter works, the conduction process is interpreted as Schottky-emission process solely due to the deviation in the barrier-lowering coefficient. The authors were obviously unaware of the fact that this deviation from the theoretically predicted value is almost always observed for the Frenkel-Poole model, specifically also in systems where the current-voltage characteristic was proven to be bulk-limited, e. g. [129].

and the estimation in section 4.2), the dynamic permittivity (at optical frequencies) is the only value in the barrier-lowering coefficient which is not a natural constant. The usually observed too low barrier-lowering coefficient may be ascribed to a permittivity greater than the corresponding literature value. This was a typical quantitative argument against the correctness of the, in some eyes, too simple model which neither takes more modern physical concepts into account nor uses a realistic potential landscape (see full discussion in section 5.6). In this work, a correction of the Frenkel-Poole model or rather the commonly used calculation of the applied field in the Frenkel-Poole model is proposed. Instead of the external electrical field, the internal field is used. This correction is completely within the concept of classical electrodynamics and, hence, also within the scope of the Frenkel-Poole model, rather than an introduction of different physical concepts like the introduction of quantum-mechanical processes. Since the novel approach of analysis, presented in this work, measures and fits resistive and capacitive properties simultaneously and fits shared parameters like the permittivity jointly, the test of the correction was a uniquely suited task for the novel approach.

Tetrahedral amorphous carbon is a specifically suited material for both, studying the Frenkel-Poole model and finding a unified microscopic theory for ac as well as dc properties. The latter mainly because it is a typical disordered system with the consequential well-known constant phase response. The former, since it is a relatively simple material, especially the in the mass-selective ion-beam deposition (MSIBD) grown variant which has a characteristically low number of foreign contaminants [101, pp. 211-213] and a high sp^3 content [154]. The amorphous structure of the thin ta-C film, which is assumed to be homogeneous, renders the material isotropic which specifically reduces the complexity of the long-range binding potential between the exiting electron and its trap, because it allows the assumption of a spherically symmetric potential (for distances sufficiently large than the lattice constant, see the specific discussion in section 5.6.4). Especially the MSIBD-grown ta-C which is particularly pure, even mono-isotopic, and has a rather high sp^3 content in comparison with other methods of synthesis, can be expected to consist almost entirely of carbon atoms. Consequently, as opposed to many other dielectrics exhibiting Frenkel-Poole conduction, polar bonds should play no role in the conduction process. Furthermore, again as distinguished from other representatives, typical bulk dielectric relaxations or resonances may be neglected below optical frequencies. Frenkel-Poole conduction may only occur in materials with sufficiently low mobility which is usually connected to some element of disorder [82]. Ta-C is a typical representative of disordered solids, including its property to exhibit a constant-phase behaviour with a constant phase around 0.8π at low frequencies. The high number of defect states in a disordered material also has the advantage that space-charge layers at the interface, inside itself, in contact with other materials are highly unusual [80]. Consequently, using metals, Ohmic contacts are rarely a problem on disordered solids. In this experiment, Au/Cr and Al/Ti contacts, evaporated onto ta-C, resulted in indistinguishable voltage-dependent immittance spectra.

Although not the primary focus of this work, the used example system ta-C/p-Si is uniquely suited to illustrate the benefits of this novel method of analysis. Furthermore, the ta-C thin films in this work, synthesised by mass-selective ion-beam deposition, could

be a candidate to resolve what is said to be one of the major challenges of solid state physics [118], or even, the 'most important unsolved problem in physics today' [147]: a unified microscopic theory for the ac and dc properties of disordered dielectrics.

1.4 Structure of this book

The theory part of this work which is divided in four different sections, can be found in chapter 2. In the first section, Maxwell's extended version of Ampère's law for the total current density and the approximation of its exclusive separation, in electric and dielectric contribution caused by static charge transport processes and polarisation mechanisms, is introduced while allowing for non-linear responses dependent on external parameters, before finally, geometries are introduced in the last part of the first section. This creates the perquisites to interpret the equation for the total current as EEC, which is addressed in the second section of the theory. Each homogeneous piece of the system can be described as universal Voigt-circuit element. Different possible arrangements of circuit components representing the dielectric contributions are presented, handling parallel processes and the combination of serial pieces to the complete system are explained. The origin of lossy polarisation processes, specifically within the region of dielectric relaxation, are focused upon in more detail, since the given interpretations of the resulting constant phase element in many other works are limited to only surface roughness, though there are much more possible reasons. The final section of the theory explains the global fitting procedure for systems involving physical models dependent on external parameters as components of the circuit and also reveals some benefits of this approach.

The next chapter shows the synthesis of the samples, their subsequent preparation for the measurement, the experimental setup itself and an explanation of the global fitting process.

The fourth chapter shows and interprets the measured immittance spectra and their fits with distinct model variants. In the first section the focus is on the depletion layer in the substrate and its dependence on the different doping levels. It is shown how a parameter can be jointly used within resistive and capacitive models. For comparison with the novel approach a conventional capacitance-voltage analysis is performed. In the subsequent section, different models for the thin film are compared. Each model uses a distinct connection between resistive and capacitive part of the thin-film immittance model. The distributions of residuals, plotted over the external-parameter space or in statistical representations, are compared to determine whether the correction, suggested in this work, to calculate the internal field (for the linear, superimposed field that lowers the Coulombic potential) can resolve the decades old deviation between the measured and predicted slope (i. e. barrier-lowering coefficient) in the Frenkel-Poole model.

In first section of the fifth chapter, the discussion, other approaches using lumped components to analyse immittance data are compared: the most common method of analysis using EECs and specific lumped solutions of the Poisson-Nernst-Planck equations. In the subsequent section, the benefits of the presented approach, specifically for the investigated material system are discussed. The next section compares different concepts of extracting the static permittivity of a material, especially in the context of findings in this work related to the correction of the Frenkel-Poole model. The fourth section of chapter 5 discusses the range of frequencies at which the exclusive separation into static conduction and dielectric processes is valid. In the subsequent section, the various benefits of this approach, which includes the full information of a conventional

current-voltage measurement, in comparison with conventional current-voltage analysis are presented. The sixth and final section of the discussion, focuses on the Frenkel-Poole model. In the fist part its advancements are presented. In the second part its remaining limits. Subsequently, the disappearance of the permittivity is discussed, before finally, possibilities why the corrected Frenkel-Poole model can explain experimental data despite its prevailing deficiencies, especially in the description of the local environment of the trap, are presented.

The last chapter of this work summarises the findings and points out future possibilities resulting from this work.

1.4.1 Typographic specifics

Sometimes, the reader will find text passages that have broader margins and smaller text as compared to the other parts. This book tries to manage the balance act of addressing advanced readers, who are considered experts in the field of immittance spectroscopy or electric properties of disordered materials and want to get more information about the underlying physics of their investigated system from of the immittance data while further find answers to the questions they were afraid to ask, as well as novices to the field of immittance spectroscopy, who want to begin their journey in the exciting field of immittance spectroscopy with a condensed, modern introduction including all need-to know facts. To accomplish this goal, parts that contain more detailed information that might not be relevant for advanced reader have wider margins and smaller text.

Besides the usual usage of *italic font* to indicate a foreign origin of words, text is slanted to emphasise key points or to introduce major keywords.

A '[...]' in direct citations indicates words that were left out, hence it is not a part of the citation, but a comment by the author of this work. Double quotation marks inside the single quotation marks of a direct citation indicate the use of quotation marks in the original text.

2 Theory

2.1 Derivation from Maxwell's equation of total current density

2.1.1 Introduction

The novel approach presented in this work, which also includes the non-linear dependence of the process-specific physical models on external parameters, especially including the applied field, requires a more general theory as compared to conventional EECs using solely idealised lumped components.

Conventional EECs are *ambiguous*, i. e. different arrangements of idealised lumped components can produce identical immittance spectra over all frequencies [192] (circuit ambiguity and its challenges are discussed in greater detail in section 5.1.1). The values of the parameters of the components, which for conventional EECs solely take the form of resistances, capacitances, inductances, etc., are, however, for each of the several arrangements of the components very different. This makes the extraction of information about the underlying physics as well as the comparison of results using different arrangements extremely difficult (compare Figure 1.1). J. Macdonald suggested finding the one, of several arrangements of components, which correctly represents the underlying physics by analysing the system at different temperatures or bias voltages [114]. This might select the correct arrangement of circuit components, however, it would still not change the fact, that the extracted parameters are resistances, capacitances etc., instead of parameters characterising the underlying physical properties (e. g. the concentration of the involved defects and their energetic distance to the conductive band). In contrast to general parameters like resistances which are independent of an underlying process, above mentioned physical properties carry a specific meaning and can be directly compared between different experiments.

The main goal of the novel approach of analysing immittance spectra, by directly including process-specific physical models as components in the electrical equivalent circuit, is to find and extract information about the underlying physics of the investigated system. An important and necessary requirement for this primary goal is to select the arrangement of circuit components that represents the underlying physics correctly and, in consequence, leads to a bijective association of circuit components to physical processes in the system under investigation, i. e. each individual process in the system should be represented exclusively by specific parts of the circuit. This one-to-one mapping of components and physical processes (as illustrated in Figure 2.1) allows extracting the physical parameters of the corresponding processes, unaltered by the influences of other accidental contributions. Furthermore, when process-specific physical models dependent on external parameters instead of idealised lumped components are included in the circuit,

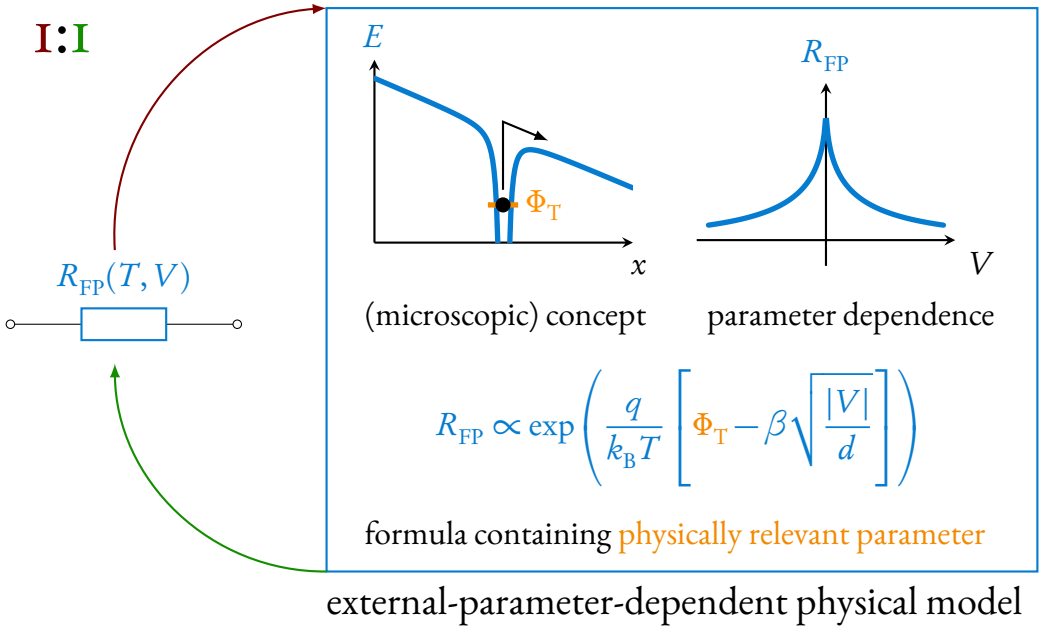

Figure 2.1: Illustration of the one-to-one assignment of circuit components with underlying physical processes, i. e. one physical process should be represented exclusively by one specific component (or one specific pair of components, for a delayed response) in the EEC and vice versa, which facilitates extracting the desired process-specific information. In the exemplary schematic the Frenkel-Poole conduction mechanism is exclusively associated with a resistor. To ensure the one-to-one assignment, in the presented approach, models are directly included as model-based parameter-dependent components of the circuit (in this example a model-based parameter-dependent resistor). The model itself consists not only of an external-parameter-dependent formula, but it further includes the underlying physical concept, e. g. a vision about the microscopic processes, and a (usually) characteristic appearance in a plot of resistance (or capacitance etc.) against the external parameters. Instead of resistances for each condition, physically relevant parameters are fitted directly, e. g. rather than fitting n resistances for n different applied bias voltages the barrier height Φ_T (exemplary included in the illustration) and permittivity (contained in β) are optimised to jointly describe the response for several conditions (compare section 5.1.1.2 and Figure 5.1). The next step is the connection of the permittivity in the barrier-lowering coefficient β of the resistive model with the value extracted from the corresponding capacitive part of the piece (confer section 2.4).

equally well fitting different arrangements of the components is no longer possible. A physical model is based on a conception of the underlying physics, i. e. dominant microscopic processes involved in the material are associated with the model. From this underlying physical concept a formula is derived that is usually, as a consequence of the dependence on external parameters of the microscopic processes, also dependent on them. The formula may further contain system-specific parameters, e. g. the density of traps and their energetic distance to the mobility edge, which would directly be fitted in the presented approach. As a consequence, fitting a component with the wrong model is either not possible at all (i. e. when there is mathematically no stable solution or the side conditions are violated) or leads to unphysical system-specific parameters (the more usual scenario). On the other hand, if a model is in good agreement with the measured data, it is very likely that the underlying physics is correctly assigned. The fact that, by fitting these models, specific parameters of the involved materials are extracted, opens new possibilities: other experiments to extract the same parameters may be used in combination to verify the plausibility or give possibly a more accurate value of a parameter, that may then be assumed fixed within the immittance fits.

Many process-specific physical models are non-linearly dependent on the applied field and other external parameters. Consequently, the derivation of the circuit to describe a single homogeneous piece[1] takes this into account. As a result, during the whole derivation non-linear dependence on external parameters is considered.

As a consequence of causality (confer [96, pp. 331-336, 349-354]), and unaffected by the consideration of non-linearity [164], any permittivity different from the one of free space requires, as can be deduced from Kramers-Kronig relations, lossy polarisation processes in the material [78, p. 49]. The polarisation processes, e. g. (partial) alignment or creation of dipoles, are unavoidably non-instantaneous [164] and therefore associated with a finite, possibly external parameter dependent, time constant. The loss of the polarisation process inevitably leads to a finite phase delay and, as later explained in detail, to complex phasors of the permittivity (confer [33, pp. 89-95]). In other words, any phase delay is connected to a lossy polarisation mechanism (and vice versa) and, as a result, the permittivity of *anything but free space* (which has only purely imaginary phasors) has complex phasors and is dependent on frequency.

For a wide variety of very different materials (see Figure 2.2), a broad distribution of resonances is observed, manifesting itself in a broad resonance peak in the typical frequency range of immittance spectroscopy [83, 84, 79]. This resonance peak, that is usually modelled with a constant phase element [25, 47] (which is mathematically identical to the 'universal capacitor' introduced by Jonscher [83, 84]), can have various reasons [79, 104, 40, 87]. Any long-tailed distribution of resonances will lead to the approximately constant phase behaviour [37, 27]. Nevertheless, it seems that many authors are still associating this effect solely with surface roughness [1]. Due to the confusion in this area, introducing lossy polarisation processes in our derivation will be more pronounced and

[1] Typically, a system under investigation consists inevitably of multiple pieces, even if a single homogeneous piece of material is investigated, contacting the material usually leads to changed properties close to the interfaces e. g. the formation of space-charge layers (compare section 2.3).

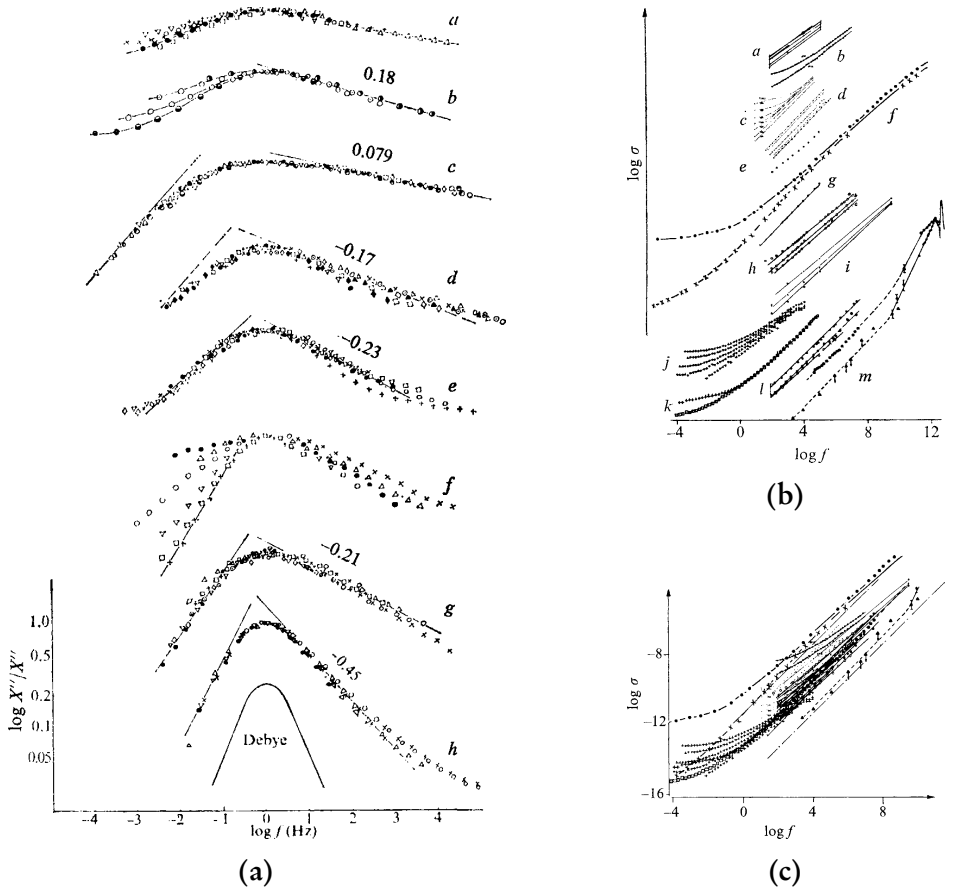

Figure 2.2: All plots from reference [84]. (a): Dielectric losses for some polymeric materials (details in [84]), point styles indicate different temperatures which were shifted laterally to make the loss peaks coincide. In comparison, an ideal Debye peak which is almost never observed in any real material. (b): Ac conductivity for different materials vertically displaced for clarity (data for one letter is on a common $\log\sigma$-scale). (c): The same data of (b) but on a common log scale showing the relatively narrow range of ac conductivity even for very different materials. Materials in (b) and (c): a single-crystalline silicon (3 K, 4.2 K, 8 K and 12 K), b single-crystalline β aluminium, c amorphous silicon (84 K to 295 K), d different chalcogenide glasses, e single-crystal anthracene at 294 K with 1 mol saline solution as contact f single-crystal anthracene (bottom) and evaporated β carotene (top), to show difference in dc properties and similarity in ac behaviour g trinitrofluorinone-polyvinyl carbazole (TNF PVK) h three glasses at room temperature: $50P_2O_5$-50FeO, $50P_2O_5$-40FeO-10CaO, $50P_2O_5$-25FeO-25CaO i $80V_2O_5$-$20P_2O_5$ glass at three temperatures j evaporated amorphous silicon monoxide 211 K to 297 K k stearic acid in the dark and in presence of ultraviolet light l amorphous (top to bottom) As_2Se_3, Se, As_2Se_3 at 300 K m As_2Se_3 at 300 K including higher frequencies. Reprinted by permission from Macmillan Publishers Ltd: Nature 267(5613), 673–679, copyright 1977.

thoroughly explained. A constant phase θ over a certain frequency range is equivalent to a constant ratio of real and imaginary part of the immittance, since e. g. for the impedance $Z = R + iX$ with reactance $X \in \mathbb{R}$ and resistance $R \in \mathbb{R}_0^+$ the phase

$$\theta = \arg(Z) = \arctan\left(\frac{X}{R}\right),$$

mathematically more strict $R = 0$ requires calculating the limits which are $\lim_{R\to 0}(\theta) = -\frac{\pi}{2}$ and $\lim_{R\to 0}(\theta) = \frac{\pi}{2}$ for $X < 0$ and $X > 0$, respectively. While the ratio between real and imaginary part of the immittance remains constant, in experiments, each value usually shows approximately a power-law dependence on frequency [37], whereas the constant phase element predicts an exact power law dependence (see section 2.2.5).

2.1.1.1 Structure of the chapter

The main goal of this chapter is to derive the correct arrangement of EEC components for a single homogeneous piece of a possibly larger system (i. e. potentially consisting of multiple pieces) and, finally, the connection of the different sub-circuits to a model for the complete system. Only using such an arrangement where each component corresponds to a single microscopic process allows including physical models dependent on external parameters that specifically describe the corresponding process as circuit component.

Before the actual derivation of the EEC, conventions in this work, especially for that subsequent derivation, are defined (see section 2.1.1.2).

In the second part of this chapter the derivation begins (see section 2.1.2), at first in time domain, the different contributions of Maxwell's equation of total current are explained and, in a nutshell, arguments for assuming the 'free' current to be caused by static charge transport models presented (the justification of this important approximation are discussed in more detail in section 5.4.1). Subsequently, external-parameter-dependent functions, as place holders for definite physical models for conductivity and permittivity, are included and their general form, especially their dependence on frequency and the necessity of their complex values, explained, while also the transition into frequency domain (see section 2.1.3) is performed.

In the third part of the derivation, geometry is included (see section 2.1.4) to finally arrive at a more general expression for the impedance of a single homogeneous piece. Since non-linear dependence on the applied field is allowed, the derived quantity is actually more than the impedance.

Details of this 'universal impedance' are addressed in depth in the last part of the derivation (section 2.1.5). After that, a short introduction into constant phase elements is given, including their possible origins (see section 2.2.5). Subsequently, see section 2.2.3, it is explained in more detail how to deal with multiple processes in a singe homogeneous piece and usual conventions for high-, respectively, low-frequency-limiting elements are presented. On the one hand, it is usually impossible to isolate a homogeneous piece of a system and, on the other hand, many investigated systems consist of several pieces anyway. Hence, in the final part (see section 2.3) of this chapter the connection of multiple homogeneous pieces is discussed.

2.1.1.2 Conventions

In the following section, the electrical equivalent circuit representing a single homogeneous, non-magnetic ($\mu_r = 1$), non-ferroelectric, isotropic bulk[2] of material is derived directly from Maxwell's equation of total current. As usual in the field of immittance spectroscopy, each piece and, consequently, the systems are described as two-port networks. It is generally assumed in this work that half of the wavelength of any applied electrical signal is much larger than any of the dimensions of the system. For the most part the derivation is, as common for immittance spectroscopy, in frequency-domain. That is why functions in time-domain have a tilde over the designation, e. g. $\tilde{\mathbf{J}}$, while for addressing a function in general, e. g. to describe a property applicable to the representative of a function in both domains, a $\star$ is used as accent, e. g. $\dot{\mathbf{J}}$. From this example, it can also be seen that spatially vectorial quantities are written as bold letters. Since the applied field $\dot{\mathbf{E}}$ (i. e. $\tilde{\mathbf{E}}(t)$ or $\mathbf{E}(\omega)$, see above) is a very important external parameter in this non-linear derivation, it is always written explicitly. Other external parameters are combined in a parameter set $\dot{\mathscr{P}}$. The idea of the other parameters is that they are potentially time dependent, since they are varied, but the variation should be between single measurements of the immittance, so that the one (complex valued) immittance is measured for each condition. During the variation of the applied field, to measure the immittance of the sample at one specific condition, the external parameters should be constant.[3] Although different processes might depend on very different parameter sets, to avoid unnecessary syntactical overhead, in the derivation all parameter sets are denoted $\dot{\mathscr{P}}$, no matter what their specific content is. Using the omitted mathematically more strict convention: a sum $\tilde{S}$ of two functions $\tilde{A}$ and $\tilde{B}$ dependent on different parameter sets $\tilde{\mathscr{P}}_A$ and $\tilde{\mathscr{P}}_B$ would actually result in their union

$$\tilde{A}(t, \tilde{\mathscr{P}}_A) + \tilde{B}(t, \tilde{\mathscr{P}}_B) = \tilde{S}(t, \tilde{\mathscr{P}}_A \cup \tilde{\mathscr{P}}_B).$$

Like in this case, also in all other cases in this work concerning the parameter sets, the tilde above the parameter set should not indicate that the set $\tilde{\mathscr{P}}_i$ changes with time, but instead its components $\tilde{p}_j$, i. e. $\forall\, \tilde{p}_j \in \tilde{\mathscr{P}}_i : \tilde{p}_j \equiv \tilde{p}_j(t)$. To avoid unnecessarily long formulae the explicit time (frequency) dependence of external parameters $\dot{p}_j$ and the applied field $\dot{\mathbf{E}}$ is, if not stated otherwise, omitted. The *explicit* time dependence of response functions, in the example above $\tilde{A}$, $\tilde{B}$ and $\tilde{S}$, shows that the functions do not instantaneously react on the changes of the external parameters but have some finite time delay. To stress the fact that almost all static current transport models (that due to a lack of alternatives have to be used to describe the dc current contribution, see section 2.1.2) are designed for

[2] As later explained in 2.3, the derived fundamental description is not different whether it is a bulk or interface piece, the models for the specific elements, on the other hand, are.

[3] These assumptions are chosen to account for realistic measurement scenarios. For example, if one measures at different temperatures, temperature will obviously vary over time. However, one would stabilise the temperature to perform the measurement of an immittance spectrum at one temperature. Varying the temperature while obtaining the spectrum would lead to results which were very difficult to interpret.

equilibrium conditions, i. e. usually do not have an explicit time dependence and, as a result, react instantaneously, there is no explicit time dependence for those functions, representing static conduction models.

In this work, it is convention for the order of harmonics of a function, periodic in time domain, to have the same numbering as the power of the fundamental frequency ω_0, hence, the 0th order harmonic corresponds to the static offset, the 1st order harmonic corresponds to the coefficient of the fundamental frequency (i. e. $\omega_{\text{harm}}^{(1)} = 1 \cdot \omega_0 = \omega_0$) and so on ($\omega_{\text{harm}}^{(n)} = n \cdot \omega_0$). Harmonics with higher order than the first order harmonic are called *higher harmonics*.

Let f be a periodic function in frequency domain with $f(\omega) = \hat{f} e^{i(\omega t + \phi)}$, with the real valued amplitude $\hat{f} \in \mathbb{R}$. The phasor $\underline{\hat{f}}$ of the periodic function f is defined as the product of the real amplitude with the complex phase term $e^{i\phi}$, i. e. $\underline{\hat{f}} \equiv \hat{f} e^{i\phi}$, so that $f(\omega) = \underline{\hat{f}} e^{i\omega t}$. In frequency domain and assuming (as usual in this work) a homogeneous, isotropic response, a response function can be represented by a complex frequency-dependent function, e. g. $\forall \omega : h(\omega) \in \mathbb{C}$. If the response function is real, e. g. $\forall \omega : h(\omega) \in \mathbb{R}$, the response is in phase with the stimulus, since it does only change the amplitude of the phasor(s) of the response.

Directly connected to the fact that an in time-domain real valued function may be described by superposition of its odd and even contributions, the response may be separated in *in-phase* and *quadrature contributions*. In frequency-domain, this corresponds to a description using real and imaginary part. To make the mathematical formulations easier, it is, if not stated otherwise, assumed throughout the work that the stimulus has a real phasor. That allows deducing that when the phasor of the response is real, consequently, the phasor(s) of the response function must be real, as well. Whether the phasor of the response is complex or purely imaginary, since a phasor of the response function with non-vanishing imaginary part leads also to a non-vanishing imaginary part of the phasor of the response, i. e., assuming causality, a delayed response to the stimulus. Non-linear response functions cause poly-harmonic responses to periodic stimulus. Hence, the response can be expressed using multiple phasors $\underline{\hat{b}}^{(n)}$ designating the phasor of the nth order harmonic with $n \in \mathbb{N}_0$. If all phasors are real, the response is, just like in the linear case, in phase with the stimulus, i. e. does not have a delay. For non-periodic signals, this means that purely real valued response functions do not lead to retardation. For more information about non-linear response functions and their different representations the review of Peterson [145] is recommended.

2.1.2 The total current density and its contributions

According to Maxwell [126] the total current density $\tilde{\mathbf{J}}_{\text{tot}}$ through a non-ferroelectric, non-magnetic, isotropic material can in time-domain be expressed as

$$\tilde{\mathbf{J}}_{\text{tot}}(t, \tilde{\mathbf{E}}, \tilde{\mathscr{P}}) = \tilde{\mathbf{J}}_{\text{free}}(t, \tilde{\mathbf{E}}, \tilde{\mathscr{P}}) + \frac{\partial \tilde{\mathbf{D}}(t, \tilde{\mathbf{E}}, \tilde{\mathscr{P}})}{\partial t}, \tag{3.1a}$$

with *'free' current density* $\tilde{\mathbf{J}}_{\text{free}}$ and *electric displacement field* $\tilde{\mathbf{D}}$.

The two different terms, of the total current density $\tilde{\mathbf{J}}_{\text{tot}}$ in equation (3.1a) the 'free' current density $\tilde{\mathbf{J}}_{\text{free}}$ and, respectively, the *displacement current density* $\partial\tilde{\mathbf{D}}/\partial t$, are exclusively associated with the two different contributions from *conduction processes* and *dielectric processes*, respectively. Throughout the whole work circuit elements or quantities in the formulae are colour coded to be clearly associated with the different contributions. In the following two sections, it is explained what kind of processes contribute to which of the two terms of the total current density $\dot{\mathbf{J}}_{\text{tot}}$. As a consequence, immittance spectroscopy related assumptions about the different contributions can be introduced yielding a description of the total current density $\dot{\mathbf{J}}_{\text{tot}}$ in which familiar process-specific physical models can be directly included. Here only an essential summary for the two different terms is given:

The first term, the 'free' current density $\dot{\mathbf{J}}_{\text{free}}$, is assumed to exclusively result from conduction processes (see below in subsection 2.1.2.1 for the discussion on the term 'free'). Those *conduction processes* must *principally* allow charge carriers to migrate from one side of the material to the other. Further, in a later defined (but for immittance spectroscopy solely important) low-frequency regime $\mathbb{L}$, the cause for the 'free' current density is the continuous movement of charges across the material that leaves the 'centre of gravity' of the charge distribution (on average) unchanged [78, p. 41]. However, in addition to the fact that this definition by Jonscher is only valid in this to be explained 'low-frequency regime' $\mathbb{L}$, one has to add that local dipoles can temporarily be created, since the local carrier distribution and their movement are commonly statistical processes. Yet, for sufficiently large volumes, the polarisation vanishes on average.

The second term, the time derivative of the electric displacement field $\partial\tilde{\mathbf{D}}/\partial t$, also called displacement current density, is exclusively associated with polarisation processes. Those processes lead to repositioning or separation of charge carriers due to the applied field, thereby creating dipole moments that in total result in a non-vanishing polarisation in the material. The statement by Jonscher [78, p. 41], that no charges may migrate through the dielectric as a result of those processes, is tendentiously vague since the conduction process and the dielectric process in a single material can originate from the same underlying mechanism [37]. For example, the Barton-Nakajima-Namikawa relation, confirmed for many materials, implies the same underlying process for static conduction and dielectric properties (confer references [36, 182] and see subsection 6.2.4).

2.1.2.1 The contributions to the 'free' current density and their properties

Time (frequency) dependence of conduction processes Beside their dependencies on external parameters (which might themselves vary in time), especially their possibly non-linear response to the applied field, that is discussed later, conduction processes are *generally* explicitly time (analogously frequency) dependent. The explicit time (frequency) dependence is a consequence of a non-instantaneous response of the resulting current to the applied field. The delay in the response to a change in field is dependent on the process itself, but always finite (as explained in [78, pp. 36-52]). It is shown below that, depending

on the relation of the magnitude of the delay to the abruptness of the time derivative of interest (analogously frequency range of interest), the response of the conduction process can be divided into three regimes.

The differential equation for the motion of a charged particle in the theory developed by Drude [4, pp. 1-20] can, omitting the specific reasons for the damping (e. g. collisions), be interpreted more generally, to approximate (with certain restrictions) any situations of damped movement of idealised charge carriers.

Of course, this reduces the situation only to the main ideas of a charge transport process, since it is a classical, mean-field, continuous media, point-charge approximation. Furthermore, the time-variant analysis of the Drude model used here is just to get a general idea of the properties of the time (frequency) dependence of conduction processes (which is rarely discussed in the context of immittance spectroscopy). In detail, especially also due to the fact that the Drude model does not include even very fundamental properties of materials, e. g. band structures, the Drude model would give a poor description for experimental conductivity data in many materials. Hence, the author does not at all want to suggest to use the Drude model to interpret any experimental data. On the contrary, the conduction in many materials is expected to be much more complicated in general, and, especially in our context, to have a more complicated frequency dependence.

However, the one very important fact, that at some critical abruptness of the stimulus (i. e. at some critical frequency $\omega_c^{(dc)}$) the conduction mechanism cannot contribute to the 'free' current $\tilde{\mathbf{J}}_{free}$ any longer, can be derived through the following theoretical analysis of the above given model by Drude.

The first fact that can be derived from the simple model given above, that does very likely not vanish for more complex conduction models, is that any form of damping, whatever its cause in the specific process, has a key influence on that critical frequency $\omega_c^{(dc)} = \frac{1}{2\pi\tau_c^{(dc)}}$, at which the charge carriers cannot follow the applied field any longer (in consequence also the corresponding contribution to the 'free' current density decreases rapidly). Even if there are several time constants or it is a distribution of values instead of a single constant, there are always slew rates (frequencies) at which the process cannot contribute any longer. The damping, in the (differential) equation of motion of the charged particle with mass of Drude, leads to a critical time constant $\tau_c^{(dc)}$ that separates the corresponding low- ($\mathbb{L} = \{\omega \,|\, \omega\tau_c^{(dc)} \ll 1\}$) and high-frequency regime ($\mathbb{H} = \{\omega \,|\, \omega\tau_c^{(dc)} \gg 1\}$) of the process. The transition region around the resonance of the conduction process ($\mathbb{T} = \{\omega \,|\, \omega\tau_c^{(dc)} \sim 1\}$) is specific to the corresponding conduction process and its form of damping. In the low-frequency regime $\mathbb{L}$ the response can be regarded as instantaneous to the stimulus. In the high-frequency regime $\mathbb{H}$, on the other hand, the charge carriers are too slow to follow the applied field. In the intermediate region, the transition region $\mathbb{T}$, the highest values of the imaginary part may be observed. The properties of this transition region itself cannot be narrowed down from the above considerations which intentionally describe the problem in the most general way possible.

Silveira and Lima [169] solve a more general version of Drude's equation of motion for the charge carrier: the stochastic Langevin equation. They show the

influence of the charged particles inertia, which was neglected in Maxwell's original theory [30]. Silveira and Lima find a finite time constant, delaying the response of the free current $\tilde{\mathbf{J}}_{\text{free}}$ to the applied field. This constant divides the conduction mechanism in its different regimes, $\mathbb{L}$ and $\mathbb{H}$. Finally, they arrive at an explicitly frequency-dependent conductivity $\mathbf{J}_{\text{free}}$. This means that, in the end, also in a more refined approach the above derived result remains unchanged.

In the case, that the applied field changes much faster than the process-specific critical frequency $\omega_{\text{c}}^{(\text{dc})}$, the contribution of the conduction process to the 'free' current density $\dot{\mathbf{J}}_{\text{free}}$ either decreases or the conduction process contributes to polarisation.

The charge transport in insulators typically involves (randomly arranged) localised electrically active states [58] while the charge transport in metals, on the other hand, is through charge carriers propagating in delocalised states [10]. As discussed in more detail later, in section 5.4.1, the critical time constant of conduction processes based on charge carriers propagating in delocalised states is too short to play a significant role in the typical frequency ranges of immittance spectroscopy. Hence, for the frequencies used in immittance spectroscopy, those metallic conduction processes can be assumed to be in their low-frequency regime $\mathbb{L}$. The process of movement of charges in insulators through randomly arranged localised states does, in the frequency range relevant for immittance spectroscopy, contribute to both, the free current and to the displacement current, at the same time (see below, section 5.4.1 and section 6.2.4). It will be shown in section 5.4.1, that it is justified to assume for insulators, just as for metals, that the contributions of those processes to the free current $\dot{\mathbf{J}}_{\text{free}}$ are in a subset of the low-frequency regime $\mathbb{L}$, at the frequencies relevant for immittance spectroscopy. As already mentioned, in the low-frequency regime $\mathbb{L}$ the 'free' current density $\dot{\mathbf{J}}_{\text{free}}$ can be assumed to result exclusively from *static conduction processes* (also called *dc conduction processes*). This does change the following properties: Generally, the non-instantaneous response of the conduction process leads to an explicit frequency (or respectively time) dependence of the conductivity. As a consequence of this delayed response, the phasors are in general complex quantities in frequency domain, i. e. $\forall n : \underline{\hat{\sigma}}^{(n)} \in \mathbb{C}$ (whereas a phasor must be in $\mathbb{C} \setminus \mathbb{R}$ to generate a delay). This allows a delayed response of the current with respect to the applied field, which is, here and everywhere else in this work, without loss of generality assumed to always have a phase of zero. In the low-frequency regime $\mathbb{L}$, on the other hand, the response of the conduction process might be assumed instantaneous and, hence, the conductivity is only implicitly dependent on the frequency (through the external parameters and explicitly the applied field), i. e. $\sigma_{\text{stat}}(\mathbf{E}, \mathscr{P})$. Furthermore, all phasors of a non-delayed response function are purely real $\forall n : \underline{\hat{\sigma}}_{\text{stat}}^{(n)} \in \mathbb{R}$, meaning that the response is in phase with the applied field. Consequently, in time domain the explicitly time-dependent conduction models can be replaced by the corresponding time-independent, hence, instantaneously responding static conduction models $\tilde{\sigma}_{\text{stat}}(\tilde{\mathbf{E}}, \tilde{\mathscr{P}})$.

To differentiate the 'free' current density $\dot{\mathbf{J}}_{\text{free}}$ in general from the 'free' current density calculated only using *static* conduction models, the latter is from now on called *static*

'free' current density $\mathbf{J}^{\star(\mathrm{stat})}_{\mathrm{free}}$.

In frequency domain, the static 'free' current density $\mathbf{J}^{(\mathrm{stat})}_{\mathrm{free}}$ can be calculated using Ohm's law (confer [93, p. 3]), which is (in this work as compared to the source) further generalised for non-linear applied-field-dependent as well as external-parameter-dependent conductivities $\sigma_{\mathrm{stat}}(\mathbf{E}, \mathscr{P})$,

$$\mathbf{J}^{(\mathrm{stat})}_{\mathrm{free}}(\mathbf{E}, \mathscr{P}) = \sigma_{\mathrm{stat}}(\mathbf{E}, \mathscr{P})\mathbf{E}(\omega). \tag{3.2a}$$

Although the static conductivity shows, in contrast to the conductivity in general, no explicit frequency dependence, the time-domain representation of the conductivity looks more complicated, since the dependence on the applied field still leads to an implicit time dependence and, furthermore, the product in frequency domain converts in a convolution in time domain, here given for a linear response,[4]

$$\tilde{\mathbf{J}}^{(\mathrm{stat})}_{\mathrm{free}}(\tilde{\mathbf{E}}, \tilde{\mathscr{P}}) = \int_{-\infty}^{t} \mathrm{d}t' \mathscr{F}[\sigma_{\mathrm{stat}}]\left(\tilde{\mathbf{E}}(t-t'), \tilde{\mathscr{P}}\right)\tilde{\mathbf{E}}(t'). \tag{3.2b}$$

As a consequence of the fact that the static conductivity is only implicitly frequency dependent through the applied field itself, its variation is (as explained above) always in phase with the applied field. The other external parameters are assumed to be constant during the immittance measurement of a certain condition (compare section 2.1.1.2 about the variation of external parameters in time).

Due to the fact that codomains of static conductivities in frequency domain are real, the static 'free' current density in time domain $\tilde{\mathbf{J}}^{(\mathrm{stat})}_{\mathrm{free}}(\tilde{\mathbf{E}}, \tilde{\mathscr{P}})$ responds instantaneously to the stimulus, meaning there is no delay to the stimulus. Additionally, this means that $\mathbf{J}^{(\mathrm{stat})}_{\mathrm{free}}(\mathbf{E}, \mathscr{P})$ has no explicit time (or analogue, frequency) dependence. Furthermore, the phasors of the static 'free' current density $\underline{\hat{\mathbf{J}}}^{(\mathrm{stat}),(n)}_{\mathrm{free}}$ are (assuming periodic stimulus[5]) purely real, i. e. in phase with the applied field, as well.

The above assumption lays the foundation for using models that were developed to describe static conduction in the corresponding medium. In contrast to conduction processes in general, those dc conduction models understandably assume equilibrium conditions and, hence, do not include (explicit) time dependence (compare examples for different dc conduction models in Table 5.1). As a result of the assumptions made above, these models can be used to calculate the (static) 'free' current density in the frequency range of immittance spectroscopy.

Due to the variation of the applied field $\tilde{\mathbf{E}}(t)$ and the other external parameters $\tilde{\mathscr{P}}(t)$ with time the (conductivity and in consequence also the derived) 'free' current density $\tilde{\mathbf{J}}_{\mathrm{free}}$

[4] Usually one assumes that the explicitly time dependent conductivity vanishes for $t > t'$ so that the integration is until infinity and it really becomes a convolution. One may still use this formula, which is valid, but then one has to use Laplace transform instead of Fourier transform. Anyway, causality forces that the current density at time t should depend neither on future values of the applied field nor future values of the conductivity.

[5] For aperiodic stimuli the phasors, otherwise discrete in frequency space, become continuous in frequency space.

is, however, *still implicitly time dependent*. Furthermore, the 'free' current density $\tilde{\mathbf{J}}_{\text{free}}$ is usually non-linearly dependent on the applied field (see the examples for process-specific physical models dependent on external parameters in Table 5.1), which is represented by its dependence on the time-varying applied field $\tilde{\mathbf{E}}$. In addition to the applied field, the 'free' current density can depend on external parameters, like the temperature (confer to models in Table 5.1), an applied external magnetic field [178, 177] or on pressure applied to the material [43]. All these other dependencies on external parameters are jointly represented by the dependence of the 'free' current density $\tilde{\mathbf{J}}_{\text{free}}$ on the external parameter set $\tilde{\mathscr{P}}$ (see section 2.1.1.2). For the conductivity these dependencies on external parameters and applied field are important, since it is known to have a much stronger dependence on those parameters than the permittivity [37].

All properties for the 'free' current density mentioned above are included in equation (3.1a) by replacing the explicitly time dependent, non-instantaneous and (in frequency space) complex 'free' current density $\tilde{\mathbf{J}}_{\text{free}} = \tilde{\mathbf{J}}_{\text{free}}(t, \tilde{\mathbf{E}}, \tilde{\mathscr{P}})$ by the above described only implicitly time dependent, instantaneously responding and, hence, having purely real phasors in frequency space, static 'free' current density $\tilde{\mathbf{J}}_{\text{free}}^{(\text{stat})} = \tilde{\mathbf{J}}_{\text{free}}(\tilde{\mathbf{E}}, \tilde{\mathscr{P}})$, resulting in

$$\tilde{\mathbf{J}}_{\text{tot}}(t, \tilde{\mathbf{E}}, \tilde{\mathscr{P}}) = \tilde{\mathbf{J}}_{\text{free}}^{(\text{stat})}(\tilde{\mathbf{E}}, \tilde{\mathscr{P}}) + \frac{\partial \tilde{\mathbf{D}}(t, \tilde{\mathbf{E}}, \tilde{\mathscr{P}})}{\partial t} \tag{3.1b}$$

The derivation itself does not require the assumptions made above. It would generally also work with a time dependent, delayed 'free' current density $\tilde{\mathbf{J}}_{\text{free}}(t, \tilde{\mathbf{E}}, \tilde{\mathscr{P}})$ and it is the hope of the author that more conduction models recognising the time dependence will emerge in the future (in this context see also subsection 6.2.4). The assumptions become necessary due to the fact that, because of the *absence of alternatives*, *dc conduction models* are used to calculate the 'free' current density. Furthermore, these dc models consider the dependence on external parameters which is, as explained later, a key feature in identifying the different parts of the system. An exemplary, but not exhaustive, list of external-parameter-dependent dc-conduction models, specifically some which are commonly found in dielectric films in CMOS technology based on transport through localised states, are given in Table 5.1.

Same underlying mechanism for ac and dc conductivity possible As already shortly mentioned in the explanation of equation 3.1a, steady conduction and dielectric processes can originate from the same underlying mechanism [37]. An example for the correlation of these processes is the experimentally verified Barton-Nakajima-Namikawa relation [37]. Another understandable example for the same underlying mechanism can be pictured at an insulator with dominant conduction through a defect band. As a consequence of an assumed spatially statistical arrangement of traps, there are situations where two traps are close to each other, have high mutual transition probability, while being spatially more isolated from other traps. The alignment of a charge carrier in these two trap states with the applied field is exactly the 'pair approximation' model for polarisation in a disordered material by Pollak and Geballe [148]. In addition to the dielectric contribution, the same traps can contribute to a steady current through the material [58].

In electrolytes charge carriers can be mobile molecules that propagate through a liquid. If these molecules are themselves polar, one molecule can contribute to the 'free' current density by spatial propagation and, at the same time, to the dielectric displacement current density by rotational alignment [33, pp. 59-76].

Excursion - The identifier 'free' In this work, the common convention in literature to call the current density already present in Ampère's law [146, pp. 16-18], which is not part of the contribution of the derivative of electric displacement field introduced by Maxwell [146, pp. 16-18], 'free current density' $\mathring{\mathbf{J}}_{\text{free}}$ is used. Consequently, the index 'free' is utilised on the respective symbols in formulae. The reader may have noticed, that the term 'free' was in this context, so far, always in quotation marks. The reason for that is, that the designation 'free' can be misleading, since the charge carriers that contribute to the corresponding current do not actually have to be free.[6] In metals, up to frequencies in the THz range [143, p. 21] which is a superset of the frequency range of interest in this work, the free current density $\mathring{\mathbf{J}}_{\text{free}}$ is caused by the charge carriers that propagate *quasi-free* through the delocalised states [10]. In most cases, immittance spectroscopy is used to investigate systems, at least, containing dielectrics. To be a dielectric, i. e. an insulator[7], the material should have as few as possible electrons or holes in its corresponding conductive bands. Often, the *parasitic* process leading to the finite resistivity of a dielectric, is a result of charge carriers propagating through unwanted (energetically and spatially randomly arranged) localised defect states [58]. Between the jumps, these carriers are not free, but the opposite, bound. Through trapping and detrapping [46] (which involves the conductive band) or hopping [136, 135] (which only involves the localised states) the charge carriers can percolate from one side of the dielectric to the other. Since new carriers are injected from one electrode and collected through the other electrode, the overall 'centre of gravity' of the charge distribution does not change ([78, p. 41] - as already mentioned above, at least in the low-frequency regime $\mathbb{L}$ and neglecting temporary local dipoles due to the statistical nature of the process) and the contribution is, hence, to the free current density $\mathring{\mathbf{J}}_{\text{free}}$. Similarly, ionic conduction in solids, which can for the following arguments be treated equivalent to conduction of charges through localised states [37], can contribute to the free current density by hopping from one side (or a specific space in an amorphous matrix) to the next. Between the jumps, the position of the ions is fixed at the corresponding lattice site and, thus, not free.

An illustrative example is the movement of electrons in a disordered insulator. Disordered insulator should not imply no order at all, but some certain random element, e. g. a crystal with some randomly arranged defects. The electrons can percolate through

[6] This distinction born out of necessity appears when dealing with the Maxwell's equations in matter (sometimes also called 'Maxwell's macroscopic equations') to distinguish the various contributions by different mechanisms to the total current, e. g. in [44, pp. 125-129] and [73, pp. 13-16].

[7] Dielectrics are insulators [78, p. 1], [39]. The two terms just emphasise different aspects of such a material [39]: Insulator, from the Latin word for island '*insula*', expresses the fact that islands of charges may exist in such a material [39] and the suffix '*tor*' creates an agent noun indicating that something is performed. Dielectric, on the other hand, is derived from the Greek word '*dia*' (prefix '*di*') meaning across , i. e. the (non-conducting) material placed across the plates of a capacitor [39].

defect-rich parts, i. e. hop from one localised defect to another, until they eventually migrate from one electrode to the other [80]. Disordered or not, in materials where current flow is the result of charge movement in localised states, the charge is bound to a specific defect between jumps and therefore not free [80]. Still, the resulting direct current density has to be ascribed to the free current density $\tilde{\mathbf{J}}_{\text{free}}$ since it is the only remaining term for a response caused by a time-independent, i. e. static, stimulus.

Special properties of the displacement current density Since most properties of the displacement current density $\partial\tilde{\mathbf{D}}/\partial t$ will become more clear later when the derivation is continued in the frequency domain, here only a summary of the most important differences will be given, that will be discussed in detail in section 2.1.3.1, delimiting it from the contribution of the free current density $\tilde{\mathbf{J}}_{\text{free}}$.

There is always a contribution to the displacement current density $\partial\tilde{\mathbf{D}}/\partial t$ from free space $\varepsilon_0 \cdot \partial\tilde{\mathbf{E}}/\partial t$ which is independent of external parameters. Since the principle of causality is assumed to be valid in this work, the contribution of free space is the only lossless contribution to the displacement current density $\partial\tilde{\mathbf{D}}/\partial t$ and, hence, the only contribution which is exactly in quadrature with the applied field $\tilde{\mathbf{E}}$. In frequency domain, this quadrature in phase, as compared to the applied field $\mathbf{E}$ (with purely real phasor), represents a contribution to the total current $\mathbf{J}_{\text{tot}}$ with purely imaginary phasors.

The remaining contributions to the electric displacement field $\tilde{\mathbf{D}}$ are combined in the *polarisation* $\tilde{\mathbf{P}}$ of the material. Although polarisation exists also in the electrostatic case, as a result of the time derivative, only polarisation varying with time can contribute to the displacement current density $\partial\tilde{\mathbf{D}}/\partial t$. The link between causality, lossy and non-instantaneous polarisation, as well as its necessity to have any other permittivity than the permittivity of free space, is explained in reference [78, pp. 36-52] with the introduction of the Kramers-Kronig relations. Any other (lossy) polarisation process in the material leads to a complex contribution with finite real components of the phasors and, hence, a larger phase shift than the case of exactly −90° of the free-space contribution. Due to causality, or more graphically, because no polarisation process, i. e. neither (partial) alignment nor creation of a dipole, can be instantaneous resulting in finite time constants, the imaginary and real phasors of the polarisation processes vary with frequency as specified by the Kramers-Kronig relations (confer [78, pp. 36-52]). Hence, the electric displacement field $\tilde{\mathbf{D}}$ is explicitly time, respectively frequency, dependent. Just like for the static conductivity σ_{stat} (for which some models are exemplary given in Table 5.1), there are also process-specific physical models for polarisation processes that depend on external parameters, e. g. polarisation is known to be dependent on pressure applied to the material [31] or the temperature can vary the speed of an orientational motion of a dipole in a viscous liquid [160]. Furthermore, for a consequent consideration of large-signal analysis the electric displacement field $\tilde{\mathbf{D}}$ is assumed to depend on the applied field.

2.1.3 The total current density in frequency domain

As immittance spectroscopy is most commonly performed and analysed in frequency domain [7, p. 4], the derivation will be continued in that domain. Since the time derivative $\partial\tilde{X}(t)/\partial t$ of a function $\tilde{X}$ in time domain becomes $i\omega X(\omega)$ in frequency domain, the Fourier transform of the total current density $\tilde{\mathbf{J}}_{\mathrm{tot}}$ in equation (3.1b) is

$$\mathbf{J}_{\mathrm{tot}}(\omega,\mathbf{E},\mathscr{P}) = \mathbf{J}_{\mathrm{free}}^{(\mathrm{stat})}(\mathbf{E},\mathscr{P}) + i\omega\mathbf{D}(\omega,\mathbf{E},\mathscr{P}). \tag{2.3}$$

It should be noted, that the parameter ω is not necessarily the frequency of the stimulus, just as t is not necessarily the length of a period. Further, the term displacement current density in frequency domain shall only designate the term $\omega\mathbf{D}$. As a result of this convention, the real parts of the phasors of the displacement current density are the imaginary parts of the phasors of the total current density.

2.1.3.1 The displacement current in detail

As already explained in section 2.1.2.1, the electric displacement field $\mathbf{D}$ can be divided in the two contributions from free space $\varepsilon_0\mathbf{E}$ and from the material, the polarisation $\mathbf{P}$,

$$\mathbf{D}(\omega,\mathbf{E},\mathscr{P}) = \varepsilon_0\mathbf{E} + \mathbf{P}(\omega,\mathbf{E},\mathscr{P}). \tag{2.4}$$

The polarisation $\mathbf{P}$ is, as also already mentioned in section 2.1.2.1, due to causality a quantity with complex phasors. It is a result of the (partial) alignment or induction of dipoles in the material. In frequency domain, it can be expressed by the product of the free-space component $\varepsilon_0\mathbf{E}$ with the dimensionless, frequency- and generally external-parameter-dependent electrical susceptibility χ with complex phasors. Hence, the electrical susceptibility χ is a measure of how strong the polarisation $\mathbf{P}$ in the material is in 'units' of the free-space component $\varepsilon_0\mathbf{E}$ of the displacement current density $\omega\mathbf{D}$, i. e.

$$\mathbf{P}(\omega,\mathbf{E},\mathscr{P}) = \varepsilon_0\chi(\omega,\mathbf{E},\mathscr{P})\mathbf{E}. \tag{2.5}$$

Due to connection over the Fourier transform, in time domain the polarisation $\tilde{\mathbf{P}}$ is proportional to the convolution of the electric field $\mathbf{E}$ with the electrical susceptibility $\tilde{\chi}$.

Complex and non-linear permittivity From Eq. (2.4) and Eq. (2.5) follows that the electric displacement field

$$\mathbf{D}(\omega,\mathbf{E},\mathscr{P}) = \varepsilon_0[1+\chi(\omega,\mathbf{E},\mathscr{P})]\mathbf{E}.$$

The term in braces is, conform to the usual definitions in standard literature (e. g. [78, pp. 36-47]) called relative permittivity and defined as

$$\varepsilon_{\mathrm{r}}(\omega,\mathbf{E},\mathscr{P}) \equiv [1+\chi(\omega,\mathbf{E},\mathscr{P})].$$

As already explained, in absence of alternatives, dc current models are used to calculate the free current density $\mathbf{J}_{\mathrm{free}}^{(\mathrm{stat})}$. These static models fail to take frequency dependence as

well as a delayed response into account. On the other hand, models for the susceptibility χ and all quantities derived from it (i. e. the [relative] permittivity $\varepsilon_{[r]}$, polarisation $\mathbf{P}$ and electric displacement field $\mathbf{D}$) consider frequency dependence and delayed response. As a consequence of the delayed response, which is, as explained below, equivalent to the fact that there can be no lossless polarisation process for anything but free space, the permittivity is a quantity with complex phasors. Separating the permittivity into its *real* component in quadrature with the applied field E (in compliance with the usual literature conventions, indicated by a ' $'$ ') and the *imaginary* component in phase with the applied field E (indicated by a ' $''$ ') leads to

$$\begin{aligned}\varepsilon(\omega,\mathbf{E},\mathscr{P}) &= \varepsilon_0\varepsilon_\mathrm{r}(\omega,\mathbf{E},\mathscr{P})\\ &= \varepsilon_0\varepsilon_\mathrm{r}'(\omega,\mathrm{E},\mathscr{P}) - i\varepsilon_0\varepsilon_\mathrm{r}''(\omega,\mathbf{E},\mathscr{P})\\ &= \varepsilon'(\omega,\mathrm{E},\mathscr{P}) - i\varepsilon''(\omega,\mathbf{E},\mathscr{P}),\end{aligned} \tag{2.6}$$

where the quantity ε, with its real ε' and imaginary ε'' components, respectively, is the permittivity of the material [33, p. 94]. In the case of non-linear responses, the phasors of the permittivity are separated in their real and imaginary parts which exclusively belong to ε' or ε'', respectively. It should be noted that, due to the multiplication with the imaginary unit i, the real part of the permittivity contributes to the imaginary part of the total current density while the imaginary component of the permittivity contributes, in turn, to the real part of the total current density.

Following the notation of Debye [33, p. 94], K. Cole and R. Cole [27], Jonscher [78, p. 46], and others, as well as most engineering textbooks, the imaginary component of the permittivity is defined with negative sign. Both notations, negative or positive imaginary part, can be used equivalently. They result from the direction of rotation of the oscillating part of the electric field in the complex plane with increasing time. This work uses the notation with the oscillating part $\exp(+i\omega t)$ for the applied field, which means rotation of the oscillating part in mathematical positive sense, and results in the negative imaginary part (compare derivation of Debye in [33, p. 91]).

Illustratively, the polarisation response in a material due to an externally applied field cannot be instantaneous [164], because the (spatial) separation of charges or (at least partial) alignment of a dipole is always associated with some inertia and hence requires a certain, sometimes very short but still finite, time. A finite delay in time domain represents an unavoidable phase shift and, consequently, a non-vanishing imaginary part of the permittivity in frequency domain. Hence, for any material (i. e. everything but vacuum) the (relative) permittivity $\varepsilon_{(r)}$ is a quantity with complex phasors (confer [33, pp. 89-95] for the linear case). Assuming causality, it can be derived from the Kramers-Kronig relations (which are also valid for non-linear systems [164]) that for any permittivity differing from the value of free space, the electrical susceptibility χ of the material has to be, first, a function with complex phasors, second, its value must change with frequency and third, *each* of its two components χ' and χ'' contains the complete information of the response [78, pp. 36-52]. As a result of their relation with the susceptibility, other frequency-domain representatives of quantities, namely the electric displacement field $\mathbf{D}$, the polarisation $\mathbf{P}$, the (relative) permittivity $\varepsilon_{(r)}$ and the displacement current density

$\omega\mathbf{D}$, have (except for free space) complex valued and frequency dependent phasors as well.

Since the real and imaginary parts of the phasors are exclusively associated with either g' or g'', with $g = P, D, \chi, \varepsilon_{(r)}$, the base function g is from now on called complex, if both parts g' and g'' are finite, independently of the form of the potentially complex oscillatory part. Furthermore, it is called purely real, if the part g'' is zero, or purely imaginary, if the part g' is zero, although in the case on non-linear response, dependent on its form, the potentially complex oscillatory part of the harmonics may always force complex values.

Inserting the formulation for the complex permittivity, equation (2.6) in the total current density in frequency domain equation (2.3), results in:

$$\begin{aligned}
\mathbf{J}_{\text{tot}}(\omega, \mathbf{E}, \mathscr{P}) &= \mathbf{J}_{\text{free}}^{(\text{stat})}(\mathbf{E}, \mathscr{P}) + i\omega\left[\varepsilon_0 \mathbf{E} + \mathbf{P}(\omega, \mathbf{E}, \mathscr{P})\right] && \text{(2.7a)}\\
&= \mathbf{J}_{\text{free}}^{(\text{stat})}(\mathbf{E}, \mathscr{P}) + i\omega\varepsilon_0\varepsilon_{\text{r}}(\omega, \mathbf{E}, \mathscr{P})\mathbf{E} \\
&= \mathbf{J}_{\text{free}}^{(\text{stat})}(\mathbf{E}, \mathscr{P}) + i\omega\varepsilon(\omega, \mathbf{E}, \mathscr{P})\mathbf{E} && \text{(2.7b)}\\
&= \mathbf{J}_{\text{free}}^{(\text{stat})}(\mathbf{E}, \mathscr{P}) + \omega\varepsilon''(\omega, \mathbf{E}, \mathscr{P})\mathbf{E} + i\omega\varepsilon'(\omega, \mathbf{E}, \mathscr{P})\mathbf{E}. && \text{(2.7c)}
\end{aligned}$$

It can be seen that the imaginary part of the permittivity ε'' belongs to the component of the total current density in phase with the driving field and consequently contributes to the power loss [78, p. 45]. Thus, $\varepsilon''(\omega, \mathbf{E}, \mathscr{P})/\varepsilon_0 = \varepsilon_r''(\omega, \mathbf{E}, \mathscr{P}) = \chi''(\omega, \mathbf{E}, \mathscr{P})$ is often referred to as the dielectric loss [78, p. 45]. The real part of the permittivity ε', on the other hand, is in quadrature with the driving field and, hence, in phase with the real part of the polarisation and electric displacement field [compare equation (2.8) with equations (2.3) and (2.7a)]. As a result, it does not contribute to the loss [78, p. 45].

Depending on the individual polarisation process, both parts of the complex permittivity can depend on various external parameters. As derived from the Kramers-Kronig relations, they are both always explicitly dependent on frequency [164]. Other dependencies vary with the individual polarisation mechanism: for example, in a material where the local dipoles are caused by field-assisted trapping and detrapping of carriers in an area of high defect concentration, analogue to the static transport [46], a dependence of temperature and electric field might be assumed. Another example, already mentioned above, may be the dependence of permittivity on applied pressure [31].

Usually, there is not one but various different polarisation processes with at very different resonance frequencies [78, pp. 50-51]. Around their resonances the loss becomes significant and both components of the permittivity change rapidly [78, pp. 50-51]. While the imaginary part of the permittivity has local maxima at the resonances the real part has smooth downward-steps with increasing frequency around each resonance while it is almost constant between resonances of large enough distance in frequency [78, pp. 50-51]. The smooth steps of the real part of the permittivity are downwards with increasing frequency since for frequencies much below the resonance, the polarisation process is fast enough to unrestrictedly contribute to the polarisation. At much higher frequencies the polarisation process is too slow to contribute. Around the resonance of the polarisation process the excitation of the process is most efficient leading to the highest dissipation of

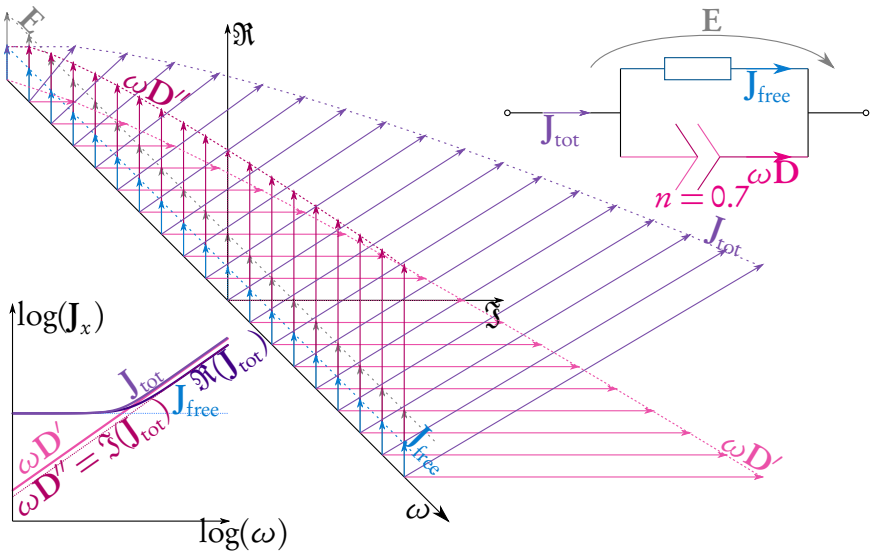

Figure 2.3: Exemplary development of the total current density $\mathbf{J}_{\text{tot}}$, free current density $\mathbf{J}_{\text{free}}$, and the real $\omega D'$ and imaginary $\omega D''$ component of the displacement current density of a resistor bypassed by a parallel constant phase element with $n \approx 0.7$ (leading to a constant phase of around −63°) with increasing frequency ω. The value is comparable with the one extracted in this work for the constant phase element of the thin ta-C film. The electric field $\mathbf{E}$ is assumed to be purely real and the orientation of the vector is shown as a reference.

energy for the corresponding process. In equation (2.7c) it can be seen that, in the regions between the resonances, where the permittivity is almost constant and its imaginary part negligible, the displacement current density ωD will be almost purely real and increase linearly with frequency. As shown later that is the reason for a capacitor to create a bypass linearly increasing in frequency between resonances.

2.1.3.2 Interpretation of the resulting total current density and its contributions

Including the formulation of the free current density $\mathbf{J}_{\text{free}}^{(\text{stat})}$ based solely on static conductivity σ_{stat}, equation (3.2a), in the formulation of the free current density, equation (2.7c), with inserted and explicitly written real and imaginary component of the permittivity, the final formula with geometry-less quantities for the total current density becomes

$$\mathbf{J}_{\text{tot}}(\omega, \mathbf{E}, \mathscr{P}) = \left[\sigma_{\text{stat}}(\mathbf{E}, \mathscr{P}) + \omega\varepsilon''(\omega, \mathbf{E}, \mathscr{P}) + i\,\omega\varepsilon'(\omega, \mathbf{E}, \mathscr{P})\right]\mathbf{E}. \tag{2.8}$$

In Figure 2.3 the development of the total current density and its different contributions is calculated for the common example of a resistor parallel to a constant phase element with $n \approx 0.7$ which results in a constant phase of around 63°. Similar to the reciprocal relation between impedance and admittance that changes the sign of the imaginary part, in the current density representation the phase of a capacitive element is, like in the admittance, positive and not negative, as it would be for the impedance.

Alternate interpretation: ac conductivity Instead of describing the current with the complex permittivity ε, some communities define the complex *ac conductivity* σ_{ac}, see e. g.

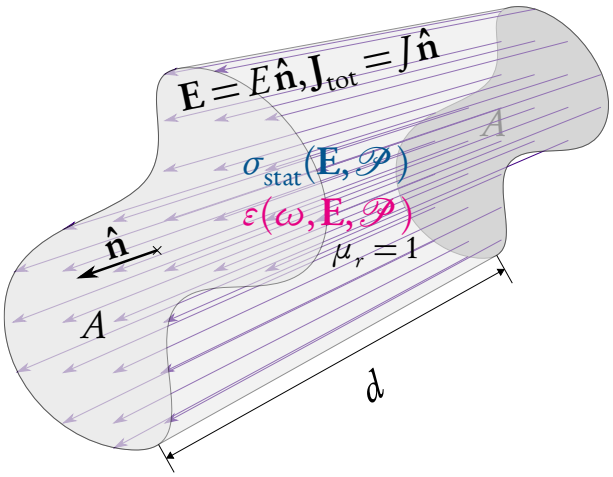

Figure 2.4: Illustration of the exemplary geometry assumed in the derivation. The area A should be sufficiently large to ignore border effects. The material is supposed to be homogeneous, isotropic, non-magnetic and non-ferroelectric, hence, all field lines are assumed to be parallel and in the direction of the field which is applied normal to the surfaces with area A. The length of the chunk of material is d, with $d, A \ll \frac{\lambda(\omega_{\text{max}})}{2}$. The surfaces with area A are normal to each other and their normal vector attacking on the centre or mass of the areas are on one straight line.

[40]. Using the assumptions in this work, the relation between these quantities can be described as

$$\sigma'_{\text{ac}}(\omega, \mathbf{E}, \mathscr{P}) \equiv \omega\varepsilon''(\omega, \mathbf{E}, \mathscr{P}) \tag{2.9a}$$
$$\sigma''_{\text{ac}}(\omega, \mathbf{E}, \mathscr{P}) \equiv \omega\varepsilon'(\omega, \mathbf{E}, \mathscr{P}) \tag{2.9b}$$

where real and imaginary part are reversed as compared to the complex permittivity [40]. One might think of the ac conductivity as expanding the free current density $\mathbf{J}_{\text{free}}$, *excluding* the dc contribution, with an additional real and imaginary term to describe the part of the displacement current density $\omega\mathbf{D}$ of the total current density while completely omitting permittivity.

2.1.4 Introducing geometry

Rather than geometry-less quantities, e. g. conductivity σ and permittivity ε, that were used in the derivation so far, EECs contain the geometry-including pendants, like resistance R and capacitance C. The geometry of systems investigated by immittance spectroscopy, and hence extraction of the corresponding geometry-less quantities, is usually much more complicated, for example, as in the case of than parallel plates. In the first step of analysing experimental results of immittance measurements, where EECs are utilised, the data is still 'affected' by geometry. Hence, in the next step of the derivation, *spatial dimensions*, i. e. geometry, have to be included. For simplicity, but without loss of generality, the problem is described assuming a parallel plate geometry, whereas other geometries would just lead to more complicated geometric factors. As explained above,

a homogeneous, isotropic, non-magnetic ($\mu_r = 1$), non-ferroelectric, bulk of material with permittivity $\varepsilon(\omega, \mathbf{E}, \mathscr{P})$ and static conductivity $\sigma_{stat}(\mathbf{E}, \mathscr{P})$ is assumed, compare illustration in Figure 2.4. Both planar, parallel contact planes with area A and genus zero are supposed to have identical shape and the axis of the non-oblique cylinder, gaplessly filled with the material, of length d should be parallel to the normal vectors of the contact areas. The area A is assumed large enough to neglect electric field lines in the volume outside and close to the border of the cylinder. Further, half of the wavelength of any applied signal should be much larger than any of the dimensions of the system. As a result, there are only straight, parallel field lines in the cylinder between, and orthogonal on, the two contact areas. It follows that the current density and electric field are normal to the two contact areas as well. Hence, the geometry allows assuming solely scalar quantities. Finally, the electric field

$$E = \frac{V}{d} \tag{2.10}$$

and the total current density

$$J_{tot} = \frac{I_{tot}}{A}, \tag{2.11}$$

where I_{tot} and V are the total current and the externally applied voltage between the contact areas, respectively. Including equations (2.10) and (2.11) into equation (2.8) yields

$$I_{tot}(\omega, V, \mathscr{P}) = \left[\sigma_{stat}\left(\frac{V}{d}, \mathscr{P}\right) + \omega\varepsilon''\left(\omega, \frac{V}{d}, \mathscr{P}\right) + i\omega\varepsilon'\left(\omega, \frac{V}{d}, \mathscr{P}\right)\right]\frac{A}{d}V. \tag{2.12}$$

By partial expansion with the geometric factor $\frac{A}{d}$ the terms in the braces can be interpreted as components of the EEC:

$$\sigma_{stat}\left(\frac{V}{d}, \mathscr{P}\right) \cdot \frac{A}{d} \equiv R_{stat}^{-1}(V, \mathscr{P}), \tag{2.13a}$$

$$\omega\varepsilon''\left(\omega, \frac{V}{d}, \mathscr{P}\right) \cdot \frac{A}{d} \equiv R_{dyn}^{-1}(\omega, V, \mathscr{P}), \tag{2.13b}$$

$$i\omega\varepsilon'\left(\omega, \frac{V}{d}, \mathscr{P}\right) \cdot \frac{A}{d} \equiv \frac{-\omega C'(\omega, V, \mathscr{P})}{i} = [iX_C(\omega, V, \mathscr{P})]^{-1} = Z_C{}^{-1}. \tag{2.13c}$$

As shown in (2.13a), the product of the static conductivity with the geometric factor leads to the reciprocal static resistance. The real part of the displacement current density multiplied with the geometric factor results in the reciprocal dynamic resistance, compare equation (2.13b). Finally, equation (2.13c) shows that the product of the imaginary part of the displacement current density with the geometric factor leads to a reciprocal capacitive impedance, since $Z_C^{-1} = [iX_C]^{-1} = i\omega C$.

With the geometry included, i. e. by inserting equations (2.13a), (2.13b) and (2.13c), equation (2.12) becomes

$$I_{tot}(\omega, V, \mathscr{P}) = \left[R_{stat}^{-1}(V, \mathscr{P}) + R_{dyn}^{-1}(\omega, V, \mathscr{P}) + i\omega C'(\omega, V, \mathscr{P})\right]V. \tag{2.14}$$

The quantity in square brackets in equation (2.14) is almost the admittance, that is the reciprocal impedance (why only almost is explained in section 2.1.5).

Alternate interpretation: complex capacitance Sometimes, the imaginary part of the permittivity $\omega\varepsilon''$ is not interpreted as a dynamic resistance as in (2.13b), but instead as an imaginary part of a complex capacitance, corresponding directly to the real and imaginary components of the complex permittivity:

$$\begin{aligned} C(\omega, V, \mathscr{P}) &= C'(\omega, V, \mathscr{P}) - iC''(\omega, V, \mathscr{P}) \\ &= \frac{A}{d}\left(\varepsilon'(\omega, \frac{V}{d}, \mathscr{P}) - i\varepsilon''(\omega, \frac{V}{d}, \mathscr{P})\right) \end{aligned}$$

(e. g. confer [78, pp. 65-66] for the linear case). This work focuses on the analysis of immittance data with EECs. From this perspective, representing the real-valued contributions to the impedance as resistors has several advantages:

As a first consequence, a resistor, in an EEC, in that case always represents a component that does not introduce an out-of-phase component with respect to the applied field and, consequently, a capacitor always represents a purely out-of-phase component with respect to the applied field.

> As explained in sections 2.1.2.1 and 5.4.1, the frequency range relevant for immittance spectroscopy is a subset of the low-frequency regime $\mathbb{L}$ of any conduction process. Consequently, the delayed response of conduction processes and, hence, its imaginary part can be neglected. As a result, conduction processes, in an EEC, are always represented by process-specific, parameter-dependent resistors that have purely real phasors. Representing the loss of a polarisation process, that is a contribution in phase with the applied field and hence a part with real phasors, as a resistor as well means that all resistors in an EEC have always real valued phasors and are in phase with the applied field.

In the eyes of the author, resistors always representing contributions in phase with the applied field and capacitors representing always an out-of-phase contribution seems more intuitive, than using the identical symbol of a capacitor for an in-phase component and a component in quadrature to the applied field.

The second consequence is that all resistors are always components of loss, while all capacitors (and inductors) are always components that store their reactive power in electric (or respectively magnetic) fields. In the end, the symbols of the components in an EEC always have the above mentioned properties and one does not have to look at the designation of the capacitor to find out weather it is a lossy component or a regular capacitance-like component.

2.1.5 Universal immittance

The quantity in square brackets in equation (2.14) is (as mentioned in section 2.1.4) only *almost* the admittance because it is, just as all other immittances, only defined for linear systems, i. e. where the response is a linear function of the stimulus.[8] The used

[8] Conventional immittance, as used in the context of immittance spectroscopy, is based on linear systems theory [111, 110] and its linearisation is the fundamental property of impedance spectroscopy [99]. However,

formulation is more general and explicitly includes non-linear response to the stimulus. In situations where this distinction is important, 'universal' is added to distinguish the regularly used (linear) immittance from the universal immittance allowing non-linear response that is derived in this work. Hence, the quantity in the brackets in equation (2.14) is the universal admittance, i. e. the inverse of the universal impedance

$$Z_{\mathrm{tot}}(\omega, V, \mathscr{P}) = \left\{ R_{\mathrm{stat}}^{-1}(V, \mathscr{P}) + R_{\mathrm{dyn}}^{-1}(\omega, V, \mathscr{P}) + \left[i X_C'(\omega, V, \mathscr{P}) \right]^{-1} \right\}^{-1},$$

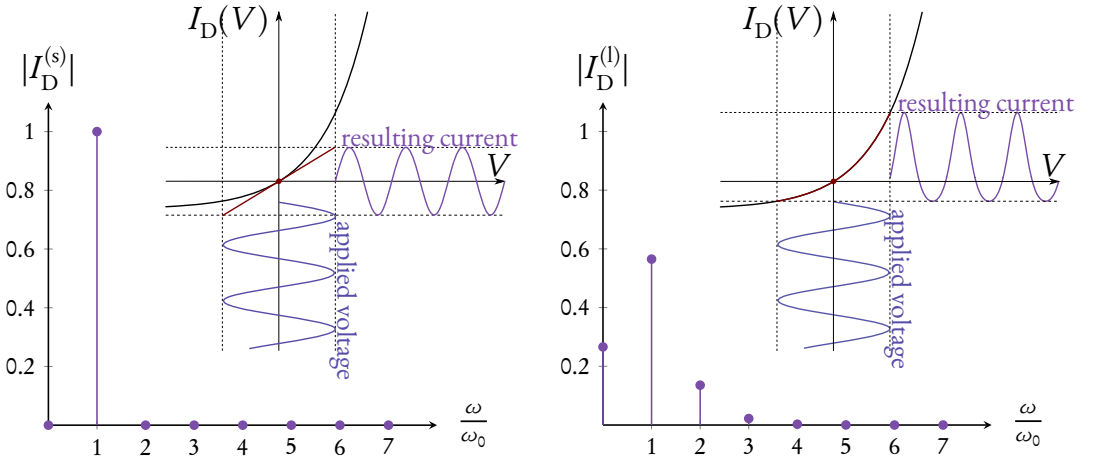

(a) Small-signal analysis **(b)** Large-signal analysis

Figure 2.5: The non-linear current-voltage characteristic of a diode in the limit for infinitesimal frequencies, i. e. purely resistive equilibrium current response. In both cases, the periodic stimulus is a sinusoidal voltage signal oscillating around a bias voltage of zero, illustrated as vertical sinus with hidden time axis. The resulting current response is given in frequency domain and in time domain right of the current-voltage characteristics with hidden time axis in the inset. In (a) the small-signal approximation is used. Consequently, the response is the same as if the oscillation took place on the shown tangent instead of the true, non-linear current-voltage characteristic. In (b), on the other hand, large-signal analysis is performed. Hence, the oscillation follows the curvature of the non-linear response.

The response of a linear system contains only the fundamental frequencies of the stimulus as well as a constant offset (zero-frequency coefficient) if the oscillation is biased (see Figure 2.5a where the unbiased situation is illustrated). In consequence, a linear system does not add multiples of the fundamental frequency, the so-called higher harmonics (see Figure 2.5b and section 2.1.1.2 for the definition of harmonics). As a result, a sinusoidal stimulus with fundamental frequency ω_0 leads to a response with exclusively frequency ω_0. This makes calculus with linear systems mathematically simpler since their response

there are and were always efforts, though different from the realisation presented in this work, to include higher harmonic responses. Possibly due to the easier handling of conventional immittance, poly-harmonic analysis is still rarely applied. Consequently, any immittance is always referring to the linear form and if higher harmonics are meant it is specifically mentioned.

can be described by a single phasor, a complex quantity that holds the information of the amplitude of the response (representing the magnitude of attenuation or gain) and the phase shift as compared to the stimulus.

The response of a non-linear, periodic system is poly-harmonic, i. e. besides the fundamental frequency higher harmonics are present, leading to a mathematically more complicated situation since multiple phasors have to be considered. Furthermore, additionally to the static offset due to a biased stimulus, the zero-frequency coefficient of the response can be influenced by the asymmetry around the operation point. Since these are, for amplifiers, unwanted, but inevitable, and well-known effects they are summarised under the term *harmonic distortion* [166]. Unlike in the development of an amplifier, in science, the observation of harmonic distortion in the investigation of a system is neither good nor bad, since it is just another property of the system under investigation and gives information about its non-linear nature and, as such, it should be exploited although it is mathematically more difficult.

> There is a distinct difference between the constant offset for linear responses and non-linear responses. In the linear case, it is just a consequence of the applied bias voltage, resulting in a steady response that is superimposed to the oscillation (as the stimulus in Figure 2.5a is oscillating around zero bias, the zero-frequency component equals zero, as can be seen in the frequency domain representation of the linearly assumed response). In the non-linear case on the other hand, asymmetry around the operation point alters the offset, in comparison to the linear case, as can be seen in the frequency domain representation of the non-linear response in Figure 2.5b.

To avoid the more complicated mathematics and more challenging experimental setups, it is quite common to linearise a non-linear response function, e. g. $\xi(E, \mathscr{P})$, at a certain *operation point* E_O, i. e. $\xi^{(\mathrm{lin})}_{E_\mathrm{O}}(\mathscr{P}) = \left.\frac{\partial \xi}{\partial E}\right|_{E_\mathrm{O}}$. If the amplitude $\hat{E}$ of the stimulus is approaching zero, e. g. $\lim\limits_{\hat{E}\to 0}\left[\tilde{E}(t,\omega_0)\right] = \lim\limits_{\hat{E}\to 0}\left[E_\mathrm{O} + \hat{E}\cos(\omega_0 t)\right]$, the linear approximation of the value of the response function at the operation point E_O becomes exact (this implies that the static value for the response is determined from the non-linear function). If the amplitudes in an experiment are sufficiently small that this linear approximation, also called the *small-signal approximation*, is acceptable, the amplitude can be ignored. This approach is called *small-signal analysis* and currently the de-facto standard in the analysis of immittance spectroscopy (e. g. see [110, 7]). The contrary approach, that takes the value of the amplitude into account, is called *large-signal analysis*.

In Figure 2.5 the difference between large- and small-signal analysis are illustrated at the example of the non-linear characteristic of a purely resistive diode (meaning that the frequency is almost zero). Since a purely resistive characteristic is assumed, the coefficients of the response function are all real values. The frequency of the oscillation is assumed to be sufficiently small, that the current response is in its equilibrium. The stimulus is a sinusoidal voltage oscillating around a bias voltage of zero. The finite amplitude of the stimulus reaches the points in the current-voltage characteristic indicated by the coloured contour. In Figure 2.5a small-signal analysis is performed. Hence, instead of following the

correct, non-linear current-voltage characteristic as marked in Figure 2.5b by the coloured contour, the response is determined by the resistance at the point of the bias voltage only, not taking the amplitude of the signal into account. This corresponds to assuming a linear relation, thus, as illustrated in Figure 2.5a, a tangent in the current-voltage characteristic. As a result, the oscillating voltage does not follow the actually non-linear current-voltage-curve, but instead oscillates on the indicated tangent. As can be seen in the illustrated response, especially in its frequency domain representation, the current response has exclusively the same frequency as the voltage stimulus. From the increasing gap between the actual current-voltage characteristic and the tangent, the deteriorating accuracy of the approximation for increasing oscillation amplitude can be seen directly. In Figure 2.5b large-signal analysis is performed. In this case, the oscillation follows the non-linear current-voltage characteristic instead of the tangent. The difference is immediately visible from the form in the given current response in time domain. The frequency-domain representation of the current response, only shown to the seventh harmonic, has in this case finite coefficients for all multiples of the fundamental frequency. The finite value at the frequency zero, represents the static offset in the current response. It can be seen in the time-domain representation at the fact, that the area of the oscillating current above and below the abscissa is not equal. Further, the non-sinusoidal form in the time-domain representation leads to the harmonics at twice the fundamental frequency and higher. In summary, using the admittedly rather large amplitude in our example while assuming small-signal-approximation, so that the measurement setup gives only the fundamental frequency response, one would only measure the fundamental coefficient of the response in the frequency-domain-representing inset in Figure 2.5b and interpret this as the actual response that would than be assumed as in Figure 2.5a. All other values in the inset would be neglected. Depending on the non-linearity of the characteristic of the system, the chosen amplitude and the purpose of the analysis, it should be clarified whether this approximation would be appropriate or not.

An important issue, especially since most available instruments used in immittance spectroscopy are still only designed for linear system response, is that one has to recognise the non-linearity of the response of the system. In an experimental setup capable of measuring non-linear response that is straight forward, since the presence of harmonics in the response can be seen directly. If the setup expects linear response, one may utilise the above given definition of the small-signal analysis: the immittance should be measured as a function of the signal amplitude, preferably under conditions where the non-linearity of the system under investigation is (expected to be) most pronounced. For decreasing amplitude the measured immittance should converge to the zero-oscillation-amplitude limit. Since the signal-to-noise ratio might become quite small at the lower end of oscillation amplitudes this characterisation of the amplitude dependence of the immittance might be performed with a sufficiently high number of repetitions.

Oscillation amplitudes smaller than the thermal voltage $V_\mathrm{T} = \frac{k_\mathrm{B} T}{q}$ should generally be small enough to neglect the oscillation amplitude and assume small-signal analysis to be valid [7, p. 5]. However, for cryogenic measurements such small amplitudes are almost impossible and, further, for measurements at room temperature hard to handle (usually

causing larger errors). With the above mentioned measurement of the immittance as a function of the oscillation amplitude, amplitudes that are sufficiently low to assume small-signal approximation but larger than the thermal voltage and, hence, in a usable voltage range can be determined. Otherwise, performing large-signal analysis is recommendable.

As already mentioned, in some cases, e. g. usually when working with high-power amplifiers [100], the non-linearity of the response has to be considered. As the understanding of the underlying physics is (as usually and understandably in that field) of lower priority, it is an accepted solution to add additional components (resistors, capacitors, etc.) in the EEC to model the harmonic response [159]. Instead of using such a descriptive approach, it can in some cases, especially when a physical model for the system under investigation is known, be advantageous to work with the universal immittance as defined in this work (or rather in the corresponding paper [3]). The direct insertion of the field or voltage and external-parameter dependent process-specific physical model then accounts for the higher harmonics.

The additional information from the non-linear part of the response might in general also be used, e. g. as additional verification that the correct model was selected. There are several ways to include the additional information from the non-linear character of the response in the analysis. The most direct one is possible if the set-up is capable of measuring the amplitude of the harmonics directly. Then the amplitudes of the harmonics, calculated from the assumed non-linear process-specific physical model, can be fitted to the measured amplitudes by adjustment of the system-specific parameters (of course, only those, not in literature). If unrealistic values are required for the system-specific parameters or the model cannot explain the observed amplitudes at all, the model should be modified or exchanged.[9] In many cases the experimental setup allows only the determination of the linear parts of the response, i. e. measurement of a regular (linear) immittance. In this case a non-linear model can still be beneficial, since part of the applied power is in the harmonics. The non-linear model can be utilised to calculate the correct fraction of the part of the power in the response with fundamental frequency. The fit of the linear immittances then considers this attenuation. The use of the knowledge of the underlying non-linear model presented last is, actually, just the correct application of small signal analysis. None the less, it is effective in ascertaining the correct underlying physics and rarely done. Usually, immittance spectroscopy is performed oscillating only around a single bias voltage, i. e. the operation point is not varied. Also variations of other external parameters are rare. By choosing a sufficiently small amplitude, the linear immittance at a certain bias voltage (or applied field) can be determined in good approximation. To utilise the known non-linearity of the model, multiple bias voltages are applied (static offsets of the stimulus are chosen). Then, a global fit (for all different bias voltages and other varied external parameters at once) of the calculated to the measured immittances gives the system-specific parameters. In that way all advantages of the traditional linear analysis, like the easier mathematics of linear system analysis as well as the possibility to

[9] This point is about the dismissal of clearly unfounded models. Of course, one may always have to accept deviations up to a certain degree, since any model is to some extent an idealisation of the real situation.

use conventional immittance measurement setups, are combined with the benefit that underlying physical processes are verifiable. If the model fits physically useful system-specific parameters can be extracted. The selection of an unsuited model cannot describe the development of the immittance with bias voltage and would lead to large differences between the measured and the corresponding calculate immittances at a high number of bias voltages. All three above explained approaches utilise the external parameter-dependent process-specific physical models instead of idealised lumped components. Hence, the underlying physical processes can be identified and the physically useful system-specific parameters extracted.

2.2 Interpretation as EEC

2.2.1 Fundamental interpretation

For the time being, let us assume solely a single static conducting process and one polarisation process in the material. In that case, the universal impedance

$$Z_{\mathrm{tot}}(\omega, V, \mathscr{P}) = \left\{ R_{\mathrm{stat}}^{-1}(V, \mathscr{P}) + R_{\mathrm{dyn}}^{-1}(\omega, V, \mathscr{P}) + \left[i X_C'(\omega, V, \mathscr{P}) \right]^{-1} \right\}^{-1}, \quad (2.1.5)$$

derived above, can be interpreted as a parallel arrangement of following circuit components:

A (frequency-independent) *static resistor* R_{stat}, that represents the dc conduction mechanism (see Table 5.1 for some examples of process-specific physical models dependent on external parameters that are commonly observed in dielectrics used in the area of CMOS technology). Particularly for this resistance it is of paramount importance that it can be dependent on various external parameters, including the applied field (e. g. for stronger dependence on temperature of the static conductivity than the permittivity confer [37]).

A *dynamic resistor* R_{dyn}, that represents the dielectric loss of the permittivity, is frequency dependent and has infinite resistance in the limit of zero frequency, since there cannot be any lossy polarisation for static fields.

A *frequency-dependent capacitor* C' that represents exclusively the part of the permittivity in phase with the applied field (hence the '′' in accordance with the usual conventions in this work).

As will be explained soon, the total permittivity of a material is given by a sum of the specific permittivities each representing a specific polarisation processes in the material (confer [143, p. 19]) and the permittivity of free space. The latter is, as already explained in section 2.1.2.1, the only permittivity that is neither dependent on frequency nor lossy. As explained later, it is beneficial to describe this purely real capacitance (i. e. purely imaginary reactance) by a separate frequency-independent capacitor, the *high-frequency limit capacitor* C_∞, in parallel to the other circuit components.

This arrangement is, however, not the only possibility. In the next section, it is explained which processes must be in parallel and which might be arranged differently, before the common case of multiple processes in a single homogeneous part of material is explained. To introduce useful simplifications for usual experimental situations, let the highest frequency in the experiment be $\omega_{\mathrm{max}}^{(\mathrm{exp})}$ and, correspondingly, the lowest frequency in the experiment be $\omega_{\mathrm{min}}^{(\mathrm{exp})}$.

2.2.2 Alternate arrangements of circuit components

Since all dynamic contributions are derived from the time derivative of the electric displacement field in equation (3.1a), they must not contribute for static signals. Hence, in the limit of a non-varying signal ($\omega \to 0$), the impedance has to converge against the static resistance of the system. Furthermore, since this is a mean-field approximation and no direct coupling is assumed between the distinct processes, all permittivities and

conductivities in the homogeneous material experience the same potential difference, excluding a serial arrangement of the dynamic components with respect to the static resistor. Hence, the static resistor has to be a parallel bypass to the dynamic part and each branch of the dynamic part, whatever the subsidiary arrangement of the dynamic resistor and capacitor, that could bypass the static resistor must have infinite impedance at zero frequency.

At extremely high frequencies (far beyond any frequency used in immittance spectroscopy) all polarisation processes and conduction processes are too slow to respond and the material becomes 'transparent' to the electromagnetic field. In this case, the only remaining contribution is the contribution of free space and, hence, the only remaining component is the high-frequency limit capacitor C_∞. Since it has to bypass all other parts and especially also the static resistor, it has to be parallel to the static resistor and all other components.

The total permittivity of a material is the result of all its electromagnetic resonances. More precisely, each resonance leads to a summand in the total permittivity of a material which is well described by (compare [143, p.19])

$$\varepsilon(\omega, \mathscr{P}_{\text{tot}}) = \varepsilon_0 + \frac{e^2}{m} \sum_{j>k} \frac{f_{ji}(\mathscr{P}_{\text{tot}}) \left[N_k(\mathscr{P}_{\text{tot}}) - N_j(\mathscr{P}_{\text{tot}}) \right]}{\omega_{jk}^2(\mathscr{P}_{\text{tot}}) - \omega^2 + i\omega\gamma_{jk}(\mathscr{P}_{\text{tot}})}.$$

where $\omega_{jk}(\mathscr{P}_{\text{tot}}) = \hbar^{-1} \left[E_j(\mathscr{P}_{\text{tot}}) - E_k(\mathscr{P}_{\text{tot}}) \right]$ are transition frequencies, between lower energy levels E_i with populations N_i and upper energy levels E_j with populations N_j, f_{jk} are the corresponding transition probabilities, γ_{ji} are the damping coefficients, m and e are the mass and charge of an electron, and $\mathscr{P}_{\text{tot}}$ shall indicate the dependence on all external parameters *including* the electrical field (hence the index 'tot'). Each distinct energy difference leads to a separate resonance. Although the physical mechanism of the excitation might be identical, in this work, every resonance is seen as a separate process. The product of the total permittivity with the applied electric field, e. g. in equation (2.7b), leads in equations (2.13c) and (2.13b) to the dynamic capacitance and resistance, respectively. Applying the distributive law to the sum, each summand, i. e. each separate polarisation process, corresponds to a parallel branch, since the electric field is always identical. The subsidiary arrangement of the real and imaginary part might, on the other hand, be both: either parallel or serial. Of course, the already mentioned very important property of the dielectric current density (that can be seen in equation (3.1a) at the fact that the dielectric current density is the time derivative of the electric displacement field) that there cannot be any dielectric contribution to the total current density at $\omega = 0$ remains. That means, that, if those dynamic components for a single process would both be arranged in parallel to the others, their impedances must both be infinite in the static limit. A closer look at their definitions, hence, leads to some restrictions: Any reactance with constant capacitance obviously becomes infinite, since $X_C = \frac{1}{\omega C}$. For a reactance with frequency-dependent capacitance $X_C = \frac{1}{\omega C(\omega)}$ (see (2.13c)) this means that (close to $\omega = 0$) for $\omega \to 0$ the capacitance must converge with frequency with a higher power than -1, i. e. $C(\omega)|_{\omega=0} = \mathscr{O}(\omega^m)$ with $m \in \{k \in \mathbb{R} | k > -1\}$. Analogue for the

dynamic resistance and the dependence of ε'' on ω, since $R_{\mathrm{dyn}} = \frac{1}{\omega\varepsilon''.\frac{A}{d}}$ (see (2.13b)). There is no reason, not to use the equivalent serial representation of these specific polarisation process describing components. In that case, only one component must be infinite at zero frequency, i. e. the restriction must only account for one of the components, either the dynamic equivalent series resistance or the dynamic equivalent series capacitance (it is important to note that the equivalent series components have very different functions). It might, however, be more intuitive that lossy and purely polarising part perceive an identical voltage drop.

2.2.3 Multiple processes

2.2.3.1 Multiple static conduction processes

It is not unusual that there are multiple static conduction processes in a material [28]. As an illustrative example, think of an insulator with energetically and spatially randomly arranged electrically active defects in the energy gap. There might be charge transport from trap to trap by tunnelling from one trap to the next. Additionally, the charges can jump from trap to trap by thermal excitation over the barriers between the neighbouring traps. Furthermore, shallow traps just below a conductive band can lead to a higher concentration of free charges (electrons or holes, dependent on whether the conductive band is the conduction or valence band) in the conductive band. Even in this very simple example which is probably a very common situation in insulators, there are three different processes. As distinct bypasses through the homogeneous material, all three processes see the same electric field and must be in parallel to each other. In the high frequency limit, they are all bypassed by their respective high frequency limit capacitors C_∞ and in the low frequency limit, all parallel conduction processes are the only remaining paths in the circuit with finite impedance.

Without the dependence on external parameters the explicit introduction of parallel conductive processes would not be possible. The corresponding parallel resistors would be indistinguishable and condense into a single resistance. Including the external-parameter-dependent process-specific physical models into the resistive components is precisely the prerequisite to separate parallel transport processes. The possibility to identify, describe and even quantify distinct conduction processes is the foundation of understanding the underlying processes in the system under investigation.

Tips for identifying unknown conduction process If the parallel process is unknown, one might start by adding a constant resistance in parallel with the known process(es). After fitting every investigated condition, the development of this resistance with the variation of the investigated parameters might give a clue about the process. This method, however, only works if only a few, better only a single, of the parallel conduction processes is unknown.

Another method of determining an unknown conduction process is to perform a global fit of the data without it and plot the residuals dependent on the external parameters. If all systematic information has been described by the EEC the residuals should be randomly

distributed, typically assumed normally distributed, since a missing process can usually not be compensated by the other processes without leading to unrealistic or at least unusual fitting parameters. Furthermore, the other processes should usually not be able to absorb all deviations of the missing process. If the fitting parameters of the known process are forced to stay within realistic values the mentioned plot of residual should show a curvature that looks similar to the missing process.

A good start for each piece that is relevant (and hence should not be simplified with the above presented approximations) is the circuit shown in Figure 2.6b. At first only include the dominant processes, e. g. the dominant conduction process, unless the other important processes are already known. Then subsequently add more details until no further models can be used to explain the remaining deviations. It is not unlikely that the residuals are not purely random. This does not necessarily indicate that there are missing processes, but it can also be due to an imperfect model itself.

Why it is beneficial to introduce a model at least in one component per piece Using only idealised lumped components changing from their parallel arrangement into their equivalent serial arrangement is straight forward, since it is only associated with changing resistance and capacitance values (compare Figure 1.1 and confer example in [114]). The changed capacitance or resistance of the respective component might, in the end, not necessarily look suspicious. By assuming a more complicated, external-parameter-dependent relation, even for either the static conduction process or dielectric process alone, the conversion, e. g. into the equivalent serial representation, would lead to a very different, unusual formulation for the resistance model. As a consequence, it becomes straightforward to spot unusual arrangements of the circuit components, even without introducing complicated models for the capacitance. The introduction of external-parameter-dependent models is, hence, an easy way to eliminate accidental misarrangement of circuit components. Since static conduction processes are usually more strongly influenced by external parameters (e. g. by temperature, confer [37]) and many models are known, they are a good starting point.

2.2.3.2 Multiple polarisation processes

Indifferent of the used arrangement (parallel or serial arrangement of the corresponding dynamic resistor and dynamic capacitor) for the single polarisation process, the components of each individual polarisation process must, as explained above, be parallel to each other. Otherwise, different polarisation processes would see different voltage drops. The individual arrangement of polarisation processes themselves and the description of multiple contributions in one material is discussed in section 2.2.2.

2.2.3.3 The 'real' high-frequency limit capacitor and the experimental high-frequency limit capacitor

It has been suggested to introduce the high-frequency limit capacitor C_∞ as separate circuit component. It has the index '∞', because for extremely high frequencies, far

beyond the frequencies of immittance spectroscopy, after all resonances of the material this capacitance will be the only dielectric contribution. Since the permittivity of free space is a constant, this capacitor represents the geometry, which is why it is sometimes called geometric capacitance. In many experiments, especially in electrochemical setups the system under investigation can have complicated, stretched-out geometries. In those cases the high-frequency limit capacitance is not defined for a single homogeneous component but for the whole system, designated $C_\infty^{(\mathrm{geo})}$, and can be used to normalise the values of other circuit components (see [7, p. 99]). Furthermore, this capacitor determines the lowest time constant of the system $\tau_{\mathrm{min}}^{(\mathrm{exp})} = R_\infty^{(\mathrm{parasitic})} C_\infty^{(\mathrm{geo})}$. However, when the highest frequency in the experiment $\omega_{\mathrm{max}}^{(\mathrm{exp})}$ is much lower than the smallest time constant, i. e. $\omega_{\mathrm{max}}^{(\mathrm{exp})} \tau_{\mathrm{min}}^{(\mathrm{exp})} \ll 1$, the high frequency capacitor might be omitted [7, p. 99].

In immittance spectroscopy the highest frequencies are below the frequencies of optical resonances and, hence, also far below the region where the 'real' high-frequency limit capacitor C_∞ becomes important. Instead, there are still some polarisation processes with resonances at much higher frequencies that are fast enough that they are almost lossless, i. e. purely real. It would be unnecessarily complicated to account for them in the fitting routine with their complex models. Since their resonances are far away and for several of those processes their corresponding contribution to the permittivity is indistinguishable in the frequency range of the experiment, all the processes relevant only at much higher frequencies can be combined in an effective high-frequency limit capacitor specific to the frequency range in the experiment. Hence, for most experiments it is useful to introduce an experimental high-frequency limit capacitor $C_\infty^{(\mathrm{exp})}$ that replaces the 'real' high-frequency limit capacitor C_∞ in the EEC. Interestingly, as described in reference [190], the experimental high-frequency limiting capacitor is frequently even used to extract the static permittivity.

2.2.4 Summarising the findings as EEC

The above-derived arrangement of components for a single homogeneous part of material is illustrated in the EEC in Figure 2.6a. The fact that dynamic components can be arranged either in parallel or in series is represented by a parallel arrangement for the first polarisation process and a serial arrangement for the second polarisation process. Further, a new dielectric component, the constant phase element (CPE), designated K, is introduced in Figure 2.6a. It is a very often used element in immittance spectroscopy and results typically from disorder causing a broad distribution of resonance frequencies. Because of its common use in immittance spectroscopy it is discussed in more detail in its own section 2.2.5.

Usually, in immittance spectroscopy only the first peak of dielectric relaxation is characterised (compare the frequency classification in Figure 5.2 and the immittance spectra of various different materials given in Figure 2.2). It is typically caused by a broad distribution of resonance frequencies and well isolated from all higher frequency responses. As a result, the latter can be combined with the response of free space in the experimental high-frequency-limiting capacitor (see the constant phase element in the circuit in Figure

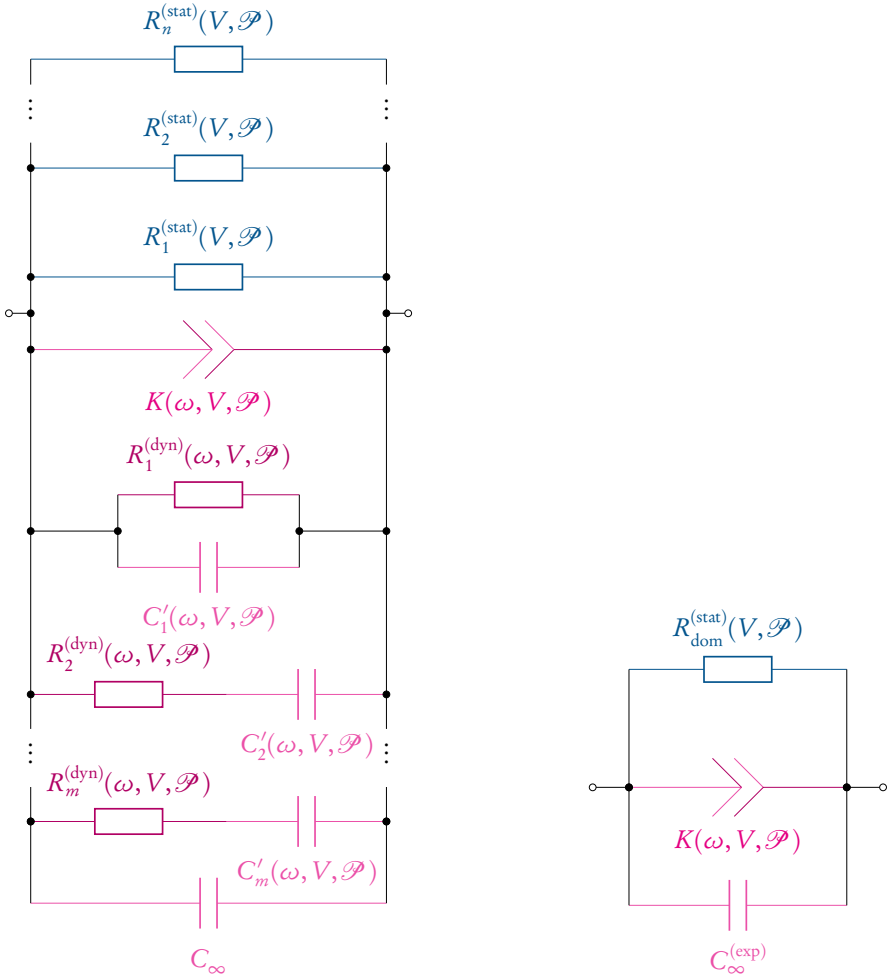

Figure 2.6: (a) The general circuit describing a homogeneous piece of material with n static conduction processes represented by the resistors $R_1^{(\mathrm{stat})} \dots R_n^{(\mathrm{stat})}$ (they determine the resistance of the material at $\omega = 0$), m distinct lossy polarisation processes that can either be represented in their equivalent serial or parallel representation and have infinite impedance for $\omega = 0$ and a distributed resonance described by a constant phase element K. Except for broadband dielectric spectroscopy there is rarely more than one resonance of distinct polarisation processes observed. The capacitor C_∞ represents the free space contribution and is, hence, purely real and frequency- and external parameter independent (unless the external parameter changes the geometry of the piece itself). (b) Experimentally relevant approximation for immittance spectroscopy, where usually only the first broad resonance peak is observed. All other resonances have much higher frequencies than the highest frequency in the experiment and hence almost no loss. As a result they can be condensed with the free-space contribution in a single high-frequency capacitor $C_\infty^{(\mathrm{exp})}$.

2.6b), that was introduced before, while the first broad resonance peak is described by the constant phase element (the capacitor $C_{\infty}^{(\mathrm{exp})}$ in the same figure). If the immittance spectra is measured in a range of conditions where there is only a single dominating transport process, the parallel arrangement of resistors can be approximated by the one representing the dominant transport process, $R_{\mathrm{dom}}^{(\mathrm{stat})}$. In the end, for most immittance measurements, a homogeneous piece of material can be described by the circuit shown in Figure 2.6b. While multiple conduction processes are quite common, observation of more than the one distributed resonance peak of the constant phase element is rather unusual in the frequency range of immittance spectroscopy. In the related field of broadband dielectric spectroscopy, the observation of the resonances of multiple polarisation processes is intended and their separate representation as shown in the circuit in Figure 2.6a advisable.

2.2.5 The constant phase element: a single lumped component combining both dynamic parts

The first step towards introducing a constant phase element was done in 1928 when K. Cole [24] introduced a constant m to describe a frequency dependent capacitive behaviour that leads to the (later) name-giving constant phases different from $\frac{\pi}{2}$ (which would be the phase of ideal, purely real-valued capacitors [47]). It is also worth noting that this is the same paper where the representation of impedances in the complex plane, later called Cole-Cole plot (after K. Cole and his brother R. Cole), is shown for the first time. It is shown that one Voigt-circuit element in series to a resistor[10] leads to a semi-circle response in the complex impedance plane. The centre of the arc is on the abscissa for $m = 0$ and deeper (with respect to $-\Im(Z)$ which is usually the plotting direction in immittance spectroscopy) for larger m, in such a situation the response is called 'depressed semi-circle'. In a slightly different description which, however, leads to the same immittance response, Fricke [47] introduced the constant phase element in the form used in this work. This is also the formulation known as 'universal dielectric response' as introduced by Jonscher in 1977 [84]. This designation subsumes the commonality of non-Debye immittance responses for the first dielectric relaxation in almost all kinds of solids (see Figure 2.2). Indeed 'pure Debye behaviour is hardly ever found in nature' [79]. In the famous [26] publication by K. Cole and R. Cole [27], that lead to the designation Cole-Cole plot, the Cole brothers associated the constant phase behaviour with a distribution of resonance frequencies. This is, indeed, the most basic physical interpretation of constant phase elements. It indicates that some 'property' is distributed which, subsequently, acts as a distribution in resonance frequencies. It does *not* have to be the surface roughness (of the electrodes) which seems to be the most commonly given reason in many experimental works (confer [1]). In fact, more accurate finite-element simulations indicate that the constant-phase elements usually associated with distributions of time constants at the surface *cannot* be attributed to 'the leading explanation' [1] of surface roughness [1].

[10] In the mentioned publication, circuit ambiguity already becomes apparent, since two different circuits are shown that both lead to the same response for all frequencies. Since the problem of ambiguity for conventional EECs was already mentioned, here circuit B is chosen, to have a single consistent example.

Distribution of any relevant physical property, including permittivity, resistivity, structure or reactivity, normal to the surface might result in such a behaviour [65]. Very different models that can explain the constant phase behaviour due to the charge transport over localised states are reviewed by Lang and Elliott [97, 40]. Other possible explanations are given in [87]. The constant phase for an extended frequency region also implies that the ratio of loss is independent of frequency in that region [79].

The constant phase element assumes a specific, often observed, relation between the real and imaginary part of the permittivity,

$$\begin{aligned}\varepsilon(\omega) &= \frac{Kd}{A}(i\omega)^{n-1} \\ &= \frac{Kd}{A}\left[\sin\left(\frac{n\pi}{2}\right) - i\cos\left(\frac{n\pi}{2}\right)\right]\omega^{n-1},\end{aligned}$$

with $n \in [0, 1]$ (where 1 would correspond to an ideal capacitor and 0 to an ideal resistor) and pseudo capacitance $K(E, \mathscr{P}) \in \mathbb{R}^+$.[11] In a case where this relation is observed, the respective dynamic resistor and capacitor for this process may be replaced by a single constant phase element. Parallel polarisation processes should still be expressed in their usual form of two components in either parallel or serial representation parallel to the constant phase element, as indicated in Figure 2.6. In many cases the constant phase element is the lowest observed dielectric relaxation and all higher polarisation effects are outside of the measured frequency range (see section 5.6.3). In such a situation all polarisation processes with much higher frequency as the highest in the experiment may be approximated by the frequency-independent experimental high-frequency-limiting capacitor $C_\infty^{(\mathrm{exp})}$. Such a circuit which should be a valid approximation for a single homogeneous part in most immittance experiments is shown in Figure 2.6b.

The many possible reasons for constant phase elements, that are also discussed and extended in section 5.6.3, clarify why it might not be possible to transform a constant phase element straight forwardly into a static permittivity, that is if it is at all a bulk property of the material and not caused by an interface effect.

[11] Additional representations of the constant phase element in different immittances, e. g. reactance, impedance or complex capacitance, are given in the publication [3] which is complementary to this work.

2.3 Modelling a complete system under investigation consisting of multiple different parts

Experimentally, the investigation of a single homogeneous piece is a rare case. Often, systems under investigation consist of multiple pieces. Since its very beginning, impedance spectroscopy has been used to investigate biological systems [56, pp. 411-418]. One great advantage of immittance spectroscopy is the possibility of *in vivo* measurements on humans, animals or micro-organisms (confer 1.2.1). It is the very nature of those specimens to consist of multiple pieces. Maybe the largest field of immittance spectroscopy, electrochemical impedance spectroscopy, involves measurement of reactions at interfaces and, hence, deals with systems of multiple pieces [110]. In almost all cases where immittance spectroscopy is used multiple pieces are present and their interface contributions important.

Even if the intention is to investigate a single homogeneous piece of material, this is usually not straight forward. Contacting a material without introducing parasitic impedances can be an incredibly complicated task. In the case of semiconductors or insulators the most common effect is the build-up of a space-charge layer which can have significant impact on the measured impedance and is usually very strongly dependent on temperature and applied voltage. Even the cause of this phenomenon itself is neither easy to understand nor to control [184]. The first idea that the effect is caused by different work functions of the involved materials which had been around some time could not explain the experimental findings [130]. Gap states at the interface introduced by the metal, by disorder, by defect-related states or by surface states, also do not seem to be the last answer[183, 185].

From these examples it can be learned that two homogeneous pieces in contact have usually to be described as at least three homogeneous components ('at least' refers to the fact that the third interface part might not be regarded as homogeneous). As a result the circuit for two stacked pieces of material in contact consist of three of the derived circuits illustrated in 2.6a. Serially stacked, meaning that while measuring the impedance in stacking direction, the circuits have to be arranged in series, since the pieces including the interface see only their respective voltage drop and have their corresponding conduction and polarisation processes (measurement contacts have been neglected in this example). While parallel stacking of the pieces, meaning measurement orthogonal to the stacking direction, leads to an arrangement of the sub-circuits in parallel, since current can flow through material A, material B or along the interface (not that unusual and important for polycrystalline materials), while the voltage drop is identical for all parts. Hence, it is important to notice that the homogeneous piece which is often mentioned in this thesis) is not necessarily a piece of bulk material.

Although the explained arrangement might seem obvious, many EECs have different, even unphysical, arrangements. This is not merely the opinion of the author of this thesis. Below are some highlights of a publication by D. Macdonald [110]. Reflecting the development of electrochemical impedance spectroscopy, D. Macdonald directly addresses the mentioned problem: '[...] the tools used to interpret impedance data fall

into two classes: (i) analogs and (ii) physical models. Analogs [...] do not pretend to describe the physico-electrochemical properties of the system, but simply reproduce the properties.', further, 'The analogs are almost always assigned without regard to the physics of the system.' and most important 'There is also a tendency to declare the first analog that is found to account for the impedance data to be the "model" [...]' [110].

2.3.1 Useful approximations and tips

Due to the limited frequency-range of an experiment, not all processes have to be included. On the contrary, explicitly including models, for example, for polarisation processes that have their resonances at far higher frequencies than the highest frequency in the experiment $\omega_{\mathrm{max}}^{(\mathrm{exp})}$ would just lead to overparametrisation. For that specific case, it was already mentioned to use an experimental high-frequency-limiting capacitor $C_{\infty}^{(\mathrm{exp})}$. Assuming a material that has no polarisation process in the frequency range of the experiment $\left[\omega_{\mathrm{min}}^{(\mathrm{exp})}, \omega_{\mathrm{max}}^{(\mathrm{exp})}\right]$ and resistance that is so high that it is already bypassed below the lowest frequency in the experiment $\omega_{\mathrm{min}}^{(\mathrm{exp})}$ (that is, the cut-off frequency ω_{co} of the material is below $\omega_{\mathrm{min}}^{(\mathrm{exp})}$, so $\omega_{\mathrm{co}} \ll \omega_{\mathrm{min}}^{(\mathrm{exp})}$). Such a material might be approximated by the capacitive components alone, or if the frequency is high enough even only by its experimental high-frequency-limiting capacitor $C_{\infty}^{(\mathrm{exp})}$ alone. This is a rather unusual case in immittance spectroscopy since the low-frequency end is usually not restricted.

More common is the opposite case, where a material is a very good conductor and its cut-off frequency is far higher than the highest frequency in the experiment, $\omega_{\mathrm{co}} \gg \omega_{\mathrm{max}}^{(\mathrm{exp})}$. In that case it is again superfluous and even adverse (again unnecessary overparametrisation, since the effect of these parameters is not significantly included in the measured data) to account for the corresponding dielectric processes. Those pieces are then best described by the static resistor only. This description is rather common in immittance spectroscopy. Leads, substrates and pieces, which have large extent (and hence low capacitance), are typically solely represented by a resistor.

The remaining component can, however, in the case of both approximations still be dependent on external parameters. Pieces of the system for which above mentioned approximations are used, should not be the one of main interest, since the experiment should be designed to have the relevant relaxations or resonances inside the frequency range of the investigation. One reason is that as a consequence of representing some parts purely as resistors, if they are in parallel without a model they would condense into a single resistor for which the separate serial parts cannot be extracted.

2.4 The benefit of combining resistive and capacitive models

It is a normal (and also advisable) procedure in physics to obtain the same parameters through different experiments or measurement techniques. Obtaining similar values from distinct observations, which usually tend to have different systematic deviations, increases the confidence in the extracted parameter itself and, since the interpretation of a measurement is usually also connected to a certain (physical) concept, it further indicates that the underlying assumptions were model-independent and reasonable, i. e. the resulting parameter is consistent with its meaning in multiple distinct models and, hence, likely not only a model-specific empirical quantity which not necessarily represents any actual property of the system. Different measurement methods can be quite distinct and, thus, need inevitably separate analysis for their corresponding results. Consequently, instead of a combined evaluation, only the end results can be correlated (and possible deviations interpreted).

The case of immittance spectroscopy is somewhat special: two distinct (i. e. principally unlinked) properties of a system, resistive (based on charge transport) and capacitive (based on dipole arrangement or generation), can be obtained in a joint characterisation. Since *the same* set-up is used and corresponding (resistive and capacitive) parts are simultaneously obtained *in a single experiment*, the extracted properties are inherently compatible and self-consistent. In contrast to many other techniques, immittance analysis and current-voltage measurements are not only very similar, but voltage-dependent immittance spectra also contain the current-voltage information anyway (temperature or any other dependence ascertained, as well). In both cases, the stimulus is the applied potential difference, though it is oscillating around a bias voltage for immittance spectroscopy. At very low frequencies, static resistors contribute predominantly and in this 'quasi-static limit', the current-voltage properties can be extracted straightforwardly from the immittance spectra.

It is, hence, quite surprising that, of all things, with this method[12], which is frequently used to extract parameters of depletion layers, a joint analysis is rarely done. Quite often even different instruments are used to extract current-voltage behaviour and capacitance-voltage characteristic. Indeed, both information are included in a voltage-dependent immittance analysis and, hence, a joint evaluation to extract the same parameters from resistive and capacitive parts of the immittance is possible. For example for a diode, the acceptor concentration or possibly the Schottky-barrier height (exceptions for letter case are discussed in the following subsection) might be obtained from the current-voltage measurement as well as from capacitance-voltage analysis (confer [176, pp. 245-297, 362-407] and [138]).

In this work, voltage-dependent immittance spectra are obtained using bias-voltage steps of 0.05 V combined with a small oscillation amplitude of 30 mV. The voltage dependence can in principle also be obtained, in a more cumbersome way: without bias steps but instead using a sufficiently large oscillation amplitude (wide enough that it encom-

[12] In this context the method is mostly referred to as capacitance-voltage analysis though it is still an immittance measurement.

passes the full range of bias voltages of interest) by extraction of the non-linearity from higher-harmonic generation. This may become increasingly difficult, with devices working in frequency space, the lower frequencies become (since latter contain the resistance-voltage information this quasi-static range should not be omitted).

Finally, voltage-dependent immittance spectra give the current-voltage characteristic with very useful additional information. Separate serial pieces of the system can be identified by their distinct capacitive bypasses and the obtained resistance specifically associated with each of these pieces. Further, the combined evaluation allows connecting capacitive and resistive parts of each piece. As they are already often theoretically linked anyway (e. g. permittivities are included to calculate internal or effective fields in the system and the acceptor concentration is a relevant parameter in capacitance-voltage and current-voltage behaviour, simultaneously), the combined evaluation can also asses whether the often only statically used models harmonise with the corresponding capacitive part at all. Since different aspects of the measured data can be used to determine identical parameters this can either be used to evaluate the quality and consistency of the used models, to check the self-consistency of the data itself (a typical task in immittance spectroscopy [42]) or, finally when consistency was validated and no model could describe the situation, to devise new explanations. Below, it is shown, using the example of the depletion-layer and thin film description in the metal/ta-C/p-Si/metal system, which and how correlations of capacitive and resistive part can be used.

Indeed, there are empirical quantitative relations between resistive and capacitive properties in systems with transport through localised states [36] that are obtained for a wide variety of very different materials [182]. This is generally acceptedly seen as an indication for a joint basis for both contributions [118]. Up to now, a unified microscopic theory that jointly explains dc as well as ac properties for such materials is missing and even considered by some authors as one of the major challenges in physics or solid state physics of our time [118, 147] The novel method of analysis, where the relevant quantities of process-specific physical models dependent on external parameters and are directly fitted in global fits of complex immittances for all conditions, is uniquely suited to validate such models: The immittance measurement allows isolating the specific contribution of the relevant (serial) piece, i. e. parasitic contributions can be removed, and the remaining relevant immittance data contains both, self-consistent ac and dc properties. The method of analysis directly extracts relevant physical parameters based on both parts and, since the data can be assumed self-consistent, the compatibility of the electric and dielectric description can be assessed with a single data set. The thoughts on this opportunity are continued in section 6.2.4. A very similar verification of the compatibility between dc and ac models is performed in the context of assessing the correction of the Frenkel-Poole model that should surprisingly eliminate a decade old quantitative deviation between theoretically and experimentally obtained barrier-lowering coefficient (see section 4.2). The basis for these evaluations is the sharing of parameters between models (especially also, but generally not exclusively limited to, resistive and capacitive models) that is presented in this section. Then again, for the analysis of a future unified theory explaining ac as well as dc properties, only one model would be used. Hence, the latter would be an intra-model while earlier mentioned assessment was an inter-model comparison.

2.4.1 The combination of models for the depletion layer

As explained above, the current-voltage and capacitance-voltage measurements are somewhat similar. Voltage-dependent immittance spectroscopy contains information of both techniques mentioned above: complementary voltage-dependent resistive and capacitive properties which are, furthermore, separably associable with each distinct serial piece in the system. Hence, an analysis of the data using jointly resistive and capacitive models simultaneously allows the extraction of parameters, present in both models, for the depletion layer based on both contributions.

In the case of the depletion layer in silicon, three fit parameters[13] are used in both models that could in principle be combined: the acceptor concentration, for which only a range was specified by the wafer manufacturer, the Schottky-barrier height and an effective flat-band voltage shift. In fact, these parameters are the only fit parameters at all for the whole depletion layer circuit (except for the power of the constant phase element which is just fitted to validate that its value is comparable to unity). All remaining parameters were taken from literature. This includes mathematical constants and natural constants but also the relative static permittivity of silicon [176, p. 849], effective masses for electrons and holes [54], the acceptor level of boron [71, p. 416], . Also all functions behind deduced values are only executed once and their results are used for both parts. This includes the Fermi-level (using a formula from Sze [176, p. 27]), the intrinsic Fermi-level (using a formula from Ibach and Lüth [71, p. 412]), the band gap (calculated using an empiric formula found by Thurmond [179]), the intrinsic carrier density (calculated using an empiric formula with parameters determined by Misiakos *et al.* [134]), the effective density of states in the valence band (using a formula from Ibach and Lüth [71, p. 411]), the total number of holes (formula again from [71, p. 419] but including effects of intrinsic charge carriers and spins) and the total number of negative charges in the depletion layer (based on the ionised acceptors using Fermi-Dirac statistics, accounting for the spin and intrinsic charge densities).

2.4.1.1 The acceptor concentration

In a first model for a similar ta-C/p-Si heterostructure [2], only the resistive model had been implemented, but the capacitance of the depletion layer was only approximated by a constant parallel capacitance. Furthermore, the acceptor concentration, which was specified through the resistivity by the manufacturer as being between 1 Ω cm to 10 Ω cm was not fitted, but instead set to a value corresponding to 5 Ω cm. After the voltage-dependent capacitance was included, still using the fixed value of 5 Ω cm, and fitted for the first time, the cut-off frequency did not fit to the experiment well. Except for the Schottky-barrier height, which was already varied in the fit (later separately, see section 4.1.2 and especially its subsection 4.1.2.1), the acceptor concentration was the only

[13] As already mentioned, in this work, the designation 'fit parameters' is only used for those parameters that have to be (or should, although there is a confirmed literature value, anyway be) determined by a fit. Of course, there are various, so-called, system-specific parameters which are shared between the mentioned resistive and capacitive description, e. g. the area, the permittivity of silicon, the energy of the acceptor level, effective masses, and also natural constants.

remaining fit parameter in the capacitance model. As a consequence of the mismatch in cut-off frequency, it was decided to also vary the acceptor concentration in the fit, as a joint single parameter for resistive and capacitive part. After the first fit with a variable, but joined, acceptor concentration, not only the capacitive part fitted the experimental data much better than the constant approximation used before, but also the resistive part had a better agreement with the data as ever before. It could be seen, how well the one acceptor concentration could describe both parts together. Additionally, this showed that the capacitive properties were much more sensitive on this parameter. The resistive behaviour had a discrepancy, but not too severe, and at that time the deviation was not identified as being connected to the acceptor concentration. The capacitive properties were, in comparison, useless with the arbitrarily set acceptor concentration corresponding to 5 Ω cm. That both parts benefited from the jointly fitted acceptor concentration significantly and are well described, with a single joint parameter that expresses a certain physical meaning, indicates that the described impedance is very likely actually from the depletion layer. Furthermore, both models seem to be compatible with respect to this parameter. The consistency of the parameter over different models indicates that its meaning is sound. Already the successful combination of this parameter between resistive and capacitive models indicates the potential of this novel approach and its leap ahead in comparison to conventional analysis that uses ambiguous EECs, based solely on idealised lumped components, where the association of different circuit components with distinct pieces in the system is inherently unreliable.

2.4.1.2 The Schottky-barrier height

Unlike the acceptor concentration that is used as joint parameter for the capacitive and resistive model of the depletion layer, the Schottky-barrier height could not be shared between both parts. Indeed, at the time of the above example about the introduction of a voltage-dependent capacitance model and the discovery that the acceptor concentration should be varied, there was still a unique Schottky-barrier height used for both models (compare Figure 2.7a). This lead to severe discrepancies of calculated and measured immittance, the highest just above zero bias voltage with decreasing differences for increasing (reverse) bias voltages and starting for frequencies from around 2 kHz (confer Figure 2.7). Especially latter property was not as salient as one might expect. In fact, the resistive model already showed pronounced deviations in a similar bias voltage region (it still does, as can be seen in Figure 4.9), so that at first, the deviation in approximately the same bias range at higher frequencies could be confused with a consequential deviation in the description caused by a bad approximation of the resistive values (compare the residuals of the model with a single joint Schottky-barrier height and with separated, effective, barrier heights in Figures 2.7a and 2.7b, respectively). However, the affected region was already at frequencies higher than the cut-off frequency and the deviation continued further to higher frequencies. Since these high-frequency values were not resistive any more, also in the calculated immittance model, the deviation could no longer be linked to the resistive part at these frequencies.

The idea of using the same value for the Schottky-barrier height is not only the first

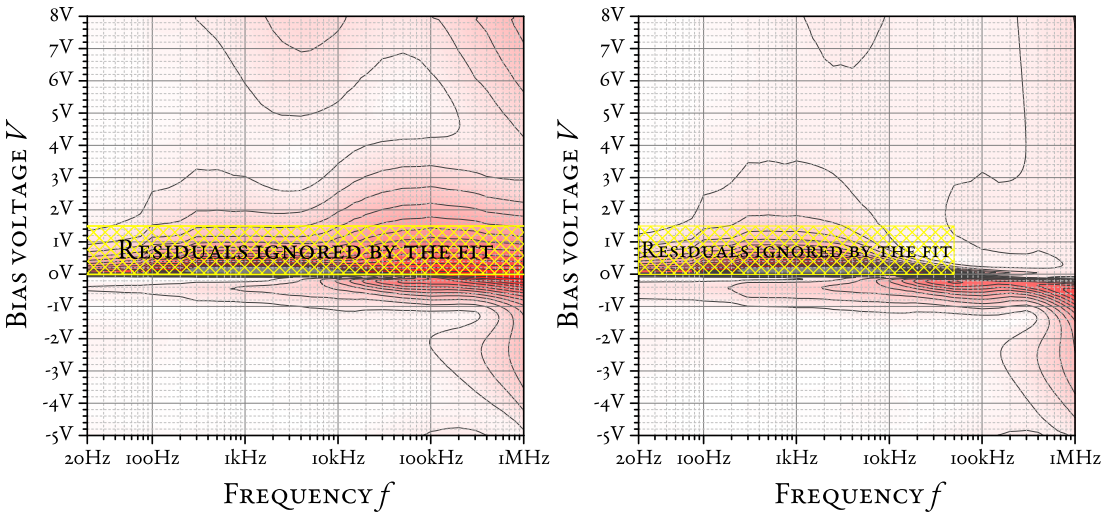

Figure 2.7: Final residuals of fits (of sample `1346aCrAu1` with thin film model 3) assuming a single Schottky-barrier height (a) in comparison of using two separate barrier heights (b) for the capacitive and resistive model of the depletion layer part. The larger residuals for voltages between 0 V and 1 V for frequencies roughly below 100 Hz are caused by a discrepancy in the resistive description that can also be found in Figure 4.9. This resistance deviation causes a subsequent deviation of the cut-off frequencies that can be seen in the range of 0 V to roughly 3 V at frequencies between 100 Hz and 10 kHz (this can, due to the absence of the superimposed capacitive deviation, be seen best in Figure (b)). The capacitive deviation if the same Schottky-barrier height as in the resistive case would be used can be seen in Figure (a). In Figure (b) the capacitive shift is taken into account using a single separate Schottky-barrier height for the capacitance model. This approximation does neither recognise the frequency dependence of the shift nor the also frequency-dependent stretch-out of the capacitance-voltage curve. The colour scale is identical to the one used in all residual contour plots in this work which given in Figure 4.20g.

logical choice, indeed, also in 'typical' literature one finds that there should not be a difference in this value whether it was determined from capacitive or resistive measurements. For example, Sze states [176, p. 292] that for intermediate contacts with clean interfaces there should be *almost no discrepancy* between Schottky-barrier heights determined from capacitance-voltage and current-voltage measurements. This statement (which seems to be the source of confusion as will be shown below) is, however, only true in the context of contacts with metals which are clean, annealed and after passivation of dangling bonds, since charged defects in insulating materials connected to the semiconductor, even for perfect trap-free interfaces, shift the flat-band voltage (from which the apparently different Schottky-barrier height would be extracted) [161]. Without converting this shift into a concentration of charged defects, this feature would appear as an apparently different Schottky-barrier height varying with frequency in the capacitive model in comparison to the resistive model (confer [138, pp. 423-491] [176, pp. 390-395]). Additionally, even for clean interfaces with metals without passivation, interface traps also lead to apparently different values of the Schottky-barrier heights from capacitive and resistive properties, because the traps at the interface lead to a stretch-out of the capacitance-voltage plot [161]. Dependent on the charge of the interface traps the corresponding stretch-out also results in a frequency-dependent contribution to the shift [161]. Furthermore, a clean interface is not expected in our case, in which the sample was not annealed after the deposition of carbon ions with an impact energy of 100 eV. This is expected to lead to a very high number of defects around the interface which are not covered by usual descriptions of such interfaces.

Interfaces can generally not be ideal in that sense, otherwise the Schottky-barrier height would be identical for both measurement methods and equal to the work function difference which is never the case [185]. Unavoidable, deviations from ideality[14] (e. g. charged defects in the insulating material [138, pp. 423-491], traps due to spatially extended disorder [176, p. 292], dangling bonds at the interface or even the difference in atom species at the interface itself [185]) lead either to traps at the interface or charged defects in the insulator. These traps or defects both influence, even dominate, the voltage-dependent resistive and capacitive properties. However, dependent on their properties, the effect on resistive properties is distinctly different from the effect on capacitive properties. In the static (i. e. resistive) case all traps and charged defects contribute with their equilibrium occupation, while for the dynamic (i. e. capacitive) case the amount of involved traps and defects decreases with increasing frequency, depending on their respective capture and emission rates [162, pp. 258-267]. Hence, the flat-band-voltage shift is even dependent on frequency (and ambient temperature). Furthermore, also in capacitance-voltage measurements the bias voltage varies slowly in comparison to the oscillating signal: the slow bias leads to different occupation statistics of the traps at the interface and the

[14] Ideality is in this context an ambiguous term, since ideal interfaces without passivation or annealing should have at least the traps caused by the contact of different materials themselves. Although, the term 'ideality' is not used in this way, e. g. in reference [176, pp. 362-430] where the ideal metal/insulator/semiconductor-structure is introduced as completely without any defects. In consequence, this work follows the established usage of the word 'ideal', within the context of interface defects, which assumes no interface states whatsoever.

oscillating signal charges and discharges, dependent on the bias voltage, other trap levels. Latter traps are then of course selected due to the frequency of the applied signal. While the slow offset always selects identical occupation statistics per voltage, the measured capacitance is decreasing at the same bias voltage with increasing frequency, since fewer interface traps are charged and discharges in a period. This leads to the so-called 'stretch-out' of the capacitance-voltage curve (confer [138, pp. 380-388] and [161]). Dependent on the type (either behaving donor- or acceptor-like) and frequency dependence of the interface traps, the stretch-out can also result in shifts that could even change their direction for different frequencies. Ignoring the origins based on disorder (structural defects at the interface and absence of atomic flatness) mentioned above for the moment, a simple image of dangling bonds is also not correct [185]. Indeed, the calculation of interface defect states, even at an atomically flat interface, is much more complex than the superposition of the different orbitals at the interface [185]. However, using much more detailed theories, as those presented by Tung [185], is (as indicated before) not justified in the case of the interfaces in this work, which are not in any way annealed or passivated after their deposition with 100 eV and may, consequently, be assumed to deviate significantly from the results for atomically flat surfaces.

To sum it up, deviations between the Schottky-barrier heights extracted either from capacitance-voltage analysis and current-voltage measurements are not unusual. In fact, the frequency-dependence of shift and stretch-out of the flat-band voltage (corresponding to the built-in potential derived also from the Schottky-barrier height) was thoroughly investigated for decades to understand the consequences of interface traps or charge defects (mobile or immobile) in the insulator and to extract the corresponding concentrations (for this quite extensive field it is conferred to its 'standard reference' by Nicollian and Brews [138][15] in which many examples of how this apparent shift in the Schottky-barrier height is converted into defect densities are given and newer works of Schroder [162, 161] which use a pedagogically more pleasant description and add some more recent insights). The different barrier heights may today only be neglected because the knowledge on metallisation of silicon (which includes 'soft' processes that do not create disorder at the interface, annealing and passivation) has advanced to such a point that above described interface defects may be ignored [162, p. 90]. The consequences of the statement by Sze, about comparable Schottky-barrier height values independent from whether they were extracted from capacitance-voltage or current-voltage measurements (already mentioned above [176, p. 292]), even seemed to have let to considerable confusion: The work of Song *et al.* [172], that investigates aluminium contacts on p-InP, explicitly mentions the statement of Sze and then tries to find reasons for different values, also referencing other works with similar findings and based on principally completely valid idea of Ohdomari and Tu [140] that the metallisation can lead to different barrier heights. Song *et al.* consequently introduced a distribution of barrier heights to explain the difference in the values of the Schottky-barrier height extracted form capacitance-voltage or current-voltage measurements. Their concept is not in question here (a distribution of barrier heights

[15] Its importance is underlined by the fact that this book originally from 1982 was unalteredly reprinted in 2003.

might very well be a contribution to the discrepancy), but the complete negligence of the long-known influence of interface traps (confer e. g. [138, 162, 161]) which are unavoidable even for extremely well prepared contacts at atomically flat interfaces [185] (and may only be rendered unimportant by passivation) is questionable. As found above, traps at the interface or in an insulator (if present) are generally not at all surprising. The work of Song *et al.* is cited over 350 times (according to the publisher website and the Web Of Science by Thomson Reuters, both visited at 29 June 2016). The most cited publication of those is by Werner and Güttler [189] which also ignores any defects at the interface, in this case potentially partially justified, for silicides on silicon, but rather not for the other mentioned materials. Any charged defect in the vicinity of the interface may contribute to the flat-band voltage shift. Except for very clean interfaces, distinct contributions changing the effectively observed Schottky-barrier height may jointly contribute. The one contribution that cannot be removed is the fundamental one due to the presence of different materials which is explained in [185]. It is highly improbable that, without mentioning any specific passivation methods etc., Song *et al.* [172] would have a distribution of Schottky-barrier heights but no other interface traps (even discounting those unavoidable ones, for the moment).

Both types of defects are expected to be present in the heterostructure investigated in this work. Since (up to now) the available immittance data does not allow distinguishing the different contributions, the densities of interface traps and charged defects in the insulator could not be separately determined. Otherwise, it would be useful to fit these values directly, instead of two Schottky-barrier heights. For now, different barrier heights have to be used for capacitive and resistive properties. Their difference is, however, interpreted in distinct extreme cases as defect concentration of either interface traps or charged defects in the insulator and analysed in more detail in section 4.1.2.1. A possible next step, after the space of measured conditions was extended so that at least some different contributions might be distinguished, would be to account for the frequency dependence of shift and stretch-out of the apparent Schottky-barrier height. Then a joint fit of the Schottky-barrier height between resistive and capacitive models might be possible.

2.4.1.3 General requirements before further combinations of fit parameters

The analytical models that were applied in this work and describe the depletion layer, are still regularly applied to analyse experimental data as well as extract certain key parameters and, further, include more effects as some models most often applied to analyse the characteristics of metal/semiconductor interfaces. For example, many publications do not include the effect of Schottky-barrier lowering, though, precisely accounting for that phenomenon solved the discrepancy between the capacitive and resistive part and, furthermore, lead to a reasonably good description of the measured reverse bias current-voltage behaviour (other authors compensated for this discrepancy by including parallel 'leakage' resistors [15] which can due to its missing voltage dependence, only be a crude approximation). On the other hand, it is still worth mentioning that to arrive at those analytical descriptions of the diode certain approximations and restrictions are

unavoidable. Indeed, there are models taking more phenomena into account or even calculate almost arbitrary geometries, doping concentrations etc. much more fundamentally, e. g. solving Schrödinger-Poisson-current equations for finite-element models and quantum-mechanically correct modelling of the interface [180]. It is expected that those highly advanced numerical models, which are usually used to simulate systems rather than fitting experimental data, would lead to much better descriptions of the experimental findings. On the other hand, it is still impressive that using these more basic, common, analytical models could lead to such a good agreement and even interesting new findings. Conclusively, there are still a lot of exciting more advanced models to combine with this novel approach of using and analysing immittance data.

This work, however, focuses on a general idea of analysing immittance data. The performed experiment is only an example to show the presented approach experimentally applied, in general, and its usefulness of extracting parameters, separating serial pieces and for the validation of models containing constants present in both, resistive as well as capacitive properties, in specific. The best possible description of the depletion layer in the investigated samples is, hence, not a priority. It is believed, that the benefits of this approach, with respect to the depletion layer, become already apparent by the successful combination the acceptor concentration in its different parts. Furthermore, the utilisation of a joint parameter for ac and dc properties is, within this exemplary experiment, also used for the thin film description. For an experiment really focusing on the understanding of a specific heterostructure, a broader range of parameters is suggested, so that also the Schottky-barrier height might be fitted jointly and the difference ascribed to interface traps or charged defects in the insulator accordingly. Further, different, more refined, models may be utilised instead of these analytic solutions.

2.4.2 The combination of models for the thin film

As explained in the last subsection, for extraction of the properties of depletion layers both approaches, using ac and dc experiments, are common. The extracted parameters can, however, dependent on which effects were included in the underlying models, have different values. For example, by including the contributions of interface traps and charged defects in the insulator, the otherwise appearing quantitative differences for the Schottky-barrier height, depended on whether it was extracted from ac or dc properties, can be mapped to densities of the respective defect type. This is, on the one hand, not the end of the road to understand the physics of the depletion layer, because these interface defects may be due to fundamentally different origins (e. g. by disorder at the interface or due to those states that would also unavoidably occur at an atomically flat surface due to the interaction of the orbitals of different materials [185]). On the other hand, it is a possibility to use a joint fit parameter for the Schottky-barrier height while the difference is at least converted to total defect densities, which might be separated further, but are at least from the present standpoint actually the source of the difference. Even to at least distinguish between the defects in the insulator or at the interface already requires the measurement under specific varied external parameters. The above described challenges may be the reason that capacitive and resistive models for the depletion layer were not

applied as combined fit models in the literature. Furthermore, the separate extraction of ac properties was usually based on the capacitance extracted form only two frequencies [138, pp.pp. 321-333, 388-389], instead of a complex immittance spectra (declaring two values not to be enough to call it a spectrum) for different voltages. From the above given example of a depletion layer, where ac as well as dc methods are both common approaches to extract fundamentally identical properties of the same system, two things might be learned for the combination of ac and dc fit parameters in the thin-film model, which unlike the depletion layer has not commonly be analysed with both methods: First, it is obviously not generally possible to straightforwardly combine parameters, since ac and dc properties are more or less sensitive to different features in the system. Secondly, for a principally common basis of the effect (e. g. in the case of the depletion layer interface effects are responsible for both properties, but their different time constants alter the capacitance dependent on frequency) the consideration of further properties in the models can explain discrepancies in the extracted parameters.

As explained above, the specific discrepancies found for the Schottky-barrier height depending on the chosen measurement method were extensively investigated in literature. Hence, utilising shared fit parameters for both, capacitive and resistive, models for the depletion layer was in case of the depletion layer more obvious. For the Frenkel-Poole model, on the other hand, a joint analysis of dielectric and electric properties, as performed in this work, with single parameters shared between the models was never done before.[16] This is actually surprising, since a major deviation of the resistive Frenkel-Poole model from measured data is connected to the dynamic permittivity, a capacitive quantity, in the barrier-lowering coefficient. The permittivity was usually taken from literature, only very rarely (e. g. in [61]) the same sample was analysed with current-voltage analysis and the permittivity measured in the same work (but then also in a second experiment with different set-up and separate analysis). The experimentally obtained value of the barrier-lowering coefficient principally suggested a larger permittivity then the literature values. Problematic may be that, although many enhanced Frenkel-Poole models exist (see section 5.6.1 where a detailed overview of the development of Frenkel-Poole models is given), most importantly the correct allowance for all three dimensions, even today the initial version by Frenkel [46] seems to be the most commonly used one. On the other hand, as the different enhancements usually (except the one of Ieda *et al.* [72] since they introduced a factor that allows freely manipulating the slope) converge against the

[16] The attempt to generalise the Frenkel-Poole model for alternating fields by Jonscher and Loh [86] takes a completely different approach (than the one presented in this work) by introducing an effective temperature, dependent on the frequency and only for the slope, in order to describe the changes in the in-phase component of the current through the thin film. The out of phase component, which corresponds to the capacitive properties, was neither determined quantitatively nor used in the analysis at all (hence, this is not a joint analysis of dielectric and electric properties). The permittivity was *arbitrarily chosen* and never discussed (it was of course unnecessary to change the permittivity since exclusively the slope was divided by the effective temperature which was redetermined for each frequency and could, hence, absorb all occurring changes). The introduction of an arbitrary effective temperature for the electron system in Frenkel-Poole models has since then been abandoned. For the above reasons and especially since the permittivity can, by compensation through an unrestricted effective temperature, be arbitrarily set in this description, its value is inherently unimportant.

same or at least a very similar slope for sufficiently high fields, the permittivity can still be regarded as principally overestimated in the Frenkel-Poole model.

As will be explained much more thoroughly in sections 4.2 and 5.6, the question arose, whether the factor in barrier-lowering coefficient was actually the permittivity at all or a dielectric constant at some other frequency. So it was suggested that it was neither simply the dynamic permittivity nor the static permittivity but some weighted mean between these values [64]. In section 4.2.1, it is estimated within the concept of the Frenkel-Poole model that the dynamic permittivity should be chosen. One reason that it might not at all be the (dynamic) permittivity is that the assumption of a Coulombic potential is essential for the specific form of the barrier-lowering coefficient. Deviations in the potential landscape could, hence, reveal themselves as different values for the barrier-lowering coefficient. That typically structural defects, which are principally not well described by effective-mass theory but rather leading to highly localised deep traps [41, pp. 281-334], are assumed to be involved solidifies the assumption that it might not be the permittivity at all. Neither are the ground states of deep traps assumed to have a Coulombic geometry at all, e. g. in strongly directional binding systems like covalent materials, (the excited states, on the other hand, may indeed have a hydrogenic characteristic [55]) nor would it be expected for such highly localised defects (maybe even on the order of one or two inter-atomic distances) that the macroscopic permittivity of the material would be relevant in the respective microscopic volume in general. Despite the limitations of the underlying concept of the Frenkel-Poole model (many were also not cleared up by proceeding enhancements, a detailed overview of the remaining limits of the model is given in section 5.6.2) and the consequent questions whether the interpretation of the barrier-lowering coefficient is reasonable altogether, in this work a connection was introduced between the permittivity in the barrier-lowering coefficient and the one extracted from dielectric components. Furthermore, it was noted that the externally applied potential difference was obviously never correctly converted into an internal field (see sections 4.2 5.6) which might be interpreted as an apparent factor for the barrier-lowering coefficient and consequently an overestimated permittivity in the Frenkel-Poole model. The field dependence in the Frenkel-Poole model arises from a barrier-lowering of the otherwise Coulombic trap potential by a superimposed field that is supposed to be caused by the applied potential difference (confer [46], but also all other subsequent advances of the model discussed in section 5.6). As will be further explained in section 5.6.3 the field that is superimposed to the trap potential must be the internal field, see equation (4.6), which accounts for the polarisability of material in which the trap exists. The usually used external field cannot be seen by the charge in the trap. It would only be correct in the vacuum case where a trap would on the other hand not occur. The internal field is calculated using the static permittivity, since the resistive part is dependent on the bias voltage which is varied comparably slow.

As a result, the model of Connell *et al.* [28] (which is three-dimensional and offers the most sound description for the escape probabilities in every direction, see 5.6) was selected and the correction to use the internal field applied. Three different models for the thin film were compared that connect the permittivity extracted from the capacitive properties in different ways with the resistive model of the thin film (see section 4.2 for a

detailed description of the different connections and section 4.2.3 for their evaluation). In the first model, the permittivity for the conversion into the internal field (which is, due to the slow variation of the bias voltage, supposed to be the static permittivity) is the sum of the contributions extracted from the high-frequency-limiting capacitor and the constant phase element (both of the thin film), while the permittivity in the barrier lowering coefficient uses only the contribution of the high-frequency-limiting capacitor (implying that it should be the dynamic permittivity only). This model would be correct if the constant phase element would contribute to the static permittivity, as suggested for specific interpretations of the element by Lunkenheimer [107, 108], and if the permittivity from the high-frequency-limiting capacitor would approximately correspond to the dynamic value.

> As explained in section 2.2.4 and Figure 2.6b, in an experiment with limited frequency range the permittivity for high frequencies leads to an effective purely real high-frequency-limiting capacitor for the specific frequency range in the experiment denoted with $C_{\infty}^{(\mathrm{exp})}$. There are usually further resonances expected between the permittivity for optical frequencies which is supposed to be in the barrier-lowering coefficient of the Frenkel-Poole model and what would be the high-frequency-limit capacitor in our experiment. Then again, specifically for this material it might (as is explained in section 5.3) be plausible to assume other polarisation processes might be negligible. For other materials, where this might not be the case, the dynamic permittivity from the barrier-lowering coefficient should however still be resembled by an extra capacitor in parallel to the other parts of the thin film. This extra capacitor would represent the contributions of the permittivity from optical frequencies and above. The high-frequency-limiting capacitor would then represent the contributions for frequencies above the highest in the experiment but below optical frequencies. The separation into capacitors guarantees that the permittivity in the barrier-lowering coefficient is not overestimated (by implying restrictions based on the dielectric part which are valid as long as the permittivity in the barrier-lowering coefficient is not in the vicinity of a resonant absorption process).

In the second model, the static permittivity was extracted only from the high-frequency-limiting capacitor, too. This approach corresponds to the procedure used by Young and Frederikse [190], who are affiliated to what is now called the National Institute of Standards and Technology of the United States of America, to compile a list of references for static dielectric constants of inorganic solids. The third model has no connection (i. e. no jointly fitted shared parameters) between the resistive and capacitive values at all. Since both 'permittivities' in the exponent of the resistive model are factors to the square root of the field and both unrestricted in this last model variant, they are combined to a single arbitrary value freely variable in the fit and unconnected to the dielectric properties. If this model would be the only one leading to a sufficiently well description of the experimental data, one could deduce that the proposed connections between dielectric properties and the resistive model do not exist. It would follow as well that the underlying assumptions of the Frenkel-Poole model itself cannot be entirely correct.

The proposed method of analysis and the usage of voltage-dependent immittance spectra, instead of conventional current-voltage analysis, are uniquely suited for the above described specific case, to determine whether a dielectric parameter plays a role in the resistive model and whether the correction to calculate the internal field introduced in this work is valid. Due to the identical set-up and simultaneous measurement of capacitive and resistive properties, the resulting immittances are self-consistent. Directly including models for dc as well as the ac parts allows global fitting of the relevant model parameters (partially shared between the models) for all conditions together. These are optimal preconditions to validate the comparability of electric and dielectric models.

In summary, different connections between the capacitive and resistive properties of the thin film are evaluated in this work. Some of them are based on an additional correction, introduced in this work, to calculate the internal field around the trap correctly within the concept of the Frenkel-Poole model. Instead of (quasi-)capacitances the permittivities are fitted in the dielectric models. Hence, dependent on which of the several descriptions for the thin film are used, the permittivity is a unique shared parameter jointly fitted for both contributions.

3 Methods

3.1 Sample preparation

Each process step, after dicing the substrates of the samples from their individual wafers, was, when possible, performed simultaneously. It will be mentioned explicitly, if samples were not in the same batch during a process step.

Using optical lithography, two rectangular aluminium back contacts (compare Figure 3.1), of 3 mm of height and 925 µm of width (thickness around 300 nm), with a gap of 1.15 mm between their long edges were deposited on the unpolished side of two types of boron-doped p-type silicon substrates (7.5 mm × 7 mm × 0.525 mm) with resistivity (as specified by the manufacturer MTI) of 1 Ω cm to 10 Ω cm and <0.005 Ω cm. Prior to thermal evaporation of 300 nm aluminium (with 5 Å s^{-1}) in a Leybold Univex 350 universal vacuum coating system, onto all samples shown in this work simultaneously, the native oxide and any contaminants, remaining after previous acetone and isopropyl alcohol treatment[1], were removed by *in situ* argon plasma etching. During sputtering and evaporation the samples were rotated while the sample holder temperature was kept constant at 295 K by water cooling. After the removal of the photoresist, including another acetone and isopropyl alcohol treatment, the polished sides of the silicon substrates were cleaned (simultaneously) by refractive ion etching (45 sccm O_2, 5 sccm CF_4) for 15 min at 300 W in an Oxford PlasmaLabSystem 100, followed by thermal annealing of the aluminium back contacts (of all shown samples simultaneously) for 30 s at 1137 K

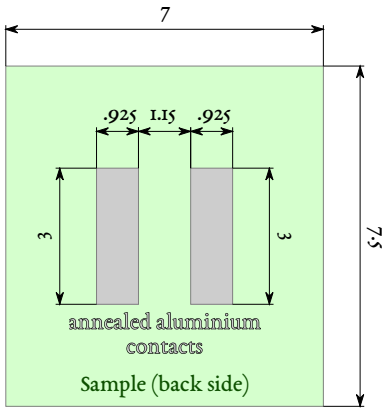

Figure 3.1: Geometries of the contact on the back side of the sample. All dimensions in mm. Scale 6:1 (when printed without scaling onto a DIN EN ISO 216 A4 paper).

[1]The standard cleaning is performed in an ultrasonic bath of acetone and subsequently isopropyl alcohol with only a single sample in one beaker at a time. Consequently, the samples were not simultaneously in one beaker. However, they were always cleaned in the same batch, i. e. without a break, with the same chemicals, with the same parameters of the ultrasonic bath, at the same day (mostly within one hour).

(30 s ramp time, using a susceptor and sapphire plates as protective covers on both sides) under argon atmosphere in an Annealsys AS-One 100 rapid thermal processing oven. All specimens analysed in this work were simultaneously carbon coated utilising mass-selective ion beam deposition (MSIBD) in the ADONIS accelerator. The coating process itself and the used set-up are described in detail in [13, pp. 21-24] and [50, pp. 45-47]. In this paragraph only some specific features of the ADONIS accelerator, that increase the film homogeneity and reduce parasitic contamination by other species, are summarised. The separation of masses, through a bending magnet, is exact enough to select a single isotope for deposition. Using an ion source after Sidenius [167] allows a sufficiently high current in combination with a low distribution of ion voltages. The identical source of the acceleration voltage of 30 kV which is used for the extraction is also applied at the target to decelerate the ions. The usage of an identical source avoids adding a voltage uncertainty by drift between separate sources. To arrive at the lower, final ion energy, a second voltage source is connected in series between the original acceleration voltage and the target. Its uncertainty is negligible against the width of the distribution of ion energies from the source, which itself has comparably low distribution of ion energies (compare [50, p. 45]). An electrostatic deflector is used to bent the ion beam by a small angle, prior to the deposition, in order to filter out neutral particles. Beside two electrostatic lenses to focus the beam, a quadrupole lens is used to create an as symmetric spot as possible. To achieve a laterally homogeneous film width, the beam is wobbled by a beam seep which is designed to leave the angle of incident unchanged.

Prior to the carbon film deposition, the native oxide and other surface contaminants on the polished side of the silicon substrates were sputtered *in situ* by 15 mC $^{40}Ar^{+}$ ions with a kinetic energy of 1 keV and normal incident angle onto the silicon surface. The about 80 nm thick ta-C film was grown at room temperature using $^{12}C^{+}$ ions with an energy of 100 eV which leads to the highest sp^3 fraction of around 80 % [13, pp. 63-66].

Two different types of top contacts were deposited on each sample by thermal deposition. Both were deposited through a gold-plated copper shadow mask with circular holes of 0.9 mm diameter in the Leybold Univex 350 (jointly on the investigated samples). One top contact variant consists of a 13 nm chrome layer on the carbon thin film, followed by a 130 nm gold layer on top. The other variant is composed of a 12 nm titanium layer on the carbon thin film followed by a 200 nm layer of aluminium on top. During the evaporation processes the samples were rotated and the sample holder constantly held at 295 K by water cooling.

The samples were mounted, in the same batch, (compare Figure 3.2) by gluing the back contacts with conductive silver paste onto two gold-plated copper bars of a printed circuit board (referred to as sample PCB). Cr/Au top contacts were bonded, in the same batch, to the gold-plated copper pads on the sample PCB using gold wires with a diameter of 30 µm, utilising a Kulicke & Soffa 4523 wedge bonder, while the sample holder was kept at a temperature of 333 K. Ti/Al top contacts were mounted in the same way, however, with the difference of using aluminium wire with a diameter of 30 µm and a sample holder at room temperature. As a result, both top contact measurements of one sample were measured with the same back contact.

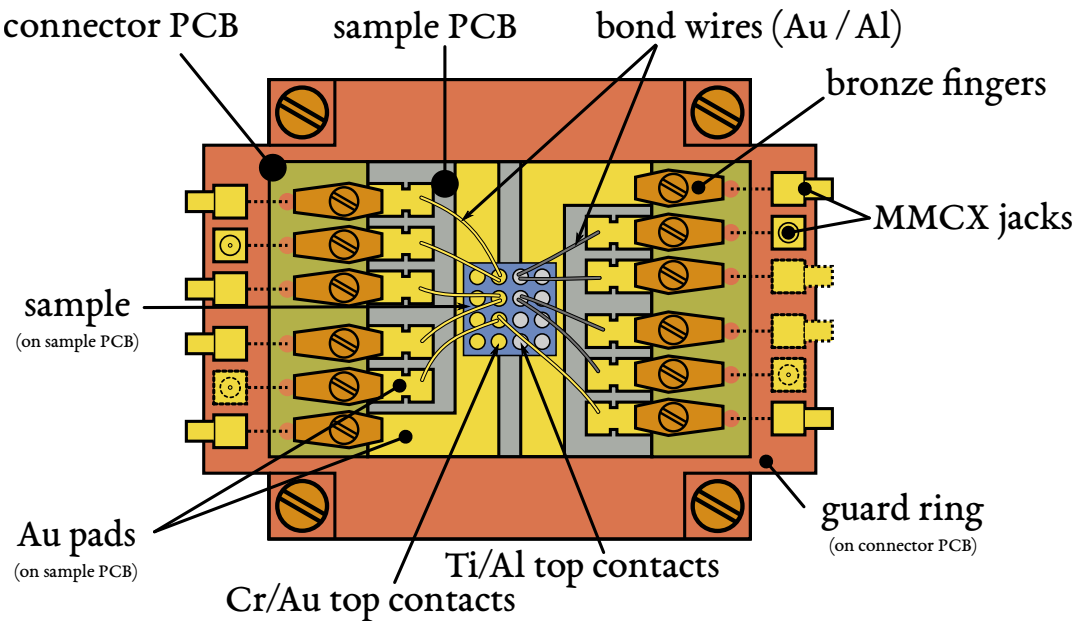

Figure 3.2: Schematic illustration of the sample holder.

3.2 Measurement

3.2.1 Impedance setup

The impedance spectra of the samples investigated in this work were determined by a HP 4284A/001 auto-balancing bridge connected in four-terminal-pair configuration continuously using 50 Ω cables and connectors. In the enclosure, which was connected to the chassis ground of the HP 4284A/001, double-sided floating shield BNC feedthroughs were used. As a result, the four terminal configuration [63] was uninterrupted until the guard ring on the connector PCB (see Figure 3.2), which surrounded the sample PCB. In addition, the connector PCB was used to connect the four terminals with the gold-coated copper pads and bars on the sample PCB via bronze fingers. All measurements were performed at room temperature.

3.2.2 Impedance measurements

The signal level was chosen by measuring the evolution of impedance dependent on the selected signal level at quasi-static conditions (signal frequency 20 Hz) and zero bias voltage (where the dependence on voltage of the samples is highest). In agreement with the voltage dependence of the resistance of the investigated system, this function is strictly monotonically decreasing with increasing signal level. As a compromise between measurement accuracy and minimal perturbation, a signal level of 30 mV_{RMS} was selected for all measurements. The measurement error for each point (frequency, bias voltage, complex impedance) was calculated according to the manual of the HP 4284A [63]. Hence, the measurement error calculation includes integration time, frequency, bias

voltage, signal level, cable length, temperature and the value of the measured impedance itself. The integration time 'long' was selected and an average rate of 3 set.

> The integration time varies the duration the analogue-digital converter has to perform its conversion. It is not a constant time but a non-linear function dependent on the test frequency (at low frequencies also other factors) which strongly increases towards low frequencies. For the full curve confer to the manual of the HP4284A auto-balancing bridge [63, chapter 9, p. 23]. As an orientation the dwell time at 20 Hz is up to around 2 s, at 100 Hz the time is typically 1040 ms, at 1 kHz around 830 ms and at all higher frequencies usually 820 ms.

High terminals of the instrument were in all experiments attached to the top contact, while low terminals where attached to the back contact. Hence, throughout this work positive externally applied voltages represent a higher potential on the top contact with respect to the back contact and, consequently, negative bias voltages represent a higher potential at the back contact in comparison to the top contact.

A complete measurement series of a sample (between 7,000 and 18,200 complex impedance values without accounting for immittances at zero bias voltage) was obtained by applying the same bias-voltage cycle for each frequency starting with the lowest frequency of 20 Hz up to the highest frequency of 1 MHz. The cycle of bias voltages was always performed in 50 mV steps starting from 0 V to the highest voltage $V_{\mathrm{b,max}}$ then to the lowest voltage $V_{\mathrm{b,min}}$ and then back to 0 V. If measured data is in this work plotted directly, generally points of both directions are shown simultaneously. A difference between immittance values measured in forward or backward direction is, however, neither visible nor significant (only 2 of the 18,200 differences between backward and forward values are larger than the corresponding mean device measurement error of the respective condition). If derived values, e. g. deviations to simulated values, are shown, the mean from forward and reverse direction is used. Since samples with low-doped substrate show a rectifying characteristic, an asymmetric voltage cycle, with maximal voltage $V_{\mathrm{b,max}} = 8\,\mathrm{V}$ and minimal voltage $V_{\mathrm{b,min}} = -5\,\mathrm{V}$, was chosen. For samples with a highly doped substrate the complete voltage-drop is assumed to be almost entirely at the ta-C layer. Additionally, the interfaces were expected and confirmed to have much lower breakdown voltages. Hence, for samples with highly doped substrate a symmetric voltage cycle was chosen, with $V_{\mathrm{b,max/min}} = \pm 2.5\,\mathrm{V}$.

3.3 Analysis

3.3.1 Preparation of measurement data for the fit and residual calculus

In order to fit the measured immittance data, it was converted into pairs of resistance and reactance. In a next step, the measurement error for each value in the pair was determined according to the specification of the device manufacturer [63]. Since the bias voltage was changed in forward and backward direction, each condition is measured twice (zero bias actually three times). As explained above, the actual measurement data is plotted in all plots containing measured data in this work and it can, hence, be seen that no visible hysteresis was found in the data.

The representation as resistance and reactance was chosen because it is very convenient for the model comparison in complex non-linear least-square fits, introduced by J. Macdonald and Garber [121]. Complex non-linear least-square fitting is the most commonly used variant in immittance spectroscopy [114]. In this work, the weighing is, however, performed differently as compared to works of J. Macdonald, where two separate weighting factors for real and imaginary part of the immittance are used [7]. The approach of J. Macdonald has the obvious advantage that differences in magnitude of both parts will be normalised by their error which is of course related to the corresponding magnitude. On the other hand, as pointed out by Boukamp [12], the individual weighing of each part would only be correct if both parts were statistically independent of each other. However, since the Kramers-Kronig relation connects real and imaginary part of the immittance, meaning their values are not statistically independent, one has to weigh the immittance deviation vector with one factor and not its components separately. Hence, following the suggestion of Boukamp, each immittance deviation vector is normalised by the length of the corresponding error vector. Of course, such a decision might lead to slightly different fit results, but the specific formulation of the residuum is not essential for the proposed method in this work. Any residuum that describes deviations plausibly for minimisation can be used.

3.3.2 Optimising the fit parameters

For the subsequent part of this section following terminology is used (which is, to be more compact, different to the syntax in any other parts of the book): A point $\mathscr{P}_i$ in the parameter space $\mathbb{P}$ for a distinct condition i is an ordered tuple with specific values for each external parameter. In this work, only bias voltage and frequency are varied. However, there are other external parameters (e. g. temperature) which are held constant during the measurement and still used in the calculation of theoretical values for the fit. Furthermore, there are parameters (e. g. signal oscillation amplitude) which are constant throughout the experiment but unused in the calculation of model values for the fit. In principle, there could be even more parameters (e. g. atmospheric pressure) which are simply not recorded during the measurement, since they are expected to be irrelevant or negligible for the measurement. For convenience, if a point in parameter space is written out, only its elements which are varied during the experiment are shown. Furthermore,

as an approximation, the external parameters themselves are assumed exact.

As a result, the measured data point for condition i, given by $\mathscr{P}_i$, is expressed by

$$Z_i^{(\mathrm{meas})} = \begin{pmatrix} R_i^{(\mathrm{meas})} \\ X_i^{(\mathrm{meas})} \end{pmatrix}.$$

A (what is called) simulated data point $Z_i^{(\mathrm{sim})}$, also consisting of resistance $R_i^{(\mathrm{sim})}$ and reactance $X_i^{(\mathrm{sim})}$, is calculated utilising the given model for the whole system, which is basically two equations, one for resistance and reactance respectively, derived from the specific arrangement of components in the circuit and, of course, using the identical tuple of parameters $\mathscr{P}_i$ as for the corresponding measurement condition. Except for the total serial resistance, which is an idealised lumped component, other components in the circuit are process-specific physical models dependent on external parameters. Their values for each specific condition i are calculated and used in the equations for resistance $R^{(\mathrm{sim})}$ and reactance $X^{(\mathrm{sim})}$ of the whole system.

During an iteration of the fitting routine all parameters have defined values. Especially also the fit parameters $\mathscr{F}$ which are varied between the iterative steps and further fixed values, e. g. natural constants and literature values, denoted by $\mathscr{C}$. Hence, for each iteration step simulated values for each condition are calculated and compared to the measured values. The comparison uses following squared residual function (as already mentioned, the weighting is according to Boukamp [12]) for each condition i

$$\delta_i^{\mathrm{res}^2} = \frac{\left(R_i^{(\mathrm{meas})} - R^{(\mathrm{sim})}(\mathscr{P}_i, \mathscr{V}_i, \mathscr{F}, \mathscr{C})\right)^2 + \left(X_i^{(\mathrm{meas})} - X^{(\mathrm{sim})}(\mathscr{P}_i, \mathscr{V}_i, \mathscr{F}, \mathscr{C})\right)^2}{\left(\sigma_i^{(\mathrm{R})}\right)^2 + \left(\sigma_i^{(\mathrm{X})}\right)^2},$$

with $\sigma_i^{(\mathrm{R})}$ and $\sigma_i^{(\mathrm{X})}$ being the measurement error of the resistance and reactance of the data point for the ith condition, respectively. Principally, not all functions use the same parameters from the tuples $\mathscr{P}_i$, $\mathscr{V}_i$, $\mathscr{F}$, $\mathscr{C}$, but for convenience (otherwise there would be even more indices) in these equations all functions get the full parameter tuple and are expected to use only those elements of it which they need. The tuple of all squared residuals $\left(\underline{\Delta}^{\mathrm{res}^2}\right)^T = (\delta_1^{\mathrm{res}^2}, ..., \delta_N^{\mathrm{res}^2})$ for all N conditions is minimised by the fitting routine by variation of the fit parameters in the tuple $\mathscr{F}$.

Specifically for the simulated values, additionally to the fit parameters $\mathscr{F}$ and external parameters $\mathscr{P}_i$, the tuple of bias voltage drops $\mathscr{V}_i$ over each serial universal Voigt-circuit element is needed. As indicated, the bias voltage drops $\mathscr{V}_i$ are dependent on the condition i. This is the case, not only since the voltage is inside the tuple of external parameters, but also because the voltage drops are influenced, for example, by different temperatures. The voltage-dependent components in a serial piece of the system are, of course, not dependent on the total bias voltage applied to the entire sample, but instead only the local bias voltage drop over their specific piece, which cannot be straightforwardly extracted from the measurement. This bias voltage drop over each specific serial part k of totally M serial parts is calculated for each condition i through minimisation of the length (Euclidean

norm) of the tuple $\Delta_i^{(V)}$ by varying the voltage-drop tuple $\left(\underline{U}_i\right)^T = \left(U_{1,i}, \ldots U_{M,i}\right)$

$$\Delta_i^{(V)} = \begin{pmatrix} R_1^{(\mathrm{sim,ser})}(\mathscr{P}_i, U_{1,i}, \mathscr{F}, \mathscr{C}) \cdot I_{\mathrm{tot}}(\mathscr{P}_i, \underline{U}_i, \mathscr{F}, \mathscr{C}) \\ \vdots \\ R_M^{(\mathrm{sim,ser})}(\mathscr{P}_i, U_{M,i}, \mathscr{F}, \mathscr{C}) \cdot I_{\mathrm{tot}}(\mathscr{P}_i, \underline{U}_i, \mathscr{F}, \mathscr{C}) \end{pmatrix} - \begin{pmatrix} U_{1,i} \\ \vdots \\ U_{M,i} \end{pmatrix},$$

where $R_k^{(\mathrm{sim,ser})}(\mathscr{P}_i, U_{M,i}, \mathscr{F}, \mathscr{C})$ represents the total dc resistance of the kth serial part from all its dc conduction processes together, at condition i.[2] That is $\mathscr{V}_i = \min_{|\underline{U}_i|}\left(\Delta_i^{(V)}\right)$. Furthermore,

$$I_{\mathrm{tot}}(\mathscr{P}_i, \underline{U}_i, \mathscr{F}, \mathscr{C}) = \frac{U_{\mathrm{bias},i}}{\sum_{k=1}^{N} R_k^{(\mathrm{sim,ser})}(\mathscr{P}_i, U_{k,i}, \mathscr{F}, \mathscr{C})}$$

is the total current dependent on the totally externally applied static bias voltage $U_{\mathrm{bias},i}$. The above described calculations are triggered again and again by the fitting routine with changed fit parameters $\mathscr{F}$ up to the point that the length of the residual vector $\underline{\Delta}^{\mathrm{res}^2}$ is minimal.[3] For simplicity, conditions with an externally applied bias voltage of 0 V are ignored in the fit.

As explained in section 2.4, an essential idea of the analysis introduced in this work is the combination of identical fit constants between different models, e. g. a shared permittivity for the conductive and resistive model or a joint concentration of traps for two different transport mechanisms. In the simple case of joint parameters, this is realised by using the same fit parameter $f_j \in \mathscr{F}$ in both models. Sometimes also derived quantities may be assumed identical: for example, the number of charges in the conduction band might be a shared quantity between resistive and capacitive properties of a depletion layer. Then, also for performance reasons, the same function to calculate the respective value is only executed once (per condition) and its result used in both (or potentially even more joined) models.

[2] This minimisation is performed using the `root` method in the `optimize` library of the SciPy package (version 0.17.0) which is implemented using a modification of the Powell hybrid method just as in MINPACK [77].

[3] This minimisation is performed using the `leastsqbound` method in the LEASTSQBOUND library (version 1.1) which is a wrapper, extending the `leastsq` optimiser in the `optimize` library of the SciPy package (which is, in version 0.17.0, implemented using MINPACK's `lmdif` and `lmder` algorithms) for possibility of boundaries as implemented in the MINUIT package [77].

4 Experimental results and simulations

The presented novel approach of analysing immittance spectra utilising physical models dependent on external parameters is, in this section, exemplary applied on the metal/ta-C/p-Si/metal system. The unique features of the approach, especially the possibility to extract the capacitive and resistive properties of the individual serial pieces as coherent entities, enabled the verification of a particularly interesting hypothesis: The solely remaining quantitative deviation of the Frenkel-Poole model (and its extensions) can be eliminated by a correct calculation of the internal field and that even without fundamentally different assumptions.

In comparison to conventional current-voltage analysis, the knowledge of the immittance spectrum allows distinguishing distinct serial pieces of the system by their corresponding capacitive bypass. On the other hand, electrical-equivalent circuits consisting solely of idealised lumped components, which are usually used in immittance spectroscopy, are ambiguous. Hence, a component of the circuit cannot be uniquely assigned to a piece in the system. The use of external-parameter-dependent immittance spectra allows a one-to-one association of different pieces in the system with separate components in the circuit while containing the full current-voltage information. In this section, the applied bias voltage is the varied external parameter. Consequently, voltage-dependent models for the resistances and (if necessary) capacitances are used to directly extract the physically relevant parameters.

> The pure assignment of different serial pieces of a sample is possible even without the use of physical models. In fact, since the utilised model for a specific piece might not recognise all features, e. g. of the resistance-voltage behaviour, of the corresponding real-world element, the respective resistance and capacitance itself could be extracted undistorted by any assumptions, negligences or deficiencies of the applied model if their values would be redetermined for any condition (to account for a possible deviation from the typical frequency dependence of a constant phase element, even for different frequencies). For latter strategy of analysis, the correct arrangement of idealised-lumped components is *crucial*, because without parameter dependence the circuit is (as mentioned above) unfortunately ambiguous. Also when models are not included, to arrive at the same one-to-one assignment between idealised lumped components and pieces in the system, the arrangement derived in chapter 2 must be used, i. e. each serial component is described by a universal Voigt-circuit element (that is like a conventional Voigt-circuit element, except for the capacitive part which might be complex instead of purely ideal and may contain several polarisation processes).

Voltage-dependent immittance spectra do not only allow the separation of serial pieces

in the system due to their corresponding capacitive bypasses, but they also include the full resistance-voltage behaviour (i. e. also the complete information of the current-voltage curve) of each piece. Hence, the presented approach allows the combined analysis of the resistive and capacitive properties, of each serial piece, as a coherent entity. Consequently, if, for example, a resistive model depends on a capacitive property of the same piece , e. g. its permittivity, it can be extracted directly from the corresponding capacitive part. Similarly, specific features of a piece might influence both, the capacitive and resistive properties, of the corresponding piece. In such a case (which is quite frequent) where the same property might be determined separately from analysing either capacitive or resistive behaviour, the presented approach offers a third opportunity: the joint determination of the feature from both parts. For example in the analysis of experimental data in this work, the acceptor concentration that determines the capacitive and resistive properties of the depletion layer in the low-doped p-type silicon substrate was jointly fitted as a single parameter that could describe both parts well. The joint value for both parts of the thin-film permittivity is, as later explained, of paramount importance for the evaluation of the corrected Frenkel-Poole model, given in this work, and consequently discussed in its own section. The concept of combining parameters (and respectively correlating properties) determinative for the behaviour of both parts, capacitive and resistive, can be used to correlate or cross-check any value affecting both parts, e. g. the thickness of a film. The extraction of correct values for these parameters is, however, influenced by the assumed models. Thus, a comparison of the extracted parameters can also be used to validate the corresponding utilised model itself or its compatibility with the associated (resistive or capacitive) counterpart.

Both major benefits of the presented approach, the separation of the system into its serial pieces and the extraction of coherent capacitive and resistive behaviour, make clear that voltage-dependent immittance spectroscopy offers a valuable complement to conventional current-voltage analysis without the necessity to create specific samples. With respect to conventional immittance analysis, the introduction of process-specific physical models dependent on external parameters leads to unambiguous circuits that allow the direct extraction of the statistically best guess for fit parameters of the model. Furthermore, the respective models weight their region of dominance in the external-parameter-dependent immittance data. As a consequence, data from transition regions can become an equally well source of information as data from regions that are dominated by a single process.

The investigated samples show, according to their doping concentration to varying extent, a significant contribution of a depletion layer in silicon. In the first part of this chapter, the model for the depletion layer in silicon is explained. Certain simplifications in the model lead to identifiable deviations between the measured and fitted immittance spectra. The origin of these deviations could be associated with the presence of traps at the interface and fixed charges in the thin film. Conventional capacitance-voltage analysis is shown to highlight its differences to the proposed model. Additionally, the conventional analysis is found leading to similar parameter for (almost) identical assumptions. Furthermore, for specific extreme cases, the magnitude of the defects at the interface or fixed charges in the thin film are estimated. Additionally, a depth profile of acceptor

concentration in the silicon substrate is shown and its validity discussed. It is found that the substrate has an acceptor concentration within the specification of the manufacturer, though a high number of defects at the interface or in the insulator lead to a strong dispersion that seems to require even higher frequencies (than the maximal frequency of 1 MHz used in this work) to observe an undistorted capacitance-voltage curve which could be used to extract more accurate doping concentrations.

As already mentioned in the beginning, the benefit of a coherent entity of capacitive and resistive information is especially useful to validate an assumption about the permittivity in the resistive part. As more thoroughly discussed in section 5.6 (although the Frenkel-Poole model uses quite basic assumptions that might not be representing the real situation in the material very well) it was found, within this work, that the single remaining quantitative discrepancy in the Frenkel-Poole model, between the theoretically assumed and experimentally obtained barrier-lowering coefficient β, can be explained by introducing a correct calculation of the superimposed internal field. This calculation requires the static permittivity of the material. Due to the above explained fact, that capacitive and resistive properties are jointly measured, the proposed method of analysis is uniquely suited to determine whether our correction is sound. For that, the fit quality and resulting fit parameter values are evaluated for three different models for the thin film in section 4.2.

4.1 Differences between the samples and experimental findings associated with the ta-C/p-Si interface effects

4.1.1 The different substrates, their associated properties and their description

4.1.1.1 Properties that are identical - a prologue

Before preceding to the details about the intentionally differently selected substrates, it is important to notice that great care was taken to ensure that all other properties of the samples are as similar and, hence, as comparable as possible: Samples `1346aCrAu1` and `1346bCrAu4`, whose immittances are shown in Figure 4.1, were both synthesised in the same batch in any production step. That includes every step in the preparation, i. e. the cleaning procedures, all steps of the metallisation of the back contact and the reactive-ion etching of the surface, as well as the coating of ta-C with the preceding *in-situ* sputtering of the surface. For all processes (except for the standard cleaning procedure, which is done without sample holder) the samples were mounted on the same sample holder, specifically including the thin film coating of ta-C. As a result, except for a possible different thickness of the thin film (due to a potential weak gradient of the thin-film thickness over the area of the sample holder), the thin ta-C film on the samples is assumed to have identical properties.

4.1.1.2 The different substrates and the resulting key differences

The ta-C film is grown on *p-type silicon substrates* with different acceptor concentrations, of which two are exemplary studied within this work. The substrate of sample `1346aCrAu1` has a *lower acceptor concentration* (sheet resistance according to manufacturer 1 Ω cm to 10 Ω cm) leading to a strong rectifying behaviour due to the formation of a depletion layer on the silicon side at the ta-C interface (best seen as resistance in the absolute impedance of positive voltages in the first row of Figure 4.1). Based on the formula of Demoulin and van de Wiele [34] and assuming the barrier height extracted from the resistive properties of the sample (the barrier heights are discussed very thoroughly later in section 4.1.2.1), it could be estimated that acceptor densities lower than around $5 \cdot 10^{11}$ cm^{-3} would be required for the formation of an inversion layer at the interface. Although this formula is for regular Schottky diodes, i. e. direct metal/semiconductor interfaces and consequently not necessarily valid for ta-C/Si structures which have a rather low conductivity, this is in agreement with the observed capacitance-voltage behaviour (see deep depletion in high-frequency curves in Figure 4.12). It is, hence, assumed that no inversion layer is present in either of the investigated samples at any condition. As a consequence, the capacitance is modelled to limitlessly decrease with increasing reverse bias voltage. The substrate of sample `1346bCrAu4` has a much *higher acceptor concentration* (sheet resistance according to manufacturer <0.05 Ω cm), hence, showing no rectifying behaviour, but only a small asymmetry between the positive and negative bias-voltage side in the immittance spectra. As the substrate is p-type silicon as well, the

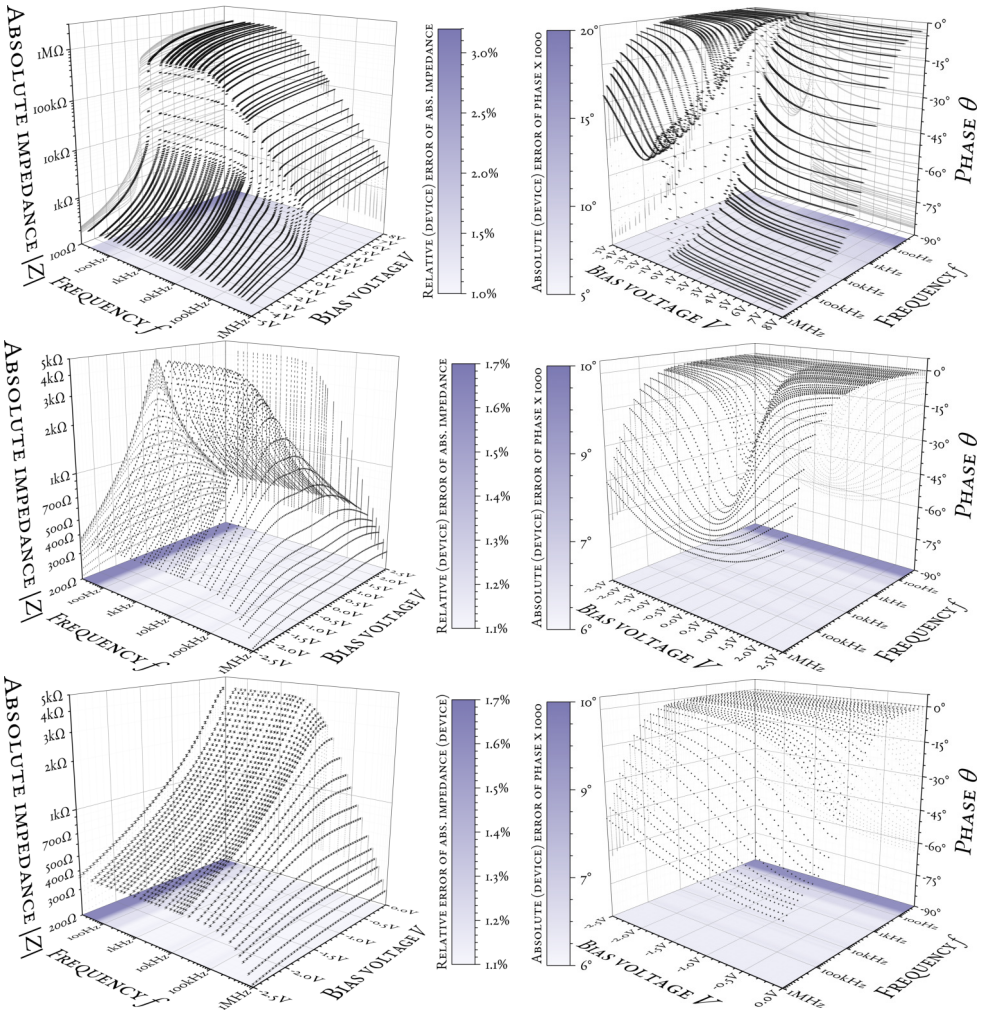

Figure 4.1: Bode plots of the measured immittances for samples `1346aCrAu1`, with low-doped substrate (top row), and `1346bCrAu4`, with highly doped substrate (middle row). The contour plots at the bottoms of the plots indicate the relative (for absolute-impedance plots) or absolute (for phase plots) value of the measurement error calculated according to the specification of the device manufacturer. The negative bias side of the immittance of `1346bCrAu4`, separately shown in the last row, is assumed to be almost unaffected by remaining depletion layer effects. Hence, solely these values are used in fits of latter sample, which is modelled without a separate circuit representing the depletion layer.

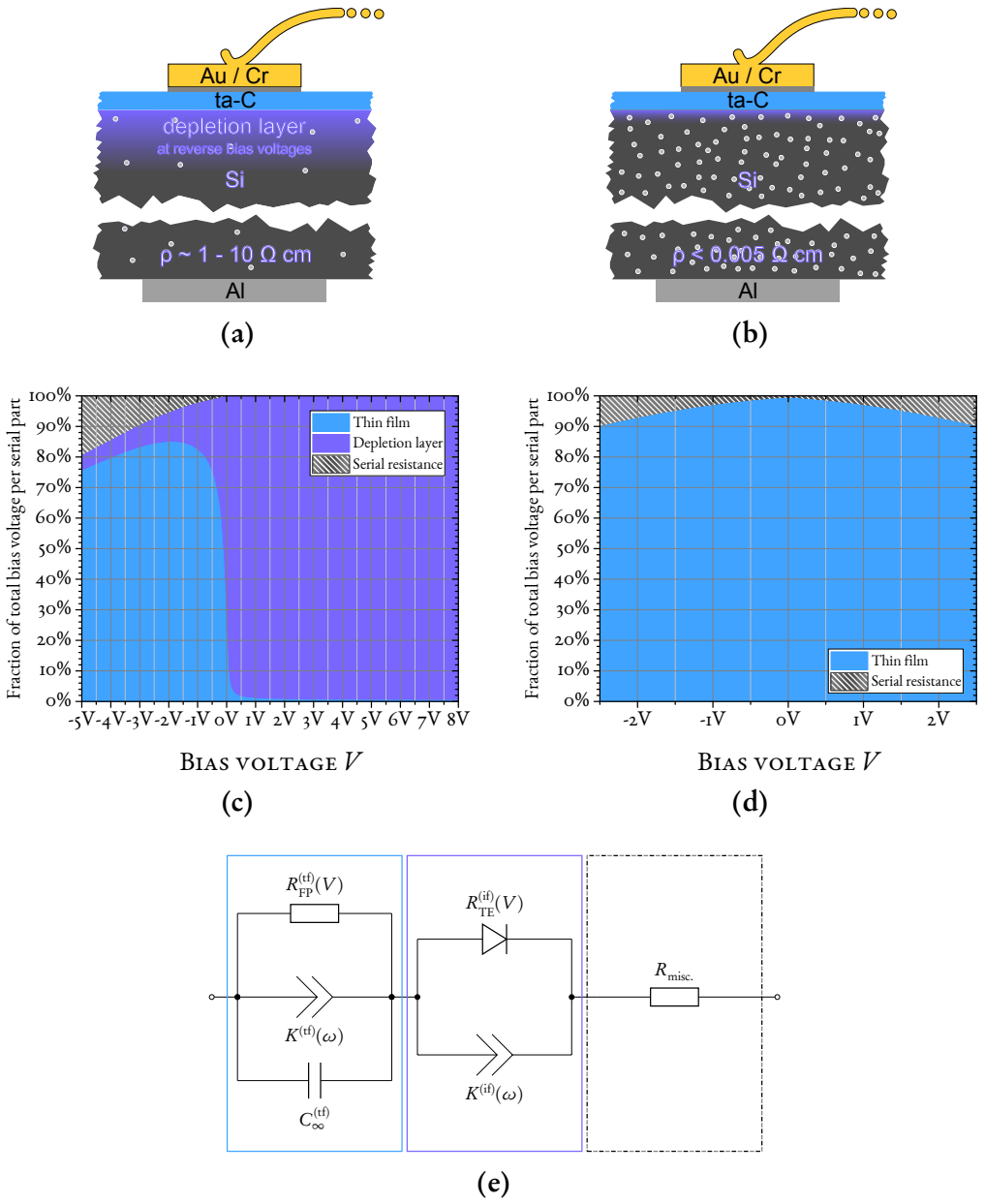

Figure 4.2: (a): Schematic of sample `1346aCrAu1`. (a): Schematic of sample `1346bCrAu4`, the length of its depletion layer is expected to be much shorter, so that it only leads to a slight asymmetry in the resistance-voltage characteristic instead of rectification. (c): Voltage drops over the different Voigt-circuit elements for sample `1346aCrAu1` using Model 3 and fit optimised for the shown sample. (d): As (c) but for sample `1346bCrAu4` where the rectifying part is assumed negligible and, consequently, not modelled. The shown voltage drops are based on models and, hence, their accuracy is based on how well the chosen description resembles the actual system. However, the observations in the measured immittance spectra are in agreement with these voltage drops. (e) A lumped component representation of the model used in this work. The interface description, surrounded by a violet rectangle, is used when modelling sample `1346aCrAu1`. The total serial resistor $R_{\text{misc.}}$ combines all serial resistive contributions with cut-off frequencies much higher than the maximal frequency in the experiment.

absolute impedance of sample 1346bCrAu4 shown in the middle row of Figure 4.1 is slightly larger for positive voltages. Since the distortion, due to space-charge effects in the silicon, should be small for the negative bias-voltage side of the immittance spectra, this side of sample 1346bCrAu4 is assumed to give almost the raw thin-film immittance. Hence, its measured immittance for negative bias voltages is explicitly given in the last row of Figure 4.1. Furthermore, as the depletion layer of this sample is not explicitly modelled: for sample 1346bCrAu4, generally, only the data for negative bias voltages (shown in the last row of Figure 4.1) is fitted.

4.1.1.3 Description of the corresponding depletion layers

According to Sze [176, pp. 254-270] there is a suited analytical theory to model the depletion layer in the low-doped substrate: the thermionic-emission theory of Bethe, extended to account for Schottky-barrier lowering in reverse bias [176, pp. 270-297]. But then, no model given in his book [176] is suited for such a high doping concentration as in 1346bCrAu4. On the one hand, the deviation from symmetry is rather small for the highly doped sample (compare middle row in Figure 4.1). On the other hand, if the best suited model (for very high doping concentrations) would be used regardless of the non-applicability, it would lead to the bizarre situation, that numerous fitting parameters would be used to describe a very small deviation (potentially even only very roughly, since no model in [176] is supposed to be suited for the very high doping concentrations in the substrate of 1346bCrAu4). Going beyond the analytical models given in reference [176] (more complicated numeric modelling might lead to a well enough description even for the highly doped sample) would significantly increase the complexity of the calculations. Though, there is no limit, in the proposed novel method of analysis, for the complexity of the models and, moreover, the computational requirements are expected to be within acceptable expenses, there is a point to which the scope of the work must be limited:

The above described systems are used as example to apply the novel method of analysis on. The properties of the depletion layer in the highly doped silicon are not actually of interest for this work. It was, hence, decided to model the depletion layer in 1346aCrAu1, the sample with low-doped substrate, but not in 1346bCrAu4, the sample with highly doped substrate. The low impurity concentration, as in sample 1346aCrAu1, is more common in the semiconductor industry, can already be sufficiently well (though not completely) described by the above mentioned analytic depletion-layer model, and is also assumed to be of higher scholarly interest. Furthermore, modelling the interface of 1346aCrAu1 already shows that the proposed method of analysis is capable of distinguishing different pieces and extract their respective useful parameters. The idea to use higher doped samples was to obtain the 'purest possible' parameters for the thin film. Since the asymmetry in 1346bCrAu4 would, however, distort the fitting parameters of the thin film, only its forward biased conditions (as shown in the last row of Figure 4.1) are used for analysis. Also, for sample 1346aCrAu1, for which the interface shall be modelled, better models for the depletion layer exist (e. g. confer [180, 185]). It was decided to model the interface with often utilised analytical models to not unnecessarily complicate this exemplary application of the novel approach to analyse samples of multiple pieces with

voltage-dependent immittance measurements. Hence, not the best description possible for the depletion layer was applied. The description is, however, good enough to give a first glance of the potential of this novel approach, while already showing that it can successfully distinguish and describe the interface and bulk parts, though, solving a very common challenge. Furthermore, perfect description of the interface is not the main goal of this work. More important is the proof of concept of the novel approach. If the exemplary system should be investigated further, introducing a more detailed model would be recommended and the next logical step. Especially a model that takes the densities of the traps at the interface and in the thin film into account, should lead to a much better agreement between the fit and measured data. These traps are assumed to be responsible for the major deviations of the depletion-layer model, including a flat-band voltage shift, in this work (confer section 4.1.2). As there is no limit of the complexity of the models, by the presented approach of analysis with voltage-dependent immittance data, the above mentioned more sophisticated (numerical [180]) models might be applied.

In summery, although better models for the depletion layer exist, they were not applied since the focus of this work is the presentation of the new concept of analysis and not on the perfect description of the exemplary sample system. For the description of the remaining 'depletion layer' in the highly doped substrate, more elaborate models would be necessary. Because of the above mentioned reasons, it was decided against the introduction of those models and instead only the experimental data for negative bias voltages (shown in the last row of Figure 4.1) were used in the fits for the sample with highly doped substrate.

4.1.1.4 Assumptions of the used interface model

As explained above, the model describing the immittance of the depletion layer, based on the thermionic-emission theory for metal-semiconductor contacts [176, pp. 255-258], considers some, but not all, relevant effects.

A very important feature, that was necessary to achieve an almost perfect fit of the reverse bias resistance at sufficiently high bias voltages, was the consideration of the *Schottky-barrier lowering*. It was modelled as described in the book of Sze [176, pp. 245-297] or in the work of Hjelmgren [67]. According to Sze [176, pp. 73,96-97,282-284], *edge-leakage currents* are 'the dominant reverse current component' [176, p. 282]. On the one hand, it is possible that the rather large contact area in this work, compared to usually used dimensions in semiconductor devices, significantly reduced the importance of edge-leakage. On the other hand, it cannot be excluded that all extracted parameters are distorted since the actual geometric factor might be different from the one assumed (this aspect is taken up again and discussed considering further arguments at the end of this section). Even so, the field enhancement at the borders of the geometry used in this work could only influence the thin film directly. It should be sufficiently reduced towards the ta-C/Si interface. The fact that the Schottky-barrier lowering, that introduces *no additional fitting parameter* and uses solely literature constants, can lead to a correct description alone, while its voltage dependence is different from that caused by the edge-effect, is a very strong indication that the edge-effect is indeed not relevant in for the depletion layer

of the investigated sample structures, though it might still be of significance for the thin film model.

The intrinsic carrier concentration was taken into account and calculated rather accurately using an empiric formula by Misiakos and Tsamakis [134, Eq. (3)]. Furthermore, the calculation of the probabilities of occupancy of the acceptor levels as well as the bands and all derived quantities took the spin into account and used Fermi-Dirac statistics. Also the band gap was calculated using an empiric formula by Thurmond [179]. The last three features will become more important when the experiment is, as suggested in the outlook, continued with varied system temperature.

An important feature of the approach of analysis of voltage-dependent immittance data proposed in this work is that the different pieces, here the depletion layer, are already isolated by design, i. e. the model accounts for the (within the description) correct voltage drop, serial resistances and capacitances of other pieces as well as other parallel contributions. As a result, the depletion layer can be modelled without influence by other parasitic parts (which are accounted for by other models like for the thin film or even only a serial resistors). This specific advantage becomes especially apparent in section 4.1.2.1, where conventional capacitance-voltage analysis is performed. Although known as a large error source, many works utilising conventional capacitance-voltage analysis ignore the serial resistance and parallel leakage. In contrast, both is modelled (even very sophisticatedly) in the presented approach. If those parasitic contributions are considered in the conventional capacitance-voltage analysis at all, they are usually added afterwards as corrections [19].

Like all models in this work, also the depletion-layer description is an effective media approach.

Though the complexity of the depletion-layer model is not limited by the approach itself, meaning that while more effects could in principle be added, not all attributes were taken into account. Very important features that were not taken into account are associated with defects and their distribution of time constants. All major deviations that can be observed between the fit and the experimental data are likely caused by these simplifications (that especially also affect the capacitive model), associated with the following: defects at the ta-C/Si interface, localised (charged) electronic defects in the thin film, the assumption of a spatially homogeneous, constant distribution of acceptor levels of one energy only, while ignoring any other electronically active localised states, e. g. traps deeper in the band gap. A strong indication for the existence of deeper trap levels, at the interface but possibly also in the bulk silicon far away from the interface, and their relevance can be seen in the frequency-dependence of the acceptor concentration, see Figure 4.14: for low frequencies also deeper traps can charge and discharge during the cycles of the ac signal. They lead to the higher value of an *effective* acceptor concentration. For increasing frequency, lesser deep traps are able to be charged and uncharged until only the shallow acceptors (most likely the deliberately introduced extrinsic impurities) remain, leading to the observable lower bound of acceptor density in the plot. All these ignored types of defects, especially those at the interface and in the thin film, lead to a significant distortion of the 'true' barrier height, easily recognisable in a large difference between the barrier heights extracted from either capacitive or resistive parts of the sample

(indicated in Figure 4.13) and pronounced artefacts in the (later explained) conventional capacitance-voltage analysis, compare Figure 4.16.

Another questionable assumption is that the *area* of the interface should be of the same size as the area of the top contact. It seems likely that the true area at the interface is different to the area of the top contact. Not only because of the expected widening of the field lines, but even much more pronounced than already in a symmetric contact geometry due to the asymmetric geometry, i. e. that the back contact is much larger compared to the top contact. Furthermore, there are likely surface variations (e. g. local variation in surface defect density) leading to regions of higher or lower barriers. It seems safe to assume, that the resistive properties are dominated by the lower barriers, while the capacitive properties are weighted by the respective ratio of the total area of the corresponding barriers [172]. Additionally, the interface region might not be as flat as expected, also changing surface defect densities and effective area of the interface. As a result, a deviation of the assumed area A distorts any (geometry-afflicted) quantity of the interface part.

4.1.1.5 Combined fitting of both samples

Due to the assumed almost identical thin-film properties, the approach was to fit both samples combinedly (their voltage-dependent immittance spectra are compared in Figure 4.3): while the sample with highly doped substrate `1346bCrAu4`, that is always restricted to its negatively biased side, is modelled with an EEC without the diode circuit in series to the thin film, the sample with low-doped substrate `1346aCrAu1`, on the other hand, has an additional diode circuit in series. Except for the thickness of the thin film that, as discussed above, might slightly vary laterally over the sample, and the ideal Ohmic total serial resistance, that also includes the resistance of the bulk silicon and its back contact which are both likely influenced by the changed doping concentration, *all other parameters*, i. e. the parameters for the immittance of the thin film, are *shared* for both samples.

Possible consequences for the serial resistance in the highly doped sample It might be expected that omitting separate modelling of the remaining depletion-layer contribution in the highly doped sample system (`1346bCrAu4`) might lead to an overestimated total serial resistance $R_\mathrm{s}^{(\mathtt{1346bCrAu4})}$ in the highly doped sample system with respect to the total serial resistance $R_\mathrm{s}^{(\mathtt{1346aCrAu1})}$ in the low-doped sample system (`1346aCrAu1`). Without this possible overestimation, the total serial resistance should be lower for the highly doped sample, because a major contribution is assumed to be due to the bulk substrate resistance, which should be decreasing with increasing acceptor concentration. However, at least for the sample with low-doped substrate, the voltage drop over the depletion-layer part is still significant, compare forward-bias region in Figure 4.2c. Consequently, though much less pronounced, the remaining depletion-layer contribution for forward bias voltages of the highly doped sample, although actually voltage-dependent, might, due to the omitted part to represent it, be falsely ascribed to the total serial resistance of the highly doped sample which makes this value possibly incompatible between samples.

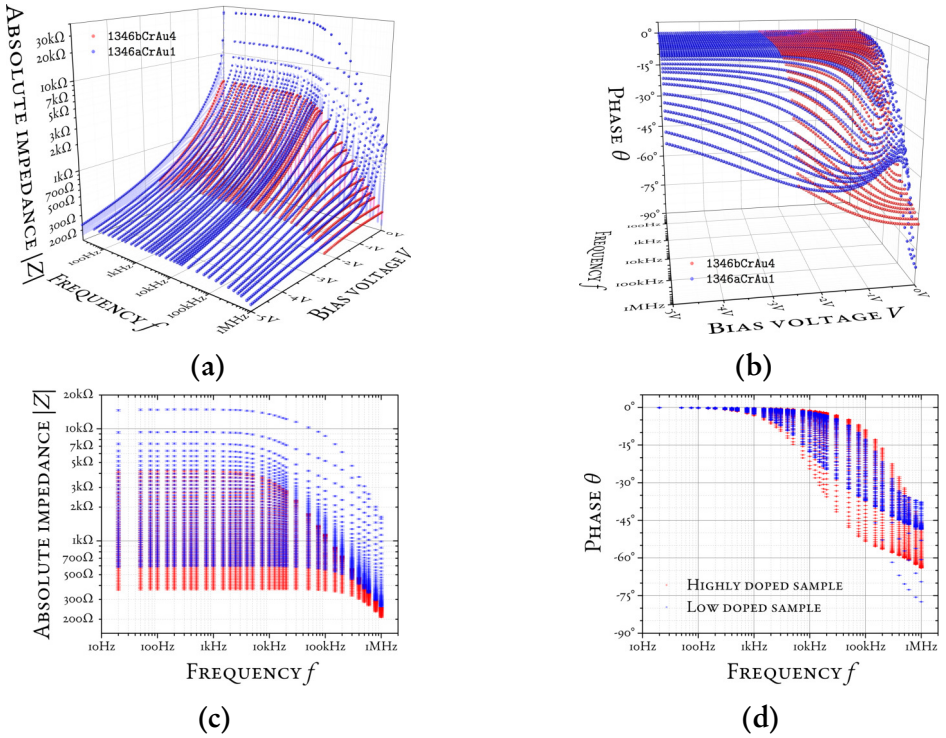

Figure 4.3: Comparison of the measured impedances of samples `1346aCrAu1` (blue, *low doped substrate*) and `1346bCrAu4` (red, *highly doped substrate*) for negative bias voltages at which thin-film properties are most prominent. Two dimensional projections of the full parameter space of absolute impedance (a) and phase (b) on the $|Z|$-f and θ-f planes, respectively, are shown in Figures (c) and (d). The absolute impedances of sample `1346bCrAu4` are always lower at identical conditions. Also after the cut-off, the absolute impedance follows a parallel straight line with lower values as compared to sample `1346aCrAu1`, indicating a larger capacitance or, assuming otherwise identical properties, a smaller thickness of the thin film. A thinner ta-C film, which might be caused by a slight lateral thickness gradient during the simultaneous deposition process, would also be in agreement with the generally reduced resistance and the observed steeper slope. As a result of the simultaneous processing (cf. sections 3.1 and 4.1.1.1), different permittivities or trap densities should be less likely. Important to note is the obviously depletion-layer-specific artefact most prominent in the phase plots, specifically (b): unlike the phase of `1346bCrAu4` which may be interpreted as the sole thin film phase, `1346aCrAu1` shows a fold in the phase that, with increasing frequency, increases in width and shifts the maximum to absolutely higher voltages. In this region, plots of sample `1346aCrAu1` show a pronounced deviation. It is shown in this section, that this artefact (connected to the shift of and stretch-out around the flat-band voltage) is caused by the influence of interface traps and charged defects in the thin film on the depletion-layer characteristic, which are currently not included into the depletion-layer description.

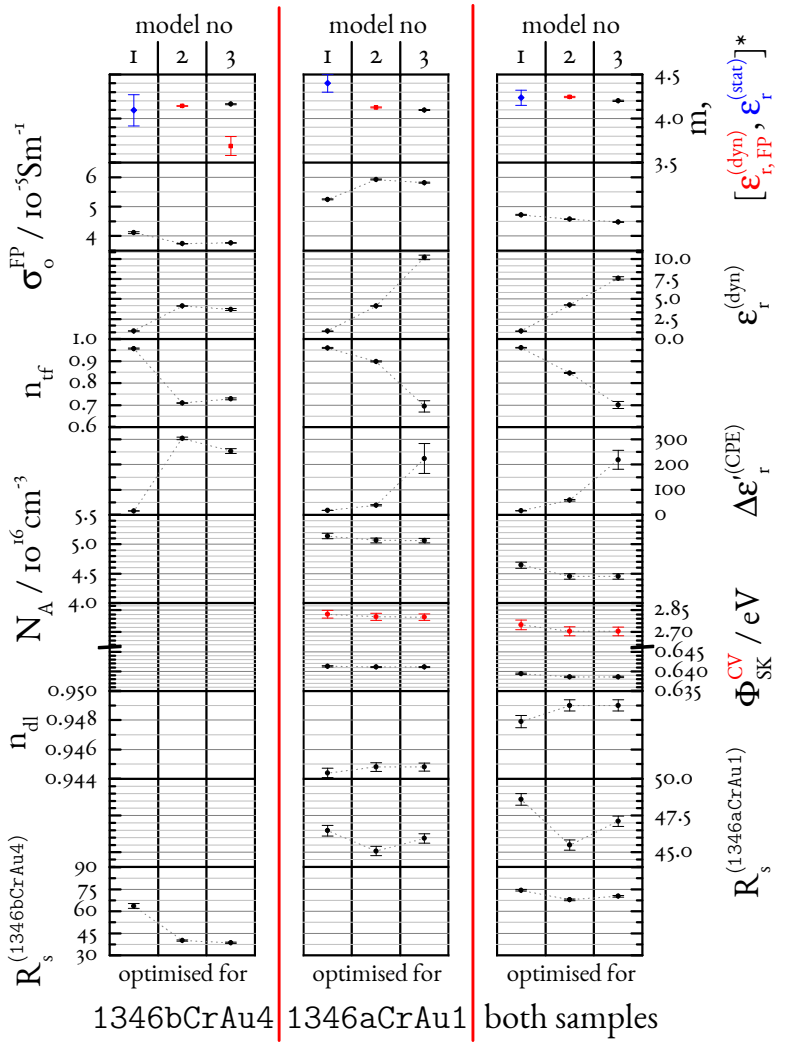

Figure 4.4: The development of fit parameters for the three different models while optimising for each sample separately as well as combined. The permittivities of the thin film of models 1 and 2 are converted to be comparable with the parameter m that combines the influence of all permittivities in the barrier-lowering coefficient (including the conversion to internal permittivity). As explained in the text, the Schottky-barrier heights Φ_{SK} for capacitive and resistive parts are separately optimised. The (absolutely) larger value for the capacitive part of the model can be explained by traps at the interface or in the insulator that shift the flat-band voltage towards even lower bias values. Since the contributions by different types of traps cannot be distinguished using the available data, it was not necessary to fit the defect concentrations rather than just using different barrier heights, see section 4.1.2.1.

In Figure 4.4 both total serial resistances for different models are compared (in the last two rows). Indeed, for the sample-specific optimisations (in the first two columns of Figure 4.4), the fit with Model 1 leads to a larger total serial resistance for the highly doped sample as compared with the low-doped sample, i. e. for Model 1: $R_s^{(1346bCrAu4)} > R_s^{(1346aCrAu1)}$. But, for all other models, where the optimisation was performed separately for the individual samples, the total serial resistance is lower for the sample with highly doped substrate, i. e. $R_s^{(1346bCrAu4)} < R_s^{(1346aCrAu1)}$ for Model 2 and Model 3. From the fact that this larger value for the total serial resistance $R_s^{(1346bCrAu4)}$ for the sample with highly doped substrate seems to be *exclusive to the first model*, it can be concluded that this deviation is a result of Model 1 itself rather than caused by the possible overestimation due to the not separately described depletion layer contribution. In fact, although the values for the total serial resistance of the sample with highly doped substrate are lower, for the two other models, the values might still be overestimated, but at least not as much as to lead to a reversal of the expected sizes. Besides being the only model that leads to the reversal of the expected sizes of the total serial resistances, there are further arguments leading to the conclusion that Model 1 does not describe the underlying physics correctly, see section 4.2 and especially the subsection 4.2.3.

The last column of Figure 4.4 shows the total serial resistances of the samples that were obtained by a combined optimisation of both of them. As explained in section 4.2.3.2 and seen directly in resistance-voltage plot of a fit optimised on both samples in Figure 4.23, although the density of points is identical for both samples, due to the broader range of applied voltages for the sample with low-doped substrate, joined thin-film parameters are preferably optimised on the sample with low-doped substrate `1346aCrAu1`. This can be seen in the resistance-voltage curves in Figure 4.23, where the fitted resistance-voltage curve does not follow the measured data of the sample with highly doped substrate very well, while the resistance-voltage characteristic of the sample with low-doped substrate is almost perfectly reproduced. The total serial resistance is a parameter determined separately for both samples. In the combined fits, its value is generally higher for the sample with highly doped substrate as it is in individual fits for the sample alone. This higher value of the total serial resistance $R_s^{(1346bCrAu4)}$ compensates for two conspicuous deviations between fitted and experimental values of the sample with highly doped substrate `1346bCrAu4`, in case of an optimisation of the combined sum of residuals: First, the deviation of the slope of the resistance-voltage curve that can still be seen in Figure 4.23. Secondly, and as found by fitting either only the resistive or capacitive parts of the immittance most importantly, the higher value compensates for the otherwise larger deviation in the cut-off frequencies. In the light of this, the generally higher total serial resistance from the combined fits should not be overrated, as it can be identified as an artefact, caused by differences between the thin-film pieces in the different samples that evidently cannot be explained by varying the thickness of the thin film alone. Indeed, this means that the separate fits should generally be the first choice for the extraction of parameters and, further, that the thin films of the two samples might not be as similar as previously expected. Assuming the thickness of the thin film to be the only difference between the thin-film parts of both samples, hence, seems insufficient. The observed form of deviation, a constant offset

in the semi-logarithmic resistance-voltage plot indicates a constant value subtracted in the exponent (as compared to the exponent of the sample with low-doped substrate). It would, however, be very unusual that the barrier height of the bulk traps in the ta-C, deposited by MSIBD, could be influenced in that way by the underlying substrate.

In summary, though the effect of omitting the immittance of the interface for the analysis of the sample with highly doped substrate might lead to an overestimation of the total serial resistance, it does not lead to such a high value that it becomes larger than the total serial resistance of the low-doped sample. In all cases where the latter was true, it could be identified as another artefact, e. g. either of a poor connection between capacitive and resistive parts of the thin film or as a result of the compensation of the effect that combined fits always resemble rather the sample with low-doped than the sample with highly doped substrate.

4.1.2 Deviations in the description of the ta-C/Si interface

In this section, different strategies to handle systematic deviations are presented at the example of two deviations in sample `1346aCrAu1` most likely linked to an insufficient description of the depletion layer (likely caused by omitting the effects of traps at the interface and in the thin film). Possible origins of the deviations are presented and used to motivate the different strategies of dealing with the deviations.

This is done in detail, since for the here proposed analysis of immittance data, jointly for capacitive and resistive parts and utilising global optimisation using process-specific external-parameter-dependent physical models, systematic deviations are expected to occur much more frequently as in the conventional analysis, especially during the process of finding the correct model. The more frequent occurrence of these deviations should not lead to an early dismissal of this novel analysis. Conventionally, fits to extract similar parameters are performed only at a certain region in parameter space, where the discrepancy from the assumptions of the model are minimal and, hence, a good agreement can more easily be achieved (e. g. confer the different methods of determining the barrier height [176, pp. 270-297] where only specific regions are fitted or the fact that commonly only two frequencies are used to determine trap concentrations and the flat-band voltage from capacitance-voltage measurements [138, pp. 383-388]). Within the measured parameter regions of the proposed method, also transition regions between two different dominant models might occur. Especially and unavoidably also between resistive and capacitive models that are usually not applied in combination in a single fit. Hence, unexpected deviations might appear in these, usually neglected, areas. The decision whether to ignore those regions, extend the model or keep the area of deviation within the fit (e. g. if the selected model is a first order approximation for the respective region) depends on the individual situation.

Furthermore, the different methods of determining the identical physical parameter might lead to methodical discrepancies of the same value: There are only very few examples where both, capacitive and resistive analysis, is used to extract the same physical parameters. A very prominent one is the extraction of the properties of interface regions

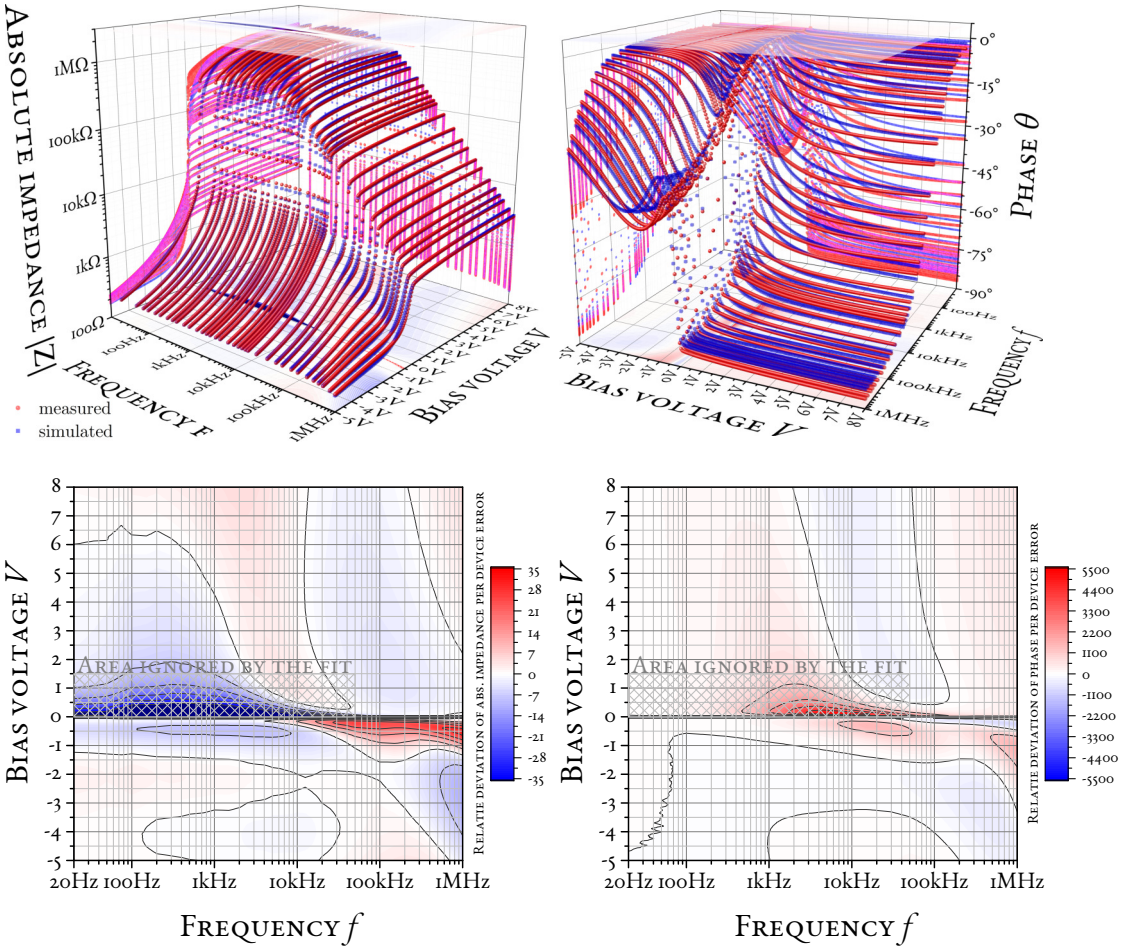

Figure 4.5: Measured and fitted values of absolute impedance and phase for sample `1346aCrAu1` and their corresponding deviations using thin-film Model 3 in an individual fit of the sample. The separately given deviation plots are repeated inside the 3D plot as projections above and below the three-dimensional data. Reasons for the seemingly striking magnitudes in deviation plots are discussed in subsection 4.2.3.1.

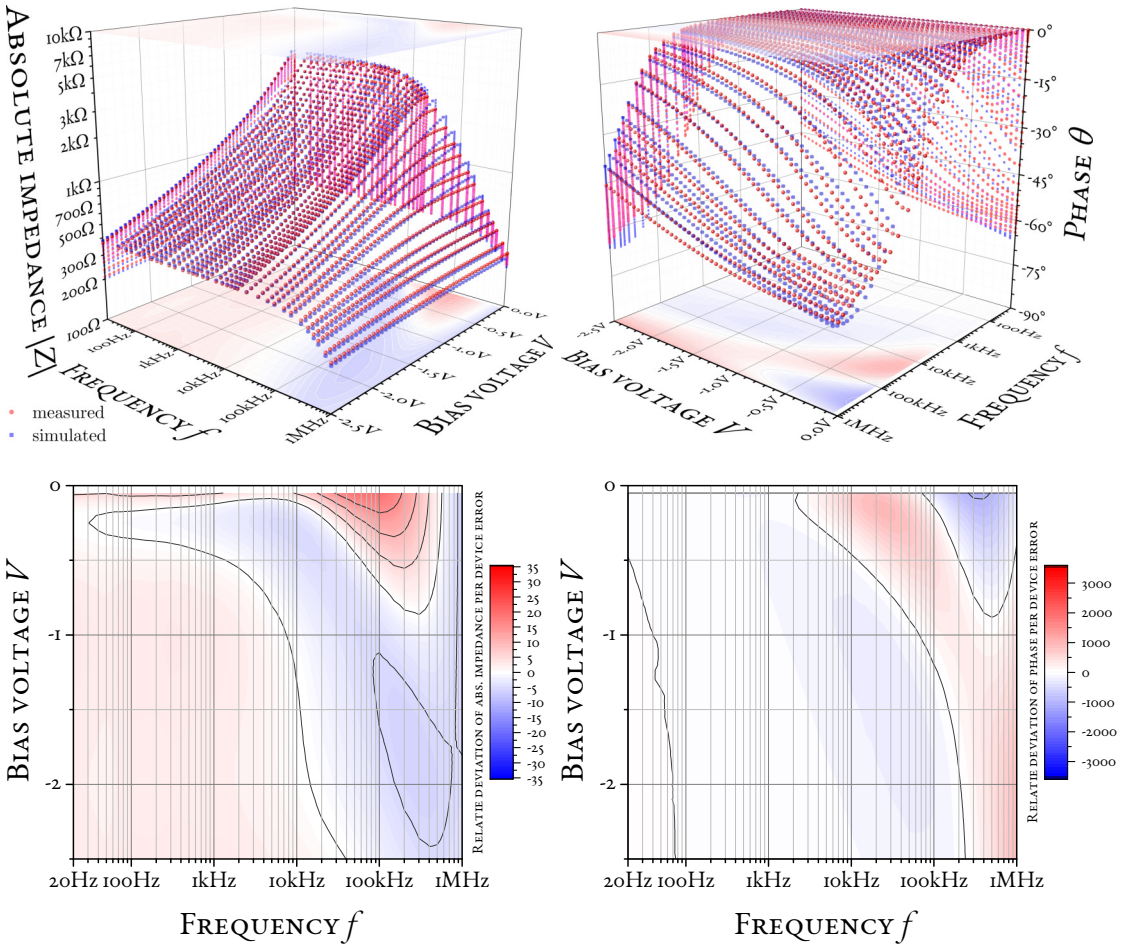

Figure 4.6: Measured and fitted values of absolute impedance and phase for sample `1346bCrAu4` and their corresponding deviations using thin-film Model 3 in an individual fit of the sample. The separately given deviation plots are repeated inside the 3D plot as projections above and below the three-dimensional data. Reasons for the seemingly striking magnitudes in deviation plots are discussed in subsection 4.2.3.1.

between (somewhat different)[1] semiconductors or a semiconductor and a metal. Dependent on whether the resistive or the capacitive methods are used, the analysis is performed either at static conditions or, respectively, at frequencies in the kilo- or megahertz range. As a result of the disjunct regions in the parameter (here: frequency) space, these models might not be suited for one another: While in the static case all traps are occupied according to the corresponding equilibrium, the (low-frequency) capacitive method measures the continuous capture and emission of charges in the traps as an additional (displacement) current, often approximated as a capacitor parallel to the actual depletion layer capacitance. The example continues as a discrepancy between high- and low-frequency conditions in the corresponding capacitance-voltage characteristics. As a result of the energetic and spatial distribution of the traps, also the time constants of the traps are distributed, i. e. the parallel capacitance is dispersive (dependent on frequency), and may be neglected for sufficiently high frequencies (typically in the MHz range [138]). Models not incorporating the contribution of these traps will unavoidably lead to different values of the extracted parameters, e. g. the Schottky-barrier height or the acceptor concentration. Indeed, commonly used models for capacitance-voltage and current-voltage modelling do not take the different trap concentrations into account: the resistive and capacitive approaches to extract the Schottky-barrier height presented in the well known and often used reference [176, p. 279-288] will lead to increasingly different values for an increasing interface trap density. As a result, the extracted Schottky-barrier heights of the different models are not compatible. The conventional strategy in capacitance-voltage analysis is to calculate the trap densities of the interface and fixed charges in the 'insulating' thin film from the flat-band voltage shift of a high- and a low-frequency curve [138, pp. 462-489]. Although these calculations might not directly have the form of an analytical model, they might be brought in such a form, provided at least some simplifications are possible, e. g. the assumption of a spatially homogeneous distribution of traps in the insulator. Otherwise, numerical models are required. Their application is, as already explained, entirely possible in the presented approach. The discussion about above-mentioned aspects, capacitive properties of the investigated system as well as conventional capacitance-voltage measurements in general, will be continued in section 4.1.2.1.

An expected deviation appearing, not only in the presented, but also in the conventional approaches, is due to the design limits of a model. Sometimes, not all relevant effects have been or can be recognised. For example, the (resistive and capacitive) depletion-layer models used here knowingly neglect the variation of the acceptor concentration with depth, which might not recognise the real situation. In the presented approach, residuals and deviations are plotted over the external parameters. On the assumption that the affected regions indicate certain processes or conditions, this might help to identify the limits of a selected model resulting from false or neglected assumptions.

Finally, at the beginning of the analysis, in most cases, not all relevant models are already known. Usually, they are identified, and subsequently introduced, in the order of recognisability and dominance in the measured parameter region. Hence, during this

[1] Meaning, that the difference might also be only in the type of doping and not necessarily in completely different semiconductors.

process of finding a good enough description (before all necessary models are identified), systematic deviation will inevitably occur. Their positions in residual or deviation plots over the external parameters are again supposed to be a valuable resource for the identification of the physical models or processes missing up to that point.

Handling the different deviations For reasons discussed later in this section, it seems that the model for the immittance of the interface piece does not describe all observed characteristics (see Figures 4.5, 4.7, 4.9, 4.19 and 4.20). Especially the steep slope of the diode resistance between 0 V and 1.5 V, designated INTERFACE DEVIATION 1 (compare illustration in Figure 4.8), and possibly also what looks like a capacitance-voltage stretch-out for forward bias voltages close to 0 V at frequencies above around 10 kHz, designated INTERFACE DEVIATION 2 (schematically shown in Figure 4.8), show pronounced deviations.

As a consequence for the interface deviation 1 (present only in sample `1346aCrAu1`), its residuals in the bias-voltage range between 0 V and 1.5 V up to the frequency of 50 kHz, are not part of the sum of residuals that is minimised by the fitting routine. This leads to an excellent agreement of the areas of the resistance which are supposed to be actually described by the model. In Figure 4.9, the reverse-bias resistance is in excellent agreement with the measured data for voltages sufficiently larger than those of the ignored area. Not ignoring the region of interface deviation 1 leads to a compromise, minimising the deviation around zero but, also, leading to a false tendency in the area of high reverse bias voltage, that in Figure 4.9 has an excellent agreement. Since the depletion-layer model includes the field-assisted barrier-lowering due to the Schottky effect and the impurities at and around the interface play a decreasing role with increasing voltage, the model is assumed to give a better description at high reverse bias voltages. As a result from ignoring the unsuited region in the fit, the model shows that it can lead to excellent agreement in the area that it is supposed to describe and also the tendency seems correct. Consequently, also the parameters extracted from, the suited region of, this fit are assumed to be as undistorted as possible (without introducing more refined models).

Generally, including a region to the fitted data with a behaviour which cannot be described by the correspondingly utilised model would distort the fit parameters of the regions that are actually represented by the model. As a result, the above mentioned region was excluded from the fit while its hypothetical, however, ignored residuals and deviations are still given in the correspondingly marked areas in the respective plots. In the next section, possible reasons for interface deviation 1 are suggested and it is discussed in detail why this lead to the decision to exclude this region from the fit.

The origins of the second major discrepancy, interface deviation 2, are much clearer as those of the first one. Due to the form of the deviation and its origin, its residuals remain in the total sum of residuals. In subsection 4.1.2.1, the likely origin of the deviation is explained and the corresponding decision to let the affected residuals remain in the fit argued.

interface deviation 1 and why the affected area is excluded from the fit Interface deviation 1 is caused by a deficiency in the utilised *resistive* model, as can be seen at the suboptimal

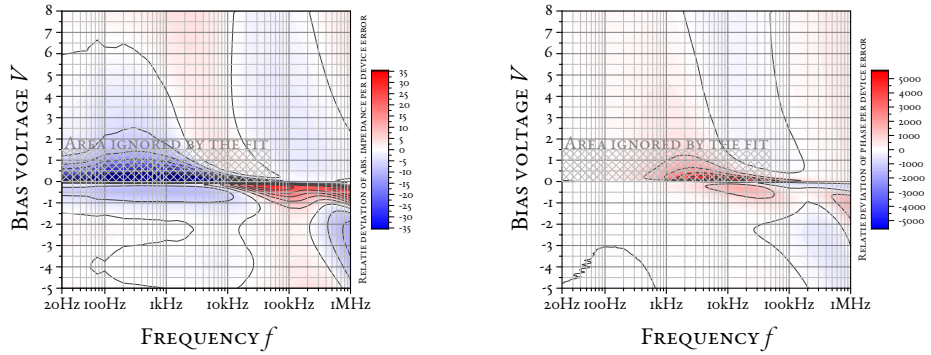

(a) Model 1, abs. impedance

(b) Model 1, phase

(c) Model 2, abs. impedance

(d) Model 2, phase

(e) Model 3, abs. impedance

(f) Model 3, phase

Figure 4.7: Deviation plots for absolute impedance and phase, normalised on the respective device error, for each of the three models, optimised on the shown sample `1346aCrAu1` with low-doped substrate. Interface deviation 1 is inside the region ignored by the fit. Interface deviation 2 can be found starting at negative bias voltages close to zero from frequencies around 10 kHz and continuously expanding towards more negative bias voltages with increasing frequency. The affected region for deviation 2 can be seen more clearly in the contour plot in Figure 4.16. Both deviation regions are further schematically shown in the illustration in Figure 4.8. Reasons for the seemingly striking magnitudes in deviation plots are discussed in subsection 4.2.3.1.

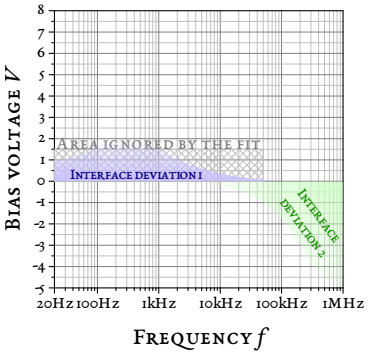

Figure 4.8: The regions of interface deviation 1 and 2 shown schematically on the parameter plane spanned by bias voltage and frequency.

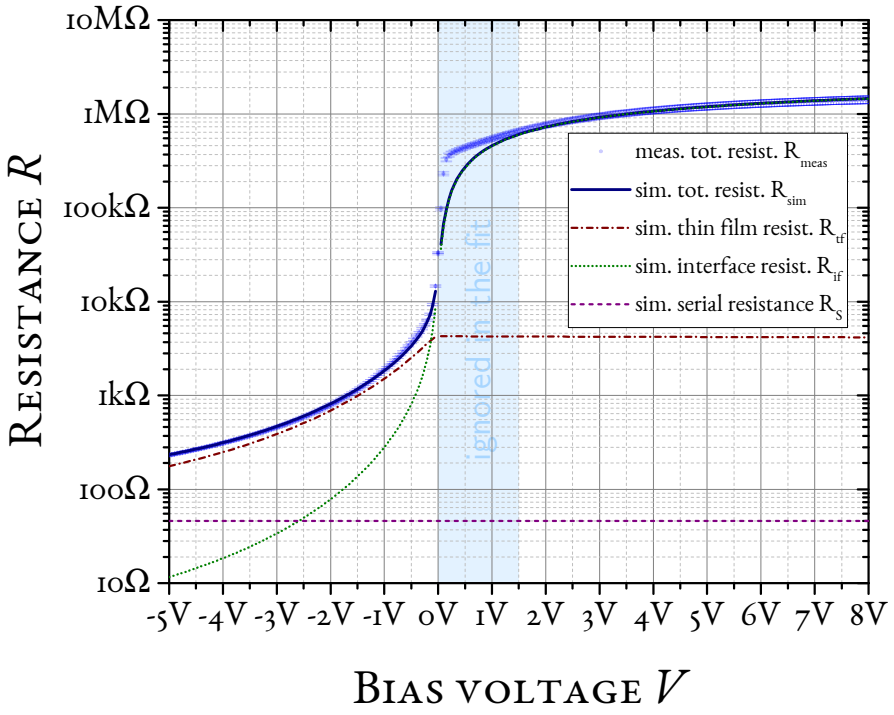

Figure 4.9: Resistance-voltage curve of sample `1346aCrAu1`: Measured data compared with the simulated data also including its individual contributions. The latter was calculated utilising the parameters from an individual fit of the corresponding sample using thin-film Model 3. It can clearly be seen that the deviation in the ignored area is associated with the resistance. The corresponding voltage drop over the different pieces is shown in Figure 4.2c. The negligible voltage drop for reverse bias conditions on other circuits than the one of describing diode explains the almost voltage-independent progression of the thin-film resistance in that region. The abbreviation 'sim.' stands for 'simulated', 'tot.' for 'total', 'resist.' for 'resistance' and 'meas.' for 'measured'.

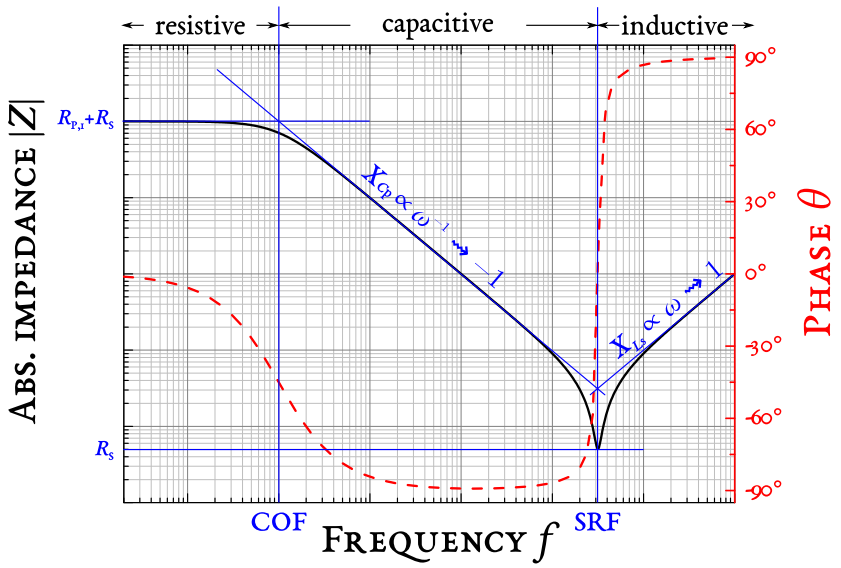

(a)

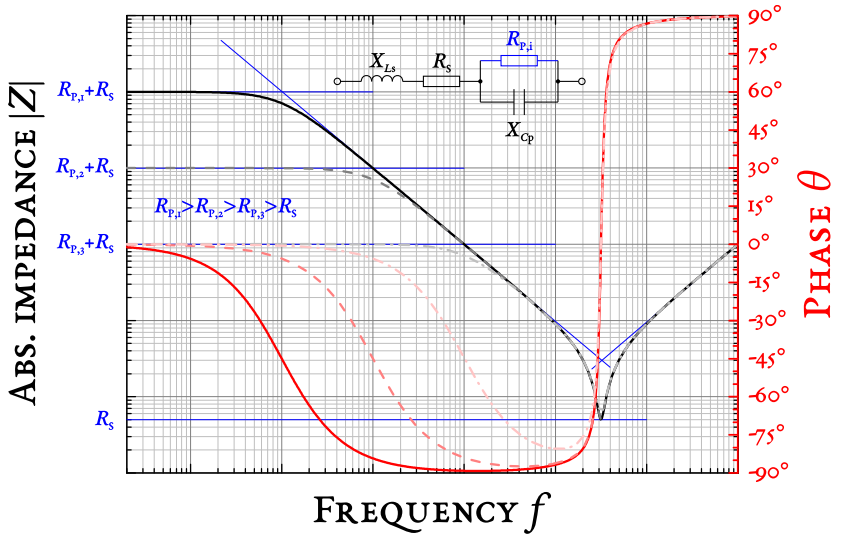

(b)

Figure 4.10: Bode plot (absolute impedance and phase versus frequency) for the circuit shown as inset in (b); (a) introduces the key parameters *cut-off frequency* (COF) and *self-resonant frequency* (SRF), furthermore, *resistive*, *capacitive* and *inductive regions* are defined, after [2, p. 64]. In (b) the response of the circuit for various parallel resistances $R_{P,i}$ is illustrated, after [2, p. 69].

agreement of the transition from forward to reverse bias in Figure 4.9. The phase deviation plots of Figure 4.7 clarify that this is a deviation exclusively associated with the resistive part, because the discrepancy of the affected area is non-existent at low frequencies. This is not at all surprising, since at sufficiently low frequencies any part is resistive and the *phase* gives no information whether there is an agreement in resistance or not. At higher frequencies, especially from around 1 kHz up to 50 kHz, there is a pronounced deviation in the phase. This is a direct consequence of a false resistive description in combination with an accurate capacitive description. The cut-off frequency, a measure for when the resistive part ends and the capacitive part begins (see Figure 4.10a), is determined by both resistance and capacitance. A different resistance leads to a different frequency of entry in the capacitively dominated region (see Figure 4.10b). Hence, the observed phase deviation is solely due to the discrepancy in the transition from resistive to capacitive part. This can be seen by two facts: First, the deviation fades for higher frequencies because of the correct description of the capacitive part itself. Secondly, the severity of deviation is coupled to the magnitude of discrepancy of the resistive part, compare with Figure 4.10. The modelled resistance is too low, as already explained clearly visible in Figure 4.9. With decreasing resistance the cut-off frequency increases. Hence, the larger the difference of the simulated resistance (i. e. the lower the simulated resistance compared to the actually measured one), the later the transition to the capacitive part and, finally, the longer the frequency region of incorrect phase. This does explain the form of the phase deviation,[2] since it is longer in frequency direction the closer the bias voltage converges to zero, just as the resistance is increasingly underestimated towards zero bias, compare resistance deviation in Figure 4.9 and range in frequency of the phase discrepancy in Figure 4.7.

The resistive model can obviously not correctly describe the onset of the reverse bias region. The much steeper slopes in the ignored area are assumed to be associated with the depletion-layer contribution and would, in consequence, correspond to significantly higher Schottky-barrier heights as those determined by the current-voltage analysis from reverse bias voltages greater than around 2 V, i. e. outside of the ignored region. Indeed, these higher barriers would rather be in the magnitude of the barrier heights extracted from the capacitive part of the measurement (see Figure 4.13 and its corresponding section 4.1.2.1). However, these unrealistically large values (compare with other barrier heights for materials on silicon given in the numerous figures and the table in [176, pp. 270-296]) are likely caused by the negligence of any defects at the interface or in the 'insulator', see section 4.1.2.1. As explained later, this flat-band voltage shift in negative direction is associated with positively charged defects [138, pp. 423-428]. The same effect, that also leads to a discrepancy between the barrier heights extracted from resistive or capacitive methods, might also be explained without any traps at the interface or in the 'insulator' but instead by a distribution of Schottky-barrier heights [172]. Latter can, however, not explain the observed resistive behaviour. For lower bias voltages the slopes are steeper, indicating a higher Schottky-barrier height. However, there seems to be no reason that the current should be at first limited by the higher barriers but then only for higher

[2] At least in a zero order approximation, neglecting the voltage and frequency dependence of the depletion layer capacitance, which of course influences the form of the deviation as well.

voltages by the lower barriers. Reasonably, the current should for a parallel arrangement of resistors, as the different barrier heights are expected to be arranged (because they represent different parallel paths through the interface), always be limited by the lower resistances. This deviation, like the other one major discrepancy from the model in the diode part, might, hence, much more likely be caused by the large number of defects at, what especially in this case (e. g. due to the synthesis process and omission of any passivation or annealing processes) clearly is, a non-ideal interface. Possibly, also more accurate diode models may reduce the deviation. Expected deviations from an ideal, defect-free, interface are discussed in the next three subsections.

4.1.2.1 Insights from *conventional* capacitance-voltage analysis

Comparability of the extracted parameters The models for the capacitive and resistive description of the depletion layer, used in the presented approach, do not include the effects of traps at the interface or in the insulator. Consequently, for direct comparison of the extracted parameters, the models chosen for the conventional capacitance-voltage analysis, performed in this section, do not include these effects either.

> Despite the fact that the presence of these defects has significant influence on the capacitance-voltage characteristic and, as a result, seriously changes the values of extracted parameters [138], it seems that it is not uncommon to neglect the influence of defects at the interface or in the insulator, even though the capacitance-voltage method itself played a crucial role in the history of identifying as well as analysing traps in the insulator [138, p. 444] and, in fact, an important role in the investigation of metal/oxide/semiconductor (MOS) structures, in general [161, p. 128]. A possible explanation is that the improvement of processes development, especially including procedures for oxide growth, thermal annealing and passivation of defects, lead to such low concentration that for metal/oxide/silicon devices their consideration became really unnecessary (according to Schroder the 'interface trap density is usually negligibly low for properly annealed, high quality SiO_2-Si interfaces' [162, p. 90]). This might explain why Sze chose to mention the discrepancy between barrier heights extracted from resistive or capacitive analysis with only two sentences in his book (see [176, p. 292]). Furthermore, in his description of the capacitance-voltage method [176, p. 286-288] only the formula ignoring any defects at the interface is given. Possible distortions of the flat-band voltage extracted from Mott-Schottky plots are discussed in the work of Cardon and Gomes [19]. Also they seem to see the usual capacitance-voltage method as being 'based upon the validity of the Mott-Schottky relationship' [19, p. L63], which does neglect any influence of defects. Subsequently, possible deviations from this ideal relationship are discussed. Also the publication of Guenther *et al.* [59], that introduces a more refined approach of extracting the actual capacitance of the depletion layer from the immittance data, does ignore the contribution of defects (though, they assume that their approach should still work when defects are recognised).

In the following paragraph, it is confirmed that the interface properties of the sample

system are dominated by defects at the interface or in the insulator. Magnitudes for the defect concentration in the insulator and at the interface are estimated. However, with the available experimental data (which is neither dependent on temperature nor does it include a thin-film thickness variation) a differentiation between the two different types of defects is, unfortunately, not reasonably possible, so that the given magnitudes are only valid in the extreme cases where only one type of defect is solely responsible for the interface properties. Generally, the conventional approach cannot gain more information from the data than the presented approach. Hence, the conventional analysis is not shown to extract further information, but rather to understand why precisely these values for the fit parameters were obtained with the presented approach. Any more refined analysis performed in the conventional way could also be included into the models used in the novel approach of analysis using voltage-dependent immittance data that is presented in this work.

Differences to the conventional characterisation of MOS structures The conventional analysis of capacitance-voltage curves in this section uses the assumption of a parallel arrangement of a capacitor C_p and a resistor R_p to convert the measured immittance into a capacitance.

To extract the capacitance for a subsequent capacitance-voltage analysis, it is quite common to interpret the system as a two component circuit consisting of one resistor and one capacitor [59]. There are two possible arrangements of the circuit elements: in series or parallel. The serial arrangement is better suited in a low impedance rage (up to around 100 kΩ), whereas the parallel representation is preferable at high impedances (starting from approximately 2 kΩ) [88].

For the intended analysis, the most important region for which the capacitance should be extracted is the depletion-layer region. It dominates the impedance at bias voltages larger than −1 V. Most of its low-frequency response has impedances that are much larger than acceptable for the serial-circuit, i. e. the R_s-C_s, approximation. For the parallel arrangement, on the other hand, the impedances of the depletion layer are in the required range for all frequencies. Furthermore, even the impedance of the thin film for sufficiently small negative bias voltages is within the acceptable region for the R_p-C_p approximation. Hence, the parallel circuit allows the extraction of the capacitance in the relevant range of parameters without a potential intermediate change in model. Furthermore, utilising the serial arrangement of resistor R_s and capacitor C_s is not recommended in this work, since the thin film is not sufficiently insulating to approximate it as a completely blocking electrode, which is implied by this arrangement (since no current may flow for dc conditions). Still, the selected parallel two-component approximation cannot describe the system at high forward bias voltages, where the total serial resistance and the thin-film immittance dominate the response of the system. Sometimes an addition serial resistance is included to enhance the description, which can result in more accurate extracted capacitances [138, pp. 222-226], [59]. If an additional serial resistance to the parallel arrangement is introduced in the conventional approach, at all, it is assumed to be ideal, i. e. not dependent on voltage and without parallel capacitive bypass. As known from the properties of the

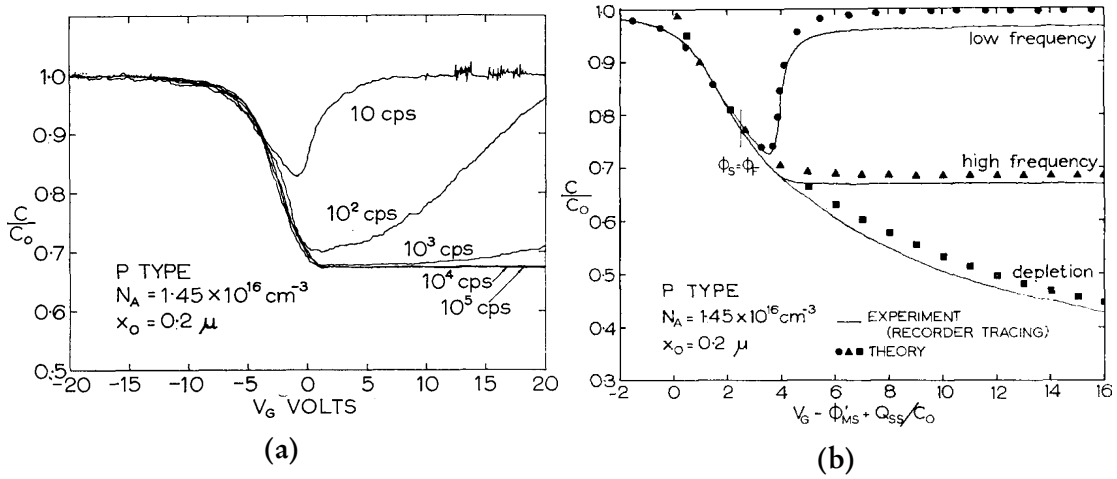

Figure 4.11: In (a) a typical frequency-dependent capacitance-voltage characteristic of a MOS structure from [57], with C_O as capacitance of the thermally grown oxide, x_O as (silicon)oxide thickness and N_A as the acceptor concentration of the p-type silicon substrate, is shown. The structure had aluminium contacts. In (b), also from [57], different forms of the MOS response are categorised. In the *low-frequency* curve, traps and minority carriers are in equilibrium: for negative values of the abscissa the majority carriers *accumulate* at the oxide, for large enough positive values the *inversion* sets in, i. e. minority carriers agglomerate at the oxide and can follow the applied field. As a result, the capacitance at those conditions rises again to the value of the oxide. For the *high-frequency* curve, the minority carriers cannot follow the applied ac signal any longer and their concentration is approximately unchanged in the inversion region. The plateau capacitance is a consequence of reaching the limit of the depletion-layer width. In the *depletion* (today usually called *deep depletion* [162, p. 71]) case, there are no accumulated minority carriers at the oxide although the band bending allows for inversion. As a consequence of the missing screening by minority carriers, the depletion-layer width continuously grows, resulting in the observed continuously decreasing capacitance. The source of such behaviour can be a leaky oxide or a bias-voltage sweep so fast that the minority carriers could not follow. All explanations, beside those explicitly cited from another source, are from Grove *et al.* [57]. Reprinted from Solid-State Electronics 8, Grove, Deal, Snow and Sah, 'Investigation of thermally oxidised silicon surfaces using metal-oxide-semiconductor structures', pp. 145-163, Copyright 1965, with permission from Elsevier.

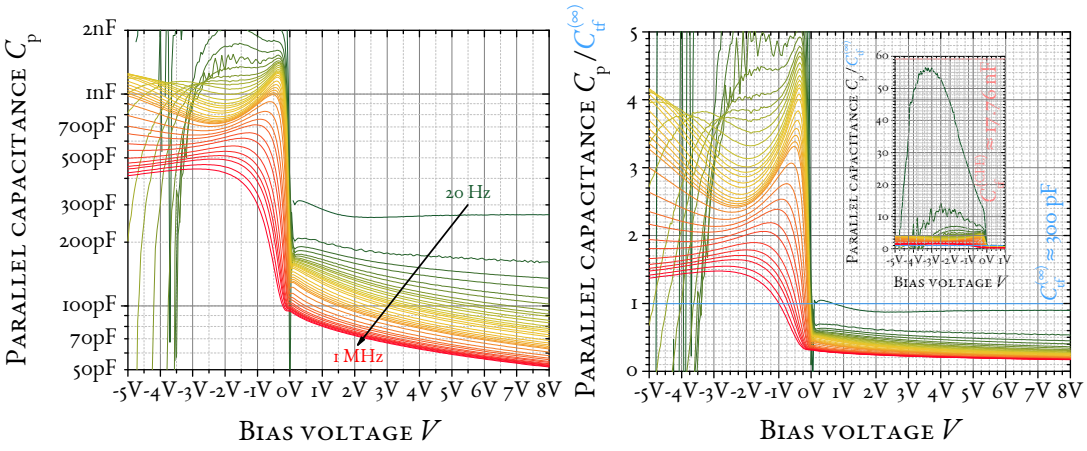

Figure 4.12: (a): plot of the parallel capacitance C_p extracted from the measured immittance utilising the simple, but not uncommon [59], assumption of a parallel arrangement of a single resistor R_p and capacitor C_p. (b) shows the same data, but (as usually for such plots, compare Figure 4.11) normalised on the thin film capacitance, extracted according to [190] from the experimental high-frequency limiting capacitance $C_{\infty,tf}^{(exp)}$ (the thin film capacitance extracted according to [108] from the constant phase element is marked in the inset for comparison). A plot including a large range of normalised capacitance values, that includes the complete forward bias data, is shown as inset. With increasing frequency, the measured capacitance-voltage curve converges against the usual characteristic at deep-depletion conditions (compare 4.11b). Latter property is likely caused by the relatively high conductivity of the insulating thin film [57]. For the lowest frequency (at 20 Hz) the capacitance at high reverse voltages reaches a value comparable with the capacitance of the thin film (as extracted from the high-frequency-limiting capacitor). This could be explained with the response of minority carriers at the interface in inversion. However, the characteristic dent due to the high depletion-layer capacitance is missing and, due to the dispersive thin-film capacitance the forward-bias capacitance seems overly large. If all these overly large capacitances for forward bias voltages would be replaced by the one calculated from the static permittivity extracted according to [190], the convergence of the capacitance against that value can also be seen in the high-frequency response, this would look a lot more like the expected response of a MOS diode. Hence, the dispersive nature of the thin-film capacitance, that in consequence leads to these (apparently) high values, might only cloud the actual response.

thin film, the serial resistance would for the sample system in this work not at all fulfil these requirements (the resistance of the thin film reduces from around 5 kΩ to only 500 Ω in about 2.5 V), compare Figure 4.9. Consequently, instead of adding an ideal serial resistor, one with the correct dependence on voltage should be introduced. Adding the voltage dependence of the thin-film resistance, i. e. introducing external-parameter dependence to a component, would, however, not be conventional capacitance-voltage analysis any-longer, but rather the approach for analysing immittance data suggested in this work.

To sum it up: In the conventional capacitance-voltage analysis very often either the R_s-C_s or R_p-C_p approach is used. For the above mentioned reason, from these two possibilities the R_p-C_p variant seems better suited for the investigated system. The selected parallel arrangement is a sufficient approximation, at least, at high reverse bias voltages where the voltage drop is supposed to be almost exclusively over the depletion layer, see Figure 4.2c. In that region, the extracted capacitance should belong entirely to the depletion layer in the silicon, since it is by far the most dominant part of the immittance, compare its resistance with those of other components in Figure 4.9. For lower bias voltages, the rapidly decreasing serial resistance of the amorphous layer and, later for even lower bias voltages, also the total serial resistance become increasingly important. This leads to deviations from the expected capacitance-voltage characteristics in the corresponding range of voltages.

In principle, one could have the idea to describe sample `1346aCrAu1` in terms of a metal/insulator/semiconductor (MIS) structure. Exemplary capacitance-voltage responses for low- and high-frequencies of the likely most thoroughly investigated MIS structure, the metal/oxide/silicon (MOS), are shown in Figure 4.11. However, the experimentally obtained characteristics, for the samples investigated in this work, are very different from those conventionally observed, see Figure 4.12.

One important cause for the deviation is the distinctly different insulator. It is much more conductive than the thermally grown oxide layers in usual MOS devices. At room temperature, silicon oxide has a resistivity in the range of 10^{14} Ω cm to 10^{16} Ω cm [176, p. 852], while tetrahedral-amorphous carbon (synthesised as in this work) has a resistivity (in the limit towards 0 V, hence, at its maximum) of only 10^{7} Ω cm [68]. As a result, ta-C can, unlike the silicon-oxide layer in conventional MOS structures, not be approximated as completely blocking. In consequence, the 'insulating' layer might be too leaky for a formation of an inversion layer at high reverse bias voltages or the agglomeration for forward bias voltages. This is expected to have a severe influence on the capacitance, since the before mentioned layers in the semiconductor with their counterparts on the electrode on the opposite site of the insulator are the reasons to measure the oxide capacitance at sufficiently high bias voltages in the respective directions.

Furthermore, the capacitance of the insulator (investigated in this work) is highly dispersive: In the conventional characteristic in Figure 4.11a the oxide capacitance variation in a frequency range from 10 Hz to 10^{5} Hz is negligible. In Figure 4.12, a frequency range from 20 Hz to 10^{6} Hz is shown. The dispersion is much larger even omitting the dispersion at very low frequencies that is depicted in the inset.

Another major difference, might be due to a higher concentration of interface defects

as well as trapped charges in the ta-C, that are expected due to different growth process (thermal oxidation versus MSIBD). Their influence on the capacitance-voltage characteristic is further investigated later in this section. Then again, silicon oxide is a much better insulator and is expected to have even fewer carriers above the mobility edge. Therefore, the possibly higher number of charged defects in ta-C might be better screened by the larger number of mobile charge carriers. Furthermore, due to the higher conductivity those charged defects, which are also traps for charge carriers can be better reached by the latter and, consequently, neutralised.

The curvature on the reverse bias side shows a capacitance continuously decreasing with voltage, rather than a plateau. As can be seen in Figure 4.11b this corresponds to the effect called *deep depletion*, i. e. there is no inversion layer of accumulated minority carriers at the interface [57]. Since each bias step takes at least a dwell in the order of a few seconds, this indicates that the insulator, ta-C, is too leaky for a minority carrier build up at the interface. On the other hand, the lowest-frequency response reaches the capacitance of the thin film at higher reverse bias voltages, if one assumes that the extraction from the high-frequency-limiting capacitor according to reference [190] is correct. Then this could be explained by an inversion layer of accumulated minority carriers at the interface.

Assessment of the acceptor concentration determined by the fit Within the already mentioned limits, the slope in a Mott-Schottky (C^{-2}-V) plot can be used to determine the concentration of acceptors in the semiconductor [138, pp. 383-385]. Such plot of the measured parallel capacitance C_p of sample `1346aCrAu1` are shown in Figure 4.13. Exemplary, two different depths in the semiconductor (represented by two different regions of voltages) are fitted. It is found that the slopes are dependent on frequency. Furthermore, that the fits do not intersect at the same point on the abscissa. Finally, the slope, and consequently the acceptor concentration, seems to be dependent on the depth in the semiconductor, i. e. the applied bias voltage.

The direction of the flat-band voltage shift and its dependence on frequency As already brought up in the last paragraph, the presence of defects at the interface and in the insulator leads to a shift of the flat-band voltage and stretch-out of the voltage scale [161]. In this paragraph, these effects are discussed in greater detail. Figure 4.13 shows a Mott-Schottky plot, i. e. the reciprocal squared capacitance C_p^{-2} plotted over the applied voltage V, using the capacitance extracted from the immittance assuming a simple conventional R_p-C_p circuit approximation. While the slopes in this simple model, as already explained, can be utilised to calculate the doping concentration in the material, the abscissa intercepts may, with the formula given in the inset, be used to calculate the flat-band voltage. In this case, the flat-band voltage obviously shows a frequency-dependent shift.

The shift in flat-band voltage was not directly expressed as defect density (neither in this conventional analysis nor in the proposed model utilising external-parameter dependence of physical models for analysis of immittance spectra), because it is, with the data at hand, not possible to distinguish whether the traps are located at the interface or if they are fixed charges in the insulator (compare different methods of analysis to obtain

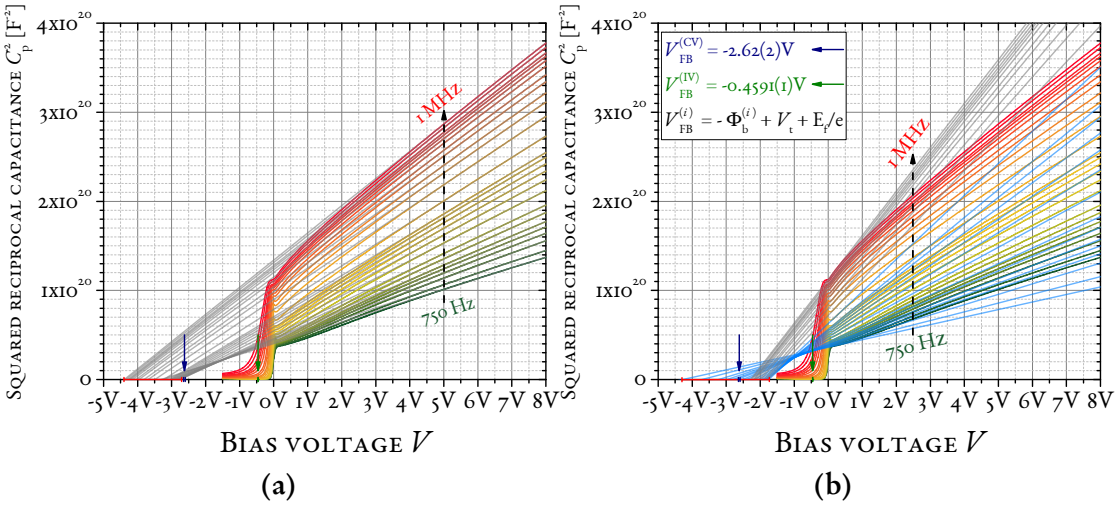

Figure 4.13: Conventional capacitance-voltage analysis (a) evaluated at relatively large bias voltages, i. e. the depletion-layer width oscillates around a region relatively far from the interface, and (b) assessed at bias voltages associated with a region of oscillation close to the interface. In the rather unrealistic ideal case of no defects at the interface or in the insulator, the intersection with the abscissa in the Mott-Schottky plots determines the flat-band voltage, from which the barrier height can be determined. The formula utilised and shown in the inset ignores the contribution of any defects at the interface or in the insulator (as do the resistive and capacitive models utilised in the presented approach, see the beginning of section 4.1.2.1 to understand why). The analysis was performed for several frequencies. In (b), where the slope at low voltages is evaluated, part of the capacitive behaviour falls into the region ignored by the fit, which is indicated by colouring the corresponding lines light-blue. The range of the abscissa intercepts is marked in red. On the one hand, the applied model, utilised in the analysis proposed in this work, assumes only a single effective acceptor concentration for the whole depletion-layer range as well as two effective barrier heights for the capacitive and resistive model, respectively. The corresponding fit results (converted to flat-band voltages) are shown in blue (capacitive) and green (resistive) on the abscissa. Unlike the fits shown here, the approach proposed in this work, bases its fit parameters on all fitted points and is, further, not limited to the very simple circuit models of conventional capacitance-voltage analysis. The plots shown above do not follow the ideal Mott-Schottky behaviour, but instead show different slopes (potentially corresponding to different acceptor concentrations) and a relatively broad range of abscissa intercepts. Such deviations are not uncommon and categorised by Dutioit *et al.* [35].

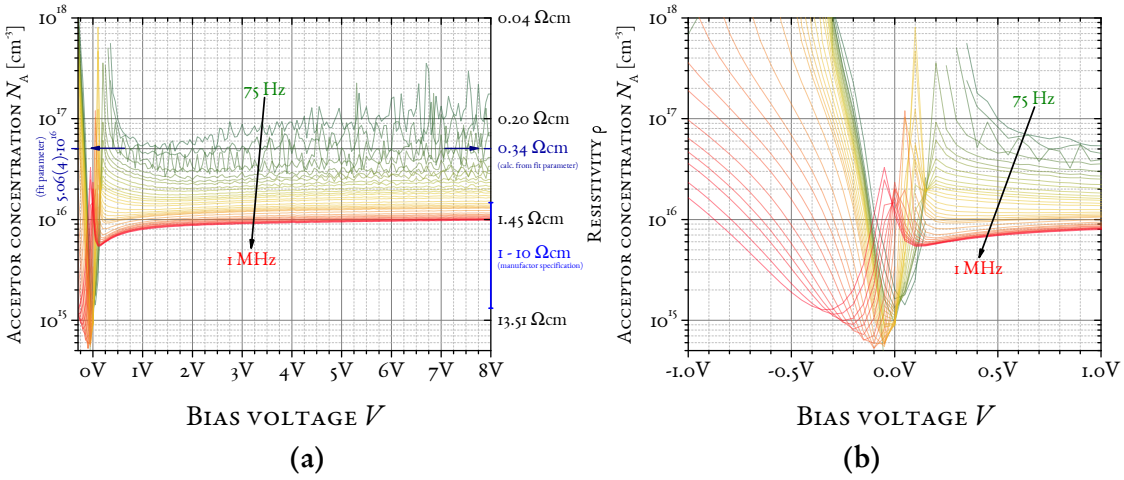

Figure 4.14: The acceptor concentrations obtained using equation (4.1) by derivation of the Mott-Schottky plot shown in 4.13 for the entire depletion-layer region (a) and around zero bias in detail (b). With increasing frequency the 'misleading' contribution by interface traps and fixed charges in the insulator diminishes. The models used in the proposed approach for immittance analysis assume only one acceptor concentration and no dispersion due to other defects (neither at the interface nor in the insulator). It is, hence, no surprise that the consequently fitted 'effective acceptor concentration', that is shown as dark-blue arrow in the plot, lies within the rather broad region of determined concentrations. Since the acceptor concentration is decreasingly influenced for higher frequencies (as a consequence of the time constants of the involved traps), the high-frequency value should be closer to the 'true' acceptor concentration (though the stretch-out correction given in equation (4.2) indicates a further reduced value). Latter acceptor concentration is approximately 10^6 cm^{-3} which corresponds to a resistivity of around 1.45 Ω cm and is, hence, within the range given by the manufacturer indicated in blue in (a).

the corresponding densities in [161]). Energetically distributed defect states throughout the complete band gap at the interface can lead to an asymmetric stretch-out that at least partially behaves like a voltage shift. If the energetic centre of gravity of acceptor-like and donor-like states is at a different depth in the gap, resulting to in each case different (mean) time constants, the shift as well as stretch-out character varies over frequency, independent of the types of the defects: whether they are in the insulator or at the interface. In general, any positive charges in the insulator or (since the contribution from interface charges has the same sign in equations (10)-(12) in [161]) at the interface shift the flat-band voltage to more negative bias voltages as compared to a defect-less situation, while negative charges shift towards more positive bias voltages [138, pp. 423-428], independent of the type of the semiconductor the depletion layer is in. As can be seen in Figure 4.13a, for the experimental data of sample `1346aCrAu1` the flat-band voltage-shift increases to even lower bias voltages with rising frequency. This could be explained by following situation: First, more positively defects have to be present, since the flat-band voltage seems already at low frequencies unusually large, indicating an excess of positive charges. Now to the second part, that the flat-band-voltage shifts further into the negative direction, with increasing frequency: This could indicate that the positive charges are at low frequencies partially screened or filled, so that not all contribute to the shift. At higher frequencies, the process shielding the effect of the positive charges continuously decreases, indicating that the time constants of this process are in the investigated frequency range. The whole effect of flat-band voltage shifting might further be complicated by a stretch-out due to the thermal equilibrium occupation of interface and charged defect states with respect to the slowly varying bias voltage. As not only one kind of defect is present, both effects are much more complicated for the investigated samples as for typical examples given in the literature, e. g. in reference [161]. The complicated observed behaviour is, actually, not uncommon [35]. Dutoit *et al.* categorise typically observed deviations from the expected Mott-Schottky behaviour. Latter may be found solely for interfaces where even the defects caused by the unavoidable change of materials themselves [185] are passivated. Even the specific frequency dependence of the voltage shift, found for the samples investigated in this work, has already been observed by Khan *et al.* [89], as a matter of fact, for diamond-like carbon. They argue that the effect is due to tunnelling into traps in the insulator, which gives an exponential distribution of time constants, rather than due to a stretch-out caused by interface traps [89]. This is explained by the fact that for a stretch-out the threshold voltage would stay the same for different frequencies, while only the flat-band voltage has the exponential time-constant dependence [89]. Indeed, in this work, the threshold voltage seem to be independent of frequency. Furthermore, the frequency dispersion is larger in, what could be, accumulation[3] than in depletion, compare Figure 4.11.

The dependence of the slope in Mott-Schottky plots on the bias voltage As already mentioned, the slope, and consequently the acceptor concentration, seems to be dependent

[3] Due to the high conductivity of the insulator, a high rate of charges escaping the (spatial) region of accumulation, close to the interface, has to be accounted for.

on the depth in the semiconductor, i. e. the applied bias voltage. The Mott-Schottky plots have been derived by the bias voltage and the obtained 'slopes' used to calculate the acceptor concentration, according to [52]

$$N_{\mathrm{A}}(V) = -2\left(e\varepsilon_{\mathrm{r}}^{(\mathrm{Si})}\varepsilon_0 \frac{\partial}{\partial V}\left[\frac{1}{\hat{C}^2}\right]\right)^{-1}, \tag{4.1}$$

with acceptor concentration N_{A} (whereas there is a discussion whether this should rather be the majority-carrier concentration than the doping density [162, pp. 61-68]), a relative permittivity of silicon $\varepsilon_{\mathrm{r}}^{(\mathrm{Si})} = 11.9$ [176, p. 850] and the hat over the capacitance $\hat{C}$ indicating a capacitance per area. The result is shown in Figure 4.14, in comparison with the range of resistivities according to the specifications of the wafer manufacturer and the value extracted from the fit using the novel approach presented in this work. As already expected from the obvious frequency dependence in the slopes (compare Figure 4.13), the acceptor concentrations seem dispersive, as well. This might, however, be a deception due to the negligence of any defects other than the acceptor states. Assuming, there are interface traps: At sufficiently low frequencies, these traps might be filled and emptied fast enough, that they are more or less occupied according to the thermal equilibrium. The charging and discharging of these traps leads to an additional current, that may (approximatively) be represented by a capacitor in parallel to the one of the depletion layer [138, pp. 181-212]. If there are various trap levels, corresponding to different time constants, the latter capacitance is frequency dependent [138, pp. 181-212]. As a result, with increasing frequency only a reduced number of deep levels can contribute, reducing the capacitance corresponding to the interface traps or fixed charges in the insulator. At high enough frequencies, the interface traps (or fixed charges in the insulator) cannot follow the applied ac signal any longer and their contribution becomes minimal (or even negligible). This trend is in agreement with the dispersion of the acceptor concentration in Figure 4.14. The acceptor concentration extracted from the 1 MHz response is already within the specified region of acceptor concentration of the manufacturer. The capacitance model used in the fit of the approach presented in this work is also based on the basic Mott-Schottky relation that neglects the presence of interface states. Furthermore, it assumes a homogeneous distribution of acceptor concentration independent of depth. It is, hence, no surprise that the single *effective* acceptor concentration fitted within the above described limits of the above mentioned model would lead to a value in-between the frequency- and voltage-dependent acceptor concentrations. This value is shown as blue arrow in 4.14a.

Even the high-frequency curve does, however, not give the correct concentrations of acceptors in the semiconductor (confer [138, pp. 385-388]). True, the omitted traps are too slow to follow the high-frequency ac signal and do not contribute to the measured capacitance in that range any longer, but the bias voltage is, neither usually nor in this experiment, varied as fast as the ac signal. Hence, the slow bias voltage changes are not only compensated by a change in charge density in the depletion layer, but also by the change in interface (or fixed insulator) charge density [138, p. 387]. This leads to a 'stretch-out' of the high-frequency capacitance-voltage curve along the voltage axis, resulting in a

decreasing slope of the capacitance-voltage curve of the depletion regime [138, p. 387]. The formula in equation (4.1) can be corrected for this stretch-out by introducing the factor [138, p. 388]

$$\frac{1-\hat{C}_{\mathrm{lf}}/\hat{C}_{\mathrm{ins}}}{1-\hat{C}_{\mathrm{hf}}/\hat{C}_{\mathrm{ins}}}=\frac{\hat{C}_{\mathrm{ins}}-\hat{C}_{\mathrm{lf}}}{\hat{C}_{\mathrm{ins}}-\hat{C}_{\mathrm{hf}}}, \tag{4.2}$$

with the low-/high-frequency capacitance $\hat{C}_{\mathrm{lf/hf}}$ and the insulator capacitance $\hat{C}_{\mathrm{ins}}$ (all per area). Since the parallel capacitance in forward bias, shown in Figure 4.12, cannot be interpreted straight-forwardly as insulator capacitance, latter is, hence, rather estimated from the static permittivity of the thin film utilising the novel approach presented in this work. Depending on the chosen model to extract the static permittivity, the factor in equation (4.2) becomes approximately 60 % (extracted according to [190], $\varepsilon^{(\mathrm{tf})}_{\mathrm{r,stat}} \approx 4.2 \rightarrow C_{\mathrm{ins}} \approx 300\,\mathrm{pF}$) or almost unity (permittivity assumed to be increasing due to hopping conductivity [108], $\varepsilon^{(\mathrm{tf})}_{\mathrm{r,stat}} \approx 250 \rightarrow C_{\mathrm{ins}} \approx 18\,\mathrm{nF}$). These different approaches to extract the static permittivity of the thin film are a main topic of this work and discussed in much greater detail later, including in sections 5.3 and 5.6.3. Consequently, the acceptor concentration might be even lower and, with that, closer to the centre of the range specified by the manufacturer. There are even more corrections to make the description of the interface more realistic and the consequently extracted parameters more accurate [138, 162, 161], which will not be applied in this work. Again, all these more refined calculations could be introduced to the model(s) in the presented approach.

Another possible contribution to the frequency dependence of the acceptor concentration could be the due to different acceptor-like trap levels with varying depth into the band gap in the silicon *bulk*. For the same argument as for the interface traps, those 'deeper' trap levels might be filled and emptied for certain frequencies until they cannot follow any longer. This would lead to a similar effect. The density of these traps are, however, likely not as large as those concentrations at the interface.

Yet another important factor to obtain a quantitatively correct acceptor concentration is the *accuracy of the assumed area*. In all formulae to calculate the acceptor concentration from a capacitance-voltage measurement, even in the correction factor to compensate for the stretch-out at high frequencies, the area is a factor. There are many obstacles to overcome gaining the 'true' interface area, see the paragraph 4.1.1.4.

So far, the focus of the analysis of the acceptor concentrations in Figure 4.12 has been on the frequency dependence. Now, it will be on the variations in the acceptor concentration with applied bias, which, finally, shall be translated in a depth profile of the acceptor concentrations. As already explained, at sufficiently high reverse voltages, the depletion-layer immittance should be the dominating contribution and the assumed R_{p}-C_{p} model is a sufficiently good approximation, so that the extracted capacitance is in that region indeed the one of the interface without too much influence of other parts of the sample. Like mentioned before, the capturing and emission of charges from traps at the interface (or in the insulator, or other traps in the bulk than the acceptor states) still influences the capacitance at all reverse bias voltages, so that it is dispersive. At sufficiently high reverse bias voltages, the acceptor concentrations are at least independent of voltage.

This is seen as indication that far away from the interface the wafer is homogeneously doped, likely even in the acceptor concentration specified by the manufacturer. More interesting than its dependence on bias voltage is the acceptor concentration as a function of depth in the silicon. Luckily, the calculation of the depth does not depend on the bias voltage. Hence, the frequency-dependent shift of the flat-band voltage (likely due to traps at the interface or in the insulator) does not falsify the resulting depth scale. However, the calculation of the depth scale requires the capacitance of the thin film $\hat{C}_{\mathrm{tf}}$. A wrong thin film capacitance leads to a shift in the depth scale. The comparison of Figure 4.12b with Figure 4.11 makes clear, that the correct value for $\hat{C}_{\mathrm{tf}}$ cannot as easy be determined for the investigated system, as for conventional MOS structures. The capacitance-voltage curve at the highest frequency (1 MHz) comes closest to one of the expected behaviours shown in Figure 4.11b. It looks like a high-frequency deep-depletion response, which is in principle fortunate, since in deep depletion the depletion-layer width w is continuously growing so that the depth profiling can advance into spatially deeper regions of the semiconductor. Furthermore, the 1 MHz capacitance-voltage curve is theoretically least affected by the interface traps. As a result, the depth profile is based on the highest-frequency capacitance-voltage curve. The depth w into the semiconductor can be directly calculated from the measured capacitances [138, p. 285]

$$w(\hat{C}(V)) = \varepsilon_{\mathrm{r}}^{(\mathrm{Si})} \left(\frac{1}{\hat{C}} - \frac{1}{\hat{C}_{\mathrm{tf}}} \right) \tag{4.3}$$

The maximum in capacitance of the highest-frequency curve $C_{\mathrm{max}}^{(1\,\mathrm{MHz})} \approx 443\,\mathrm{pF}$ is assumed to be the capacitance of the thin film $\hat{C}_{\mathrm{tf}}$ in equation (4.3). The maximum is at a voltage of about −2.8 V. Not only for higher (as expected from the usual capacitance-voltage behaviour shown in Figure 4.11), but also for lower bias voltages the capacitance is decreasing. This is assumed to be an effect of the increasing influence of the total serial resistance (compare voltage drops in Figure 4.2c) and, hence, not shown (a capacitance decrease in that direction leads to an opposite sign in the doping concentration, representing donor states). It should be kept in mind that the maximal resistance $C_{\mathrm{max}}^{(1\,\mathrm{MHz})}$ is still in the dispersive region, i. e. it has not yet arrived at its high-frequency limit, that is supposed to be around 300 pF. Hence, there might be an offset to the actual depth. Since the capacitance is directly used (and not their derivative) to determine the depth scale, neither the offset due to the flat-band voltage shift nor the stretch-out in its scale will have an effect on the depth scale itself. However, the acceptor concentration itself is calculated from the derivative of the squared reciprocal capacitance with respect to the voltage $\frac{\partial}{\partial V}\left(\frac{1}{C^2}\right)$. Hence, the values for the doping concentration are affected by the stretch-out. Since none of the measured low-frequency responses showed a behaviour similar to the expected one, the stretch-out correction of the acceptor concentration using low- and high-frequency values could not be performed.

In summary, the depth was calculated according to equation (4.3) for the response at the highest frequency (of 1 MHz, see Figure 4.12) and assuming its maximal capacitance to be the one for the thin film $\hat{C}_{\mathrm{tf}}$, though the dispersion is likely not finished at this

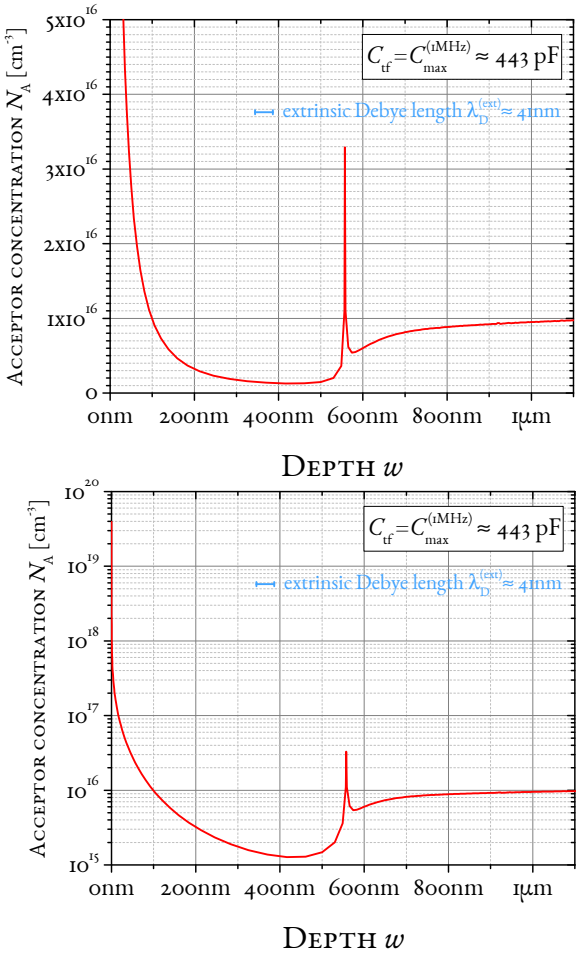

Figure 4.15: Depth profile of the acceptor concentration extracted from the highest-frequency 1 MHz capacitance-voltage curve, assuming its maximal capacitance was the one of the insulator (knowingly ignoring the facts that the dispersion of the insulator capacitance was likely not finished at 1 MHz, that due to the simplified R_p-C_p circuit the capacitance values become increasingly unreliable for voltages below zero and that not necessarily all acceptor-like states are fully depleted.) Any stretch-out or shift in the voltage does not affect the depth itself, since it is calculated from the capacitance value itself. Stretch-out and shift of the voltage axis will, however, effect the acceptor concentration. The prominent peak in the depth profile is corresponding to a peak in the acceptor-concentration-voltage curve closely below zero bias (compare Figure 4.16). The extrinsic Debye length, given in the plots, is considered to give the magnitude of the depth resolution in such plots [162, pp. 65-67]. Spatial variations of doping profiles below this distance cannot be resolved by capacitance-voltage measurements. The high values towards zero and the subsequent valley are expected artefacts when neglecting interface effects and assuming complete depletion [162, p. 68].

frequency (potentially resulting in a constant offset of the depth scale). Using this in combination with the acceptor concentrations shown in Figure 4.14, that are (for the above explained reasons) calculated without correcting for the probable stretch-out on the voltage axis (potentially resulting in distortion in the concentrations), leads to the depth profile of acceptor concentration shown in Figure 4.15. Further to the profile, the extrinsic Debye length $\lambda_{\mathrm{D}}^{(\mathrm{ext})}$ is shown in the plots. These depth profiles are very similar to those shown in [162, p. 68], where certain artefacts of the used approximation are shown. From the comparison with the plots in the reference, it seems probable that the observed dent (roughly between 100 nm to 800 nm) is due to the presence of interface traps and, furthermore, that the increase in acceptor concentration is an artefact of the depletion approximation.

The resolution of the depth profile is expected to be limited to this length or at least some value in the order of it. The extrinsic Debye length $\lambda_{\mathrm{D}}^{(\mathrm{ext})}$ is given by

$$\lambda_{\mathrm{D}}^{(\mathrm{ext})} = \sqrt{\frac{\varepsilon_{\mathrm{r}}^{(\mathrm{Si})}\varepsilon_0 k_{\mathrm{B}} T}{e^2 |N_{\mathrm{A}} - N_{\mathrm{D}}|}},$$

with the donor concentration N_{D} [162, p. 67]. For sample `1346aCrAu1` the extrinsic Debye length is around 41 nm.

For all frequencies the acceptor calculations depicted in Figure 4.14 show a high peak around zero that is with increasing frequencies shifting from a bias voltage of roughly 250 mV, at low frequencies, to a bias voltage of approximately −50 mV, at 1 MHz. This shifting peak is magnified in Figure 4.14b and can also be identified as a line in the contour plot in Figure 4.16. It becomes obvious in the latter plot, as well, that the peak is not always in positive direction. This might indicate, that this peak is actually caused by defects at the interface and not deeper in the semiconductor. The different voltages and frequencies might then select the energetic depth in the band rather than the spatial depth in the semiconductor. Then again, this peak, which is around −50 mV for the capacitances obtained at 1 MHz is the very prominent peak at a depth of approximately 560 nm. This also means that all acceptor concentrations in the depth profile left of it belong to the bias voltages below zero. As a consequence of assuming solely a R_p-C_p circuit, this region might be influenced by the thin film as well as the total serial resistance and, consequently, these values might either not really be inside the semiconductor or they might not represent the depth profile correctly. There is no process step that is expected to cause a high doping concentration at a depth of 560 nm. Furthermore, the peak is not for all frequencies registered as acceptor-like but sometimes also as donor-like state, see Figure 4.14b. Consequently, it rather is supposed to be due to the many expected energy levels of the defects at the interface. In this context, such artefacts can be seen in reference [176, pp. 287-288].

Magnitudes for defect concentrations causing the flat-band voltage shift assuming different extreme-case scenarios The negligence of interface as well as insulator traps affects

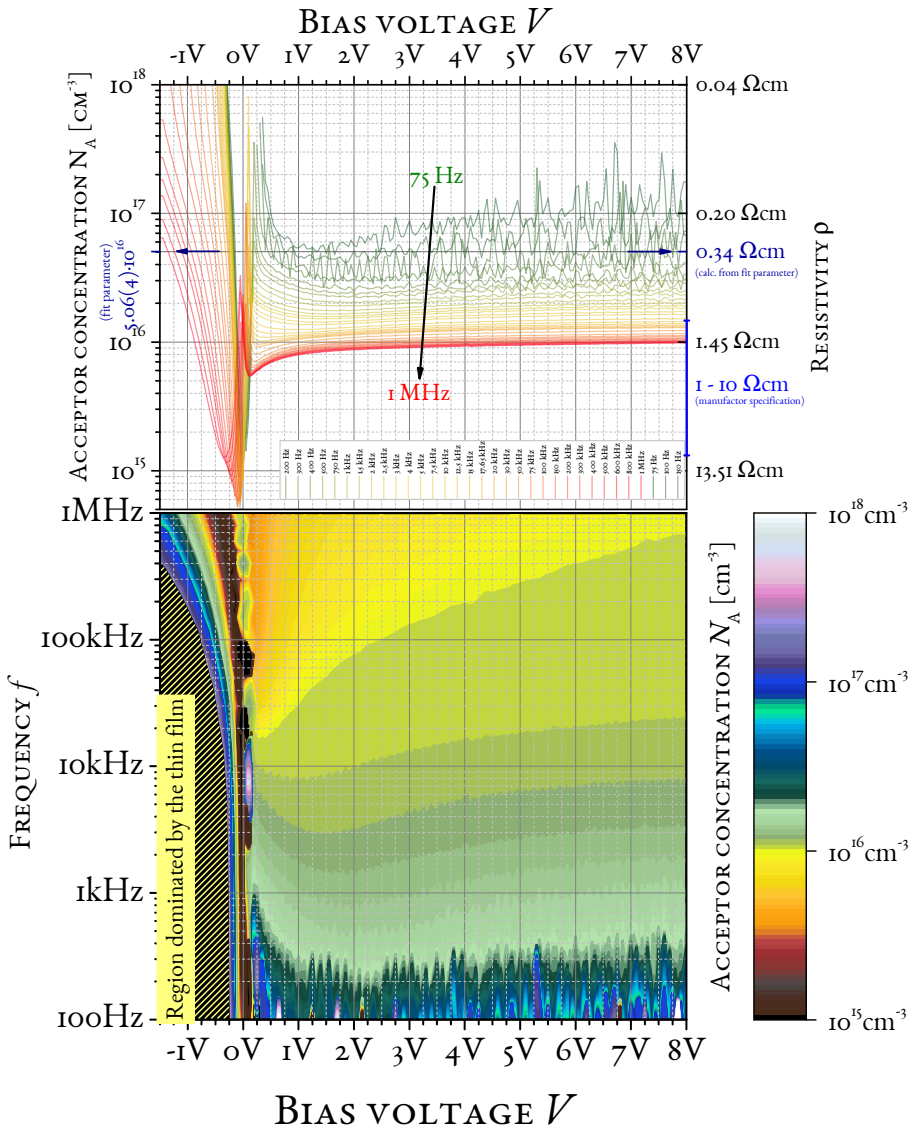

Figure 4.16: While the upper plot repeats Figure 4.14a (all relevant information for the upper plot can, hence, be found in its corresponding caption), the lower plot shows the extracted values as a contour plot. Notable features are the peak around zero that shifts only very slightly with frequency (while its type varies between acceptor and donor-like for different frequencies) and the transition to a very high capacitance (region dominated by the thin film) with a preceding valley that shifts strongly in negative voltage direction with increasing frequency. Latter might be associated with an exponential time-constant distribution indicating a contribution of defects in the insulator (with increasing time constant for deeper traps) while former may be associated with defects located directly at the interface.

models at different frequencies, i. e. especially also resistive and capacitive models, differently. The association of the differences with different types of traps is sadly not possible with the obtained data. Hence, since it is unclear which type of defects are the source, or better what fraction of the shift is caused by which defect, it was decided against fitting only one barrier height and a defect concentration that could explain the discrepancy. Instead, two barrier heights are extracted, one for the resistive response at one 'effective' barrier height for the capacitive response. Both (capacitive and resistive) models ignore the contribution of interface as well as insulator traps. The resistive barrier height is around 0.641 eV while the capacitive one is in the order of 2.8 eV. The difference between barrier heights $\Delta\phi$ is about 2.16 eV. Assuming this difference would be caused solely by charges in the insulator (and, further, there are no states at the interface), their concentration would be about $8 \cdot 10^{16}\,\mathrm{cm}^{-3}$.

The barrier height difference $\Delta\phi$ from charges in the insulator Q_{ins} is given by

$$\Delta\phi = \frac{Q_{\mathrm{ins}}}{C_{\mathrm{ins}}},$$

with C_{ins} as the capacitance from the insulator [138, p. 426]. An insulator capacitance of 300 pF is assumed. To convert the total number of acceptor-like defects in the insulator into a defect concentration, the cylindrical volume $\mathfrak{V}_{\mathrm{ins}}^{(\mathrm{cyl.})}$ of the insulator beneath the metal top contact with a homogeneous distribution of defects is assumed for normalisation. This approximation completely ignores a potential weighting of the effect of the traps due to their individual distances from the interface and geometry is also only roughly approximated:

$$N_{\mathrm{A}*}^{(\mathrm{ins})} = \frac{\Delta\phi \cdot C_{\mathrm{ins}}}{e \cdot \mathfrak{V}_{\mathrm{ins}}^{(\mathrm{cyl.})}} \tag{4.4}$$

Both types of traps can (assuming equal sign of charge) contribute in the same way to a flat-band voltage shift [138, p. 466], so that in the second extreme case, that there are no defects in the insulator but instead all at the interface, the only thing that changes with respect to equation (4.4) is the normalisation. Instead of normalising on the volume, all traps are now assumed to be at the interface of tetrahedral-amorphous carbon and silicon. The area of the interface is assumed to be identical to the area of the top contact. As a result, an interface state density of $6 \cdot 10^{11}\,\mathrm{cm}^{-2}$ is determined. This value is (keeping in mind the rough process of deposition in comparison to thermally growing an oxide film) surprisingly, close to interface defect densities obtained for thermally grown silicon oxide layers, compare values in [57].

Other effects not recognised by the utilised capacitive models Beside neglecting the contributions of the different types of defects, other assumptions were made when determining the barrier height from the intercept. Due to the focus on the novel approach presented here, this conventional analysis does (actually, like most publications) not use all possible tweaks and extensions to compensate for deviations caused by not exclusively

measuring the isolated capacitive response of the depletion layer. As mentioned in the introduction of the section about conventional capacitance-voltage analysis, the results are extracted to understand and compare them to the novel approach.

Unlike in the model for the novel approach which assumes a serial resistor and a resistive as well as a capacitive model for the thin film, the conventional analysis in this section does not assume any resistance or capacitance in series to the parallel pair of resistor and capacitor that is assumed to represent the depletion-layer properties. Since the voltage drop over the thin film is dependent on the total of externally applied bias (compare Figures 4.2c), which is ignored by the conventional analysis, the observed stretch-out and shift of the flat-band voltage are expected to be influenced by neglecting the correct voltage drops over the different parts of the system.

Additionally, in both types of analysis, the models assume that all acceptor states are completely ionised. Furthermore, a spatially homogeneous distribution of those states is assumed, which seems, considering the results from the conventional analysis, to be a quite good approximation deep enough in the semiconductor. As already mentioned in paragraph 4.1.1.4, the knowledge of the area of the interface A is critical, since it affects almost all extracted quantities. Unlike in the presented approach, in the conventional analysis the voltage-dependent barrier lowering was not taken into account in any calculation.

4.1.2.2 Interface deviation 2 and its potential origins

In this paragraph, possible reasons for interface deviation 2 are discussed. Some facts were already mentioned in the last section that addressed the conventional capacitance-voltage analysis of the experimental data.

Distinctions to the other deviation The residuals of the region that is possibly affected by a dispersive flat-band voltage shift are not excluded in the fit, although they are expected to distort the parameters especially of the capacitive part of the thin film. The mentioned deviation is present in both samples, although its severity seems less for the highly doped sample. A distinct difference to the ignored region of the low-doped sample around interface deviation 1 is that the deviation 2 is only present in the capacitive region and leads to overestimation for one voltage side, but underestimation for the other. Hence, unlike for the other deviation, the used model seems to be a valid zero-order approximation. Consequently, it was assessed that the differences of the used model to the real situation could be identified more clearly by explicitly including that region and observing its residuals or deviation plots.

Possible reasons for the deviation Possible reasons for the deviation might be a pronounced capacitance-voltage stretch-out due to the extremely high number of interface defects expected by 100 eV carbon ion deposition or by fixed charges in the respective amorphous thin film. A capacitance-voltage stretch-out is quite usual for any interface due to unavoidable interface defects active in the respective frequency range (see [185] for the fact that defect states exist at interfaces and [161] that interface defect-states lead to a

capacitance-voltage stretch-out). As compared to interfaces created by other methods, ion-beam deposition with 100 eV carbon ions is expected to create more damages close to the overall more disordered interface. Furthermore, the ta-C film itself is under a lot of stress which also affects the substrate. To avoid changes in the electrical properties of the thin film, the samples were neither annealed nor passivated. As a result of the above mentioned differences to usual interfaces, a much higher number of interface defect is expected. Since the intensity of the capacitance-voltage stretch-out is a measure for the amount of electrically active interface states or fixed charges in the insulator (confer [161] and [138, pp. 424-428]), it is expected to be even more pronounced for the investigated samples than for usual interfaces. Khan *et al.* [89] explored the possibility that the frequency-dependent flat-band voltage shift is only similar to a capacitance-voltage stretch-out, but shows some distinct differences that are supposed to indicate that the origin of this behaviour are fixed charges in the insulator rather than states at the interface (though also the states in the insulator have to be in the vicinity of the interface). The observed exponential distribution of time-constants (its beginning can be seen in the contour plot in Figure 4.16) is supposed to be a typical consequence of the different depths of traps in the insulator. The frequency-independent threshold voltage, visible in the resistive properties, should be another clue supposing this interpretation rather than the capacitance-voltage stretch-out.

Different barrier heights from resistive and capacitive properties To extract an identical value for the barrier height from capacitance-voltage and current-voltage measurements the interface has to be very clean [176, pp. 292-293]. Contaminants at the interface, intervening insulating layers, edge leakage current or deep impurity levels can cause large differences between the barrier heights for each different method of extraction [176, pp. 292-293]. The barrier height obtained from capacitance-voltage measurements is usually higher than the one determined by current-voltage measurements [172]. Most interpretations of this feature are associated with disorder, e. g. a distribution of barrier heights by surface inhomogeneity, contaminants or roughness, or intervening insulating layers (since for some nanometres the carbon mixes with the silicon, this might appeal as a thin amorphous SiC interlayer) [172]. Such systematic deviations between the different measurement methods are usually investigated at well prepared, thermally annealed interfaces (at least in comparison to the samples investigated in this work). Considering this, it seems consistent that classical capacitance-voltage analysis of the investigated samples, showed, in agreement with the parameter obtained from the immittance model fit, a much higher increased Schottky-barrier height (about four times the current-voltage value) in comparison to the oversize (up to about 20%) observed by Song *et al.* [172]. The presence of a high number of interface states as well as a high number of fixed charges in the insulator are expected to strongly influence the properties of the interface immittance. It would be surprising not to find a strong capacitance-voltage stretch-out in such a system.

Independent of whether the real barrier height is closer to the value obtained by the capacitive or current-voltage analysis (latter seems more likely), the flat-band condition

(which determines when the depletion layer really vanishes) lies in the negative voltage range. Since the voltage drop over the thin-film piece is significantly larger in that region (compare Figure 4.2c), the voltage drop over the depletion layer is rather small in comparison. The observed capacitive deviation for negative voltages might, however, still belong to the depletion layer because the voltage drop over the interface has not yet reached the flat-band condition so that the voltage drop might still be large enough to charge and discharge a significant amount of charges at the interface. Furthermore, the mentioned feature around 100 kHz does not extent much further into the negative-voltage range than the lowest determined barrier height. The effect must, however, not necessarily be a capacitance-voltage stretch-out, though this seems still the most likely explanation, but could potentially also be just another manifestation of the poor description of the depletion layer around low voltages. The capacitance-voltage analysis shows a strong increase in apparent doping concentration for regions closer to the interface. If changes in the defect concentration were the cause, they would have to be associated with the interface defects created by the ion-beam deposition, rather than the intentional acceptor concentration of the substrate, since the feature is present in both samples and, hence, independent on the initial impurity concentration. Whether this increase is really connected to any real traps at all, can not be assessed from the capacitance-voltage analysis in this work. Much more elaborate modelling would be required. This is, however, not justified within this work, which focuses on a completely different approach and shows a conventional capacitance-voltage characterisation just as a demonstration of usual analysis as well as to compare the results on the same basis of assumptions.

Exploration of different possibilities including reasons for a change in sign of the deviation at sufficiently larger bias voltages Although it might, in light of all of the above arguments, be tempting and also likely to be correct to identify the deviation, at forward bias voltages and higher frequencies, solely as a capacitance-voltage stretch-out (a regular one or a dispersive stretch-out with the properties according to Khan *et al.* [89]), it might yet be due to other effects: The parameters of the proposed models seem to adjust to have a higher absolute impedance at low forward voltages and a lower value at higher forward bias voltages (compare Figure 4.7). Latter voltages seem too high to be still associated with charging and discharging the interface defects. Either this is just an effect by the fit that tries to find a compromise to minimise the deviation or it is an indication that the model is missing a higher-order effect like a voltage-dependent capacitance. Considering that the voltage dependence is rarely considered in immittance spectroscopy (common models for bulk capacitance do not include bias-voltage dependence, as well), a bulk capacitance in a non-polar material with such a high sensitivity to the applied voltage seems surprising.[4] Another cause of such a behaviour could be a highly voltage-dependent resonance

[4]Long has considered the voltage dependence in the pair-approximation model, due to the necessity to account for the relatively high fields at low temperatures [104]. This is caused by the limit of low-field approximation which decreases with temperature, since $eE_z d_z \lesssim k_B T$ with the applied field (without loss of generality assumed solely in z-direction) E_z and thickness d_z. In this context, Long mentions the remaining demand of field-dependent characterisations. It should however be noted that no static bias was discussed in the manuscript of Long. The field was rather considered to be caused by the oscillating part of

with a time constant in the investigated frequency range. Indeed, a capacitance-voltage stretch-out would just be an example for such an effect caused by the interface. But it does not necessarily have to be due to interface defects, though bulk mechanism are not expected to be sensitive to voltages. Finally, such a behaviour may also be explained by another generalised Voigt-circuit element in series with the others. However, against this last explanation for the deviation speaks that its resistance would have to be at least in the order of the rather high Frenkel-Poole resistance around 0 V. Ignoring such a large resistance should, on the other hand, have a more pronounced impact. The back-contact interface resistance that could in principle become that large, should increase with higher absolute voltages and, hence, have a low value around zero, but instead a higher value for more negative bias voltages. Moreover, the resistance of the back contact was separately voltage-dependently analysed to be negligible in the used voltages. Another cause for the additional generalised Voigt-circuit, a yet unknown bulk part, is not that likely, since it requires a voltage dependence significantly stronger than that of the Frenkel-Poole part.

The cause of this deviation is also not too important, since this work does not focus on a perfect understanding of this particular material system, but instead, on presenting the novel analysing technique based on a modified voltage-dependent immittance measurements that gives unambiguous circuits and insights in the underlying physics while allowing simultaneous consistency check of static and dynamic parts of the applied model. In fact, it can be seen that the structural ambiguity of circuits for a system as depicted in Figure 1.1, which is unavoidable for EECs consisting only of idealised lumped components, can already be removed with models only roughly approximating the specific pieces. Also the above mentioned joined fitting of parameters shared between resistive and capacitive models, could be illustrated already using the utilised models with their limits.

4.1.2.3 Comparability of the different samples

Since the substrates (though from the same manufacturer) are from different ingots, other differences might principally be possible, although the surface preparation was identical (and the investigated samples always in the same batch, see section 3.1). However, different ingots are not necessary to explain the observed differences: Interface deviation 2 is (for the reason explained above) very likely caused by the charging and discharging of states at or close to the interface, and should, hence, not be influenced too much by the bulk doping concentration. Consequently, it is consistent that this deviation from the model may be seen in both samples (see Figures 4.7 and 4.18) because, although the higher acceptor concentration might significantly reduce the depletion-layer width, the potentially responsible states at the interface or in charged defects in the insulator should have very similar characteristics between the samples. Latter is expected due to the identical processing of both samples. In the case of this deviation especially due to the simultaneous cleaning of the surface with refractive ion etching, the *in situ* argon sputtering prior to the coating and the subsequent ion beam deposition of carbon (in all mentioned processes the samples were next to each other on the sample holder). Furthermore, the deviation

the signal.

is much less pronounced in the highly doped sample 1346bCrAu4, although in this case the depletion layer was not modelled at all, which may in comparison with sample 1346aCrAu1 (where the depletion layer has been modelled with its voltage-dependent capacitance) might lead to an overly conspicuous appearance of this deviation. The low severity of deviation 2 in sample1346bCrAu4 may be seen especially well in the comparison of phases between both samples in shown Figure 4.3 and can, additionally to the reasons given above, be explained by the reduced voltage drop over the interface in this sample. The phase of the highly doped sample seems as an almost undisturbed continuation of the phase corresponding to the thin-film immittance. Beside the slight variation in depletion layer deviation 2 and the obviously different properties with respect to rectification, the thin-film part has a principally lower absolute impedance, also in the region of the capacitive decrease. This could indicate a slightly smaller film thickness of the highly doped sample in comparison to the low-doped sample.

To rule out that neither a potentially wrong assumption of comparability between the samples nor a poor model quality hide the effect of the different models the fits for each model are performed separately for both samples and in combination (compare fit parameters of the different scenarios in Figure 4.4). As a side effect, the comparability of the samples dependent on the chosen model is evaluated as well.

In *Variant A* only the residuals of the highly doped sample 1346bCrAu4, with negligible rectifying behaviour, are minimised.

In *Variant B* only the residuals of the low-doped sample 1346aCrAu1, with strong rectifying behaviour, are minimised.

In *Variant C* the fit is performed to minimise the residuals of both samples. Since the density of measurement points is identical, the residuals of both samples are equally weighted (still using the corresponding errors for normalisation). To compensate for different substrate resistances and a potential variation in the thickness of the ion-beam deposited thin film, the serial resistances and the thin-film thicknesses remain separate fit parameters for the samples in combined fits.

4.2 Evaluation of different models for the thin film

In this section, different variants of describing the immittance of the thin film are presented and their quality of description of the measured data assessed. The differences between those models are their connection of the resistive and capacitive part of the thin-film immittance. The novel approach of voltage-dependent immittance analysis, presented in this work, that gains all needed data in a single experiment resulting in a coherent entity of capacitive and resistive information, allows this correlation in a consistency probably never reached before . Using this connection of resistive and capacitive part, it will be shown that a correct conversion of the externally applied potential difference to the internal field, accounting for the polarisability of the surrounding media, could resolve an over 50 years old, yet unresolved, quantitative discrepancy between the theoretically predicted and the experimentally observed barrier-lowering coefficient that has been identified by many authors as the (only remaining) main discrepancy of the Frenkel-Poole model.[5] Since these new findings do not resolve the questionable fundamental assumptions of the Frenkel-Poole model, it is all the more surprising that this theory can, despite its often criticised simple and semi-classical basis, lead to a quantitatively correct description of the measured immittances (reasons why this model leads to good agreement despite its fundamental shortcomings are proposed in section 5.6.4).

In order to understand the selection of the different variants of thin-film models, it is important to be aware of the historic challenge of the discrepancy between theoretically predicted and observed barrier-lowering coefficients in all Frenkel-Poole model variants up to the present day. Hence, in the first subsection a short summary anticipates the later given, more thorough explanation of the omitted permittivity in the conversion from applied potential difference to the internal field observed by the mobile charge carrier. The detailed discussion, including a review of major steps in the development of the Frenkel-Poole model over the years, is given in the discussion in section 5.6.3. In the second subsection the above mentioned model variants for the immittance of the thin film are introduced. In the third subsection the residuals of fits for distinct samples, fitted separately or combined, are compared utilising different models (connections of resistive and capacitive parts).

4.2.1 Solving the historic challenge of the prediction of too steep slopes

The barrier-lowering coefficient determines the slope in a Schottky plot, i. e. plotting $\log J$ versus $\sqrt{E}$, for sufficiently large fields. It has been found that its experimentally determined value deviates from the theoretically predicted one. As all other values in the barrier-lowering coefficient are natural constants, the discrepancies are typically mapped

[5] Almost all publications about the Frenkel-Poole model from the 1960's on at least mention this discrepancy. In many works the deviation is the centre of the discussion, e. g. including [129, 61, 80, 170, 60, 72, 81, 28, 32]. Others directly present it as a major problem [144, 163]. There are different approaches that eliminate the low-field discrepancy, that was previously considered the only other large deviation, making the quantitative difference between observed and calculated barrier lowering even the only remaining quantitative challenge faced by the Frenkel-Poole model.

completely onto the relative permittivity. Hence, the (in comparison to the theoretically predicted value) too shallow slopes that are observed in experiments are often interpreted as permittivities larger than the respective literature values from optical frequencies. As serial parts are explicitly taken into account in this work, a reduced voltage drop at the thin film could not explain the, in comparison to the predicted value, shallower slope obtained using the usual interpretation.

In the Frenkel-Poole model, the electric field seen by the escaping charge carrier (see Figure 4.17) is composed of the Coulombic potential and the superimposed linear field caused by the externally applied potential difference. For each of the two contributions to the field, perceived by the electron (or hole) exiting the trap, different time scales and, hence, distinct permittivities are relevant. The specific frequency ranges for the distinct parts of the potential landscape, resulting in potentially different permittivities will each be derived in the following two paragraphs. The consequent thoughts are consistent with, but as a result also limited to, the assumptions within the concept of the Frenkel-Poole model. This includes the persistent principle assumption, that remained unchanged over all extensions of the Frenkel-Poole model, that the current in the system is limited by the number of 'quasi-free' mobile charge carriers and that the field-assisted de-trapping of these trapped charge carriers is the fundamentally important process which leads to the resulting current-voltage relation. Consequently, the Frenkel-Poole model, as well as most of its extended versions, focuses on the process of the *emission* of trapped mobile charges into the conductive band, while there are only few works debating the *fate* of the mobile charges after the de-trapping process (for a discussion of different possible scenarios of fate for the mobile charges after the emission into the conductive band confer [144]). Continuing in this legitimately debatable concept, the potential landscape discussed in the following paragraphs is the based on the *perspective of a single mobile charge exiting the trap*, i. e. this is not necessarily the potential around the trap in general, which would for example be perceived by a 'quasi-free' mobile charge while passing by the trap.

Within the above explained concept, the *Coulombic part* of the field is caused by the attractive interaction between the exiting mobile charge carrier and its oppositely charged immobile trap. This part of the total potential landscape, in this form, only exists for the short amount of time while the mobile charge carrier is exiting the range of influence of the attractive electromagnetic field caused by its former immobile trap. For the same reasons as described above, it is only consistent to also estimate the relevant time scale, the mobile charge carrier perceives the attractive force of the trap, in the same spirit of assumptions as the Frenkel-Poole model. Furthermore, the calculation is oriented at the (within the above described scope indeed realistic and for the characteristic of ta-C relevant) example given in Figure 4.17. With the given conditions, the distance of the barrier maximum from the trap centre in z direction z_{max} is about 12 nm. The minimal energy needed to overcome the remaining energetic barrier in z direction $e\Phi_{\mathrm{bar}}^{(\mathrm{FP})}(\mathbf{E})\Big|_z = e\Phi_{\mathrm{bar},0}^{(\mathrm{FP})} - \sqrt{\frac{e^3\mathbf{E}\cdot\hat{\mathbf{e}}_z}{\pi\varepsilon_{\mathrm{r}}\varepsilon_0}}$ in the example is around 202 meV, where the initial barrier height $e\Phi_{\mathrm{bar},0}^{(\mathrm{FP})}$ was assumed to be 250 meV. From that, the minimal velocity of an electron (assuming unchanged

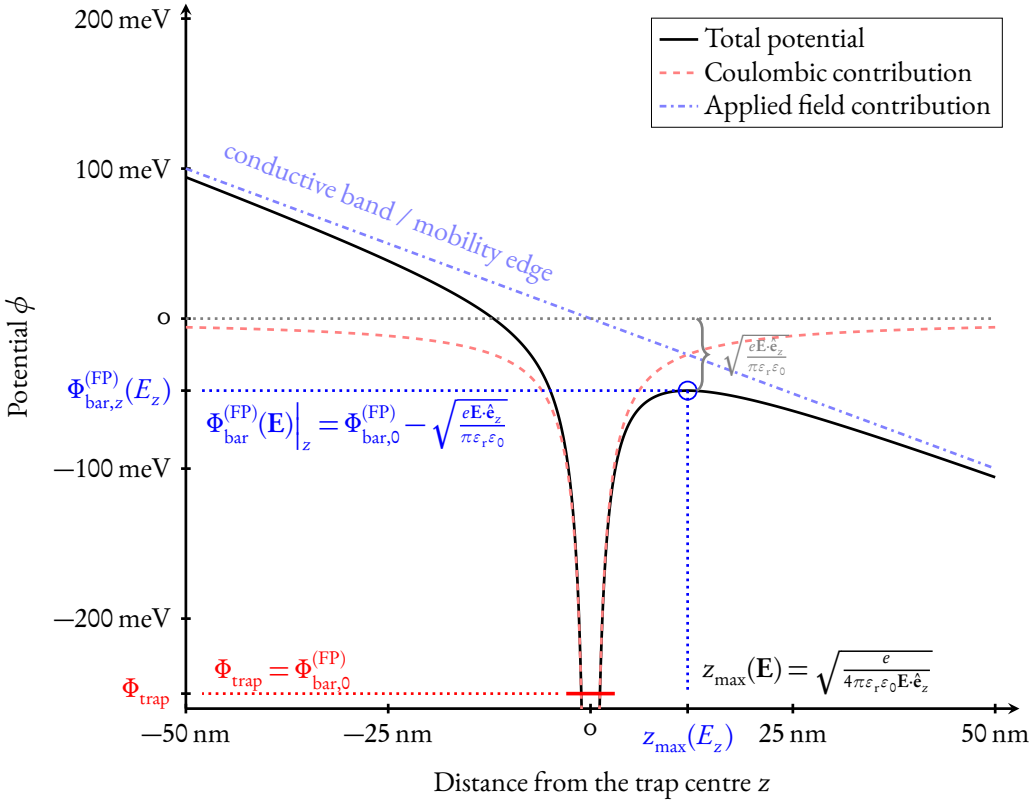

Figure 4.17: Example of the potential landscape (in z direction) assumed by the classical Frenkel-Poole model (and correct calculation of the internal field) in a fictive material with relative permittivity $\varepsilon_r^{(\mathrm{stat})} = \varepsilon_r^{(\mathrm{dyn})} = 5$, a resulting internal field of 2 MV m^{-1} (a field present, for example, if a voltage of 1 V dropped over 100 nm of the fictive material), and a trap depth of 250 meV beneath the respective conductive band or mobility edge. The boundaries and any other traps are assumed to be in infinite distance.

mass m_e)[6] classically capable of exiting the trap in z direction can, in agreement with the concept of the Frenkel-Poole model, be calculated as $v_{min} = \sqrt{\frac{2}{m_e} e\Phi_{bar}^{(FP)}(\mathbf{E})\Big|_z}$. In this example, its minimal necessary velocity in z direction is about 266.6 km s^{-1}. Assuming this is the slowest possible speed, the maximal time to pass through the maximum of the energetic barrier, and hence exit the attractive region of the potential, the maximal time of exiting the barrier t_{max} is calculated as $t_{max} = \frac{z_{max}}{v_{min}}$. In the given example, the maximal time to exit the trap, hence, the maximal duration of interaction between the immobile trap and the exiting mobile charge is 45 fs. Behind the energetic maximum the Coulombic interaction becomes negligible. As a result, an infimum for the frequency range relevant for the Coulombic interaction and, hence, for the permittivity can be estimated as $f \geq f_{min} = \frac{1}{t_{max}}$. In this example the infimum of the frequency range is about 22 THz. Comparison with the frequency ranges of different plateaus of the permittivity in Figure 5.2, it can be confirmed that the dynamic permittivity, for visible light, should be used in the Coulombic part since it is just above the ionic resonance, especially for a material like ta-C which is supposed to have no ionic polarisation. The above calculation, to determine the relevant frequency region, is *brutally crude*: no quantum mechanics, no relativistic effects considered ($v_{min} \sim \frac{1}{1000} c_0$), effective media approximation, Coulombic potential assumed, only in z direction, *but* the treatment is in the spirit of and suitable for the Frenkel-Poole model that imposes very similar restrictions and, hence, self-consistent.

Now to the above mentioned second term describing the *superimposed static field caused by the applied potential difference*: Within the framework of classical electrodynamics and continuous-media approximation, the unavoidable polarisation of the surrounding medium (represented by a relative permittivity larger than unity[7]), causes the charge to perceive different fields inside medium with respect to vacuum, though externally applied field $\mathscr{E}_{ext}$ and geometry are assumed to be identical. Although required by classical electrodynamics to convert the externally applied potential V_{ext} (here V_{tf}) to the internal field $\mathscr{E}_{int}$ [150], that is the static component of the field actually seen by the mobile charge exiting the immobile trap *inside the medium*, for the superimposed static field the permittivity of the material has never been considered before (for a detailed overview, including various references, of the missing permittivity and how the publications were missing a constant factor of the size of the forgotten permittivity confer section 5.6.3). The source of this contribution to the potential landscape is the applied potential difference that leads to a voltage drop V_{tf} over the thin film. Beginning with the publication of Frenkel [46], all works extending and most works using the Frenkel-Poole model were formulated using geometry-less quantities, e. g. conductivity σ, current density J and field E instead of resistance R, current I and potential difference V. The used geometry-less formulae were correct (and of course also the author of this work encourages the use of

[6] Typically, effective masses in insulating or semiconducting solids are lighter. Hence, this assumption gives a tendentiously lower estimate for the minimal velocity.

[7] Frequency ranges much outside of those relevant for the scope of this work or other exotic exceptions with permittivities smaller than unity are explicitly ignored in this explanation (e. g. metamaterials [157] or some permittivities for x-ray-frequencies [171]).

geometry-less quantities). However, the problem lied in the conversion of the applied field, that was rarely explicitly given since the originally measured quantities like current or voltage were not mentioned any-longer at all. In those works where the conversion was explained, the superimposed field was calculated by

$$\left(\mathscr{E}_{\mathrm{ext}} = \mathscr{E}_{\mathrm{int}}^{(\mathrm{vac})} =\right) \frac{V_{\mathrm{tf}}}{d_{\mathrm{tf}}}, \tag{4.5}$$

where d_{tf} is the thickness of the thin film. As indicated in equation (4.5), this particular calculation generally gives the *external field* which is identical to the internal field *only* in free space, where $\varepsilon_{\mathrm{r}}^{(\mathrm{vac})} \equiv 1$. In those other cases where the conversion was not described, the static permittivity $\varepsilon_{\mathrm{r,tf}}^{(\mathrm{stat})}$ was neither given, quoted, fitted, estimated, determined by a measurement nor mentioned at all. Combined with the fact that the permittivities extracted form the fitted barrier-lowering coefficient were overestimated as well, it is assumed that also these publications did not calculate the internal field. For that matter, the latest publication explicitly mentioning the conversion, *still not taking the permittivity into account*, is from 2015 [163]. The charge carrier influenced by the applied field can, however, not perceive the external field, but only the internal field. Since the Frenkel-Poole model describes an effect in a medium (*not* in free space) which generally has a permittivity different from unity, the correct calculation of the internal field from the potential difference is

$$\mathscr{E}_{\mathrm{int}} = \frac{V_{\mathrm{tf}}}{\varepsilon_{\mathrm{r,tf}}^{(\mathrm{stat})} d_{\mathrm{tf}}}. \tag{4.6}$$

In the very early work by Pool [149] , who still used the relation between current and voltage, he directly comments on omitting this permittivity since the behaviour should only be described *qualitatively*. Later works (e. g. [144, 163]), however, criticise the *quantitative* difference of the predicted versus the measured slope, while still omitting the important factor of the static permittivity for the superimposed linear field. Again, using the geometry-less quantities is not the issue, that is actually better than using harder to compare geometry-afflicted observables, however, it might have lead to overlooking the missing permittivity, as the conversion from the original observables was conventionally omitted and also since these originally measured observables were not any-longer explicitly shown.

In contrast to the Coulombic potential, which is dynamically generated by the interaction of the mobile charge carrier *moving* out of the trap, the externally applied potential difference is supposed to be stationary, meaning that the field is assumed to be applied long enough so that all polarisation processes in the respective materials finished their rearrangement or reorientation. In this case, the internal field is reduced as compared to the externally applied field by the static polarisation of the surrounding material. Hence, the calculation of the internal field uses the static permittivity $\varepsilon_{\mathrm{r}}^{(\mathrm{stat})}$.

The static permittivity is the sum of all permittivities caused by all (higher) resonances (confer section 2.1.3.1). In the case that there are no more resonances for lower frequencies than those causing the dynamic permittivity, the static permittivity would be identical to

the dynamic one. It cannot be lower. As a result, the works omitting that permittivity would at least make an error of the factor of the square root of the dynamic permittivity, but entirely possible one of a higher factor (factors with respect to the barrier-lowering coefficient). Since the static permittivity is a divisor to the potential difference that follows *in* the square root after the barrier-lowering coefficient, its negligence would lead to an overestimation of the permittivity in the barrier-lowering coefficient or, if the permittivity is not varied but taken from literature, to a too steep slope in a Schottky plot.

In summary, the until now omitted static permittivity $\varepsilon_r^{(stat)}$ necessary to calculate the *internal* field $\mathscr{E}_{int}$, which represents the effective field that the mobile charge can actually perceive from the originally applied potential difference V_{tf}, may explain the often observed and criticised deviation of the barrier-lowering coefficient. The three different models (presented in the next subsection and visualised in Table 4.1) are specifically designed to, on the one hand, experimentally verify the correctness of this assumption and, on the other hand, ascertain whether the static permittivity should be extracted from the constant phase element or the experimental high-frequency limiting capacitance.

An important recognition, discussed in detail in section 5.6, is that for both assumptions, a Coulombic trap potential and the mean internal field to be equal to the local field, the electrons contributing to the Frenkel-Poole process have to be in excited trap states.

4.2.2 The different models for the thin film

As explained before, the different models for the thin film exclusively vary the connection between the capacitive and the resistive part in the description. It is found that the introduction of the correct determination of the internal field seems to resolve the, at least over 50 years old challenge of, quantitative discrepancy between theoretically calculated and experimentally determined barrier-lowering coefficient in the Frenkel-Poole model, while giving a reasonable value for the permittivity of the material.

Specifically the novel approach of voltage-dependent immittance analysis, presented in this work, made the missing factor apparent and allowed simultaneously to evaluate the compatibility between the capacitive and resistive model. Conventional approaches measure solely the static current-voltage behaviour or only the immittance response at a single bias voltage. One key idea of the presented approach is to determine the immittance spectra for a range of bias voltages. As the dc resistance is part of each spectra (assuming that low frequencies are part of the spectra), the full information of the current-voltage behaviour is included. Since the spectra also include the capacitive bypasses and the different bias voltages emphasise distinct pieces according to the correspondingly varying voltage drop over the specific piece, the serial pieces of a system can be separated (also without explicitly using external-parameter-dependent physical models which is, though not utilised here, explained in detail in section 5.5). Consequently, their specific permittivities, like the one of the thin film which is relevant for this subsection, can be determined.

Another key idea of the proposed approach is connecting resistive and capacitive models of each significant piece of the system. In this way, it cannot only be checked whether the capacitive or resistive model are separately applicable to a piece, but (without

Model 1	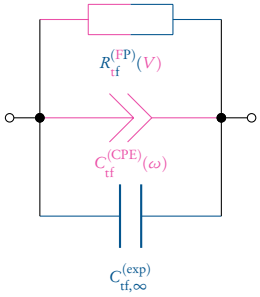	$R_{\mathrm{tf}}^{(\mathrm{FP})}(V) \longrightarrow \ldots \sqrt{\frac{e}{\pi\varepsilon_0\varepsilon_{\mathrm{r,tf}}^{(\mathrm{dyn})}}} \cdot \sqrt{\frac{\lvert V\rvert}{d\,\varepsilon_{\mathrm{r,tf}}^{(\mathrm{stat})}}} \ldots$ $C_{\mathrm{tf}}^{(\mathrm{CPE})}(\omega) = \varepsilon_0 (i\omega)^{n_{\mathrm{tf}}-1} \Delta\varepsilon_{\mathrm{r,tf}}^{(\mathrm{CPE})} \frac{A}{d}$ $C_{\mathrm{tf},\infty}^{(\mathrm{exp})} = \varepsilon_0 \varepsilon_{\mathrm{r},\infty,\mathrm{tf}}^{(\mathrm{exp})} \frac{A}{d}$	$\varepsilon_{\mathrm{r,tf}}^{(\mathrm{stat})} = \varepsilon_{\mathrm{r,tf}}^{(\mathrm{dyn})} + \Delta\varepsilon_{\mathrm{r,tf}}^{(\mathrm{CPE})} \cdot \sin\left(\frac{n_{\mathrm{tf}}\pi}{2}\right)$ $\varepsilon_{\mathrm{r,tf}}^{(\mathrm{dyn})} = \varepsilon_0 \varepsilon_{\mathrm{r},\infty,\mathrm{tf}}^{(\mathrm{exp})}$
Model 2	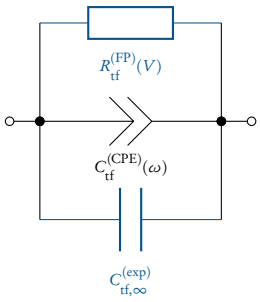	$R_{\mathrm{tf}}^{(\mathrm{FP})}(V) \longrightarrow \ldots \sqrt{\frac{e}{\pi\varepsilon_0\varepsilon_{\mathrm{r,tf}}^{(\mathrm{dyn})}}} \cdot \sqrt{\frac{\lvert V\rvert}{d\,\varepsilon_{\mathrm{r,tf}}^{(\mathrm{dyn})}}} \ldots$ $C_{\mathrm{tf},\infty}^{(\mathrm{exp})}(\omega) = \varepsilon_0 \varepsilon_{\mathrm{r},\infty,\mathrm{tf}}^{(\mathrm{exp})} \frac{A}{d}$ No link of $C_{\mathrm{tf}}^{(\mathrm{CPE})}(\omega)$ with resistive part.	$\varepsilon_{\mathrm{r,tf}}^{(\mathrm{stat})} \simeq \varepsilon_{\mathrm{r,tf}}^{(\mathrm{dyn})}$ $\varepsilon_{\mathrm{r,tf}}^{(\mathrm{dyn})} = \varepsilon_{\mathrm{r},\infty,\mathrm{tf}}^{(\mathrm{exp})}$
Model 3	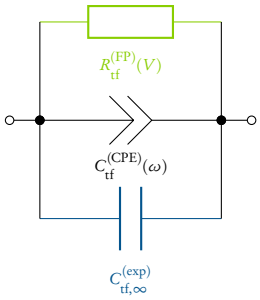	$R_{\mathrm{tf}}^{(\mathrm{FP})}(V) \longrightarrow \ldots \frac{1}{m} \sqrt{\frac{e}{\pi\varepsilon_0}} \cdot \sqrt{\frac{\lvert V\rvert}{d}} \ldots$ $C_{\mathrm{tf},\infty}^{(\mathrm{exp})}(\omega) = \varepsilon_0 \varepsilon_{\mathrm{r},\infty,\mathrm{tf}}^{(\mathrm{exp})} \frac{A}{d}$, no link to $R_{\mathrm{tf}}^{(\mathrm{FP})}(V)$. No link of $C_{\mathrm{tf}}^{(\mathrm{CPE})}(\omega)$ with resistive part.	$m \overset{?}{\longleftrightarrow} \sqrt{\varepsilon_{\mathrm{r,tf}}^{(\mathrm{stat})} \varepsilon_{\mathrm{r,tf}}^{(\mathrm{dyn})}}$ $m \longleftrightarrow \varepsilon_{\mathrm{r},\infty,\mathrm{tf}}^{(\mathrm{exp})}$

Table 4.1: Visualisation of the connections between resistive and capacitive parts of the thin-film circuit in the different models (other serial generalised Voigt-circuit elements remain unchanged). The models are designed to evaluate if the proposed revision of the Frenkel-Poole model can resolve (the ongoing discussion about) the discrepancy between experimentally observed and theoretically predicted barrier-lowering coefficient as well as, if confirmed, whether to extract the static permittivity from the constant phase element or the ideal high-frequency limiting capacitance.

accidental influence of other pieces in the system) also whether the models are compatible to each other at all. Latter can be determined by fitting parameters that appear in both, the capacitive and the resistive model, as a single parameter for both models together. Although this combined analysis seems to be an obvious step, usually the capacitive and resistive parts are analysed separately and only afterwards the respective results are compared. Most likely also, because voltage-dependent immittance measurements are already unusual on their own, in other contexts than capacitance-voltage analysis. For the heavily investigated system of semiconductor interfaces, on the other hand, the same parameter of the Schottky barrier height is known to have different values when it is extracted either from capacitive or resistive properties as long as interface traps or charged defects in the insulator are not included in the models (e. g. confer [172, 189, 128] for the discrepancies and [138, 162, 161] for how to convert the different flat-band voltages for high and low frequencies into defects in the insulator or traps at the interface), which is why in this specific case, the presumably shared parameter had to be interpreted as two separate parameters (the different results, for a combined value or two separate values of the Schottky-barrier height extracted from capacitive or resistive properties and its reasons, are further discussed in section 2.4.1). As a result of taking these steps on a new ground for other models, it must be evaluated if these shared parameters, present in both, capacitive and resistive models, are comparable at all and, if so, which fulfil this requirement. For the thin film this concerns the dynamic and static permittivity.

The resistive part is described by the Frenkel-Poole model. This current-voltage (and -temperature) behaviour of ta-C has been identified in numerous publications (e. g. [38], [168, 91][8], [90], [53], [132]), in general, and for samples synthesised in the same set-up by Ronning *et al.* [156], Hofsäss [68] and Brötzmann *et al.* [15], in particular. Especially for the dynamic permittivity, in the barrier-lowering coefficient, the systematic deviation from literature values, obtained through optical measurements, is a well known problem for the Frenkel-Poole model in general. Furthermore, there are eligible doubts (discussed in section 5.6 and specifically in its subsection 5.6.2) that the bulk dynamic permittivity of the material as well as the assumed Coulombic potential, leading to this specific barrier-lowering coefficient in the first place, are at all physically reasonable assumptions [80, 163]. Hence, the interpretation of the dynamic permittivity in the barrier-lowering coefficient is questionable.

As mentioned before, in this work, a corrected conversion from applied potential difference to the internal electrical field is suggested. Since the Frenkel-Poole model assumes a stationary superimposed applied field, this calculation involves the static permittivity. The measurements of the impedance of the thin film piece (see Figure 4.1) show a constant-phase behaviour in the frequency range from around 5 kHz to 1 MHz. There are various different explanations for such a constant-phase behaviour at low frequencies [107, 108, 190], that are discussed in detail in section 5.3. The most common explanation is the appearance of the Maxwell-Wagner effect [187, 107, 108, 190]. It leads to the observation of apparently large permittivities for low frequencies and is caused by interfaces of

[8] In both works the authors interpret their findings as Schottky-emission process since they are obviously unaware that the observed deviation in the barrier-lowering coefficient is normal.

two or more 'materials' of either different sized permittivities of usual magnitude (with identical conductivities) or identical permittivities of normal magnitude in combination with different conductivities (of usual size) or a combination of both [187]. A typical structure where a single solid alone can lead to the Maxwell-Wagner effect is a polycrystalline microstructure (which was already suggestively described in the original work of Wagner by spheres of different conductivity and permittivity as the surrounding matrix) [187]. Furthermore, with the usual approaches it is very difficult to measure the isolated contribution of a separate piece alone, that is without the parasitic Maxwell-Wagner contribution of at least the interfaces at the contacting electrodes. As a consequence (according to Young and Frederikse not only because of the proper Maxwell-Wagner effect in its narrower sense, confer to the discussion in section 5.3), the low-frequency part is in general omitted for the determination of the static permittivity [190]. However, in the here investigated case of ta-C, there are three clues indicating that the constant phase element, observed at low frequencies, is not caused by the Maxwell-Wagner effect:

First, due to the new approach of analysing voltage-dependent immittance spectra, in this work, different serial contributions can be separated (a novelty previous works did not have). Hence, the constant phase element should exclusively describe the ta-C film without Maxwell-Wagner effects at interfaces to different materials that could lead to apparently large permittivities at low frequencies. Secondly, ta-C itself might have certain regions of slightly varied properties caused by unavoidable statistical fluctuations, but as an amorphous material it is not supposed to have any real internal borders, like grain boundaries in a polycrystalline material. Thirdly, as also supported by the observation of Frenkel-Poole conduction (and variable-range hopping at lower temperatures [50, pp. 63-108]) [107, 108], ta-C falls in the quite large group of materials that observe the so-called 'universal response' [148, 84, 78, 79]. This ac conductivity effect caused by the dominance of localised states in the transport and a certain element of disorder, leads to a constant phase behaviour at low frequencies [84, 78, 79, 107, 108]. According to Lunkenheimer [107, 108], this effect leads to an actual increase in permittivity towards lower frequencies.

It remains, however, unclear if this part of the permittivity should be considered a real and not an apparent contribution to the bulk static permittivity. It seems to be caused by an effect inherent to the bulk and not by the interfaces (Maxwell-Wagner polarisation) which are in this work explicitly taken into account. Also, it seems plausible to assume that pronounced ac conductivity properties exist in this material. The ac conductivity *is defined* in a way that it is closely associated to the permittivity (confer [40] as well as equations (2.9a) and (2.9b) with the corresponding paragraph in 2.1.3.2), but this is *just a convention* that interprets any part of the dielectric term in equation (2.3) as the frequency-dependent contribution to the conductivity, while excluding the dc contribution. Just as the convention excludes the static conductivity σ_{dc} in the real part of the ac conductivity σ'_{ac}, the conversion back into the complex permittivity might generally include contributions that are actually from the retarded response of the free current. As was already elaborated in the theory, in section 2.1.2 and will be discussed in section 5.4, the convention always maps the complete parts (i. e. any frequency-dependent contribution) to one of each other, and that might not necessarily represent the real contributions of the

different parts. The very fundamental question arises, how a frequency-dependent part of the free current can or should be distinguished and separated from the permittivity. The form of the Kramers-Kronig relation requires that all frequency-dependent contributions are included in their respective parts. Hence, a retarded conduction process should contribute to polarisation if it cannot follow the applied field any longer. The constant ignorance of the low-frequency contributions of any material whether it observes ac conductivity or not [190] indicates that it is not easy to determine which contributions to the permittivity are apparent and which true. Hence, whether this constant-phase behaviour, assumed to be caused by the *conduction processes* in the material, is really an effective contribution to the static permittivity and, consequently, influences the internal field is discussed in section 5.3. The uncertainty about whether the universal response leads to a real (and not just another apparent) contribution to the static permittivity, consequently, manifests itself in the presence of two different models to extract the static permittivity.

In summary, this leads to two questions that should be answered by the three different models: First, does the correct calculation of the internal field in the Frenkel-Poole model solve the quantitative discrepancy between the experimentally observed and the predicted barrier-lowering coefficient at all? And, if yes, is the static permittivity extracted from a region described by a constant phase element, either caused by a Maxwell-Wagner effect or, more likely, as a consequence of hopping conduction, a valid summand in the static permittivity or not?

Three models, depicted in Table 4.1, are proposed to introduce the connection between the above described permittivities in the Frenkel-Poole model and the determined capacitances of the thin film:

In **Model 1**, it is assumed that the dynamic permittivity in the barrier-lowering coefficient is identical to the one in the parallel experimental high-frequency limiting capacitance $C_{\infty}^{(\mathrm{exp})} = \varepsilon_0 \varepsilon_{\mathrm{r},\infty}^{(\mathrm{exp})} \frac{A}{d}$. The static permittivity is supposed to be the sum of the already mentioned dynamic permittivity $\varepsilon_{\mathrm{r},\infty}^{(\mathrm{exp})}$ and the real part of the permittivity extracted from the constant phase element of the thin film, i. e. $\Delta\varepsilon_{\mathrm{r,tf}}^{(\mathrm{CPE})} \cdot \sin\left(\frac{n_{\mathrm{tf}}\pi}{2}\right)$. There are several requirements for this model that might not be fulfilled: First, the idea behind the Frenkel-Poole model must be correct at all, e. g. the assumption of Coulombic traps and that the conduction process in the material is limited by the number of electrons in the conductive band which are field-assisted thermally excited from the aforementioned traps. Secondly, the dynamic permittivity for the 'relatively large' whole thin-film volume must be identical to the permittivity of the local 'relatively small' volume around the trap. Otherwise, the constant in the barrier-lowering coefficient should be some effective local permittivity that could have a very different value, more accurately describing the local environment around the trap. Thirdly, it must be possible to extract the dynamic permittivity from the experimental high-frequency-limiting capacitor. For the investigated thin-film material, it is quite reasonable to assume that the value of the dynamic permittivity extracted from this capacitor remains unchanged up to the frequencies relevant for the Coulombic interaction, since most polarisation processes with intermediate resonances are not at all or not significantly present in an amorphous material with covalent bonds and only

Assumptions	Model 1	Model 2	Model 3
The current-voltage relation follows a $\log(I)$-$\sqrt{(V)}$-law.	✓	✓	✓
The general idea of the Frenkel-Poole model is rudimentary correct.	✓	✓	
The connection, of the dynamic permittivity with the voltage dependence of the resistance, as described by the Frenkel-Poole model is valid.	✓	✓	
The correction to calculate the internal field using the static permittivity is valid.	✓	✓	
The relevant dynamic permittivity can be extracted from the high-frequency-limiting capacitor.	✓	✓	
The effective medium approximation is still valid in the local environment of the trap, i. e. local and global relative permittivity are identical.	✓	✓	
The constant phase element is a genuine contribution to the bulk static permittivity of the thin film.	✓		
The constant phase element behaves like a relaxational and not like a resonant dispersion.	✓		
The bulk static permittivity of the thin film should be extracted from the high-frequency-limiting capacitor instead of from the constant phase element.		✓	
The static and the relevant dynamic permittivity are approximately identical in ta-C, i. e. there are no polarisation mechanisms with resonances between their frequencies that give relevant contributions.		✓	

Table 4.2: Assumptions that are required for each model and, hence, verified if the sum of residuals of the corresponding model is not significantly higher than the model(s) with more degrees of freedom. Since already the invalidity of one of the several assumptions should lead to significant deviation and, in consequence, dismissal of the respective model, which assumptions was incorrect cannot be determined without further investigations. Another fourth model which did not even require $\log(I)$-$\sqrt{(V)}$ behaviour but only a weaker $\log(I)$-V^{ξ} relation, did obtain $\xi \approx 0.5$ and, hence, shows no visible difference to the third model. In consequence, its results are not shown.

one element. Fourthly, the constant phase element has to be a contribution to the static permittivity at all. Finally, as usual in this frequency range, a relaxational rather than a resonant dispersion is assumed. This means that the total real part of the permittivity step of the resonance corresponding to the constant phase element is a summand in the static permittivity. As already explained, the low-frequency regime, at which the constant phase element is observed, is usually strongly influenced by contributions of interfacial polarisability [190], also caused by random inhomogeneities in the dielectric and the interface. Such contributions are not part of the bulk static permittivity responsible for the lowered internal field as compared to the external field [190].

As the last two requirements of Model 1 might be invalid, in **Model 2** it is assumed that the permittivity extracted from the constant phase element is not comparable with the missing summand for the static permittivity. As a result, the dynamic permittivity is used as an approximation for the static permittivity without any other summand, i. e. $\varepsilon_{\mathrm{r,tf}}^{(\mathrm{dyn})} \simeq \varepsilon_{\mathrm{r,tf}}^{(\mathrm{stat})} = \varepsilon_{\mathrm{r},\infty,\mathrm{tf}}^{(\mathrm{exp})}$. This is in agreement with the suggestion by Young and Frederikse who assess that 'it usually is impossible to measure the static dielectric constant in the low frequency range' [190, p. 317]. Furthermore, this is exactly how Young and Frederikse [190] extracted the static permittivity of many solids, including different allotropes of carbon. Now, one could identify the product, of the barrier-lowering coefficient in the exponent $\beta = \sqrt{\frac{e}{\pi\varepsilon_0\varepsilon_{\mathrm{r,tf}}^{(\mathrm{dyn})}}}$ of the Frenkel-Poole model with the subsequent factor of the square root of the internal applied field $\sqrt{\mathscr{E}_{\mathrm{int}}} = \sqrt{\frac{|V|}{d\,\varepsilon_{\mathrm{r,tf}}^{(\mathrm{dyn})}}}$, as a squared dynamic permittivity in an *effective* barrier-lowering coefficient $\beta_{\mathrm{eff}} = \sqrt{\frac{e}{\pi\varepsilon_0\left(\varepsilon_{\mathrm{r,tf}}^{(\mathrm{dyn})}\right)^2}}$ (resulting in a linear factor of the permittivity in the exponent) if the vacuum conversion for the internal applied field from the potential difference $\sqrt{\mathscr{E}_{\mathrm{int}}^{(\mathrm{vac})}} = \sqrt{\frac{|V|}{d}}$ would be used. Since, in direct comparison with Model 1, the parameters of the constant phase element can be varied freely from the resistive part of the thin film, the degrees of freedom of the fit are increased with respect to Model 1. This model still needs to meet the requirement that the local and the global dynamic permittivities are comparable, i. e. the effective-medium assumption should not break. Furthermore, the connection, between the barrier-lowering coefficient and the permittivity, as suggested by the Frenkel-Poole model (including the corrections of this work) must still be valid. This also implies that the assumptions of the Frenkel-Poole are not completely unjustified. Moreover, it has as well to be true, that the permittivity for the relevant frequencies can be extracted from the experimental high-frequency-limiting capacitor after all.

If one of these requirements would not be justified, the permittivity extracted form the capacitance should not be connected to the resistive Frenkel-Poole model at all. This possibility is taken into account with **Model 3**. Consequently, the dynamic permittivity was removed from the exponent (equivalent to setting it one in the barrier-lowering coefficient) and instead a *free* divisor m was introduced that divides the barrier-lowering coefficient (hence the parameter m is *not* inside the square root). This parameter is independent of any capacitive element. There is no restriction imposed on it by any other

element. As a result, in Model 3 resistive part and capacitive part of the thin film are completely independent. As compared to Model 1 these are two and in comparison to Model 2 one more degrees of freedom for the fit. Model 3 makes the parameters in the exponent essentially free, however, the form of the relation between current and voltage, $I \sim V \exp(\sqrt{V})$, remains fixed.

To permit further variance, at least to some extent, in the connection between current and voltage, in **Model 4**, another free parameter ξ that allowed the power of the field in the exponent to deviate from the square root was introduced, i. e. $\left(\frac{|V|}{d}\right)^{\xi}$ in the exponent instead of $\sqrt{\frac{|V|}{d}}$ with $\xi = \frac{1}{2}$. However, the fitting routine did not change the parameter significantly from 0.5, so that showing the results of model 4 (indistinguishable from those of Model 3) was omitted. Hence, even if the extremest point of view, that the idea of Frenkel is totally wrong, was true, it still seems that the current-voltage relation follows a $I \sim V \exp(\sqrt{V})$ law for high applied fields.

Finally, Model 3 has enough degrees of freedom to cover the case that only the current-voltage relation is correct, too. If no other model than this, without any connection to the measured permittivity, could fit the measured data well, this would also indicate that the suggested correction to calculate the internal field would not solve the problem of the too high barrier-lowering coefficient. It would of course further indicate that the Frenkel-Poole model does not describe the underlying physics at all.

4.2.3 Evaluation of the residuals of the fits for different models and samples

4.2.3.1 Residuals and deviations normalised on the device error plotted over the external parameters

In Figure 4.18 the external-parameter-dependent deviations of absolute impedance and phase, normalised on their respective device errors, for the three different models are compared. In order to exclude potential influences arising from a combined optimisation of both samples, the shown deviations were obtained for optimisations specifically of sample `1346bCrAu4`, i. e. the one that does not have a pronounced rectifying behaviour. Similarly, deviations plots for sample `1346aCrAu1` were already shown in 4.7. In Figures 4.19 and 4.20 residuals are plotted over the external parameters for each model and optimisation of each sample separately as well as combined.

About the magnitudes of the device-error-normalised deviations The magnitudes of the deviations due to the normalisation with the device errors might be misleading. As can be seen in the contours of Figure 4.1 a deviation unit in the absolute impedance plots is comparable to 1 %, so that the deviation scale reaches from —35 % to 35 %.

> Why only normalised deviations are shown is illustrated at the following example: Regarding the deviations of the phase without normalisation on the device error, the most prominent deviations would be seen for low frequencies, where the expected

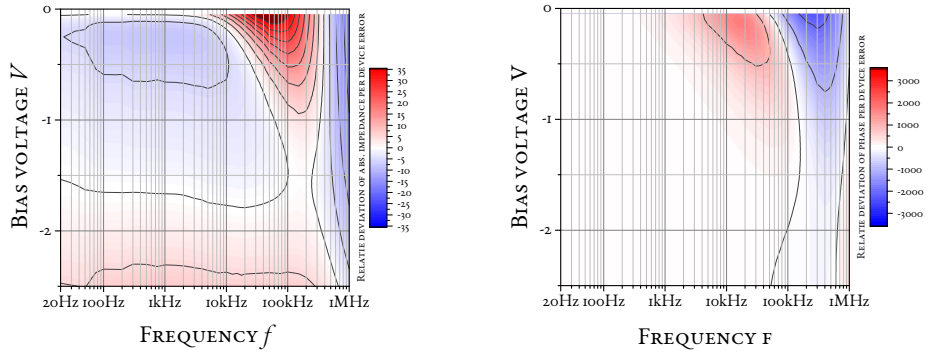

(a) Model 1, abs. impedance

(b) Model 1, phase

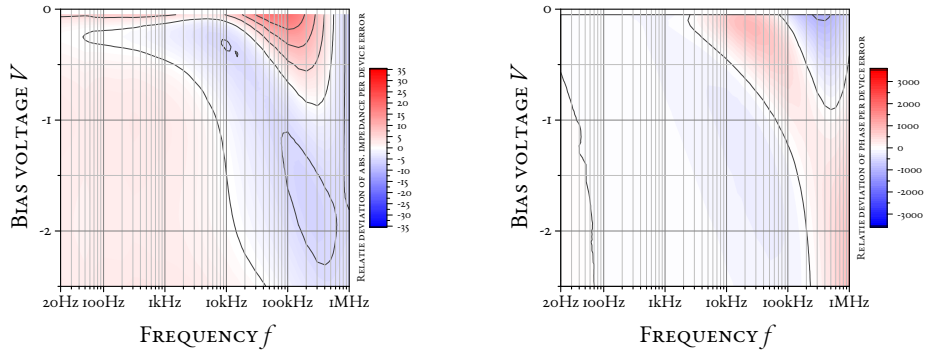

(c) Model 2, abs. impedance

(d) Model 2, phase

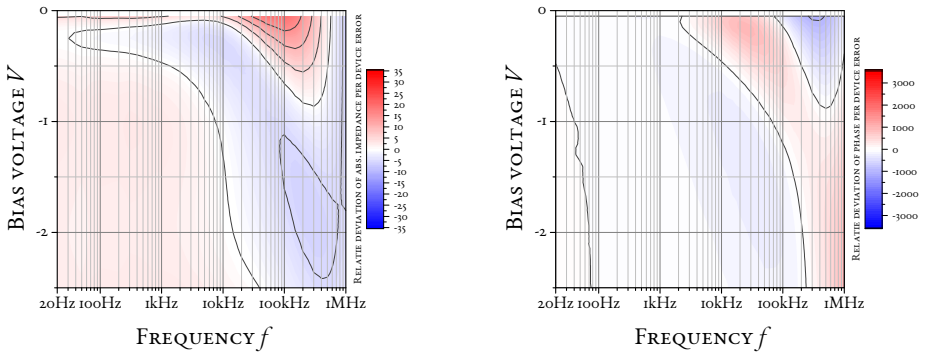

(e) Model 3, abs. impedance

(f) Model 3, phase

Figure 4.18: Deviation plots for absolute impedance and phase, normalised on the respective device error, for each of the three models, optimised on the shown sample `1346bCrAu4`. Reasons for the seemingly striking magnitudes in deviation plots are discussed in subsection 4.2.3.1.

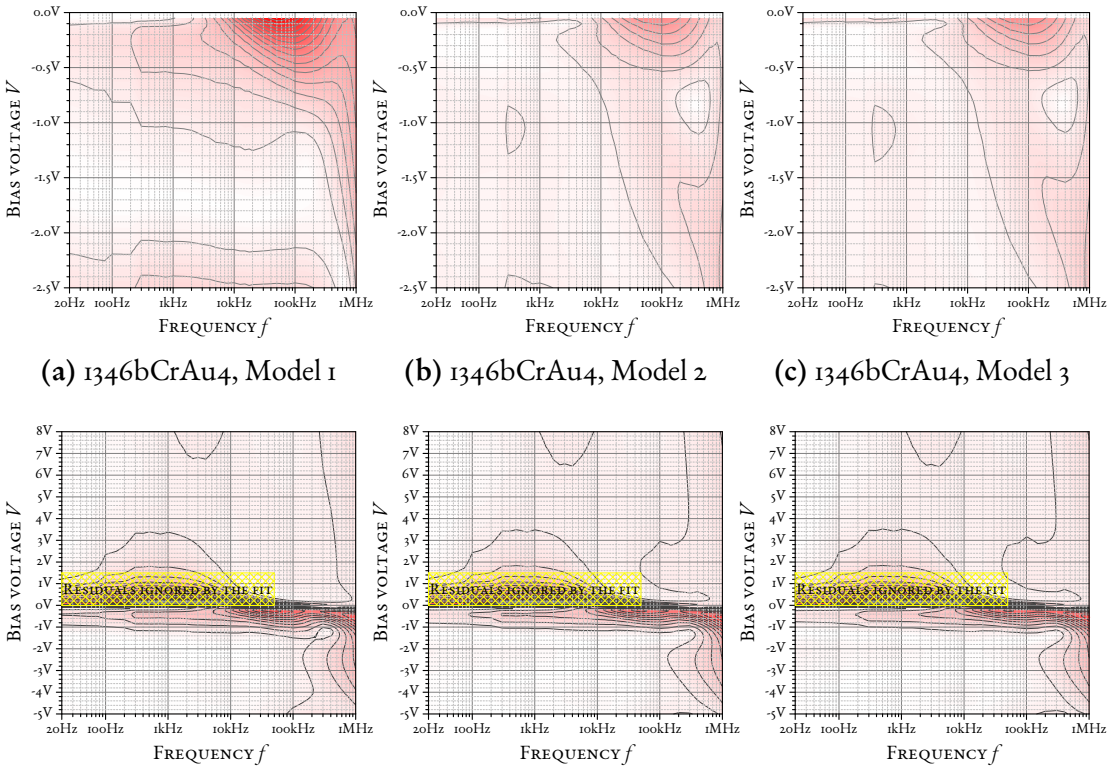

(a) 1346bCrAu4, Model 1 **(b)** 1346bCrAu4, Model 2 **(c)** 1346bCrAu4, Model 3

(d) 1346aCrAu1, Model 1 **(e)** 1346aCrAu1, Model 2 **(f)** 1346aCrAu1, Model 3

Figure 4.19: All residual plots use the scale given in Figure 4.20g. The residuals of which sample were optimised for and which model was selected is given in the subcaption. In (a)-(c) the contours plots of the residuals of sample `1346bCrAu4` and in (d)-(f) the ones of sample `1346aCrAu1` are depicted. Indicated residual regions of sample `1346aCrAu1` are ignored in the fit. Contours in this Figure only show fits optimised for a single sample. In Figure 4.20 joint optimisations for both samples can be found.

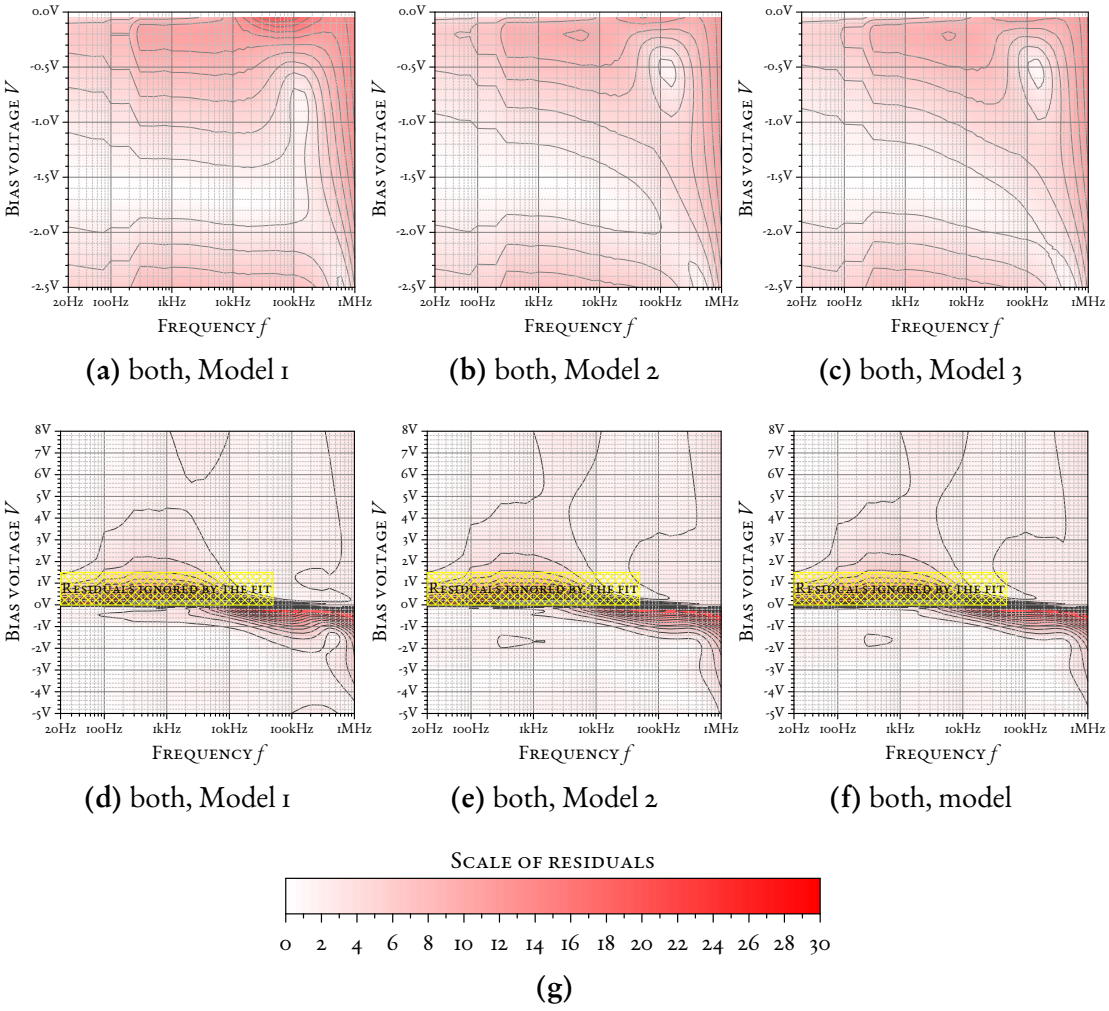

(a) both, Model 1 **(b)** both, Model 2 **(c)** both, Model 3

(d) both, Model 1 **(e)** both, Model 2 **(f)** both, model

(g)

Figure 4.20: (a)-(f): Contour plots of the residuals using different models while always optimising jointly for both samples. In (a)-(c) the contours plots of the residuals of sample `1346bCrAu4` and in (d)-(f) the ones of sample `1346aCrAu1` are depicted. The used model is given in the subcaption. Indicated residual regions of sample `1346aCrAu1` are ignored in the fit. Contours in these Figure only show fits optimised for both samples. In Figure 4.19 separate optimisations of single samples can be found. (g): Scale that is used for all plots in this Figure and Figure 4.19.

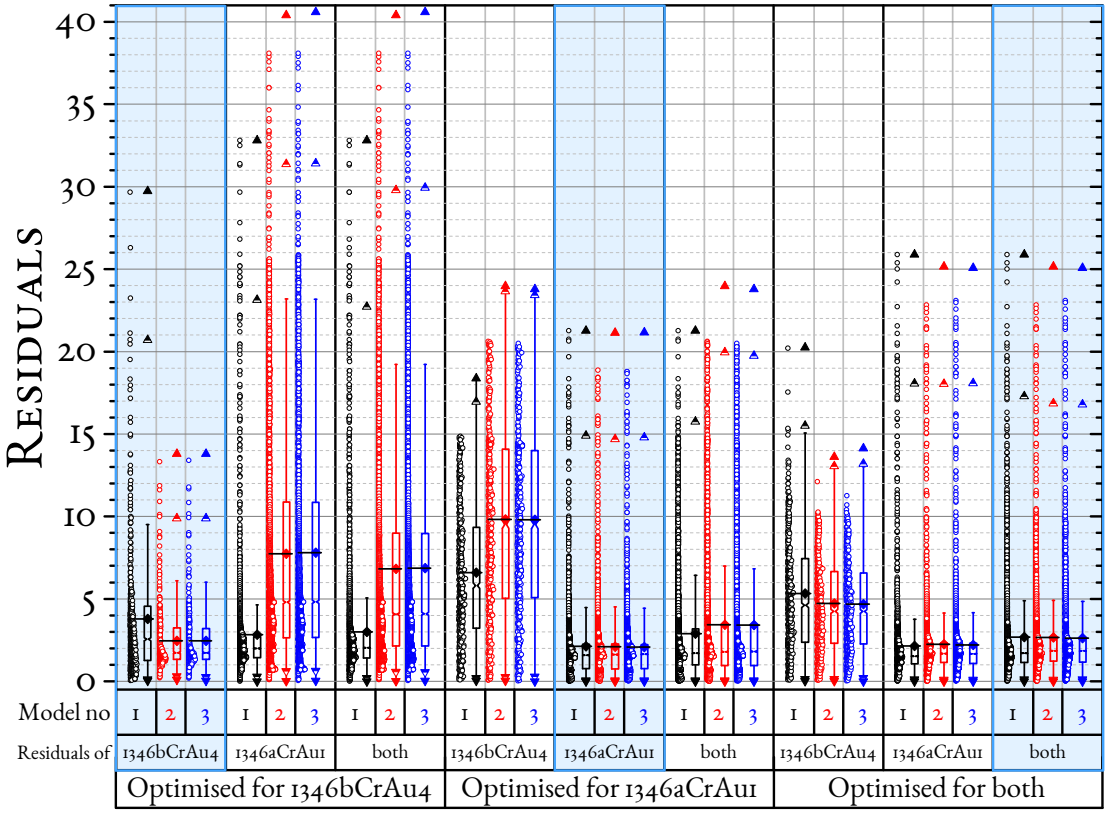

Figure 4.21: Key values of the residual distributions (*as they were given to the fitting routine*, i. e. without residuals of the ignored region) to asses the quality of the fits for different scenarios. The three main columns indicate on which sum of residuals the fit routine was optimising: only for sample `1346bCrAu4`, solely for sample `1346aCrAu1` or both combined. In these main columns the statistics of the residual distributions of each sample and the combination are separately given while highlighting the residual distribution key parameters that were optimised for in the fit with a blue box and light blue background behind the subcolumns title. Each of these subcolumns is divided in three different models that were assumed in the corresponding fit. Example: The fifth distribution from the left, visualised by its key parameters, are the residuals of sample `1346aCrAu1` for performing a fit using Model 2 only optimising on the residuals of sample `1346bCrAu4`, i. e. the calculated residual distribution is shown for sample `1346aCrAu1` while actually the other sample was fitted using Model 2.

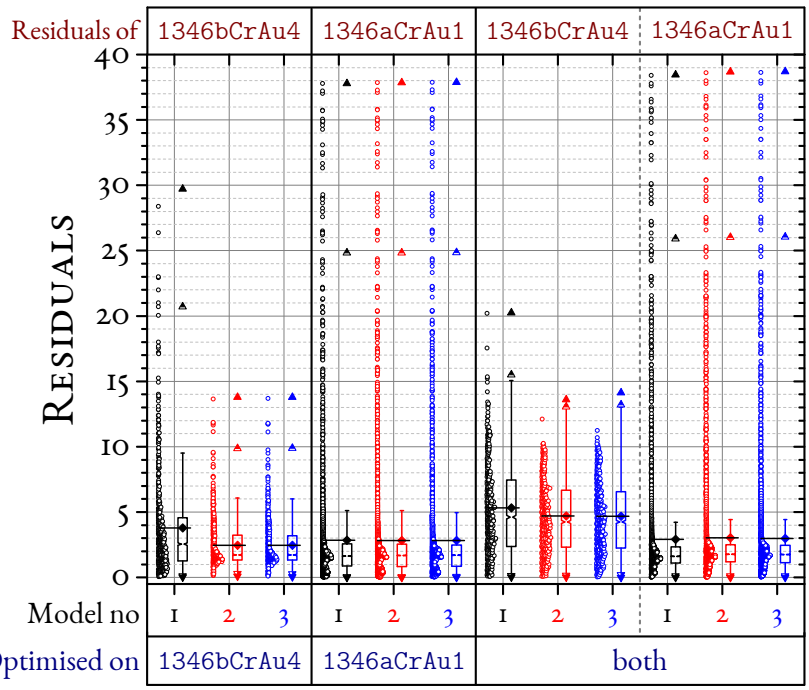

Figure 4.22: Distributions of residuals, *including those in the region ignored by the fit* (as marked in the detailed residual plots in Figures 4.19 and 4.20). The residual distributions of the combined fit are shown per sample.

> phase is zero. The measured phases, in this region, are very small but not exactly zero whereas the simulated values really are zero (within the machine precision). Hence, the relative deviations in that region are of the order of unity, i. e. 100 %. Since the 'actually relevant' deviations are, as already mentioned above, inside a −35 % to 35 % interval, they would be hard to separate from this 'irrelevant noise' that is a result of the finite measurement error.

The error of the phase calculated according to the specifications of the manufacturer is relatively small. Although its value is highest for what is expected to be a purely resistive plateau at low frequencies (compare with the example above), the observed invariably statistical variation of the measured phase seems to be significantly larger than the error given by the manufacturer. Even so, the weighting due to the variation of the magnitude for different regions of bias, frequency and complex impedance values seems to reflect the size of the statistical variation correctly. As indicated by the resulting deviation plots where all relevant deviations are clearly visible. Determination of a correction factor for the device error would dissolve the probable overestimation of the model error. It would, however, neither change the physical understanding of the system nor, since it is probably only a constant factor, alter the regions where the chosen models deviate from the measured behaviour. Moreover, as mentioned above, all relevant deviations are well recognisable.

From the contour plots of the phase error in Figure 4.1, it can be seen that the absolute value of the phase error is quite small. As a result, the highest point of normalised

deviation in Figure 4.18b, that lies in an area of systematic deviation (with a measured feature that cannot be described by our model), corresponds to a relative deviation from the measured value of 34 %, in Figure 4.18f even 'only' 18 %. That is why one should not be confused by the high numbers in the scale of the phase deviation plots. Hence, it was chosen to postpone above mentioned cosmetic changes of the statistics for a later time while, for now, concentrating on the physical interpretation.

The deviations of absolute impedance for **Model 1**, compare Figure 4.18a, show that using the permittivity extracted from the constant phase element in both, resistive and capacitive, parts of the thin film models leads to a compromise with a poor description of either part. In combination with Figure 4.4, it can be seen that the relative permittivity of the resistive part must be around 4.2. As part of the exponent, the resistivity, and with that the overall impedance, is very sensitive to this parameter. A connection with the permittivity of the constant phase element, as introduced in Model 1, forces its permittivity to a much too low value. As can be seen in the development of the real part of the permittivity of the constant phase element for sample `1346bCrAu4` in Figure 4.4, after releasing this connection its value becomes much (by around a factor of 20) higher and then remains on that high level for both other models.

To obtain the permittivity in the barrier-lowering coefficient comparable to the almost always used Frenkel-Poole model with a faulty conversion of the applied field, one has to square the values given at the row of factor m in Figure 4.4. Thus, using the conventional model with faulty conversion of the applied field, the permittivity would range approximately from 16 to 20, for which even the lowest value is unreasonably large.

A very important result with respect to the permittivity correction may be noted in Figure 4.4: While the fit parameters for the permittivity extracted from the high-frequency-limiting capacitor $C_{\infty}^{(\mathrm{exp})}$ is in **Model 3** completely independent from the value m in the resistive model, their fitted values are for a fit of sample `1346bCrAu4` comparable (as indicated by including the permittivity value extracted from the capacitive part in the same row of Figure 4.4 as the parameter m). Obtaining similar values for the same parameter in distinct contributions (resistive versus capacitive) in a free fit may be seen as an indication that the correction of the Frenkel-Poole model, proposed in this work, actually resolves the usually observed discrepancy. That this similarity is obtained only in the fit for sample with highly doped substrate might be ascribed to the strong influence of the flat-band voltage shift and capacitive stretch-out from the depletion layer that reaches far into the negative bias voltage region and is assumed to distort the extracted thin-film capacitance (compare Figure 4.3).

4.2.3.2 Comparison of the overall fit quality for different samples and models

In the last section, different models to describe the measured data were proposed. As explained, each of these models is associated with different interpretations of the underlying physics. One of the aims of this section is to compare the goodnesses of the fits to decide which of the models describes the measured data correctly, and in consequence test whether the introduced correction in the Frenkel-Poole model leads to a quantitatively correct barrier-lowering coefficient. Ideally, this comparison of the quality of the fit

should be possible across the fits of different samples as well as combined fits.

In order to meet these self-imposed requirements, in the first part of this section, it will be explained, what distribution of residuals is expected and why the deviations from the model are, in this case, not normally distributed. Before finally comparing the different fits, a general introduction in the chosen visualisation of the fit quality is given, which shall allow us to compare the different fits comprehensively over multiple samples and models. Reasons for and possible difficulties of the chosen representation are discussed.

Expected distribution of the residuals To perform a least-square regression analysis, the deviations from the model function are usually assumed to be normally distributed (with zero mean) per value and uniformly between values (with suitable normalisation, resulting in an identical normal distribution around zero for each error) [131, pp. 104-105 and pp. 168-169] Meaning, that there is no more information in the deviations (the deviations arise only by chance), also implying that the model function has to describe all aspects of the measured data to be fitted. *Only* in this case (potentially with suitable normalisation), the residuals would be χ^2 distributed.

> The χ^2 distribution is only mentioned in this context because many authors give the χ^2 value after a fit of immittance data with an EEC to show the significance of the fit. Indeed, since EECs are used only to fit a spectrum recorded at one condition, the deviations from the model can for a well designed circuit be assumed solely statistical in nature and normally distributed. In this case, and assuming a high enough number of data points [29], the χ^2 test can be used to quantify the goodness of a fit. Due to the circuit ambiguity, the goodness of a fit itself does unfortunately not guarantee that the chosen representation of circuit elements is representing the underlying physics, or in the words of D. Macdonald 'while the analog may produce plots that are impressive in their fit to the experimental data, they do little to advance the science' [110].

The non-normally distributed errors do, however, not make the least square estimator a bad choice [131, pp. 409-411]. The heteroscedasticity (variation in variance for different conditions) and correlation between errors, both due to systematic deviations, on the other hand, do [131, pp. 409-411]. None of the utilised models describes all features of the measured data. This can be seen by the regions of systematic deviation, e. g. in Figures 4.19, 4.20 or any of the other plots comparing measured and simulated values over the external parameters. This has consequences for the statistical analysis as well as its representation:

Obviously, the residuals might no longer be χ^2 distributed. The heteroscedasticity is not connected to the measurement error (compare Figures 4.1 with 4.7 and 4.18) and can consequently not be dissolved by weighting with the latter. Since there are several (but not many) distinct regions of systematic deviation with specific severity of discrepancy, each of them could enter as a separate mode additional to the statistic deviations. Consequently, the distribution must be assumed to be multimodal. That this is actually the case can, for example, be seen in the histogram-like data representation in Figure 4.22 (as already mentioned, the visualisation will be explained in detail below): The residuals for the fits

of sample 1346aCrAu1 (located in the middle black-framed box of Figure 4.22), clearly show two distinctly distinguishable hills. Actually, neither a mean with its standard derivative nor a notched box plot is a suited representation of multimodal distributions. Histograms or better yet extraction and separate analysis of the regions of deviation would be a better approach from the standpoint of statistical analysis, but only if including better models (which can likely explain at least some of the observed deviations), which is always preferable, was not possible. In an even better way than histograms, namely connected to their corresponding regions in external-parameter space which allow extraction of physical explanations, the separate deviations can be seen in the contour plots (or residual plots) and are well explained in the corresponding parts of this chapter. The distributions are visualised without their conditions solely for the purpose of quick comparisons across different models and samples. Since the distribution is asymmetric (skewed), extremely long-tailed and can only lead to positive real values, displaying them with notched box plots is still preferable to a mean standard derivative representation.

Another consequence of the systematic deviation is not only the display of the distribution, but also the fact that the residuals do not strictly fulfil the requirements to perform a least-square regression on them. The deviations, which cannot be explained within the models, might, hence, influence the fit result. There are other regression estimators than the ordinary least-square method, which are potentially more robust against outliers [158]. However, it is assumed that none of the other regression estimators could reduce the effect of the deviation as much as the elimination of the deviations themselves by a better description would. In this work, a novel method of analysing immittance spectra is proposed. At some points, it was explicitly decided against using even more advanced models, because the perfect description of the exemplary used material system is not a primary goal of the example (e. g. see sections 4.1.1.3, 4.1.1.5 or 2.4.1, especially also including 2.4.1.3). It would be inconsistent to utilise highly advanced regression estimators which are, judging from pathological mathematical examples (which might not even be significant for such specific systematic deviations), more robust against outlier, whereas they could potentially just be eliminated by including, so far, deliberately ignored more elaborate models for the different pieces. The ordinary least-square regression estimator is, on the other hand, relatively straightforward, very common and easy to understand, i. e. the influence of the estimator by certain kinds of deviation easily comprehensible. Moreover, the author has, within the field of immittance spectra, never seen the use of any other regression estimator. Potentially, because non-linear least-square analysis has been explicitly modified to fit complex immittance values [121] (this method is today found under the designation CNLS fitting for complex non-linear least-square fitting [7, pp. 194-204]). As explained in section 3.3.1, the complex extension of non-linear least-square fitting itself has raised question of the weighting for which no unique answer within the field exists. It is, consequently, without further research not easy to determine whether the more robust regression estimators maintain their superior robustness in combination with the selected complex extension, especially with the (controversial) weighting factor. For all the above reasons and since the estimator is only used to obtain the fit parameters, but explicitly not to evaluate quality of the fit itself (this is done with histograms and box plots in section 4.2 and, hence, not relying on the regression estimator itself), it was

decided against more elaborate regression estimators.

Visualisation of the residual distributions for direct comparison across samples and models In order to compare the fit qualities spanned over the different samples as well as several models, two things have to be achieved: First, a measure for the goodness for each approximation has to be established. Secondly, a criterion to decide, whether a fit quality is significantly different to another, is needed. Preferably, both should lead to a visualisation of the fit quality that make them easy to compare with each other.

In Figures 4.22 and 4.21 the distributions of the residuals and their key parameters are shown. All fits were performed by minimising the sum of the corresponding squared residuals. That is why the mean, an otherwise unsuited value for such broad asymmetric distributions, is shown as one of the key parameters of each distribution: it is nothing else than the sum of residuals normalised for the number of points (at least if the residuals are really those summed for the fitting routine as in the case of the residuals in Figure 4.21). Hence, the square of its value, multiplied with the corresponding number of points, is the parameter minimised by the fitting routine.

Fitting both samples combined, means that the sum of all residuals (of both samples except the ignored region) is minimised. As the density of the measurement points is identical, no additional weighting factor (supplementary to the already used error normalisation) between the samples was introduced. Unlike in Figure 4.21, where the residuals of the regions ignored in the fit are not shown (i. e. selected distributions in Figure 4.21 show the actual distribution relevant to the fit), in Figure 4.22 the residuals of those regions ignored in the fit are included to calculate the visualised key parameters of the distribution. Furthermore, in Figure 4.22 residuals of different samples are always shown separately, also in the case of the combined optimisation of both samples. Meaning, that in contrast to the fits of single samples, the sample-specific mean does not have the same importance in Figure 4.22 .

In both Figure 4.22 and Figure 4.21 the distribution of residuals is depicted on the left and key parameters of the respective distribution are shown in a notched box plot on the right side (critics about this display for multivariate distribution was already given above). The convention in all notched box plot in this work is the following: Whiskers represent the range of the residual distribution without outliers. The box shows the range between the first and third quantile. The notch is at the median, the notch width indicates its confidence interval. The mean is depicted by a filled diamond and additionally by a line extending into the distribution. The upper triangles represent the maximum (filled triangle) and 99 % percentile (semi-filled triangle). Analogously, the lower triangles the minimum and the 1 % percentile. Important: The residual distributions of Figure 4.22 include the areas ignored by the fitting routine, which can lead to additional outliers and broader distribution as compared to those of Figure 4.22 that only includes residuals given to the fitting routine.

The plots of deviation contours, residuals and the visualisation of the residuals as histogram as well as notched box plot are used to visualise whether a change in model improves or deteriorates the quality of the fit significantly as compared to another representation.

For example, the fit quality of sample `1346bCrAu4` in Figures 4.19 and 4.20 improves from Model 2 to Model 3 only very slightly (the slight changes might be seen best in the deviation plots 4.18). The quality of the fit has to improve, or at least stay the same, since the degree of freedom increases while the model keeps otherwise identical. The intention of the visualisation as box plots is to have a measure for the *significance* of the changes. For the present distributions the standard deviation would *not* be a suited measure. Whether the width of the interquartile range is a good measure or not is debatable, however, it is at least a key size to orientate the decision at.

For sample `1346bCrAu4` it is decided that Model 1 leads to a significantly poorer description than Model 2 or 3 while, on the other hand, the improvement does not increase significantly from Model 2 to Model 3.

> The differences between Model 1 and the others are deemed significant, because of following properties: The mean of the residual distribution using Model 1 lies outside of the interquartile range of models 2 and 3 and is in the top third of its interquartile range while it is almost centred in the others (see Figure 4.21). It is almost half a interquartile range of Models 2 and 3 larger in Model 1. Also, the interquartile range for Model 1 is about one half larger as for the residual distribution using the other models. The median of the residual distribution of Model 1 is raised about one half of an interquartile range of Model 2 or 3. The range of residual distribution of Model 1 without outliers is almost reaching the value of the 99 %-percentiles of the other distributions.

Both results can also be seen in the strong change of the form of the distribution from Model 1 to Model 2 and its almost unchanged form from Model 2 to 3.

The distributions of sample `1346aCrAu1` for the different models are very similar. A very outstanding shared feature is their very long tail towards high residuals. Since the tail remains (almost) identical for fits with the different models, these residuals are apparently associated with deviations not addressed by the different models. Examination of Figure 4.19 clarifies that this feature can be connected with an almost unchanged pronounced deviation just below zero bias voltage with increasing severity towards higher frequencies. The deviation is not addressed by any of the three models. The reasons for these deviations and why no model is covering for them is discussed above in the discussion about interface deviation 2. Finally, it is ascertained that the different models, for the thin-film permittivity connection between its resistive and capacitive part, fit the measured data at this feature equally well.

As expected, the residuals for the minimisation of the combined sum of both residuals, the residuals are worse than when fitted for each of the separate samples alone. While the increase in the quality of the fit from Model 1 to Model 2 and its constancy between models 2 and 3 is still visible, all has been overlapped by another deviation significantly broadening the 'main hill' of the deviation. Although the density of points is identical for both samples, meaning that the same parameter ranges of the samples have identical numbers of points, the bias voltage ranges are different. The reason is that the bias-voltage range for the same feature (the forward bias region dominated by the thin-film immittance and influenced by the total serial resistance) is larger for the low-doped sample than for

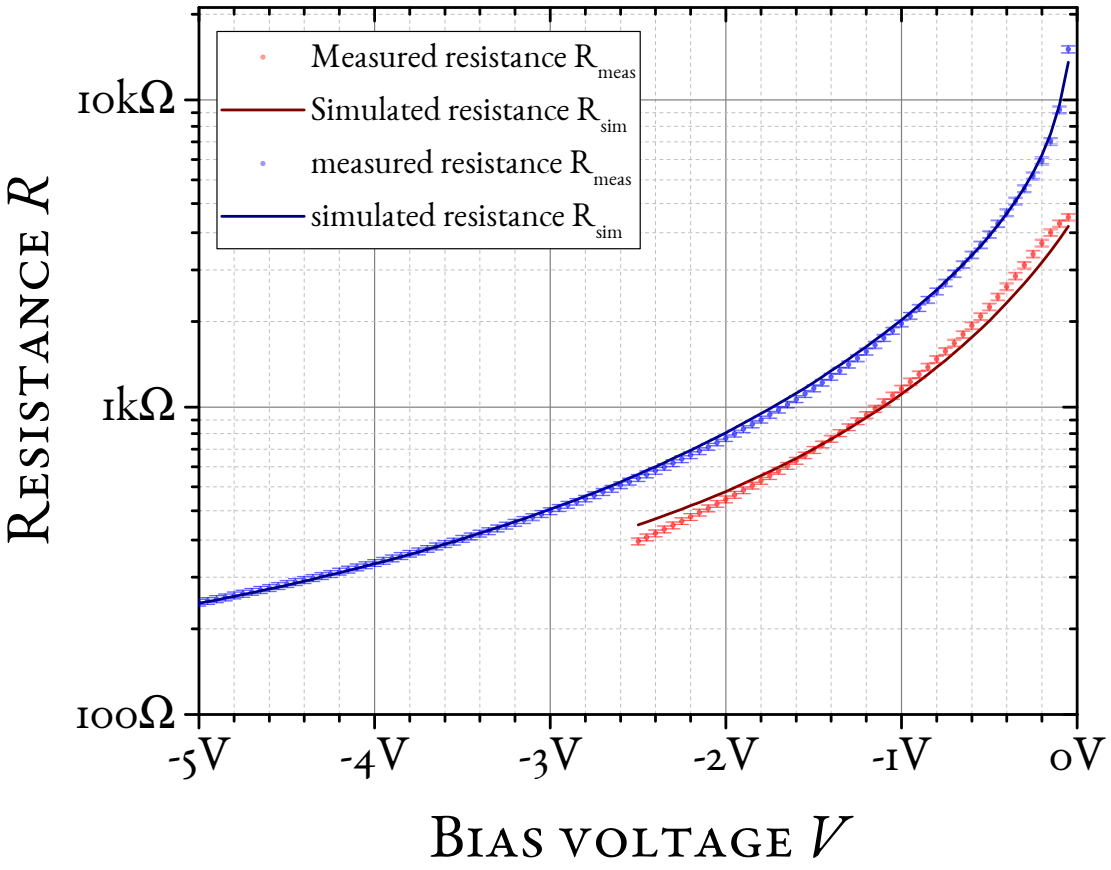

Figure 4.23: The voltage-dependent resistance at forward bias voltages for the samples with high- (red) and low-doped substrate (blue) in comparison. A *combined fit* of both samples with the same density of points optimises the thin-film parameters to preferably fit the sample with low-doped substrate, because of its larger measurement range. The comparability of these samples, created in the same batch, was discussed above. The almost parallel trend of the measured data sets of both samples could correspond to a constant offset in the exponent, e. g. a different barrier height, or another factor before the exponential term, e. g. a varied zero-field conductivity. Both exemplary explanations are actually not expected for a film synthesised in the same batch (i. e. all process steps were performed simultaneously for the shown samples, see sections 3.1 and 4.1.1.1).

the highly doped sample. Though, despite the fact that the density of points is identical, the regions for which the same part of the model dominates are different. More precisely, the impedance of the thin film is the major contribution from −2.5 V to 0 V for the highly doped sample while the range of domination for the low-doped sample is larger, namely from −5 V to about −1 V. Hence, although the density of points is identical, if the characteristics of this part would be different, for each sample the combined sum of residuals would have more residuals from the low-doped sample for the affected part of the model than for the highly doped one. In consequence, a compromise fit parameter value would be closer to the optimal value of the sample with low-doped substrate. And this is exactly what is observed. The resistance-voltage behaviour is optimised preferably approximating sample `1346aCrAu1` and not sample `1346bCrAu4`, see Figure 4.23. The resulting deviation in all residual distributions of sample `1346bCrAu4` is causing the very broad hill in the residuals superimposing the usual deviations of the different models. The caused major deviation can also be clearly seen in the first row of Figure 4.20 that shows the residuals of sample `1346bCrAu4` for each model when optimising for the combined sum of residuals of both samples. This unwanted but accepted weighting also expresses itself in the significantly larger mean and median values for this sample. The mean and median values of sample `1346aCrAu1`, on the other hand, are not significantly worse than for the sample-specific fits. Though, the form of the almost bimodal looking distribution for the sample-specific plot changes into a broader hill spanning the range of the former both. The observed deviations for both samples due to the combined optimisation can be directly compared in Figure 4.20. While the second row of residuals for sample-specific plots of sample `1346aCrAu1` remains almost unchanged as compared to the residuals of the combined optimisation shown in the last row, the sample-specific fits of sample `1346bCrAu4` in row one, look much brighter as those in row three, that are the result of the combined optimisation.

This cast doubts on whether the comparability between the samples is allowed with the thin film thickness (and the total serial resistance) being the only possible difference between them. Since the only intentional difference between the samples is the substrate, the cause should lie within that scope, however, the form of the deviation does, at least not straightforwardly, point to some obvious substrate related property. A top contact diameter of 0.9 mm should be large enough to average out statistical deviations of the amorphous film and interface roughness, which are all suspected to be below the μm range.

Another approach of assessing the comparability is pursued in Figure 4.21. All residuals shown in this plot do *not* contain the area ignored by the fit. Hence, the sum of the square of these residuals represents actually the values the fitting routine minimises. Except for the fact that the ignored area is not contained in Figure 4.21, but is included in Figure 4.22, the residuals in both Figures are calculated based on the same fit results. After the sample-specific fits were performed, their respective fit parameters were fixed and only the remaining parameters optimised against the respective other sample. As a result, not only the residuals of the primarily optimised sample are shown, but also the residuals of the remaining sample and the distributions of all residuals of both samples together. In the first of the three main parts of Figure 4.21, the residuals are primarily optimised on sample

1346bCrAu4, with low-doped substrate, which is indicated by the blue box around its respective residuals. Its respective residuals for each model are shown in the first three notched box plots with the according data on the left. These optimised residuals are also always highlighted by changing the line colour of the surrounding box to blue. The next three representations (containing the data on the left and the notched box on the right side) of residual distributions show the result for sample 1346aCrAu1 where only the diode parameters and its serial resistance were fitted, while all thin-film parameters are still optimised on sample 1346bCrAu4. All residuals together give the combined residual distribution of both samples and are given in the last three data sets of the first third. The subsequent third is optimised for sample 1346aCrAu1. Its data sets for each model fit are represented by the tree notched box plots in the mid-position. Left of those are the ones of sample 1346bCrAu4 with parameters from the diode sample, except for the fitted serial resistance. Right of the optimised residuals are again the combined distributions for each model. In the last third, the residuals of both plots combined are optimised. In fact, the mean shown in the last three distributions, which as mentioned before represent the residuals of both samples combined, is the square root of the normalised parameter that is minimised by the fit for combined fitting of both samples. In the first and second sub-third of that last third, the distributions of the individual sample are given.

One major message of Figure 4.21 is, again, that the parameters obtained by fitting the one sample do not describe the other sample very well. The different samples are qualitatively very similar, but seem quantitatively not comparable. At least when using the proposed models, with their known restrictions, one sample should *not* be used as reference for the other. There is, of course, still the possibility that the deviation in forward bias, that makes both samples quantitatively incompatible, is caused by ignoring certain effects in the interface model (e. g. contributions by fixed charges in the insulator or defects at the interface). However, especially since the discrepancy is affecting the resistive properties, the voltage-range of the constant offset in Figure 4.23 seems too large (since the effect of defects only ranges below −2 V for high frequencies). At this point, it cannot be decided whether the observed derivations are either caused by a disregarded property of the system, i. e. some unexpected effect of the different doping concentrations in the substrates, or if the reproducibility in the same batch is really that low. Maybe the preparation in the same batch was not enough to reduce pre-existing differences of the samples in addition to the doping-concentration, however that could cause this kind of deviation. As already mentioned for the interpretation of Figure 4.22, it can be seen especially clearly in Figure 4.21 that sample 1346bCrAu4 with its lower number of points for the same feature, while still having the same density of points, has a reduced impact on shared fitting parameters than the sample 1346aCrAu1. In cases of combined fits, its residual distribution changes the most.

The change from Model 1 to Model 2 increases the goodness of the fit significantly for sample 1346bCrAu4, while the change from Model 2 to model three seems to have no significant effect. For sample 1346aCrAu1 on the other hand all models lead to an approximately equally good fit. Though, from a close look to the distribution, it can be seen, that the lower hill of the (approximately) bimodal distribution increases notably from Model 1 to Model 2, while remaining almost unchanged from Model 2 to Model

3. This might indicate that, although some regions of strong deviations were neither included in the fit nor the shown residual distribution, the more frequent deviations for the rectifying sample mask the change of goodness of the fit due to the different models. The latter is definitely the case for the combined fitting of both samples.

Findings of comparing the different fits

Results of combined fitting The measurements of both samples have the same density of points. However, the part of the parameters space dominated by the thin-film contribution, the forward-bias region, is larger for the sample with low-doped substrate. As a result, combined fitting bases the optimisation mainly on sample `1346aCrAu1`, with low-doped substrate, while the properties of the thin film from sample `1346bCrAu4`, with highly doped substrate, are recognised only to a lesser extent. This effect leads to a much worse approximation of the thin-film part in both samples than any change in model. The analysis of the model quality should, hence, not be based on the distribution of combined fits.

Comparison between the models Model 1 is significantly worse in describing the residuals of sample `1346bCrAu4` than Models 2 and 3. Both latter models lead to almost indistinguishable fit quality. This observation can be confirmed with the changes in fit parameters in Figure 4.4. The resistive properties are much more sensitive to changes of the permittivity then the capacitive part. This forces a value of around 4.2 for the relative permittivity affected factor m in the exponent of the Frenkel-Poole model. All fit parameters for sample `1346bCrAu4` change massively from Model 1 to Model 2 and barely from Model 2 to Model 3. As Model 1 describes the experimental data significantly worse and leads to very different fit parameters as compared to both other models, it is concluded that the static permittivity should not be calculated from the constant phase element parameters. This is in agreement with the suggested method to extract the static permittivity according to Young and Frederikse [190]. Above result is further discussed and brought in context with the literature in section 5.6.3. The differences in fit quality between Model 2 and 3 are not significant for any sample. While its fit parameters are also very similar for sample `1346bCrAu4`, there seems to be a trade-off between capacitive parameters of the thin film for sample `1346aCrAu1`. It should however be noted (see Figure 4.5) that the capacitive part of the thin-film-dominated region for latter sample is recorded only in its beginning. Consequently, the fit parameters for sample `1346bCrAu4` are considered more reliable. Another finding is that there seems to be little to none trade-off between the thin-film-dominated parameter regions and the diode part. This underlines one of the mentioned advantage of the presented approach of analysing immittance data, e. g. over conventional current-voltage analysis: the separability of different parts.

4.2.3.3 The correct calculation of the internal field

The different models represent distinct connections between the resistive and capacitive part of the thin film. The only difference between Model 1 and 2 is a different way of calculating the static permittivity. Only Model 3 does not connect the permittivity extracted from the capacitive data with the resistive part at all. It was found that Model 2 describes the immittance of the thin film equally well as Model 3. Consequently, the correct calculation of the internal field proposed in this work seems to resolve the decade-old problem of a quantitative difference between the observed and theoretically derived barrier-lowering coefficient. Interestingly, the quantitative deviation could be resolved within the concept of the semi-classical Frenkel-Poole model, without including fundamentally different physics, e. g. correct quantum-mechanical calculation of the problem. As previously explained, already the publication by Poole mentions, the negligence of the permittivity, i. e. the weakening of the field by the polarisation in the dielectric, though quantitative description was never seen as a goal in his work. The extraction of the static permittivity ignoring the first frequencies of the dispersive region, that is Model 2, is in agreement with the conventional way of extracting the static permittivity [190]. The first dispersive region of frequencies is often superimposed by Maxwell-Wagner response of the interfaces [190]. For the approach presented in this work, straight-forward Maxwell-Wagner response caused by the ta-C/Si interface is already included in the model, while other interfaces seem to have a negligible immittance contribution. Possible reasons why the dispersive region might not be a contribution to the bulk static permittivity of the thin film are discussed in section 5.3. In section 5.6.4 it is speculated why the Frenkel-Poole model can lead to a quantitatively correct description of the experimentally observed behaviour despite its approximations that ignore, not only the correct quantum-mechanical description, but also the 'true' local potential landscape. In a covalently bound material the latter is expected to show a strong dependence on direction and, hence, supposed not to be well described by a (three-dimensional) Coulombic potential.

5 Discussion

5.1 Comparing the presented approach with other methods of analysis

Two major categories of modelling immittance spectra may, utilising the terminology of Grimnes and Martinsen [56, pp. 284-286], be distinguished: descriptive versus explanatory models. None of them is better or worse than the other. Which of them is suited, is based entirely on the application, i. e. the goals of the investigation. In industrial scenarios, it is often not important to understand the cause of the response of a system or specific device, but rather to know the response under certain conditions of stimulation. In such a case, a preferably compact (in case of an embedded *in-operando* analysis also easy to calculate) descriptive model, for the specified region of operation, is favourable. This 'equivalent' is then used as representative of the specific device for calculations of larger circuits. While this is completely legitimate for a descriptive application, it is questionable to associate different components of such a circuit with specific real corporal pieces of the system and, in consequence, extract physical parameters from a descriptive model. The criticisms of D. Macdonald of using 'analogs' refers to this interpretation of underlying physics from descriptive models and the 'tendency to declare the first analog that is found to account for the impedance data to be the "model"' [110]. Such 'analogs' usually take the form of electrical equivalent circuits (EECs). The latter may in principle also be designed to represent the underlying physics and are, hence and due to their common usage, compared with the approach introduced in this work in the next subsection.

However, this work focuses on finding explanatory models. These models help to understand the underlying mechanisms and should allow the extraction of meaningful physical parameters, like an impurity concentration, a barrier height or a mobility. Next to the approach of developing models introduced in this work, also Poisson-Nernst-Planck models[1] belong to the class of explanatory models in the field of immittance spectroscopy. These models are compared in the second subsection of this chapter.

A general challenge in the analysis of immittance spectra (and one reason why it might not be obvious at a first glance that only an equivalent is regarded) is that only the response of the full system under investigation is known, while the details of the constituting pieces remain hidden. In other words, the response of a whole (linear) system is described by one complex value, i. e. one immittance value, per condition. Without further knowledge of the underlying system, the resulting black box could have many possible arrangements

[1] In this work only those distinct analytic solutions of the Poisson-Nernst-Planck equations that were intended for the analysis of immittance spectra are compared, see section 5.1.2 for details.

leading to the observed immittance. Such a black box could be modelled with conventional EECs, i. e. those only consisting of idealised lumped components. The circuit with the least components that has a sufficiently similar response can then be used as equivalent for the investigated system. The indirect analysis of any system under investigation is an unavoidable fundamental restriction of immittance spectroscopy. As mentioned above, a descriptive model can not be used to extract fundamental information of the underlying system directly. Instead, an explanatory model, which is in most situations almost impossible to find only relying on the immittance data, is required. Hence, without any prior knowledge, e. g. by combination with other measurements, it would be impossible to extract any relevant underlying parameters. Fortunately, a situation where there is not any further information besides the immittance spectrum of a system is (at least in scientific investigations) rather unusual.

Typically the different pieces of a system are known, for example because the setup of an experiment or the synthesis of a sample is known. Different semi-circles in a Nyquist plot may then be associated with distinct serial pieces. Subsequent analysis of the separate contributions may then allow to extract physically relevant information.

As already mentioned, the most common method of analysing immittance spectra is utilising conventional EECs [110]. As known already for a long time [192], arrangements of lumped components are ambiguous, i. e. the same number of differently arranged components can approximate the immittance spectra equally well. Extracting parameters from an accidentally wrong arrangement would result in, at least, distorted parameters. Furthermore, when fitting capacitances and resistances, it is not easy to recognise whether an arrangement, correctly representing the underlying physics, i. e. where each component represents an underlying physical process, was chosen. It seems that in many cases the analysis ends with the resistances and capacitive values fitted using the first circuit that could approximate the measured data, although such quantities are not that meaningful [110]. Furthermore, identical materials are often described by different arrangements of the corresponding idealised lumped components (e. g. see the example in Figure 1.1) which makes the comparison of results from different scientists very difficult.

There are other models to analyse immittance data beyond conventional EECs. In this work, a model is presented that is based on modelling immittance spectra with lumped components. In this light, the given comparison is restricted to models that take the form of lumped components, as well: for one thing, the most common method of analysis utilising EECs consisting of idealised lumped components, for another thing, Poisson-Nernst-Planck models that take the form of lumped components. The latter concept tries to solve one of the challenges in the analysis of immittance spectroscopy which is also targeted in the approach presented in this work: the extraction of relevant physicochemical parameters. Principally, Poisson-Nernst-Planck models encompass a much broader field than those specific solutions [74, 75, 116, 22, 76, 117, 120, 112, 119] compared in this work and associated with this term in the context of immittance spectroscopy. Instead of using the mentioned specific solutions that take the form of lumped components (compare also [115]) the differential equation system of Poisson-Nernst-Planck equations can be combined with finite-element methods to model almost arbitrary geometries and forms (e. g. microscopic grains in some bulk material) of specific parts, within continuity and

mean-field approximation. For high frequencies, also the locally different concentrations of mobile charges may be investigated (though, at some frequency, it may become necessary to take the inductive properties into account, as well). Using spatially extended modelling is not only very interesting (since spatial distributions of field and current might be seen directly), but can certainly lead to more realistic models as any lumped-circuit approximation. The approach presented in this work is neither supposed to nor can it replace a well made spatially extended Poisson-Nernst-Planck model. The presented approach is rather supposed to exhaust modelling with lumped components. In fact, even the specific solution of Poisson-Nernst-Planck models, that are specifically intended to describe immittance spectra (they can be applied without changes to almost all typical immittance measurements) and are available in a freely-downloadable fit software since about 1992, are rarely used [119]. Spatially extended Poisson-Nernst-Planck models are in comparison much more elaborate to apply than these specific solutions. Hence, although these spatially extended models have certainly a lot of potential, there seems still to be demand for lumped-component models that can extract relevant physical parameters. In order to do that, resistances and capacitances have to be replaced or converted into more meaningful parameters. Preferably, these quantities should be comparable between other experiments and the obtained arrangement of circuit elements shall be unambiguous. Furthermore, the resulting arrangement should resemble the underlying physics which means that the different components of the circuit should be one-to-one associated with the underlying physical processes.

With regard to these requirements, the approach presented in this work is, in the following subsection, first compared to conventional EECs, the most common means of analysing immittance data. In the following subsection, a comparison is made between the presented approach and specific solutions of Poisson-Nernst-Planck models for immittance spectroscopy that take the form of lumped components. Also a possible combination between Poisson-Nernst-Planck models and the fundamental concept of this work, to include external-parameter-dependent process-specific physical models directly in the model and perform global fits over the full parameter range, is suggested. This is found to be a promising path to take for the future of the analysis of immittance spectra.

5.1.1 Comparison with conventional EECs

5.1.1.1 Conceptual main differences between the approaches

The most common method of analysis of measured immittance data uses conventional EECs [110], i. e. circuits consisting only of *idealised* lumped components. These idealised lumped components, e. g. ideal resistors, ideal capacitors and constant phase elements, (except for the latter which is, at least, a frequency-dependent capacitor) do not include any dependence on external parameters. Assuming a correct number and arrangement of the components as well as no parallel transport processes in the system, a conventional EEC can have a one-to-one association between one circuit component and one process in the system. In this case and assuming that the values of each component represent solely the intended process (which is, as explained below, not simple to achieve in an

EEC), (a component of) the EEC does not solely emulate the response of the system, but is a physical model, though a simple one. Only then, each component is a first-order approximation of the response of a specific part, e. g. a resistance is a first-order approximation of a *current* transport process and, hence, a physical model, though one without dependence of external parameters.

5.1.1.2 Challenges using conventional EECs and resolving them by the presented approach

Circuit ambiguity The variety of above-mentioned assumptions presages the challenges, one is confronted with, when using EECs as valid physical models that enable extraction of relevant parameters or understanding of underlying physical processes. As mentioned before, a prominent problem is the ambiguity of circuits that consist only of idealised lumped components [114]. Different arrangements of the components can lead to an equally well agreement with the measured data [192]. Consequently, identification of the correct arrangement is a challenge. J. Macdonald [114] suggested that measurement over a range of temperatures or potentials (bias voltages) might help to establish which of several possible arrangements might be the physical reasonable one. This is also the direction the presented approach takes. However, not all arrangements are equally likely from the start: with the theoretical deviation of an universal EEC for a single homogeneous piece (see section 2.2) and their arrangement for multiple parts (compare section 2.3), many ordinarily used arrangements (including the one shown in [114, Figure 8] and its interpretation of components) became already theoretically less likely. Variation of external parameters and modelling using conventional EECs can help to identify the correct structure, but since the various contributions may react in their distinct way onto the variation, an exclusive association of different processes to the components in the circuit is still not an easy task. The certain behaviour of a resistance as expected for a specific process might only show that the component is predominately representing the specific process but not necessarily exclusively. Unlike in the proposed method of analysis, where the actual model with its dependencies is included as a circuit component and which substantially restricts its possible behaviour, in a conventional EEC the probability that a component might still partially 'absorb' the response of other process is significantly higher. This also means that some mistakes in the arrangement might not be as easy to find since they get more easily absorbed by other components. Though this problem is not completely resolved with the proposed method (since it is present in any fit), its much more restrictive properties, combined with the fact that only physical parameters are fitted and not a resistance *for each condition*, makes false association less likely. A conscientiously assessment of the used models, the arrangement of components and the fit result (obviously not always given [110]) is necessary for any model, also when using the presented approach (which makes accidentally wrong arrangements easier to find, though).

A typical goal of immittance spectroscopy in science is (or rather it should be, compare [110]) the extraction of certain relevant parameter(s) of the underlying system instead of just finding suitable resistances and capacitances for some arrangement. Extraction of the

correct value for the parameter(s) is only possible in EECs where the component really represent the properties of the specific process. In this case, the parameters are extracted in a subsequent step form the value of the component or the progression of its values over a varied external parameter under the assumption of a certain model for the process.

Parallel processes Especially complicated, when analysing using conventional EECs, are parallel process. Ideal parallel capacitors or resistors simply conflate into a single component, respectively. Consequently, there is no deviation that would alert one about the joined fit of two processes. Decoupling may again be achieved by variation of external parameters or by determining the other processes with alternate methods. Using the proposed method of analysis, an initially assumed single process could not describe the external-parameter dependence correctly and leads to systematic deviations. From these, the requirement of a parallel process can be seen. This means one is immediately alerted about the missing process. Furthermore, the parallel process may even be identified by the progression of the deviations with certain external parameters.

Many fit parameters required to model multi-condition measurements conventionally Another consequence of using conventional EECs, present for analysis under different conditions (sets of external-parameter values), that was already implied in the last paragraph, is a larger amount of fitted values (compare Figure 5.1). For each condition every component in the circuit (sometimes a subgroup of components might be assumed constant under certain external-parameter variations) may have different values. Since the fits for each condition are independent of each other, the contributions of a process might shift between different components, i. e. through this intermediate step of fitting resistances and capacitances information may be lost.

The fit of external-parameter-dependent physical models, on the other hand, connects the different conditions. Since not resistances and capacitances, but the underlying parameters responsible for their values are fitted, fewer parameters are necessary. Furthermore, the restrictions of the models reduce the 'absorption' of deficiencies in the model (missing processes, bad descriptions, wrong models for other parts). If, despite the restrictions, deficiencies are 'absorbed' the underlying parameters make spotting this problem more easy by resulting in suspicious values. The sensitivity for wrong values of a resistance, that even contains the geometry, might not be as high as for a quantity embedded in a more vivid physical concept (and the assessment of meaningfulness of such a resistance is often omitted [110]). In Figure 5.1 the reduced amount of fitting parameters of the novel presented approach is compared with the number of fitting parameters required using a conventional EEC for the analysis.

5.1.1.3 Different types of analysis for different situations

Despite its obvious disadvantages, when the goal is gaining an understanding of the underlying physical processes or the extraction of relevant parameters, modelling with conventional EECs can still be useful and in some cases even superior.

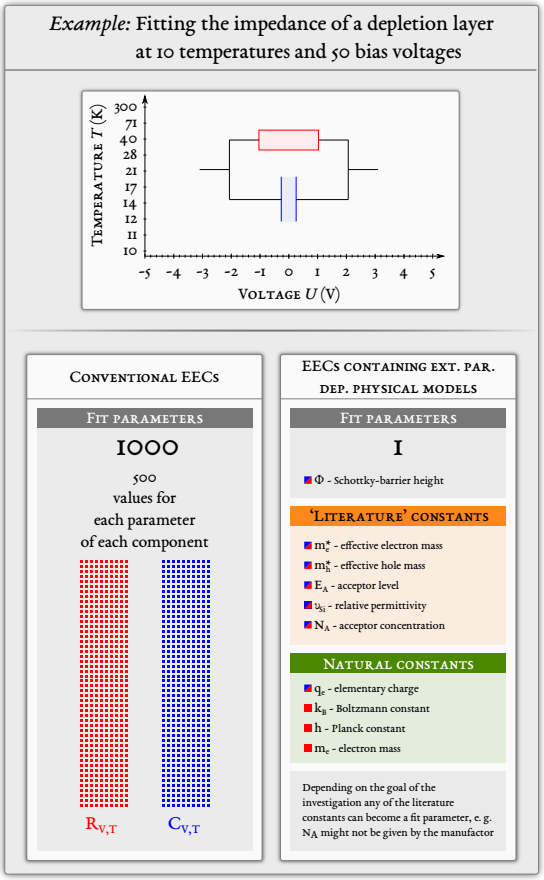

Figure 5.1: The number of fit parameters using analysis with conventional EECs in comparison to the suggested approach for the typical example of a depletion layer under plausible parameter ranges (10 temperatures and 50 bias voltages). The assumed circuit and the parameter ranges are indicated in the upper part of the figure. Each coloured square in the lower part represents a fit parameter. Red colour indicates that the fit parameter represents a resistive property, blue colour correspondingly indicates a capacitive property (both colours consequently indicate that the parameter is used in models for capacitive as well as resistive properties). The squares for the novel approach are bigger just to increase visibility. The acceptor concentration is not really a 'literature constant' but a value that may be given by the manufacturer. Since the manufacturer only gave a rather broad range of resistivities for the low-doped wafer used in this work, it was also a fit parameter in this particular case (meaning twice as many parameters were fitted for the depletion layer part: two instead of one). To summarise, the use of the novel approach presented in this work can significantly reduce the amount of fit parameters, in comparison with conventional EECs while further eliminating circuit ambiguity (thereby leading to a correct assignment of contributions by the different parts to the specific circuit components) and extracting relevant parameters directly (without a potential loss of information by the intermediate step of fitting resistances and capacitances). Similar illustration already used in reference [3].

The presented approach might be seen as supplement to using conventional EECs. In the moment of analysing the experimental data for the first time and without an idea of what processes might be involved a conventional EEC can be a good point to start. Subsequently, the presented approach might be applied (step by step replacing idealised components) to extract parameters of the underlying system or separate parallel processes. If the system is not already well known or the assignment was not already gained in another way, the novel approach might also help to find a circuit with one-to-one assignment between processes circuit components.

There are systems which do not fulfil the requirements for the presented approach to be useful. Batteries, for example, are usually characterised using the open-circuit potential and under normal operation conditions. Varying the temperature in a battery test significantly from the point of operation might help identify processes but can also activate completely different processes (which are never relevant in its normal operation) that might even irreversibly change the properties of the sample. Generally, it makes no sense to apply the presented approach on any system that gets inevitably changed permanently by applying the different conditions.

In some situations analysis using conventional EECs might be superior to the presented approach. The components do not impose as many restrictions as physical models dependent on external parameters. Their values are redetermined for every condition and almost any arrangement can be used. All these liberties can be used to achieve a better agreement with the measured data. As already explained many times in this work, the circuit ambiguity (that is unavoidable in circuits solely using idealised lumped components) makes it difficult to determine whether the chosen arrangement of components has anything to do with the real structure of underlying processes. Hence, if understanding the underlying physics is less important as accurate emulation of the sample and saving data points for each condition, conventional EECs may be superior to the presented approach. Although separate values for the components at each condition have to be known, the computation of such linear EECs may be performed faster than the calculation of external-parameter-dependent physical models, which are often nonlinear and involve rather often exponential functions or square roots. Consequently, in highly-specialised embedded devices, e. g. a battery management system in an electric car, where the integration of complex floating-point units is expensive and would otherwise be unnecessary, a conventional EEC might be advantageous. At least as long the range of external parameters is not too large, requiring too many sets of saved values (compare with paragraph 5.1.1.2 and Figure 5.1).

5.1.1.4 Introducing process-specific external-parameter dependent physical models *after* an analysis using conventional EECs

One approach, to extract relevant physical parameters from conventional EECs, might be to start the analysis using conventional EECs and subsequently use physical models to analyse the progression of a certain component with variation of external parameters. This way allows determining whether the chosen arrangement of components represents the underlying physics correctly or at least whether one component may (dominantly)

represent a certain process. This is actually *not a different approach but rather a properly finished analysis using conventional EECs* [110]. A final result of an analysis is supposed to be a specific, relevant and (between different works) comparable property, e. g. a reaction rate or a doping concentration, but not a resistance.

In comparison with the presented approach, this *complete* analysis using conventional EECs has still some drawbacks. If some component was accidentally omitted or there are (at that time) unexplainable contributions, other elements in the circuit might absorb these contributions. A certain components that is still dominated by one process would contain other contributions which distort the extracted values. Suppose the arrangement and number of circuit components would correctly represent the underlying physics, which can, as explained before in the absence of restrictions due to specific external-parameter dependence, not be guaranteed in the first part of analysis without models (further, parallel processes would necessarily be lumped together). Assuming the same models are used, due to the fitting in two steps (one intermediate step for resistances and capacitances) either the resulting parameters are identical or worse, because of a loss of information in the intermediate step. Since the correct association is in particular difficult in transition regions, they are usually excluded from such an analysis. A lower number of data points used for the analysis also means a loss in information and consequently lower confidence in the fitted parameters. The global fits based on circuits with external-parameter-dependent models, on the other hand, can use all data points, also those in transition regions, to find the best guess for the parameter. In summary, using conventional EECs followed by the analysis with physical models can at best lead to equally good guesses for the parameters. Due to a possible loss of information, the result is likely less accurate. An exception may exist if the utilised physical model is only very rough approximations of the observed situation. In such a case, especially if only specific pieces in series to the 'weak' model are of interest, it may be better to use an idealised lumped component instead of the 'weak' description, because it will fully absorb the (irrelevant) serial contribution. Then the parameters of the actual process(es) of interest may be less distorted. It is, however, required to know that the above mentioned situation of rough model is indeed the problem. Unless the system under investigation and its impedance response are really well understood, it may be easily overlooked that actually some other model has a bad description or some process is missing. A potential approach with 'weak' models might be to find the correct arrangement with this approach and subsequently use the circuit as a conventional EEC to fit the data. This ensures a one-to-one assignment of processes and circuit components and fit values without the (negative) influence of the 'weak' model.

5.1.1.5 The presented approach, its benefits, requirements and new possibilities

The approach presented in this work and its benefits In the presented approach, idealised lumped components are exchanged by process-specific physical models dependent on external parameters. Due to their restricted dependencies, this promotes a one-to-one assignment between circuit components and processes in the system. All conditions are fitted in a single global fit of underlying physical parameters, directly, instead of resistances

and capacitances. The dependencies of the model weight the region of dominance of the different parameters, since only residuals in the regions that may be affected by the model can be changed by the corresponding parameters.

> In the experiment in this work, for example, the Schottky barrier height can only influence the reverse bias region. Fitting only forward bias values, the assumed error of the fit parameter would be very large, since its variation would have little effect. Although the fitting routine minimises the sum of residuals and does not see the different regions of deviation, the fact that the significance of certain parameters is restricted to specific regions decouples the parameters. This means that models acting in disjunct regions cannot influence the respective parameters of the other model.

Since the dependence on external parameters is a property of the respective model, transition regions may be included in the determination of the fit parameters. Some parameters may even be involved in both, resistive and capacitive models, leading, on the one hand, to an assessment of compatibility between the different models and, on the other hand, to a consistent value for both parts validating the chosen description even further.

> This circumstance was exploited in the part of the experiment where the additional factor for the barrier-lowering coefficient and the correct calculation of the internal field was investigated (see section 4.2). The permittivity is expected to be more accurately extracted from the capacitive properties of the thin film. In the Frenkel-Poole model it is, however, also present in the resistive part. By introducing a correction to calculate the internal field, the permittivity extracted (according to Young and Frederikse [190]) from the capacitive part of the thin film lead to a quantitatively correct description of the Frenkel-Poole model. This means that capacitive and resistive models are compatible and that the resistive model seems to describe the underlying process, at least, essentially correct.

As a result, the obtained fit parameters, which are physically relevant parameters of the process, may statistically be better guesses as compared to a subsequent analysis of the resistances and capacitive values.

> Using the same models, the intermediate step over resistances and capacitances can only retain the same information or lead to a loss of it.

Additionally, due to the connection to the underlying physical concept over- or underestimated values might be detected more easily.

> In section 4.1.2.1, the source of the extracted acceptor concentration and flat-band voltage shift could be understood and its value was found to be in agreement with the information about the acceptor concentration of the manufacturer and the voltage shift was estimated as interface traps or fixed insulator charges with concentrations in agreement with the values from the literature. However, repeating the experiment with measurements dependent on temperature and thin-film thickness would allow even better modelling and, consequently, more accurate parameters.

Furthermore, the external-parameter dependence of the models and fixed parameters like literature constants, i. e. their restrictions, lead to a correct arrangement of circuit components and systematic deviations in the residual plot allow identification of missing processes or properties.

> The remaining deviations suggest a flat-band voltage shift with exponential dependence on frequency. This might indicate that traps in the thin film, close to the interface, play a role in the voltage shift, since their time constants vary exponentially with depth. Furthermore, the deviations in the intermediate steps before arriving at this model already helped in its refinement.

Requirements An obvious requirement of the novel approach of analysing immittance data, presented in this work, is the necessity to perform measurements for a range of external parameters, i. e. for multiple conditions. Furthermore, the varied external parameters should be capable of decoupling the involved processes: The models (which are required to exist or be devised, as well) must dependent on the chosen parameters and their reaction should be sufficiently different to separate distinct processes (especially for parallel ones). Sufficiently different should not imply completely varied powers of a parameter. Depending on the measurement range even a different factor in front of the parameter might be enough to separate the processes.

It is neither necessary (but of course beneficial) to know every process in the system nor to replace every circuit component by a model. Only the relevant contributions, that are those which are dominant and/or of interest (for which parameters shall be extracted) are recommended to be exchanged by external-parameter-dependent models. In a well-designed experiment, the parts of interest should be the dominant contributors to the immittance. Of course, there are sometimes reasons why above condition is not fulfilled: in such a case, the dynamic of the measurement limits the accuracy of the parameters of interest. Finally, it is at least easier to investigate a system using immittance spectroscopy with some prior knowledge about the system (immittance spectroscopy is not a good choice for a completely unknown sample).

New possibilities in the analysis This paragraph does not list all new possibilities of the approach (more features are mentioned in section 6.2) but one specific advantage concerning the process of finding a correct model. In conventional analysis, there are no restrictions imposed on the component values. Resistances and capacitances are fitted separately for each condition with the mere goal of minimising the deviation at every condition individually. If a process has no specific component in the circuit representing it, other parts may 'absorb' the consequential deviation. Dependent on the progression of the deviation with the varied external parameters the compensation may appear on several components with varying intensity. This makes it hard to identify or even realise the missing process. In the presented approach, external-parameter-dependent physical models restrict the possibility, of absorbing wrong arrangements or missing processes, significantly. Even more so, because joined parameters are used within different models for the same piece. As a result, the agreement might not be as good as using conventional

EECs. However, the deviations from an omitted component or wrong arrangement leads to *systematic* deviations. Dependent on the external-parameter-dependence of an omitted process, deviations (or residuals) will vary their magnitude with the conditions. A plot of deviations (preferably normalised on the measurement error, otherwise one may be hunting ghosts) or residuals over the external-parameter space can give valuable insights to identify missing processes, inadequate descriptions (like omitting interface traps or fixed charges in the thin film) or wrong arrangements.

5.1.2 Comparison with the analysis of immittance data using specific Poisson-Nernst-Planck models

5.1.2.1 Introduction

For systems that have one piece with a single dominating transport process for each of the up to two types of charge carriers with opposing sign and arbitrary valence, specific process-independent solutions of Poisson-Nernst-Planck models, that are compared with the presented approach in this subsection, allow extracting relevant physicochemical parameters, for the corresponding piece, from immittance data.[2] It is not unusual to account for other pieces of the system with idealised lumped components, i. e. the selected specific process-independent solutions of Poisson-Nernst-Planck model is one component in a circuit consisting otherwise only of idealised components [115].

Process-specific versus process-independent In this context, process independence indicates (confer [119]) that it is neither distinguished nor necessary to know what the exact types of propagation of the charge carriers are, e. g. whether the charges move by small ions migrating through interstitial sites of a crystalline solid, electrons thermally excited into the conduction band, charges hopping through localised states or mobile ions in an electrolyte. The Poisson-Nernst-Planck models discussed in this work extract parameters including mobilities, charge carrier concentrations and their valence. Identifying the origins of, for example, the mobility is neither necessary to know for the Poisson-Nernst-Planck models, shown in this work, nor extracted by them. Subsequent analysis of the parameters can, however, be utilised to narrow down the processes, e. g. the mobility of ions migrating in a solid is expected to be much lower than electrons in a conduction band.

In the novel approach presented in this work, process-specific physical models dependent on external parameters are used to globally fit immittance spectra for multiple conditions. Each model carries an underlying physical concept of, to remain with the example of mobility, how the carriers propagate. The assumption of the specific process is actually what determines the distinct dependence on external parameters. The differences between the models described above are summarised as being process-independent or process-specific. In Table 5.1 examples for process-specific models important in CMOS technology are given.

[2] For an introduction in the use of Poisson-Nernst-Planck models in the field of immittance spectroscopy, including a review, confer reference [119].

Bulk-limited conduction processes

Frenkel-Poole conduction (original one-dimensional form):

$$J_{\mathrm{FP}}(E,T) = e\,\mu(E,T) N_{\mathrm{C}} E \exp\left(\frac{-e}{k_{\mathrm{B}}T}\left[\Phi_T - \sqrt{\frac{eE}{\pi\varepsilon_{\mathrm{r}}^{(\mathrm{dyn})}\varepsilon_0}}\right]\right)$$

Hopping conduction:

$$J_{\mathrm{H}}(E,T) = ean(T)\nu(T)\exp\left(\frac{-e}{k_{\mathrm{B}}T}\left[\Phi_{\mathrm{T}} - aE\right]\right)$$

Trap-filled limited / Space-charge limited conduction:

$$J_{\mathrm{TFL/SPL}}(E,T) \propto \mu(E,T)\frac{E^2}{d^5}$$

Electrode-limited conduction processes

Schottky emission:

$$J_{\mathrm{SE}}(E,T) = A^* T^2 \exp\left(\frac{-e}{k_{\mathrm{B}}T}\left[\Phi_{\mathrm{B}} - \sqrt{\frac{eE}{4\pi\varepsilon_{\mathrm{r}}^{(\mathrm{dyn})}\varepsilon_0}}\right]\right)$$

Fowler-Nordheim tunnelling:

$$J_{\mathrm{FN}}(E) = \frac{e^2E^2}{8\pi h\Phi_{\mathrm{B}}}\exp\left(-\frac{8\pi\sqrt{2em_{\mathrm{T}}^*}}{3hE}\Phi_{\mathrm{B}}^{3/2}\right)$$

Thermionic-field emission tunnelling:

$$J_{\mathrm{TE}}(T,E) = \frac{e^2\sqrt{mk_{\mathrm{B}}T}E}{2h^2\sqrt{\pi}}\exp\left(\frac{-e}{k_{\mathrm{B}}T}\left[\Phi_{\mathrm{B}} - \frac{e\hbar^2E^2}{24m(k_{\mathrm{B}}T)^2}\right]\right)$$

Table 5.1: Exemplary list after [23] (not intended to be exhaustive) of *process-specific* physical models dependent on external parameters for current transport processes in solids and at their interfaces, which are commonly found in dielectric films in CMOS technology. Each model is connected with an underlying concept and, consequently, certain assumptions. Furthermore, these models are non-linearly dependent on the applied field, underlining how important it was to allow for non-linear field-dependence in the conversion from Maxwell's equation of total current density to an electrical equivalent circuit. The used symbols have following meaning: μ electron drift mobility, N_{C} density of states in the condition band, $e\Phi_{\mathrm{T}}$ trap energy level, $\varepsilon_{\mathrm{r}}^{(\mathrm{dyn})}$ dynamic relative permittivity (at frequencies of visible light), a mean hopping distance, n electron concentration in the conduction band, ν frequency of thermal vibration of electrons at trap sites, d thickness of dielectric thin film, A^* effective Richardson constant, $e\Phi_{\mathrm{B}}$ Schottky barrier height, h Planck constant, m_{T}^* tunnelling effective mass in the dielectric

The specific Poisson-Nernst-Planck models discussed in this work This work follows the usual conventions in the context of immittance spectroscopy regarding the term 'Poisson-Nernst-Planck model' which restricts it to specific solutions derived to analyse immittance spectra using lumped components, like the specific solutions derived in [116, 117, 120]. In general, Poisson-Nernst-Planck models may encompass any model, especially including those using finite-element methods, that describes the (spatially resolved) ion or charge flux considering the gradient of concentration, the influence of the electric field and, possibly, chemical reactions. Meaning that general Poisson-Nernst-Planck models are extremely versatile and limited only by the assumptions of an effective-medium and by disregarding the spatial extent of the charge carriers (which may, however, be specifically important for electrochemical experiments with ions in an electrolyte where agglomeration of molecules at the electrodes has a significant influence on the measured immittance)[3].

In combination with finite-element methods complex inhomogeneous media with arbitrary geometries may be modelled. However, though some properties are known, e. g. the distribution of grain sizes and their respective properties, the actual form of an underlying inhomogeneous material is usually unknown. Hence, such an approach is limited to simulate random structures with similar properties, e. g. generating a structure with identical grain-size distribution and corresponding phase and orientation properties, which only emulates the actual situation in a 'real' sample. Furthermore, the actual size of the sample might be too large while the important structures are too small to simulate a full-sized system in the necessary detail, i. e. a macroscopic piece of a nano-crystalline material. Instead, a smaller volume of only few detailed structures might be simulated and the result respectively scaled.

It should be possible to include any process that can be embedded within an effective-medium approach in such models, also those with non-linear dependence on the field like the Frenkel-Poole conduction process. It could be introduced as carrier generation rate of an element dependent on its local internal field (generation and recombination of charges was introduced in [120], but without utilising local properties as the internal field). Similarly, electrode limited processes, like Schottky emission, may be included in Poisson-Nernst-Planck models by respective boundary conditions or field-dependent rates of injection from the electrodes (electrode-discharge effects have been introduced in [117], but without dependence of the local field at the interface).

The general idea of this work, i. e. introducing process-specific physical models dependent on external parameters, can, as indicated in the above examples, be combined with finite-element models. It may even be the next logical step and possibly very fruitful, especially when dealing with inhomogeneous systems. However, such intriguing future advancements of this concept of analysing immittance data lie outside of the scope of this

[3] At interfaces between electrical and ionic conductors so-called electrical double layers form which have a very significant capacitive contribution and importance in many electrochemical applications. The structural and, consequently, the derived electrical properties of electrochemical double layers require a realistic modulation of the agglomeration of ions at the interface which should, as it turns out, recognise the finite size of the ions. For information about double layers and an overview of different descriptions see [173, pp. 27-34]

work, which primarily focuses on the first step of utilising external-parameter-dependent physical models, namely, analysis based on lumped components. As already mentioned, there are specific solutions of spatially extended Poisson-Nernst-Planck models that take the form of lumped components. Exactly those models are advertised to be used in the analysis of immittance spectra [119]. Consequently, the comparison of the novel approach presented in this work with Poisson-Nernst-Planck models is restricted to those that take the form of lumped components.

Historical development towards Poisson-Nernst-Planck models utilisable in the analysis of immittance spectra This is only a very short summary of the historical development of Poisson-Nernst-Planck models. It is focused exclusively on key points in the development of models specifically designed for the application in immittance spectroscopy. The first Nernst-Planck solutions that took time dependence into account and calculated polarisation response were developed in 1933 by Jaffé [74, 75]. These works did not take carrier generation or recombination into account, but instead assumed constant numbers for both. In the first work [74], the discharge at the electrodes was forbidden which makes the presence of a dc current impossible. In the second publication [75], another type of ion species ('Ionen zweiter Art') was introduced that could discharge at or traverse through the electrodes. In 1952 Chang together with the author of the first works refined the previous model by introducing more realistic boundary conditions that would be suited for the description of electrolytic solutions [22]. Therefore, the discharge at the electrodes is assumed to be a rate process. In the second publication of this series Jaffé and Rider [76] introduced different mobilities for positive and negatively charged ions since this let to a more satisfactory agreement with presented experimental results. The works of Jaffé and its coworkers were further refined in 1953 by J. Macdonald [116] especially by assuming partial dissociation of positive and negative ions from a neutral species and taking recombination of carriers into account. Furthermore, for the first time the Poisson equation was properly included. In 1978 the description of the situation in electrolytes and semiconductors was again improved [120]. Charge carriers were now assumed to have arbitrary valence and, further, to recombination to as well as generation from neutral centres, charges can be emitted or absorbed from immobile donor or acceptor like centres. As illustrated, Poisson-Nernst-Planck models for the analysis of immittance data have an already more than eighty year old tradition and became incrementally refined, e. g. to include dc bias [45] or to account for anomalous diffusion processes [122]. However, they have not yet found widespread application for the analysis of immittance data [119].

5.1.2.2 Advantages of Poisson-Nernst-Planck models over conventional EECs

Instead of resistances and capacitances, Poisson-Nernst-Planck models extract physico-chemical properties on the basis of underlying assumptions. Typical parameters defining a Poisson-Nernst-Planck model which can, consequently, be determined in fits (some parameters are coupled, i. e. not all of them can be jointly fitted, the corresponding counterpart should be known) are [115]: the concentration of dissociable entities, valence number ratio between the two species, their corresponding mobilities, generation and

recombination rates, reaction rates at the electrodes.[4] If the extracted values are really connected to the underlying mechanisms (challenges achieving this are discussed below) they are much more meaningful than resistances and capacitances. Furthermore, there is no intermediate step of fitting EECs that may lead to loss of information.

5.1.2.3 The dangers of extracting effective values

In the last paragraph, it was established that the extracted parameters itself can be meaningful physicochemical parameters. This is, however, only the case if the extracted parameters actually correspond to some 'real' feature of the underlying process. For this, two conditions have to be fulfilled: First, the Poisson-Nernst-Planck model must be capable to describe the corresponding part of the system at all. Secondly, exclusively the immittance of this part must be associated with the fit parameters of the Poisson-Nernst-Planck model. Otherwise, effective parameters might be extracted which might not even give any indication that they have nothing to do with the real properties of the component.

The exclusive association is challenging, because currently used lumped-component Poisson-Nernst-Planck models do not include external-parameter dependence. Just as in the case of conventional EECs, it can, because no restrictions through specific dependencies are imposed, not be ensured that the lumped Poisson-Nernst-Planck component really describes exclusively the intended piece of the system. If by accident, contributions of multiple components are interpreted by the Poisson-Nernst-Planck model, it might simply 'absorb' the distortion of the false contributions. It is entirely possible that these extracted *effective* parameters might not be conspicuous at all. As a result, reasonable looking parameters might be extracted which might actually not correspond at all to any 'true' underlying property. Even if it could be ensured that only one part of the system is exclusively analysed with the Poisson-Nernst-Planck model, this part would have to fulfil certain requirements to extract relevant physicochemical parameters and not only effective ones. The part should at most have two types of charge carriers with opposing charge (they can be generated or recombined if necessary) whereas the charge injection may be limited by the electrodes (defined by specific rates). The boundary conditions have to be fulfilled. Without external-parameter dependence there might be no indication whether these requirements are not met or not.

An example that could exist in that form: assume a material where the transport is in parallel by two very different processes, a Frenkel-Poole conduction process and variable range hopping, both with electrons. Without external-parameter dependence, it is not possible to decouple two parallel Poisson-Nernst-Planck models. Additionally, without further knowledge only one transport process might be assumed. Fitting with a Poisson-Nernst-Planck model and assuming one mobile species, namely the electrons, effective parameters would be gained for the mobility, concentration, valence, etc. When varying the temperature, these effective parameters would change, however the involved underlying processes, their actual parameter and the fact itself that two processes are

[4] Here, the more common experimental situation is assumed, where the dimensions, e. g. the distance between the electrodes, are known and above parameters unknown. In principle it could also be the other way round.

involved would not be indicated. One could assume two mobile species (since they are not generated from each other with two concentrations and without generation and recombination), though they are actually not of opposing signs. With some knowledge, e. g. of the different mobilities or concentrations, the other parameters of the two sets may then possibly be associated with the different processes. Using the analytic solutions of Poisson-Nernst-Planck models for immittance spectroscopy, it would however not work for more species. So if an electrolytic solution with two solved species, e. g. NaCl and $CaSO_4$, is analysed, the parameters are inevitably effective values.

The result of the Poisson-Nernst-Planck models is compared with the novel approach presented in this work in the previous example. Of course, external parameters have to be varied, e. g. temperature and bias. One might assume a Frenkel-Poole conduction process. After fitting the experimental data and analysing the residuals one might find that this alone could not describe the experimental findings. Hence, variable-range hopping is added and one finds that the residuals do not require another process. With a bit more effort the fit does now agree with the experimental data, just as in the case of the Poisson-Nernst-Planck model before. However, the result contains more information as the models are more restrictive. Since the parameters of the Frenkel-Poole model were fitted for multiple temperatures and voltages, the activation energy and defect centre concentration may be extracted. Latter can then be compared with the density of centres determined form the mean hopping distance to determine whether or not the same centres that emit charges into the conductive band could principally also be those dominating the hopping contribution.

In summary, a good fit of a Poisson-Nernst-Planck model does not necessarily mean that the extracted parameters are really representing some underlying property. Any deviations could be absorbed by effective parameters. It is, hence, necessary to acquire some previous knowledge about the system under investigation. This could be the case for electrolytic solutions. Still, including external-parameter dependence can be utilised also in electrolytes. Similar to the field-dependent emission of a charge carrier from a trap, the dissociation of weak electrolytes has a field-dependence [144].

5.1.2.4 Describing parallel charge transport processes

Poisson-Nernst-Planck models can describe transport processes with one mobile charge by assigning its mobility, concentration of charge carriers, valence etc. As mentioned above, these parameters describe the transport of charges independent of the actual process itself. Meaning that, for example, subsequent tunnelling through localised states (that is hopping) would be assigned an appropriate mobility. Actual underlying process-specific parameters, e. g. the mean hopping distance, would not be extracted. Also two charge species with opposing sign can be well described. However, again without extracting the process-specific parameters. Except for an electrolytic solution with no more than one dissociated electrolyte species (it is one specific case the lumped Poisson-Nernst-Planck models were designed for) would be described well and the parameters would be appropriate for the underlying process. More then two charge transport processes or more than two types of ions in the solution cannot be described without fitting effective

values. Lumped Poisson-Nernst-Planck models cannot be arranged in parallel because their values would be coupled.

5.1.2.5 Decoupling multiple parallel transport processes and extracting process-specific parameters

There are two possibilities that enable decoupling of multiple different transport processes and extraction of process-specific underlying parameters: using the novel approach presented in this work or using a combination of its main idea, i. e. including process-specific physical models dependent on external parameters, with Poisson-Nernst-Planck models.

Using the novel approach presented in this work First, the transport processes dependent on external parameters is included as parallel resistors in the universal Voigt-circuit element that is supposed to describe the respective piece of the system (other parts are similarly modelled). Secondly, the parameters that cannot or should not be taken from literature or other sources are globally fitted. In the example given above, the concentration of defects that participate in the hopping process (derived from the mean hopping distance), the density of traps from which electrons are thermally excited into the conductive band as well as the corresponding energy barrier can be obtained. A comparable concentration may indicate that the involved traps could be identical. If possible, inter-process correlations should be utilised, e. g. the permittivity from the parallel capacitance can be used as joined constant for the permittivity in the barrier-lowering coefficient.

Combining the main idea of the novel approach presented in this work and Poisson-Nernst-Planck models The second method of analysis to decouple the parallel transport processes in the given example is a combination of the general idea of the presented approach with the Poisson-Nernst-Planck models. Sometimes specific physical processes may be assumed to determine certain internal properties of the system. In the example given above, the internal property of the number of charge carriers in the conduction band were supposed to follow a specific process, the field-assisted thermal emission (i. e. Frenkel-Poole model). Also the process of injection at the electrodes and its dependence on external parameters, like temperature and applied field, might be known. The central idea of this work, utilising process-specific physical models with their dependence on external parameters, can also be used to extend Poisson-Nernst-Planck models. Including these process-specific properties in conventional EECs allows decoupling of parallel processes or finding correct arrangements of components to obtain a one-to-one assignment of physical processes and circuit components, while also allowing global fitting over immittance spectra of various different conditions. Using the corresponding external-parameter-dependent physical processes to calculate the properties used in the Poisson-Nernst-Planck models, e. g. the temperature and field dependence of the concentration of charge carriers of one species, of its mobility or the injection rate at the electrodes, evokes similar advantages as in the case of the conventional EECs. In this way, also Poisson-Nernst-Planck models could be used in global fits over various conditions. Furthermore, parallel processes with

sufficiently different dependencies of the parameters of the Poisson-Nernst-Planck model can be decoupled. Also, possible intra-model coupling would be reduced.

In the example of a n-type semiconductor, mobility and number of mobile charge carriers is dependent on the temperature and total donor concentration [71, pp. 416-427]. Instead of fitting the mobilities directly, e. g. n mobilities for n different temperatures, one inserts the corresponding model for the mobility in the Poisson-Nernst-Planck model. This enhanced Poisson-Nernst-Planck model only fits the parameters of the underlying models necessary to subsequently calculate the number of carriers and their mobility for the various temperatures. The donor concentration, in particular, is a parameter acting on both, the mobility and the number of electrons in the conduction band [71, pp. 416-427], that may be extracted by varying the temperature in the relevant range. It is, hence, an example for a parameter that connects two distinct properties in the Poisson-Nernst-Planck model and, in this way, enforces self-consistency. Such restrictions can help finding the correct arrangements of components also when they are part of a Poisson-Nernst-Planck model element. Furthermore, also the distortion by other contributions can be reduced in that way. Similarly to the above mentioned example, restrictions through external-parameter dependencies can be employed for other materials and processes, too.

Process-specific physical models with their external-parameter-dependence should be included in an as early stage of the analysis as possible. They allow a drastic reduction of fit parameters for the analysis of measurements under various conditions and allow global fitting of all immittance spectra at once. This reduces accidental association of distorting contributions from other elements and can, hence, lead to better estimates for the physicochemical parameters. Since the models also carry a physical concept, the successful application also means understanding the underlying physics of the system and possible connections of one or more different models with the same constants checks not only the compatibility of the models with each other, but also the consistency of the assumptions about the underlying system itself.

There are two reasons why a fit (with the novel approach proposed in this work) of the enhanced Poisson-Nernst-Planck model does not resemble the experimental data although the theoretically derived arrangement (compare section 2.2) was used: First, the model itself cannot be applied on the intended piece of the system, hence extracted parameters would not make sense anyway. Another process must be responsible and different descriptions may be tried. Secondly, the system consists of more or less parts than expected, i. e. the number of components is not correct. Maybe another process is missing. Just as in the case of the novel approach proposed in this work, evaluation of the residuals over the external-parameters might help in this identification.

Although (systematic) deviations might be perceived as negative at first glance, more information can be gained in comparison to conventional Poisson-Nernst-Planck models. The latter would just, without warning, map any deviating behaviour on its parameters. That would mean that the extracted parameters are only effective quantities with values actually not present anywhere in the system. In other words, although process-specific external-parameter-dependent physical models impose more restrictions and can, in consequence, lead to worse approximations of the measured data, their application is easier to validate and a good description also likely means a good understanding of the

system. However, in comparison to conventional Poisson-Nernst-Planck models which require only a single condition, to apply the enhanced Poisson-Nernst-Planck model (or the novel approach proposed in this work), immittance spectra have to be obtained for a large enough number of sufficiently different conditions.

5.1.2.6 Summary

Whether the novel approach of analysing immittance data, directly, or in, the above explained, combination with Poisson-Nernst-Planck models is used, the consideration of external-parameter-dependence decouples parallel processes, allows global fitting, automatically weights the regions of importance for the specific parameters which in the end result in both, potentially better guesses and improved understanding of the underlying physics. In contrast to conventional Poisson-Nernst-Planck models, these process-specific approaches facilitate that not only effective parameters are extracted. Hence, whether the processes are assumed correctly is assessed as well (also indicating a valid understanding of the underlying physics) and, finally, other process-specific parameters, e. g. the energetic levels of the defects involved in the charge carrier emission may be obtained additionally.

5.2 Benefits of the new model using the example of metal/ta-C/Si heterostructures

In order to resolve a quantitative deviation between the measured barrier-lowering coefficient and its prediction by the Frenkel-Poole model, the calculation of the superimposed linear field was corrected. Instead of using the external field (which cannot be seen by a charge between plates that are filled with a dielectric) the *internal* field was introduced. Already without this correction, the Frenkel-Poole model that describes field-dependent resistive properties does include a parameter of the respective dielectric part of the material, namely, the dynamic permittivity. The above mentioned correction additionally includes a dependence on static permittivity to determine the resistive characteristic of the thin film. As already explained before, in such a situation the novel approach presented in this work (which uses external-parameter-dependent process-specific physical models to extract relevant parameters in global fits with joined parameters, as the mentioned permittivities, and includes the full information of a current-voltage analysis) can especially display its advantages: while different pieces can be separated, joint parameters, especially spanning over resistive and dielectric properties, can be used within the specific pieces. If the found models can successfully describe the immittance spectra, the used process-specific descriptions are compatible and the intended piece is investigated with minimal distortion by accidental contributions of other processes. It is, hence, also unlikely that another piece is described or that the models only fit accidentally.

In contrast to a conventional current-voltage characterisation, the different serial pieces can be separated by the specific parallel capacitive bypasses. The capacitance and resistance of the depletion layer, both dependent on voltage, are fitted by parameters which are physically relevant and better comparable as resistances and capacitances: the (effective) acceptor concentration (which is jointly used for the capacitive and resistive part), two Schottky barrier heights (since the voltage shift was not explicitly ascribed to either interface defects or fixed charges in the thin film, two barriers were determined, alternatively one barrier height and one defect concentration could be fitted) and the constant-phase characteristic (which is almost unity and was fitted mainly to confirm that). It is hence (almost) impossible that the fitted immittance does not belong to a depletion layer. If this piece would really have been important in this investigation, even more elaborate models could be applied leading to yet more meaningful parameters, potentially including more information about the involved defects. Using this 'unfinished' depletion-layer model is still helpful to gasp the potential of the novel approach of analysing immittance spectra presented in this work: Missing features of the depletion-layer description, e. g. the omitted defects at the interface and in the thin film, could be associated with specific regions found in the corresponding plots of deviations and residuals over the external parameters. Although the fit might have absorbed certain fractions of the deviations in the parameters of the utilised models, it could be seen how well their restrictive nature protects the models from absorbing other contributions. The presented approach is, hence, very useful to spot incomplete descriptions of certain processes or to find out if some are missing completely. It is also expected to be quite successful in the extraction of

parameters with low distortion from fragmentary models, since the approach does not tend to absorb too much of the distortions unaccounted in the model.

In the thin-film circuit, only the resistance is voltage dependent, while the capacitive part is constant. The fact that the permittivities of the constant capacitive component and the voltage-dependent resistor could be connected and both together describe the observed behaviour (complementary to the depletion layer part) very well, strongly suggests a correct identification of the underlying processes in the system. A requirement for the connection described above was the introduced correction to calculate the superimposed field in the Frenkel-Poole model, with it, the resistive part is compatible with the capacitive model (i. e. the permittivity). A similar confident decoupling of the different parts would not have been possible using conventional current-voltage analysis. Later characteristic is completely contained within the voltage-dependent immittance spectra.

In addition to the better separation and more confident identification of processes, the involvement of the permittivity in resistive and capacitive part was especially important to test the proposed correction. Three different connections between the resistive and capacitive part were compared. The first two tested different ways of extracting the capacitance. The third assumed no connection between both parts at all. Why the presented approach was optimal for testing these three hypotheses is explained in the following part of the discussion.

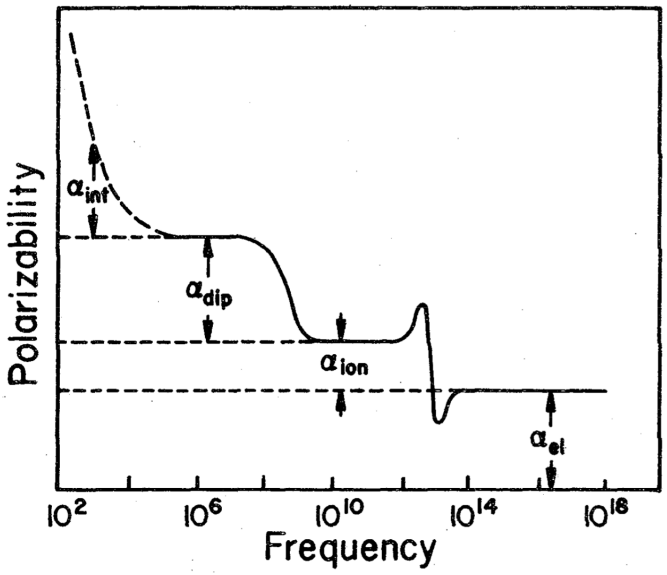

Figure 5.2: The classification in different contributions and their corresponding typical frequency ranges (apparently in Hz) from Young and Frederikse [190]. The interfacial polarisation α_{int} is supposed to occur in the measurement range of this work (20 Hz to 1 MHz). According to Young and Frederikse 'The real value of the [static] dielectric constant excludes the interfacial polarisation' [190]. Reprinted from Young and Frederikse (1973): 'Compilation of the Static Dielectric Constant of Inorganic Solids'. Journal of Physical and Chemical Reference Data, **2**(2), pp. 313-409, with the permission of AIP Publishing.

5.3 Extracting the bulk static permittivity of ta-C

There are various reasons to obtain unusually high ($\varepsilon_r \gtrsim 100$) or at least apparently high values of the permittivity at low frequencies [108]. The most common effect of apparently large permittivities, known already for a very long time, is the Maxwell-Wagner effect which belongs to the group of interface polarisations [187, 106, 108]. Essentially, the presence of (microscopic) regions of different permittivities or conductivities, which on their own have usual magnitudes, can in combination lead to apparently very large permittivity of the whole system, especially at low frequencies [187, 106]. These interface polarisations[5] explicitly include those caused by depletion layers, at metal contacts or grain boundaries [190, 108], which are in this work summarised as external origins of interfacial polarisation. According to Young and Frederikse [190], also the defects, such as voids, dislocations, clusters of vacancies, interstitials or impurities can lead to the accumulation of charges in the bulk of the dielectric and contribute to the interfacial polarisability, here internal interfacial polarisability. All these interface polarisations are very common effects which supposingly do not contribute to the true bulk static permittivity [190]. In the

[5] Although the effect leading to the apparently large permittivities is, fundamentally, still the Maxwell-Wagner effect, this work follows the convention of Young and Frederikse [190] to use the more general term of interfacial polarisation for interfaces like depletion layers and grain boundaries. This should reflect the importance of the statistical character of these interfaces, which leads to a much more complicated frequency dependence and characteristic differences from the original Maxwell-Wagner model.

compilation of static permittivities from the National Bureau of Standards [190], today called the National Institute of Standards and Technology, it says: 'All these mechanisms contribute to the interfacial polarisability α_{int}. As a result one often observes at low frequencies dielectric constants much in excess of the real value for the pure bulk material. (The real value of the dielectric constant excludes the interfacial polarisation.) Because of this effect it usually is impossible to measure the static dielectric constant in the low frequency range; for the great majority of substances the measurement has been performed at 10^3 Hz or higher (sometimes as high as 10^8 or 10^9 Hz)'. The observation that the permittivity extracted from the constant phase element is too large to correspond to the static permittivity (which is assumed in the corrected version of the Frenkel-Poole model) is, hence, in agreement with the interpretation of Young and Frederikse. Furthermore, their method of extracting the static permittivity at higher frequencies, after the contribution of the interfacial polarisation becomes negligible (as shown in Figure 5.2), corresponds to extracting the static permittivity from the experimental high-frequency-limiting capacitor $C_{\text{tf},\infty}^{(\text{exp})}$. As a result, according to the interpretation of Young and Frederikse, not Model 1 but Model 2 extracts the 'true' static permittivity of the material. As can be seen by the deviations of Model 1 and in agreement with their prediction, the permittivity extracted from the constant phase element is too large while the permittivity extracted from the high-frequency-limiting capacitor $C_{\text{tf},\infty}^{(\text{exp})}$ has just the right value to resolve a decade-old quantitative deviation of the Frenkel-Poole model.

In Model 2, the permittivity from the experimental high-frequency-limiting capacitor $C_{\text{tf},\infty}^{(\text{exp})}$ is not only used as static permittivity, but also as an approximation for the dynamic permittivity. Why this is expected to be a good approximation is explained in this paragraph, by discussing one resonance in Figure 5.2, and its respective contribution to the permittivity, after another. A covalently bound material, like ta-C, is not expected to have relevant amount of molecular dipoles that could be oriented. Consequently, the process responsible for dipolar or orientational polarisability α_{dip} in Figure 5.2, should either give little or no contribution to the permittivity at all. The same should apply for the subsequent ionic polarisability α_{ion} (again in Figure 5.2), since ta-C is a material of one atom species only, the carbon atoms are covalently bound and under the conditions of the experiment rarely expected to be ionised. Furthermore, the number of contaminants for mass-selective ion-beam deposition which may lead to bonds with potentially ionic character is expected to be not particularly high, even especially low in comparison to the majority of other deposition methods,[6] as well. It is, hence, within this context entirely possible that the permittivity relevant for the Coulombic contribution to the potential of the exiting mobile charge, the dynamic permittivity, is for ta-C almost the same as the static permittivity, for frequencies higher than the supposed (confer [190]) to be excluded interfacial polarisation . Hence, by determining the static permittivity with the procedure as suggested by Young and Frederikse and by assuming that the dipolar and ionic contributions to the permittivity are negligible for ta-C (which is for the above mentioned

[6] Specifically for ta-C mass-selective ion-beam deposition leads to the films with highest sp^3 content [154] and lowest impurity content [101, pp. 211-213].

reasons quite reasonable), the calculation for the internal field leads to a quantitatively correct slope of the Frenkel-Poole model.

Unlike in this work, to determine the permittivities, or the dielectric spectrum of a material, usually the, in that case, 'parasitic' contributions like space-charge layers are not explicitly modelled. Of course, for this alternative goal, the structure of the sample is optimised to prevent parasitic pieces. Still, these parasitic contributions at low frequencies, associated with interfacial polarisation by Young and Frederikse, seem to be unavoidable [190, 106, 108]. In fact, most large permittivities at low frequency can be explained mostly by Maxwell-Wagner contributions [106], specifically by those caused by 'depletion layers at the interface between sample and contacts or at grain boundaries' [106]. In the present work, no (non-metallic) piece of the system is expected to have grains, and hence also no grain boundaries. Unlike for the usual method of determining permittivities, in this work, different pieces of the sample have been explicitly modelled. As a result, the different permittivity contributions to the total system by the thin film itself and the depletion layer in the substrate have been explicitly taken into account. The apparently large permittivity of the system ta-C/p-Si caused by the Maxwell-Wagner effect between silicon and ta-C has, hence, been accounted for. With the analysis in previous works [2] and by unpublished results of current-voltage analysis of the annealed aluminium back contacts, it can be deduced that there is no depletion layer at the Al/p-Si back contact side. Different top-contact material systems of Al/Ti and Au/Cr each on the ta-C film have lead to no significant differences in the immittance response. This, at least, indicates that there is no significant depletion-layer formation at the metal/ta-C interface. Depletion layers in disordered materials, like ta-C, that observe defect-driven conduction mechanism are, also due to the very high number of defects and their presence at almost all energies, anyway unlikely [80]. Still, quite unlike the ta-C/p-Si interface, where the different permittivities are explicitly considered, the (abrupt) permittivity transition, at both metallic contact sides of the system, has been ignored. Then again, they do not lead to large contributions to the resistance and, consequently, only have a very small ratio of voltage drop. More importantly, the constant phase element relevant in this context is identified as the dielectric contribution parallel to the Frenkel-Poole conductivity and, hence, associated with the bulk or at least internal contribution of the thin film. Meaning that, if this apparently large permittivity at low frequencies would be caused by the interfacial polarisation, its source should rather be the inhomogeneities inside the ta-C bulk, i. e. the internal interfacial polarisation. Due to the amorphous nature of the carbon film neither sharp gradients in the permittivity, as for grain boundaries, nor large variations in permittivity at different locations in the film, like for crystalline materials that can appear in different phases, are expected.

One possible explanation could be that the interfacial polarisation at those other interfaces is falsely identified as a contribution parallel to the Frenkel-Poole conduction that describes dominant conduction process in the ta-C bulk. This seems, however, unlikely, since the assumption of this voltage-independent constant phase element parallel to the Frenkel-Poole resistance with very specific voltage dependence leads to a correct cut-off frequency for almost all bias voltages. Additionally, these different interfaces are, on the one hand, known to have only little contribution to the resistance, with the

consequence of a very low voltage drop, and, on the other hand, it is extremely unlikely that their voltage dependence should be similar to the one of the Frenkel-Poole process of the ta-C bulk.

Believing (for the moment that the circuit assumed in this work is correct) that the constant phase element is parallel to the Frenkel-Poole resistance, another possible explanation of falsely assuming the constant phase element to be a ta-C bulk property, could be caused by the misconception that the Frenkel-Poole effect would describe the bulk conduction, while it would actually be an interface effect. The possibility of an interface effect at the silicon side can be excluded by the fact that conductive ion tracks can be formed in ta-C [127, 188]. Assuming that what is identified as the Frenkel-Poole behaviour would be an interface and not a bulk effect: As there is no other significant resistance (for highly doped substrate) the bulk conductivity of the ta-C must be quite high. Furthermore, in this case, the ion tracks would not shortcut the highly conductive ta-C, but only very locally reduce the high resistance at the ta-C/Si interface. Since ta-C would in this scenario have a large bulk conductivity, the reduction of the resistance at the interface by an ion impact could impossibly lead to a very sharp (few nanometres diameter) island of high conductivity at the top surface of ta-C. Quite the opposite, the sharp conductive 'hole' in the interface would be smeared out by the good conduction of the ta-C bulk and, in the end, only a globally higher conductivity could be measured. The remaining interface is the one at the surface of the ta-C. It seems unlikely that the interface at the top of ta-C should show the same high-resistive characteristic for different metal contacts, including planar Al/Ti and Au/Cr contacts, wolfram- and diamond-coated AFM tips, and more contact materials used by other researchers finding the same current-density-voltage properties [21, 38, 132, 53], but exhibit no significant interface resistance at the substrate side (of the amorphous carbon). As already mentioned, electrode effects are not expected to be prominent in disordered materials, anyway [80].

Finally, having dismissed external interface-related effects, it can be assumed that the constant phase element really describes the low-frequency contribution of the bulk ta-C. From the list of other explanations given in reference [108] only one explanation remains: the already mentioned power-law derived by Jonscher [84] for a large variety of materials, hence termed 'universal dielectric response', only sharing the property that they are in some way disordered. This effect is associated with charge transport involving localised states. It leads to very high permittivities but also involves a very large loss ratio. It is in agreement with the presence of the Frenkel-Poole conduction and other properties of the material, like its amorphous nature and the fact that its Fermi level is inside the gap (i. e. beneath the mobility edge / conductive band), extremely likely, that ta-C should exhibit the universal dielectric response and that the observed constant phase element is its result.

In the end, three possible explanations are remaining: Either internal interfacial polarisation by slight random internal fluctuations that are, due to the amorphous nature of the material, expected much less sharp, not as pronounced and with much smaller spatial extent than grains. Or the much more likely, even surprising if not present, universal response due to the charge transport involving localised states with a certain randomness.

Assuming the cause of the oversized permittivity is indeed, as expected, due to the

latter: although a large part of the permittivity is associated with loss, the real part of the permittivity is still much larger than 10. This is not in agreement with the suggested correction for the calculation of the internal field in the Frenkel-Poole model. Hence, this could mean that the suggested correction does not fix the quantitative problems of the Frenkel-Poole model. On the other hand, *this part of the permittivity spectra is generally not used to determine the bulk static permittivities* [190]. This was justified with the association of the corresponding response at low frequencies with interfacial polarisation [190]. The correctness of this assumption might neither have been nor be universally true. It is entirely possible, that the obtained high permittivities were not always connected to interface effects, especially since the low-frequency part was in general just discarded (see reference [190]). According to Young and Frederikse [190], this type of polarisation is also caused by voids (probably generalising vacancies and clusters of such), dislocations, impurities or interstitials. All these nanoscopic defects cannot (explicitly) be described with effective media approaches. As a consequence, the effects of these localised defects cannot have anything to do with the (original form of) Maxwell-Wagner effect, that is based on effective media approximations and necessarily requires the resulting effective large-scale quantities like permittivity and conductivity. Hence, it may be interesting to further investigate whether the very lossy, but still high real permittivity values, due to hopping conduction, are contributing to the static permittivity in a way that they lower the internal field for a charge in the material or that they are not really a part of the static permittivity. It may have been oversimplified to generally associate the low-frequency part with interfacial polarisation and, consequently, to disregard it. There may be other effects not part of the static permittivity leading to apparently large real parts of the permittivity.

So far, the different interfaces which have only little resistance and, hence, negligible voltage drop were not considered to be a source of the capacitive dispersion for low frequencies. In principle, however, any capture and emission process of a trap leads to a contribution to the dielectric current. The voltage drop over the different components indicates not only their respective regions of dominance, but also that the fields in these regions are correspondingly higher than in the others under respective conditions. What if already the low field at other interfaces, while the major part of the voltage drops over the thin film, is enough to charge or discharge the traps close to the interface? For example, at the generally low-resistive back contact, consisting of an annealed aluminium/silicon, there might still be a high number of electrically active defects. Supposing they are shallow enough, they might be charged and discharged while there is almost no voltage drop around their region. If now a condition is selected where the voltage drop is primarily over the thin film but the defects close to the back contact were charged and discharged due to the applied signal, this would be falsely interpreted as a contribution to the thin film. The question is: Knowing that the signal amplitude is only 30 $\mathrm{mV_{RMS}}$ and the major part of this rather small voltage drops over the thin film, can the remaining fraction still influence the occupation statistics at another part enough to lead to a significant contribution to the dielectric current? If the answer would be yes, this could lead to a dispersion that is not actually in the thin film, but would seem that way. The interface at the back contact was just an example for the purpose of illustration. In the case that this effect exists, any region of defects which changes the occupation statistics due to this

fraction of the applied signal could lead to such a false contribution as explained above.

Another explanation would be the form of the polarisation resonance. At these low frequencies, the change in permittivity is usually assumed to have the form of relaxational dispersion instead of a resonant dispersion. Resonant dispersion would lead to very large permittivities around the resonance while the permittivity step between both sides far from the resonance, the actual contribution to the static permittivity, is much smaller (compare resonant dispersion at the ionic resonance in Figure 5.2 where the permittivity values for frequencies just below the centre of the resonance are much higher than the true contribution). The dispersion corresponding to the dipole relaxation in the same figure is a relaxational dispersion: its permittivity neither over- nor undershoots around the resonance.

An explanation why the higher permittivity values extracted from the constant phase element would have no effect on the barrier-lowering, though they would be caused by the contribution of hopping conduction in the ta-C, could be a thin-film-specific effect. In section 4.2 the distance of the maximum of the barrier height was estimated to be around 12 nm in a material with a relative permittivity $\varepsilon_\mathrm{r} = 5$ and an internal field corresponding to a voltage drop of 1 V over 100 nm thin film. Assuming, although this distance decreases for higher fields and increases for lower fields, this might be a relevant magnitude. The Coulombic traps in the thin film would have to be separated by at least 24 nm from each other to avoid an influence between them that would be strong enough to lead to serious deviation from the Frenkel-Poole model. The thickness of the thin film is, depending on the sample, supposed to be between 60 nm to 80 nm. This work uses the advanced Frenkel-Poole model by Connell *et al.* [28] which includes a three-dimensional Coulombic potential. Like most extension of the Frenkel-Poole model, the introduction of the three-dimensional potential landscape is still based on the idea of Jonscher [80]. This means that the linear superimposed field is, without loss of generality assumed in only one effective direction, while its effect on the otherwise Coulombic potential is calculated with respect to the angle in field direction (followed by integrating the escape probability over the sphere with the respective barrier heights). In this work, the *internal field* is assumed for the linear superimposed field while the rest of the calculation remains identical. For the investigated *isotropic, homogeneous* material, neglecting the influence of neighbouring traps, the field can safely be assumed to be directed normal to the sandwiched structure of the system, i. e. orthogonal to the lateral side of the thin film. Due to this fact, only very few (in the mean between one to two) traps are before or after a specific trap in the field direction. Assuming that the same traps that lead to the dispersive contribution of the capacitance at low frequencies are those responsible for the Frenkel-Poole effect, the low number of those traps in the relevant direction (normal to the thin film surface) may *break the effective medium approach*, i. e. the polarisation due to hopping might still be significant due to the relatively large lateral dimensions leading to a high number of contributing hopping centres for the measurement of the total capacitance of the complete thin film. For an individual trap, however, the contribution in the relevant direction would only be caused by few hopping centres, probably not enough to allow assuming the extracted effective permittivity, especially since for the usually utilised pair approximation the dipole is assumed to be

due to two hopping centres [104]. The possible explanation given above, that might not necessarily be the true situation, belongs to a whole class of scenarios that are all based on the fact that the effective media approximation breaks. A very simple and even extremer version of the latter example would be that the thin film could in lateral direction be divided into many cubes of two types with similar frequency: one would be a Frenkel-Poole-like conductor with the permittivity without low-frequency polarisation by charge movement in traps and the second type would contain defects that lead to a distribution of polarisation processes in latter low-frequency regime, but had no conductive contribution whatsoever. Additionally, the defects responsible for the polarisation in the second type of cubes should be too far from any neighbouring traps responsible for conductive contributions. The result would be a constant-phase response for the dielectric properties. The traps involved in conduction (in type 1 cubes), on the other hand, would not perceive the low-frequency permittivity caused by the low-frequency polarisation in the type 2 cubes. This is, of course, a pathological example which would not exist in a real-world material. As explained later, the Barton-Nakajima-Namikawa relation given in equation 6.1 even indicates that (a subgroup of) the same defects responsible for the conduction in a material are also those involved in the polarisation of disordered materials. However, from the fact that dielectric properties are much less dependent on external parameters, like the temperature, as corresponding conductive properties [37], it may be deduced that static conduction involves also contributions of very slow jumps (a theory already mentioned by [80]). These unlikely jumps are frozen long before the highly probable jumps responsible for the constant-phase behaviour freeze. Hence, only a smaller number of traps is responsible for the dielectric properties. Since a thin film is investigated, in the direction of the applied field only few of these defects responsible for the constant-phase behaviour are in series to the many defects involved in the static conduction process. As a consequence, latter might not perceive the high low-frequency permittivity caused by hopping processes. Although none of the above examples may be present in exactly the described variant in the material, these examples shall stress one very important point: *awareness of deviations caused by utilising the effective media approach*, which could explain the absence of the high values of relative permittivity, observed in the low-frequency dielectric response, in the actual static relative permittivity used in the model for the conduction process.

Since the actual origin of the constant phase behaviour is not yet entirely clear, a straight forward extraction of a permittivity from the constant phase element might not necessarily be correct. Models with distributions of resistivity but permittivity of normal magnitude can lead to an apparently high value for the permittivity [65]. At the end, fluctuations of resistance in the amorphous bulk could explain the apparently high permittivity values.

In summary, the low-frequency region associated with the response of the constant phase element is usually not regarded as a part of the *bulk* static permittivity [190]. There are specific exceptions that could appear for the investigated disordered system, since it has a charge transport mechanism based on localised states [108]. The proposed correction of the Frenkel-Poole model leads, for the first time, to a quantitatively correct description of the measured data, if the extraction is performed according to reference [190], i. e. ignoring

the dispersive capacitance at very low frequencies. This indicates that the constant phase element is either not connected to the bulk static permittivity or, if it is, that this part of the bulk static permittivity plays no role in the calculation of the internal field (some possible reasons for both are given above).

5.4 The exclusive separation of the total current density into static conduction processes and dielectric processes

As explained in 2.1.2, the two terms on the right-hand side in the equation (3.1b) (repeated below) for the total current density

$$\tilde{\mathbf{J}}_{\mathrm{tot}}(t,\tilde{\mathbf{E}},\tilde{\mathscr{P}}) = \tilde{\mathbf{J}}_{\mathrm{free}}^{(\mathrm{stat})}(\tilde{\mathbf{E}},\tilde{\mathscr{P}}) + \frac{\partial \tilde{\mathbf{D}}(t,\tilde{\mathbf{E}},\tilde{\mathscr{P}})}{\partial t}, \tag{3.1b}$$

are assumed to exclusively represent either dc or ac properties of the non-magnetic piece of material. From its first definition on, this exclusive separation is followed through until the interpretation as electrical equivalent circuit, i. e. an interpretation as lumped components for an actually spatially extended piece of material. As a result, the static resistor $R_{\mathrm{stat}}(V,\mathscr{P})$ is assumed to be caused solely by the dc transport process(es), while both dynamic components $R_{\mathrm{dyn}}(\omega,V,\mathscr{P})$ and $X'_{\mathrm{C}}(\omega,V,\mathscr{P})$, in either parallel or serial arrangement, are associated with the dielectric properties only. From this assumption follows that the static resistance has to be parallel to the dynamic components (independent on their arrangement), since it is the only remaining resistance for zero frequency. The dielectric part necessarily has, independent on whether the circuits for its polarisation processes are arranged in their parallel or serial representations, an infinite immittance at zero frequency. Any magnetic contribution, unavoidably present for any material including those with relative magnetic permeability of unity ($\mu_{\mathrm{r}} = 1$) is neglected. In systems with low conductivity (e. g. non-metals), which are usually investigated by immittance spectroscopy, this assumption is quite reasonable. It makes however clear that this separation (which also assumes the free current density J_{free} to be independent of frequency), the negligence of any magnetic contributions and, especially, ignoring the spatial dependence of these quantities, can only be an approximation.

The assumption of a frequency-independent free current density J_{free} was necessary, because including external-parameter dependence is the central idea of this novel approach, and most available external-parameter-dependent conduction models are only designed for the case of static conduction. In fact, the free current density J_{free} is dependent on frequency and its association with the dc conductivity, as already done by Jonscher [78], is only an approximation. In the next section, it will be discussed up to what frequency the dc model may still be used. It is found that assuming the dc conductivity as source for the free current density J_{free} is valid for a rather large frequency range that very likely includes all frequencies usually used for immittance spectroscopy.

> It should, however, be noted that all discussions about the frequency dependence of the free current density J_{free} do *not* affect the present version of the immittance simulation used. Currently, the simulation only uses the bias voltage to calculate the free-current contribution (more precisely the static resistance of each component). This is a typical small-signal approximation which, consequently, ignores the potentially asymmetric behaviour of the conductivity model in the voltage range of the oscillation. Due to the non-linearity and asymmetry of the model, the mean

conductivity might be different to the conductivity of the mean voltage. Furthermore, the varying voltage will also vary the voltage drop over every serial circuit component which makes the calculation of the real conductivity for each time step rather expensive.

Besides the breakdown of actually static conduction models, which seems to be outside the frequency range relevant for immittance spectroscopy, the free current density J_{free} becomes also frequency dependent because spatial dimensions and magnetic effects are ignored. With increasing frequency the 'skin effect' (see [95] and [62, p. 45]) becomes increasingly important, i. e. the self-induced magnetic filed induces a current that reduces current flow in the centre of a conductor. As a result, the effective area of the conductor is decreasing with increasing frequency (since the current in field direction is only flowing in a region, close to the surface of the conductor, which decreases with frequency). When concentrating exclusively on Maxwell's generalisation of Ampere's law *without* spatial dimensions, e. g. assuming lumped components, this effect will appear as a decrease in the amplitude of the free current density J_{free} with increasing frequency. Since this effect does involve the creation of a magnetic field from the current through the conductor and induction of an eddy current in the same material, it only plays a role in good conductors. Those are rarely investigated in immittance spectroscopy, except in the field of engineering.

5.4.1 Using static current models for the free current

This exclusive separation has also been used by Jonscher [78, pp. 40-41]. He associated the dc conductivity σ_{dc} with the free current, i. e.

$$\mathbf{J}_{\text{free}} = \sigma_{\text{dc}}\mathbf{E},$$

where σ_{dc} is assumed a purely real constant that would be obtained under steady-state conditions at infinite time, i. e. σ_{dc} is independent of frequency [78, pp. 40-41].[7] The calculation of the free current $\mathbf{J}_{\text{free}}$ via Ohm's law was already introduced by Maxwell [126]. Furthermore, Maxwell also ascribed the polarisation to the dielectric displacement [126]. On the other hand, Maxwell only mentions the proportionality between the free current $\mathbf{J}_{\text{free}}$ and the applied field ('electromotive force') and, in this context, introduces the reciprocal of the specific resistivity ('specific resistance') ρ as proportionality constant [126]. In the syntax of this work, assuming a homogeneous, isotropic material, Maxwell defines

$$\mathbf{J}_{\text{free}} = \rho^{-1}\mathbf{E}.$$

Maxwell did neither specify whether the specific resistivity should be a constant, independent on frequency, or even identical to the dc value [126]. This work adopts the exclusive separation and, consequently, the interpretation of the free current $\mathbf{J}_{\text{free}}$ by Jonscher [78]. Otherwise, the conversion into frequency domain would have also lead to an imaginary component of the free current, i. e. in quadrature with the driving field, and

[7] As in the derivation, the material is assumed homogeneous and isotropic. If not mentioned explicitly, the assumptions of the derivation are used also in this section.

frequency dependence (also of the derived components) resulting in a different electrical equivalent circuit. The derivation would have been more complicated, but still possible. There is, however, another reason why the exclusive separation of dc and ac contributions is used although it is only an approximation: in the following part of the section, it will be shown that within the frequency range of dielectric relaxation, i. e. the range relevant for immittance spectroscopy, the assumption of the exclusive separation of dc and ac contributions is a valid approximation.

The above mentioned fact, that this exclusive separation is an approximation, becomes apparent when frequency dependence is introduced for the static transport process. The frequency dependence becomes unavoidable, because the dependence on external parameters, that is included, can lead to an implicit frequency dependence. Generally, the resistivity might be dependent on the applied field, which is a quantity that is varied (periodically) in the experiment with varying frequency. A dc conductivity model, which usually assumes the system has reached its steady state (under static conditions), would independent of frequency lead to purely real values for the resistance, only. The response of a purely real-valued resistor, however, would be *always in phase with the driving field* and result in the *equilibrium current of the currently applied field at any time*, independent of the frequency of the signal. In the following paragraphs it is assessed up to which frequency the approximation of utilising the dc model may be assumed valid. There are two very different types of conduction that are considered separately: conduction through delocalised and localised states.

The situation is well investigated for the former case: *metallic conduction*, i. e. conduction through delocalised states (e. g. confer [143, pp. 16-22]). In a basic description, the equation of motion for a charged particle is assumed to consist of the constant acceleration due to the applied field and a frictional term that reduced the speed of the particle through collisions [143, pp. 16-22]. The mean-time between collisions is reciprocally linked to the dampening constant of the friction term. In a typical conductor it is of the order of 10^{-14} s, e. g. for copper $\tau = 2.4 \cdot 10^{-14}$ s [143, pp. 16-22]. From such mean times between collisions and other material specific parameters the plasma frequency can be determined [143, pp. 16-22]. It is found, that the conductivity of a metal may be considered independent of frequency as long as it is sufficiently lower than the corresponding plasma frequency which is in the terahertz range for typical metals [143, pp. 16-22]. Hence, the form of electrical equivalent circuit proposed in this work can, for a metallic part of the system, be used in all typical frequency ranges of immittance spectroscopy.

As shown in this and the two following paragraph, in parts with *conduction involving localised states*, this separation remains valid up to frequencies sufficiently lower than those at which modulation quanta are absorbed or emitted by the charge. At a first glance one might think that the *lifetime* of a trap, that is the time a charge carrier occupies a trap before it is released, might be connected to the high-frequency limit of the approximation in a material where charge transport is dominated by processes involving localised defects (for simplicity, but without the loss of generality, only one type of trap is assumed). Using the lifetime of the charge carrier in the trap (in combination with the corresponding trap density, energy differences, possible final states, recapture probability, etc.), a net jump rate r_i for charges successfully leaving the trap in a unit volume can be derived. As no

quantitative result shall be calculated, it is here not relevant what fraction of these jumps lead to an actual contribution to the current, as a result, without the loss of generality the net jump rate r_i should only include the fraction of those jumps that do contribute. Generally, the jump rate may be influenced by external parameter, e. g. the applied field or the temperature. Consequently, it is implicitly dependent on time. It is not explicitly dependent on time, because the trap should not memorise prior conditions, the trap system shall be time invariant (the derivation was restricted to a non-ferroelectric, non-magnetic material). This means that the probability of leaving the trap has as such no time dependence, i. e. applying the *same conditions* today, tomorrow any other day will result in the same probability. Of course, changing the conditions may change the probability, e. g. a higher temperature could lead to an increased jump probability. Using the familiar syntax of this work for parameter dependence while additionally stressing the fact that the parameters themselves are explicitly dependent on time the jump rate might be written as $r_i\left(\tilde{\mathbf{E}}(t), \tilde{\mathscr{P}}(t)\right)$. To calculate the number of successful jumps n_i in a time interval (t_1, t_2) may than be calculated by integrating the net jump rate

$$n_i = \int_{t_1}^{t_2} r_i\left(\tilde{\mathbf{E}}(t), \tilde{\mathscr{P}}(t)\right) \mathrm{d}t. \tag{5.1}$$

For increasing frequency the length of the time interval, at which the condition can be assumed constant, decreases. However, the calculation of the total number of successful jumps n_i remains valid, even when the length of the time interval falls below the mean lifetime (but is still above the already mentioned actual limit), because, as long as the number of traps is sufficiently high, the corresponding fraction of them still performs jumps, i. e. the number of successful jumps will decrease, but according to the ratio of the constant condition. For example, if the field is applied for only a tenth of the time to have N successful jumps, in the mean only $\frac{N}{10}$ of the jumps occur. Hence, interval length below the mean jump rate (but above the frequencies for absorption or emission of modulation quanta for the charge) result in a reduced current, but do not represent a general limit.

Another important time constant for conduction processes involving localised states is the *traversal time*. This is the time the trapped charge requires actually passing through the barrier [16]. Usually this time is much shorter than the lifetime of an occupant in the trap [3]. In their work [16], Büttiker and Landauer discuss the influence of electrical fields varying with time on the barrier and the corresponding traversal time through it. They find that, as long as no modulation quanta is transferred, the barrier remains effectively the same. There are two cases: First, the applied signal has a low frequency, with a huge wavelength in comparison to the barrier width, in this case the situation for the charge looks like the respective static condition. Second, the applied signal has a wavelength in the order of or sufficiently higher than the barrier width, corresponding to a frequency in the order of or higher than the inverse of the traversal time. In latter case, the barrier becomes actually modulated, but the relevant effective barrier remains identical. As a result the frequency range of validity (of utilising a dc model while ignoring any delay for the resistance) is not dependent on the traversal time (confer [16]).

Finally, if the frequency reaches a range where modulation quanta are absorbed or

emitted by the charge carrier, the probability of passing through the barrier is changed [16]. At such frequencies the rate integrated in (5.1) deviates from the dc behaviour and the approximation becomes invalid. It is entirely possible that this frequency is lower than the inverse of the traversal time. The moment, modulation quanta become important, is not only when the proposed approximation breaks, but also the upper frequency limit of the range at which immittance spectroscopy is typically performed. According to the definition by Jonscher [78, p. 6], dielectric relaxation is observed in the '"low-frequency" sub-quantum' limit and, hence, ends below the above described frequency range of charges interacting with modulation quanta. As a consequence, for frequencies around or larger than this limit, the static conductivity σ_{dc} has to be replaced by a dynamic conductivity that recognises the frequency of the applied signal and allows a delayed response (an imaginary part that represents the component of the conductivity in quadrature to the driving field). In the limit of low frequencies the dynamic conductivity must converge against the static conductivity. At the above described high-frequency limit the question arises how to separate the response into dc and ac part. It might well be that such a separation is neither needed nor possible any longer. Also, the effect of dissipative tunnelling through the barrier was recognised in the work of Büttiker and Landauer [16]. While this would lead to longer traversal times, it does not change the above derivation of the frequency limit.

> Regarding the influence of dissipation: the processes of overcoming a barrier by thermal emission, thermionic emission or even through tunnelling are usually dissipative, e. g. they involve absorption or emission of a phonon or photon. Even for tunnelling processes, because initial and final states may not be of an identical type and, hence, require the absorption or emission of a phonon or photon to conserve momentum or energy [37]. The statement of Jonscher that the frequency range of dielectric relaxation is in the 'subquantum limit' is of course not intended to restrict in this context.

This section does only assess the applicability of dc models to correctly account for their contribution to the free current density J_{free} in situations with ac signals. It does not asses whether they correctly contribute to the polarisation. Staying within the example of transport through randomly arranged localised states: The random arrangement of these traps leads to the formation of percolation paths through the material. With increasing frequency some jumps in these paths might become almost impossible to overcome. The charges trapped in a region of more easy jumps will then align their spatial distribution in the available traps with the applied field while other traps remain unfilled and, hence, represent a certain net charge. The movement of the remaining empty traps with the applied field can be interpreted as the alignment of bound charges with the applied field. Furthermore, this process is, in almost all cases, lossy. With increasing frequency the regions of possible jumps become smaller and smaller, until reaching the limit of this polarisation process: the pair approximation. In this high-frequency limit a single mobile charge is aligning between only two traps. After this most elementary form of dipoles by traps cannot follow the applied field any longer, the contribution by hopping ceases.

In the presented assessment of the frequency limit of the actual dc conduction model, this conversion from free-current contribution to a dielectric contribution was ignored entirely. In fact, a part (probably even the major part) of the measured constant phase element is very likely due to this effect (compare the discussion about the value of the static permittivity in section 5.6.3). A static conduction model does not include this potentially important feature. In the reviews of Long [104] and Elliott [40] various models to describe the ac contribution of randomly arranged traps are discussed. A microscopic unified theory that can explain both, conductive and dielectric processes jointly, is however still missing and deemed one of the major challenges in solid state physics (see section 6.2.4).

5.5 The underappreciated method: Enhancing current-voltage analysis using voltage-dependent immittance spectroscopy

5.5.1 Goals of conventional current-voltage analysis

Current-voltage characterisation is very common method of analysis which is applies to many very different material systems. A very prominent application is the *identification of charge-transport processes* (i. e. understanding the underlying physics) and the subsequent *determination of its relevant parameters*, e. g. Schottky-barrier height, concentration and energetic distance of donor or acceptor levels from the mobility edge, other activation energies with the help of temperature dependence (confer [176, pp. 84-96, 254-270, 279-286, 402-405]). Of course many parameters, including the given examples, may potentially be determined independently using distinct, sometimes better suited, methods of measurement. Still, current-voltage analysis is a very common and accepted method which is very often used to extract parameters of the charge-transport process, especially in combination with temperature dependence.

5.5.2 Challenges in conventional current-voltage analysis

Only very rarely all pieces of interest can be studied separately. One notable, quite common, challenge is the agglomeration or depletion of charges around the interfaces, leading to unavoidable as well as significant contributions in the current-voltage relation. There is no shortage of awareness of the presence of these barriers, but the magnitude of their contributions seems sometimes underestimated.

5.5.3 Immittance spectroscopy as logical consequence? Similarities between the different measurements.

In this section, it will be shown that voltage-(and temperature-) dependent immittance spectroscopy can improve the processes of identifying the charge-transport process as well as the subsequent parameter extraction. Voltage-dependent immittance spectroscopy contains the capacitive response of the system *further* to the full (see details in 5.5.7) information of the corresponding current-voltage analysis while it adds, except for the different but very similar measurement setup, no additional requirements with respect to the sample. The basic idea is that the capacitive information can be used to distinguish and separately extract different serial impedances. In consequence, the current-voltage curve (plus any other external parameter dependence) can be separately extracted for each serial piece. The knowledge of specific models for the different resistances or capacitances is not mandatory, but can improve the differentiation.

5.5.4 Solution by immittance spectroscopy

With the complementary frequency information, this new approach allows distinguishing different contributions to the measured current-voltage characteristic. A typical serial distortion is caused by additional resistances through space charges at the interfaces.

A very common problem, which is already manageable without additional frequency-dependent information, is to reduce the influence of contacts. This can, in usual current-voltage analysis, already be done in two ways:

First, by utilising selected materials at the contacts, often in combination with specific pretreatments of the surfaces prior to metallisation and possibly complicated subsequent annealing programs (e. g. confer [6] for an overview of Ohmic contacts for III-V compound semiconductors). While these processes are known for common materials and anyway necessary to develop devices, in science one is often confronted with materials for which such processes are not yet known. Developing low-Ohmic contacts for such latter cases may be a tedious and lengthy process.

Secondly, which is normal procedure, by performing a measurement using the four-point probe method [162, pp. 2-21]. In this way the contribution of the contacts can (in many cases) be removed, since the measurement of the voltage-drop is separated from the current measurement. With the goal on gaining knowledge about a material rather than developing a device, the four-terminal sensing can in most cases render the step of finding low-Ohmic contacts unnecessary.

Our approach offers a third method of separation by utilising the distinct capacitive bypasses of the corresponding pieces. This can be useful in the (admittedly) rare cases where a four-point probe method is not applicable and, more importantly as explained below, when the relevant piece of interest is itself a (hetero)structure consisting of several homogeneous pieces.

As distinguishes from the four-point probe method, the presented approach is not limited to eliminate the serial resistance contribution of contacts, but can be used to distinguish various serial pieces. Hence, the benefits of this approach emerge primarily for more complicated sample structures with several serial pieces. Unlike for the four-point probe method which eliminates the (parasitic) distribution, the presented approach allows separate extraction of all individual distributions. For example, if the investigated system is a more complicated structure of several layers. It might be desired to characterise the bulk contributions of each layer and its interfaces separately. Instead of synthesising different samples to study each interface and each bulk material separately, the pile of all layers can be measured together and different contributions extracted.

5.5.5 Requirements for and limits of the distinction of different pieces using immittance spectroscopy

A necessary prerequisite remaining is that at least at some point in parameter space the piece(s) of interest must have a significant contribution. The presented approach requires a measurable contribution of the piece(s) of interest in the total impedance of the system. With decreasing impedance ratio, of the piece(s) of the sample that should be extracted

normalised on the total impedance of the system, the dynamic of the extracted data for the piece(s) of interest decreases. In addition to the increasing dynamic requirements, natural limits in the maximal applicable (total) bias voltage, usually because of some threshold at which the sample (or some piece of it) gets irreversibly damaged, might significantly reduce the possible voltage range for the piece(s) of interest, for a decreasing impedance ratio. Hence, for the explained method of extraction to work, the impedance of interest should not have little contribution as compared to other serial pieces of the system. Otherwise, the extraction of the current-voltage characteristic of the piece(s) of interest becomes increasingly difficult.

For example, if the piece of interest is the bulk of material X and the metal contacts at both sides form a depletion layer in X that is very high-Ohmic in comparison to the resistance of the bulk of X, this approach might not help to avoid developing a low-Ohmic contact on X. For positive and negative voltages, the depletion-layer width would be increased on one side and take the major part of the voltage drop. Further to whether the bulk resistance can be extracted at all, which depends on the dynamic of the measurement setup, the voltage range of the current-voltage curve would be limited to the maximal and minimal voltage drop of the corresponding part. Hence, for the given example, it might still be necessary to find a way of creating a low-Ohmic contact to the material X.

In summery, the piece(s) to be extracted needs to be a significant or, better, dominant contributor to the total impedance. In any other case, the parasitic contributions have to be reduced, e. g. , continuing in the context of the example given in the introduction of this subsection, better contacts or samples for the separate parts alone are imperative.

Not always parasitic effects are, as contact resistances, in series to the piece(s) of interest. Other, typically parallel examples are: conductive bypasses through grain boundaries, the surface or randomly arranged 'percolation paths' of higher conductivity. Grain boundaries can of course also present barriers for charge carriers with very low conductivity. If these alternate paths are arranged in parallel, only the dependence on external parameters can decouple the different contributions. Just as in the case of a pure current-voltage measurement. Hence, in this situation, the additional capacitive information can only help by ensuring that there are no serial contributions, but does not enhance differentiating the distinct parallel parts. Furthermore, also potential capacitances arranged in parallel can only be distinguished by additional parameter dependence.

5.5.6 The concept of distinguishing serial pieces explained

The concept of identifying serial pieces of a system using impedance spectroscopy is not new. The semicircle representation, introduced by K. Cole[8] for permittivities and Nyquist [139] for impedances, in the impedance plane allows direct identification different serial pieces and their key parameters, since each (generalised) Voigt-circuit element is represented by a separate semicircle in the complex impedance plane (e. g. confer [7, pp. 14-20]).

[8] This representation was originally already introduced by K. Cole [24] alone. It is however usually referred to as Cole-Cole plot, since the two brothers worked together from 1931 and, since then, published together several well-known publication using these plots [26].

The extraction of individual current-voltage curves for each serial piece, proposed in this work, is based on the above-mentioned, already known and often used method of separating serial pieces due to their distinct capacitance-resistance characteristic in impedance plane plots. To arrive at current-voltage curves, the bias voltage applied to the total system has to be varied. The voltage drops over the individual serial pieces determine the voltage ranges of the corresponding current-voltage curve. This leads, as already mentioned above, to a restriction of the voltage range to the voltage drops at the respective piece. The distinct serial pieces are described by the generalised Voigt-type circuits, introduced and explained in detail in section 2.2, see also Figure 2.6. Preferably, external-parameter-dependent models, representing the underlying physics, should be used for all components. Without physical models, the association of the different serial contributions to actual pieces of the system and the tracking of its changes over the range of different conditions may be more difficult. As long as the modelling scheme introduced in the theory section is followed, mainly, because the association of the different semi-circles, while they change their properties under the varied external conditions, might be ambiguous and the consistency check of capacitive and resistive part is not possible. Introduction of physical models with their corresponding, typically quite unique, dependence on external parameters, as described in theory section, automatically associates different contributions with underlying physical processes. This typically allows deducing the origin of the contribution.

5.5.7 Possible restrictions using immittance measurements

It was already mentioned at some passages in this work, that the full current-voltage characteristic of the sample is included in the voltage-dependent immittance spectrum. In this subsection, the limits of validity of this statement are defined. The restricting property in this context is the finite accuracy of any measurement.

A source measurement units which is specifically built to perform current-voltage characterisations may in comparison to, for example, an auto-balancing bridge, which measures immittances, be capable to measure smaller currents or may have a higher range in general.

Furthermore, an immittance measurement on principle always needs a signal that varies (most often periodically) in time. Such a signal might lead to an increased deviation from the 'true' static resistance of the investigated system. However, at least at sufficiently high temperatures the signal variation is usually restricted to amplitudes smaller than the thermal voltage $\frac{k_b T}{e}$, so that the influence may be neglected. Additionally, it is good practice to characterise the measured immittance dependent on the oscillating amplitude and choose one in the region of saturation at the low amplitude side. If possible this test should be performed in the region most strongly dependent on voltage. Furthermore, a higher dependence on the oscillating signal might be expected around (absolutely) small bias voltages, since this leads to a large ratio of signal amplitude per offset voltage.

For very high resistances (i. e. low currents) the immittance might already at very low frequencies contain a significant imaginary contribution. Dependent on the remaining

dynamic of the measurement for the real part and the accuracy of the phase at low frequencies (as can be seen in the Figures 4.1 the accuracy of the phase is decreasing with lower frequencies) the measured static current may have a higher uncertainty as compared to a measurement with a source measurement unit.

In summary, the full current-voltage characteristic is contained in voltage-dependent immittance spectra only in the limit of infinitesimally small measurement error and signal amplitude. For any real device it has to be decided whether the dynamics, specific ranges or accuracies are sufficient for the experiment (as it would be necessary for any source measurement unit, as well).

5.5.8 Additional benefits

It is worth mentioning that the capacitances contain the additional information about either the permittivity or the thickness of the corresponding piece (assuming the area is known). If models are used, this allows correlations between resistive and capacitive parts as discussed in section 2.4. In this work, the extracted permittivity could be utilised successfully for the calculation of the internal electric field. Furthermore, the resistive and capacitive models of the depletion layer use, with one justified exception (see section 2.4), the same parameters. Since the measured data can be well approximated by the combination of these models, this means that they are both compatible with each other in that respect and, furthermore, that it is unlikely that the process has mistakenly been selected.

It is also conceivable that for different thin-film thicknesses and identical contact areas (assuming no significant deviation of the lateral spatial extent of the field), the extracted capacitance values could be used as measure for the film thickness, missing only a constant factor to the thickness. The resistance for the corresponding piece could be normalised by the capacitance divided by the permittivity of free space, hence, eliminating any geometrical contribution.

There is still more information that can be extracted from the capacitive part, even without using specific models:

Bulk capacitances should be almost independent of the applied voltage as compared to the capacitances at the interfaces that are results of band bending and, hence, usually more strongly dependent on the applied voltage. Consequently, the voltage dependence of the extracted capacitances can be utilised to distinguish between interface and bulk processes, also for the parallel resistance. Offering a straight-forward solution for the, since then almost forgotten, struggle about whether a process is electrode or bulk limited, is especially relevant when differentiating between the Frenkel-Poole or Schottky emission process [85, 80, 170, 129].

Interfaces do not necessarily have to be at heterojunctions, i. e. at the borders between different materials. Crystalline materials can consist of grains. Consequently, the conduction can either be preferably through the grain boundaries or hindered, e. g. by space-charge layers, at the grain interfaces. If a certain element of disorder is present, statistically, more conductive pathways may form, leading to a conductive bypass of the *actual* media. Depending on the geometry of the sample and the investigated material,

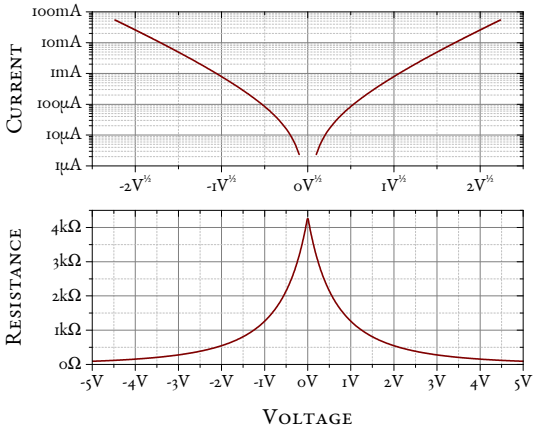

(a) Extracted thin-film current and resistance; square-root of voltage on abscissa in upper plot.

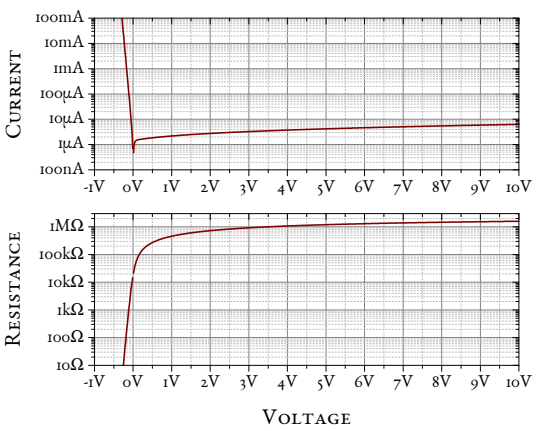

(b) Extracted interface current and resistance

Figure 5.3: Example of current- and resistance-voltage curves extracted form experimental voltage-dependent immittance data (here from sample `1346aCrAu1` interpreted with fit variant B and model 3) using global fits with process-specific external-parameter-dependent physical models. In this particular case, the global fit extracts the relevant parameters of the models directly. As a result, the data for the plots is calculated by inserting the extracted fit parameters into the model functions. Alternatively, different serial resistance contributions can (due to distinct combinations of capacitive bypass and resistance, i. e. unique cut-off frequencies) be extracted with conventional EECs. Since latter are ambiguous, correct arrangement is rather hard to verify (see 5.1.1). However, usual process-specific models may not explain all observed features. In such a case, the extracted parameters may, depending on the extend of the deviation, not represent 'actual' values. Then and if it can somehow be verified that the conventional EEC is arranged correctly, a conventional EEC may extract less distorted resistance-voltage curves (i. e. curves independent on process-specific model assumptions).

the surface can be a conductive bypass, as well. Immittance spectroscopy cannot (or at least not straightforwardly) isolate the contribution of these parasitic effects. However, the frequency dependence and the magnitude of the permittivity can at least indicate the presence of the above mentioned structures (confer [107, 108]). In combination with temperature-dependence, the different activation energies might be decouples and possibly, if the distribution is not too large, trapping and detrapping rates might become apparent, which may be correlated with the activation energies.

5.5.9 Extraction of the current-voltage curves of individual pieces of the ta-C/p-Si system

In this work, global fits over all conditions with models were used to directly extract the relevant parameters. This has the advantage that for this specific model of the whole system good guesses for the fitted parameters may be extracted. Furthermore, the different processes are now identified. It is still possible that limits in the model could be partially

absorbed by distortion of other fit parameters (though as explained before to a much lesser extent than for other models, see section 5.1). Especially, because selected models do not describe all observed features. A model that does not restrict the voltage dependence of the resistances while, further, utilising the obtained arrangement of components may lead to a more correct assignment of serial resistance contributions to the separate pieces, since it is not forced to follow some specific voltage dependence while the determined capacitive bypasses separate the different contributions.

For this case, where the fit parameters of all process-specific physical models dependent on external parameters were directly obtained, the separate current-voltage relations are simply plots of the corresponding models with the respective parameters. The extracted current-voltage curves of the thin film and the depletion layer are given in Figure 5.3.

5.5.10 Avoidable mistakes

It seems that a usual approach to identify the transport process in a material is current-voltage-temperature characterisation using static voltages. An additional analysis with frequency-dependent response seems not as common, except for the characterisation of depletion layers or doping levels [138]. One of the reasons might be that the permittivity is not (assumed to be) relevant. Even if that would be the case, while working with metal/ta-C/Si heterostructures the author found that ac analysis is useful, independently of whether the frequency dependence or permittivity of the material is of interest or not. Measuring solely the static resistance, one can often not distinguish the serial pieces of the system under investigation. While focusing on the piece of interest in the sample, the resistance of contacts or other unexpected effects of interfaces might be underestimated. As a result, the model for the expected process for the single material is fitted to the measured data for the complete system. This leads to distortion of the fitted parameters.

One example is the analysis of metal/ta-C/Si/metal and metal/BN/ZnO/metal heterostructures that has been revisited by Brötzmann and co-workers [14, 15]. Before the work of Brötzmann *et al.* ., researchers actually interested in fitting the rectifying behaviour at the semiconductor interfaces, were frequently not taking into account the serial resistances due to contacts and the (often) high-Ohmic semiconductors directly. Instead, the ideality factor in the Schottky-diode model was exploited, to absorb the missing serial pieces, using much larger values than the highest theoretically explainable factor of two. By increasing the value of the ideality factor, the voltage drop over the diode could be decreased. This necessity is an indication for serially arranged resistances, since the actual voltage drop seems to be smaller than the complete applied voltage. Although the arrangement of components was still not entirely correct, Brötzmann *et al.* could use ideal diodes (that is without using unrealistically large ideality factors) by adding a Frenkel-Poole resistance in series to the diode, that accounts for the current-voltage dependence of the large-band-gap semiconductors, and another Ohmic resistance in series, that would account for the contact resistances (although not including their voltage dependence). If the measurement had been combined with or replaced by immittance analysis the above mentioned frequent violations of the ideality factors (identified by Brötzmann *et al.*) could have been avoided, in the first place. As explained above, the

different serial pieces of the system have unique capacitances: The capacitance of the contacts and the interface between the semiconductors are typically much larger than the bulk capacitances and, furthermore, voltage-dependent. The voltage-dependence on the other hand should be different due to the different contact types of metal/semiconductor and semiconductor/semiconductor interface. Additionally to being independent of voltage and smaller, the capacitances of the two bulk materials are very different since the substrate is much thicker than the thin film of the large-band-gap semiconductor. So even without directly including models and performing the novel approach of analysis presented in this thesis, the ac characterisation would already have been beneficial. It would have resulted in at least three different Voigt-circuit elements (or three different semicircles in a Cole-Cole plot) that would have indicated at least three different resistors in series and it would have been clear, that fitting the total resistance with one model (in this case a non-ideal diode with arbitrary ideality factor to compensate for missing serial pieces) could not work. For minimal overhead, the additional immittance spectrum could have been even been performed for a single set of external parameters, still immediately giving the number of distinct serial pieces that have to be taken into account. Recognising the usefulness of immittance spectroscopy in its simplest form complementary to static current-voltage analysis, immittance spectroscopy seems to be an under-appreciated method. On the other hand, the presented, more complex, analysis of immittance spectra could replace the static current voltage characterisation altogether.

5.6 The Frenkel-Poole model

The Frenkel-Poole model designates a class of semi-classical explanations for the field dependence of bulk conductivity in (disordered) insulators, or semiconductors, all based on the field-assisted thermal ionisation of charges from electrically active defects into conductive bands. Mainly the exclusive assumption of thermal activation over the barrier delimits it from other bulk transport processes connected to localised states, e. g. tunnelling or phonon-assisted tunnelling. The initial derivation of the Frenkel-Poole model, on which all subsequent extensions are based on, was introduced by Frenkel in 1938 [46].[9] In this publication, Frenkel mentioned the empirical relation of $\sigma = \sigma_0 \exp(\alpha E)$ for the dependence of the conductivity σ on the electric field E, determined by Poole. In his publication from 1916 [149], Poole found $I = \mathscr{A} \cdot V \exp(\mathscr{B} \cdot V)$ as relation between current I and voltage V of a mica film.[10]

Although all subsequent theoretical derivations, including the one by Frenkel [46], predict a somewhat different relation between current and voltage, Poole already introduced important interpretations explaining why an exponential behaviour was observed in the experiment: He suggested that the transport in the material is limited by the number of charge carriers that could contribute to the conduction process. Furthermore, the exponential behaviour was associated with the Maxwell distribution of carrier velocities. Narrowed to only the few electrons (the most energetic in the distribution) in an insulator that have enough energy to escape their bond to a specific atom. Although his argumentation is from our 100 year later perspective not in all details on the current state of research, the basic idea, that the exponential formulation is associated with the probability of charge carriers to escape by thermal activation and that the limited number of these carriers which can contribute leads to the observed voltage-dependent bulk conductivity in corresponding materials, is still the interpretation of the more advanced models derived from the Frenkel-Poole model today.

Unlike the work of Poole which was focused more on the experimental part, Frenkel [46] concentrated on deriving a semi-classical, microscopic model to explain the field dependence of the conductivity. Again, the conductivity was assumed to be limited by the number of carriers in the conductive band (e. g. conduction band or delocalised states beyond the mobility edge). Frenkel further assumed, that the charge carriers are thermally excited into the conductive band from states that are neutral when occupied. The potential of the trap was assumed Coulombic and lowered by the superimposed applied field. A critical discussion of the appropriateness of the assumptions, their consequences, improvements of the model introduced over time and its remaining limits is given in the following parts of the section.

Another very important remark in the publication of Poole [149], especially in the

[9] The theory was published in detail in Tech. Phys. U. S. S. R **5** (1938) p. 685 which is not as easy to get as the usually cited letter to the editor in Phys. Rev. The latter contains a short summery of the derivation, so that understanding the origins and assumptions behind the model are comprehensible.

[10] In the expressions $\mathscr{A}$, $\mathscr{B}$, σ_0 and α are constants and, from comparison, $\mathscr{A} \equiv \sigma_0 \cdot \frac{A}{d}$ and $\mathscr{B} \equiv \frac{\alpha}{\varepsilon_r \cdot d}$, with area A, thickness d and relative permittivity ε_r (assuming a simple parallel-plate symmetry with $A \gg d^2$).

context of one of the findings in this work, is a footnote: Since the goal of his fundamental work was finding a qualitative rather than a quantitative relation between current and voltage he explicitly neglects the 'internal field due to the polarisation [...] as [...] it will not affect the form of the result'. Interestingly, except of two works [151, 32] that recognised what they call 'internal field' by including contributions of neighbouring defects in the (three-dimensional) local environment directly as additional linear fields with arbitrary angle to the externally applied field, the internal field was not even mentioned in subsequent works. None of the publications after Poole, including [151, 32], seemed to have used the permittivity of the polarisable media to convert the externally applied field into the internal field (in the proper meaning of the word in the context of electrodynamics, i. e. the mean field inside the polarisable media). On the contrary, many authors found that the experimentally obtained barrier-lowering coefficient $\beta = \sqrt{\frac{q}{\pi\varepsilon_0\varepsilon_\mathrm{r}^{(\mathrm{dyn})}}}$ is smaller than the theoretically calculated one.

Neglecting the *reduction* of the field $E_\mathrm{int} = \frac{E_\mathrm{ext}}{\varepsilon_\mathrm{r}^{(\mathrm{stat})}}$ that a charge perceives in a polarisable material (i. e. $\varepsilon_\mathrm{r}^{(\mathrm{stat})} > 1$) would result in an apparently lower barrier-lowering coefficient β, sometimes interpreted in an unexpectedly large relative permittivity $\varepsilon_\mathrm{r}^{(\mathrm{dyn})}$.[11] In this work, the influence of the polarisation of the surrounding material on the barrier-lowering coefficient shall be recognised (consistently with the Frenkel-Poole model still within the mean-field approximation and ignoring the influence of the exiting charge on the surrounding polarisable media). Since impedance spectroscopy allows combined measurement of the static current-voltage relation and the permittivity, it offers a unique opportunity to validate the assumption (and evaluate different possible ways to extract the static permittivity). The assessment of the different models using experimental data can be found in section 4.2. Possible explanations why the Frenkel-Poole model works despite its fundamental deficiencies (deficiencies are listed in section 5.6.2) are given in 5.6.4. Before this, the development of the Frenkel-Poole model over time is introduced in this subsection. Different enhancements are shown, several subsequent extensions were combined to the three-dimensional approach on which this work is based on. Other enhancements were not directly applied but are still relevant to understand how different omitted effects, e. g. of the fields of neighbouring defects, affect the current-voltage relation. Some of these lead to interesting arguments that may also be applied in the context of this approach.

5.6.1 Advancements of the Frenkel-Poole model

The original model published by Frenkel 1938 [46] was one dimensional. In 1967 Jonscher [80] extended the model to three dimensions, by introducing an appropriate lowering of the Coulombic potential in other directions of the forward hemisphere (around the

[11] The term in the exponent for the field-dependent barrier lowering including the effect of polarisation in the material is $\beta\sqrt{E_\mathrm{int}} = \sqrt{\frac{q}{\pi\varepsilon_0\varepsilon_\mathrm{r}^{(\mathrm{dyn})}} \cdot \frac{E_\mathrm{ext}}{\varepsilon_\mathrm{r}^{(\mathrm{stat})}}}$. Hence, ignoring the relative static permittivity $\varepsilon_\mathrm{r}^{(\mathrm{stat})}$ could be misinterpreted as too large dynamic permittivity $\varepsilon_\mathrm{r}^{(\mathrm{dyn})}$, which is *the* usual deviation using the Frenkel-Poole model [163].

applied field) and integrating over the escape probabilities of the complete forward hemisphere. This was only one of several aspects of the publication of Jonscher. Maybe that is why one sometimes finds authors giving Hartke, who performed exclusively that exactly same derivation in 1968 [60], as source of the three-dimensional extension of the Frenkel-Poole model. Also all subsequent models by Hill [64], Ieda *et al.* [72], Connell *et al.* [28], Martin at al. [125], Potemski and Wilamowski [151] and Dallacasa and Paracchini [32] are three dimensional.

Besides the obviously more realistic description of the situation in the material, this advancement also addressed one of two major deviations of the original Frenkel-Poole model from the experimentally observed behaviour: *the deviation at small fields*. Until the works of Hill and Ieda *et al.* the conduction process at low fields had always been described apart from the mechanism at high fields [64, 72]. Experimental data, on the other hand, show almost identical activation energies for high and low fields [72], indicating that the low-field process should be connected with the thermally activated escape from the same defects. Unlike expected from the original model, the conductivity at low fields converges against a constant, higher value as predicted [151]. Every new variant of the Frenkel-Poole model shown here has lead to an improvement of the behaviour for low applied fields as compared to the initial theory (not necessarily each other), i. e. brings the theory closer to the experimentally observed behaviour around zero applied field[32].

After the introduction of three dimensionality, the next major extension concerned the charge exiting in directions of the backward hemisphere. Originally it has been assumed that the charge cannot escape in backward direction [46]. According to Hill [64], the three dimensional extensions by Jonscher [80] and Hartke [60] implicitly assumed that the emission probability in reverse direction remains constant with a probability $\exp(-\frac{E_\mathrm{i}}{k_\mathrm{B}T})$, where E_i is the ionisation energy of the trap. Re-examining both works, it is found that Hills assessment is only correct for the work of Hartke. Jonscher, like Frenkel, ignores emissions in backward direction (though, since the model is three-dimensional, this time the complete backward hemisphere is ignored). Hill [64] assumed that the barrier in the reverse direction increased in the same amount that it is lowered at the forward site. There is, however, a distinct difference between the forward and the backward site. At the forward site, there is a maximal barrier height to overcome, while in the reverse direction the barrier is continuously increasing with distance. As noted by Connell *et al.* [28] neither assuming no change in barrier height in the reverse hemisphere nor considering the same amount of increase as decrease in the corresponding forward direction is appropriate. They propose to calculate the escape probability in reverse direction by integrating over the continuously decreasing probabilities of escape in reverse direction. Connell *et al.* could show, that approximating the backward-emission probability with its low-field approximation will always give an error below 6%. Ieda *et al.* [72] proposed a distance from the ionised centre $r_\delta = \frac{e^2}{4\pi\varepsilon_0\varepsilon_\mathrm{r}\delta}$ at which a particle should be considered free. The energy δ should be sufficiently small, that a phonon would likely raise an electron only that small energy below the conductive band in the delocalised state, hence, in the order of the thermal energy $k_\mathrm{B}T$. The barrier height (i. e. the energetic distance to the ground state) at the projection of the distances $\pm r_\delta$ in the

corresponding hemispheres is then used to calculate the emission probabilities. Pai [144] not only criticises the arbitrary choice of the cut-off energy δ, but also the possibility to manipulate Frenkel-Poole barrier-lowering coefficient freely with this constant, since it introduces a free offset to the exponent. Not exploiting this energy cut-off, the solution gives approximately the same characteristic as the extension of the Frenkel-Poole model derived by Connell *et al.* [144].

The alternative construction by Potemski and Wilamowski [151] in 1985 takes a completely different path than the extensions of the Frenkel-Poole model above. They extended the original model by Frenkel to include the influence of local fields caused by statistically distributed charged centres in the material. Using vector sums of the different fields (hence, allowing for arbitrary angles) acting on the potential around the trap, this is also a three-dimensional extension. Like the other extensions to three dimensions, it leads to Ohmic behaviour and increased zero-field conductivity as compared to the expected value from the original model if the applied field is much smaller than the local field. For fields significantly larger than the internal field, this extended model shows the conventional Frenkel-Poole behaviour. A remaining challenge is the unknown local-field distribution. In the absence of a better alternative, they assume the local field to be equally probable in every direction and a direction-independent mean value of the field strength. Using these assumptions, the mean local field may be extracted. For their measurement of CdF_2:Y this leads to local field strengths around $10^3\,V\,cm^{-1}$. The same idea of including the local fields by other randomly distributed charge centres was implemented by Dallacasa and Paracchini in 1987 [32]. Using an approximated result in the end and a slightly different derivation, this work arrives at local field strengths around $10^4\,V\,cm^{-1}$ for CdF_2:Y crystals. The comparability of the samples of both publication cannot be assessed from the sparse information about the samples in the work of Potemski and Wilamowski [151]. Although both theories include important properties, that can be expected to play a significant role in the local potential environment around the trap while simultaneously making it more realistic, the theories (as well as the others) are unable to include the strong directional dependence of the bonds that are present in many investigated materials. Both works include, for a specific trap, only a local field in one direction superimposed to the applied field and, *still*, the Coulombic potential. Up to now, all models are therefore restricted to describe the situation in materials with either weakly oriented bonds or materials where the central part of the potential of strongly oriented bonds can be reduced to its role as origin of the binding energy. The two latter models may then be suited especially in those situations mentioned above, where a high concentration of defects renders the recognition of contributions by neighbouring defects important. Tetrahedral amorphous carbon, an example which shows Frenkel-Poole behaviour, has covalent bonds which are strongly directional, whilst due to its amorphous characteristic many possible defect types with very different and complicated local potential environments around the trap are thinkable. Hence, extraction of more detailed information about the local structure around the defects might, due to the many possible very different individual local situations, not be possible. An exception would be, if the distance of the bound charge carrier is rather large from the centre, so that the complicated local fields can be approximated by a (screened) Coulombic field. A very

large volume of localisation of the charge bound to the trap would render comparable permittivities possible in the first place, as well. For an amorphous system this could also validate the assumption of isotropy. In this context, it may be important to note that Frenkel-Poole conduction is observed for various, very different, materials (e. g. Si_2N_4 [175], Ta_2O_5 [129, 170, 60], SiO [170, 80, 60], Al_2O_3 [60], layered crystalline solids [GaTe, CaSe] [82], ta-C [68] and many others) The asymmetric central potential of a covalent bond, and consequently also of highly localised structural defects that are expected to be a significant source of deep-level trap states in otherwise intrinsic materials, is very sensitive even to slight changes of the involved species [41, pp. 281-334]. From the fact that the Frenkel-Poole effect is observed almost universally for a wide variety of materials it may, hence, be deduced that the very different central potential parts of the traps do not dominate the response of this high-temperature process. A more thorough discussion of the local environment is given in section 5.6.2, which critically reviews the assumptions of the different models, and section 5.6.4, where the actual local potential is described and speculated why the Frenkel-Poole models leads to a good description despite its deficits.

In 1967, Simmons [170] is the first to analyse the energetic distribution and the occupation statistics of traps as well as donor states in the band gap in the context of Frenkel-Poole conduction. One of his assumptions is that the traps which experience field-assisted barrier-lowering are not necessarily the donor states. Consequently, different concentrations of trap- versus donor-states and their energetic arrangement, to themselves as well as with respect to the Fermi level, are discussed. An important finding is that, dependent on energetic arrangement and concentration of the respective states, the barrier lowering and the initial barrier height are, within the scope of the usual Frenkel-Poole effect, divided by a factor of one or two. This is essential, because the Schottky-emission model (an electrode limited process) has the identical current-voltage relation as the Frenkel-Poole model (a bulk-limited phenomenon) except for a barrier-lowering coefficient of half the size of the initial Frenkel-Poole model. Hence, Simmons could show, that the value of the barrier-lowering coefficient cannot be used to interpret whether a bulk- or electrode-limited process is observed. Furthermore, this is a possible explanation for the typical observation of shallower slopes.

To decide whether the measured conductivity is electrode or bulk limited, Mead [129] has suggested a method which does not require the knowledge of the film thickness. However, due to the high density of states in the band gap, amorphous materials, for which Frenkel-Poole conductivity is often observed, rarely are electrode limited [83]. As confirmed also in this work, the difference between a chromium/gold top contact and an aluminium/titanium top contact on tetrahedral amorphous carbon were negligible.

The work by Connell *et al.* [28] picks up the occupation statistics of the traps and their energetic distribution from Simmons [170] while discussing it from the standpoint of compensation between acceptor and donor levels. Furthermore, they clear up with the common misconception that finding a single activation energy indicates one energetic distance of the traps to the conductive band. A single activation energy can also be found for a continuous distribution of donor levels, as it would be expected in an amorphous semiconductor. The degree of compensation, in such a more complicated system, then leads to a continuous factor $m \in [1,2]$ by which initial barrier and barrier-lowering

coefficient are divided.

As distinguished from other extensions of the Frenkel-Poole model, Connell *et al.* [28] and Hill [64] are not focusing on the single trap alone. The fate of the charge carrier after leaving the trap is analysed in more detail. In the usual Frenkel-Poole model, the distance of the local maximum of the potential that has to be overcome by the charge to exit the trap increases with decreasing field. Assuming more than few traps in the material, there is a minimal field at which the barrier for the charge is already in the next trap. At this point the original Frenkel-Poole model breaks. The model derived by Connell *et al.* does in the limit of low fields converge against an Ohmic conductivity which is in agreement with the experimental observations.

Pai [144] criticises for all above mentioned extensions from before 1975 that the details of the escape process itself have not been considered. Using a similarly old theory, as the Frenkel-Poole model, by Onsager [142, 141], which was intended to describe the separation of the individual ions in dilute electrolytic solution and, further, assuming one species as fixed, a similar characteristic as the Frenkel-Poole behaviour can be derived [144].

5.6.2 Description of the local environment and general restrictions of the model

Despite all its extensions, the Frenkel-Poole model maintained some systematic limits. Most advancements of the model tackle the details of the escape or introduce more refined statistics. However, its characteristic form is primarily caused by the local potential landscape and sometimes also by the fate of the charge carrier after exiting the trap. The use of the Coulombic potential would rather be expected for very shallow traps whereas the observation demand deeper traps and their form is expected to deviate significantly from the Coulomb potential [80]. Except for Martin *et al.* [125] who investigated non-Coulombic potentials (Yukawa, polarisation and dipole potential), the other variants of the Frenkel-Poole model assume Coulombic traps. These forms of the potential are the basis for deriving the specific current-voltage behaviour. The problem of expecting Coulombic traps in these materials is probably one of the most criticised assumptions, e. g. already by Jonscher [80]. Considering the usually amorphous or extremely disordered nature of the materials, the assumed highly symmetric and long-ranged trap forms by Martin *et al.* may seem also not as likely. As will be explained in section 5.6.4, traps due to structural defects, which likely are those relevant in undoped tetrahedral amorphous carbon, are deeper, much more localised and have a very different local potential than those shallow traps that can, at least in some materials, be explained by Coulombic potentials.

In almost all advancements, the superimposed electrical field is approximated as the mean-field that uniformly drops over the material, ignoring the lowering of the internal field by the surrounding polarising media. Some authors [151, 32] assume superimposed local fields caused by neighbouring defects which is certainly an important improvement because the fields of neighbouring defects might be quite high as compared to the applied field. As the local structure around a trap is essentially unknown, the addition of the

local environment is connected to an introduction of further fitting parameters which do, however, not enable extraction of the form of the local potential itself, but only a mean field effect. Furthermore, from the works of Potemski and Wilamowski [151] as well as Dallacasa and Paracchini [32], it is found that such superimposed fields of neighbouring defects only influence the low-field properties, by, on the one hand, leading to a approximately Ohmic behaviour for small fields, and, on the other hand, determining the field strength at which the transition between Frenkel-Poole behaviour and Ohmic part begins. The slope at high fields, the second major deviation, is not affected by these corrections.

Another point of critic is that the Frenkel-Poole model is a semi-classical model that uses Boltzmann statistics. Even in the work of Simmons [170], who was the first to introduce an otherwise statistically correct calculation of the probability of occupation that recognised the presence of multiple trap states, and later extension by Connell *et al.* [28] which also allowed for compensation by different types of traps. The Frenkel-Poole model is restricted to thermal activation over the barrier and ignores any quantum-mechanical processes like (phonon-assisted) tunnelling.

Using the Frenkel-Poole model to describe experimental conductivity data, there are usually two major quantitative deviations: the experimental data shows an approximately Ohmic behaviour for low fields and a shallower slope as predicted [48]. For both, many explanations have been suggested. The former could be explained by three dimensional extensions of the geometry with [151, 32] or without [80, 60, 64, 72, 28, 125] taking additional local fields by neighbouring defects into account. For the deviation in the slope, Simmons [170] proposed the already mentioned compensation effect of different states in the band gap while Jonscher [81] introduced an effective temperature and Ieda [72] a truncation parameter. Interestingly, though this is a quantitative problem, it seems that none of the works have correctly calculated the internal field that is superimposed on the potential of the trap. Some of the times, probably because the static permittivity necessary to calculate the internal field was unknown and not determined. Since the static permittivity necessary to calculate the internal field cannot be smaller than the dynamic permittivity, without the need of any further information, at least a square root of the extracted oversized permittivity could have been performed. Unlike most others, Hartman *et al.* [61] determined the low-frequency permittivity but then did not use it to calculate the internal field (commendably they describe how they performed the conversion from external potential difference to internal field). As will be explained in detail in the next part of this section, the static permittivity is a significant factor, that might be seen as neglected divisor, in the barrier-lowering coefficient. It further has the correct magnitude to resolve the usually observed (and last remaining) deviation of the Frenkel-Poole description from experimental data.

As already mentioned, various different materials show a bulk conductivity that has Frenkel-Poole behaviour. A necessary prerequisite is a low mobility of electrons, since heating of the free-carrier system is a competing process that depends on the square of the field E^2 and leads to impact ionisation, while field-enhanced barrier-lowering only shows square-root dependence of the field $\sqrt{E}$ [82]. Hence, a Frenkel-Poole behaviour at

high fields is often observed for amorphous materials, though, there are also crystalline examples [85, 137]. Since disorder typically leads to low mobilities, it is not surprising that many materials displaying Frenkel-Poole conduction are disordered in some way.

5.6.3 The omitted factor: the static permittivity

As mentioned before, Poole [149], in his intention of finding a purely qualitative description for the field-dependent conductivity, consciously omitted calculating the internal field that is caused by the polarisation in the material. In contrast to Poole, the subsequent publications that intended to extend the theoretical model, including the original work of Frenkel, did not use quantities that include geometry, e. g. current I and voltage V, but rather geometry-free values, like conductivity σ, current density J and the electric field E, directly [149, 46, 80, 170, 60, 72, 64, 28, 144, 151, 32]. Whether these theoretical works also compared their results with experimental data or experimentalists used the Frenkel-Poole model, the data was usually plotted over geometry-free quantities as well. Sadly, the calculation to arrive at the geometry-free values was almost never given. However, in most works, the static permittivity of the material investigation was neither determined nor cited. Also, there was no mention of any factoring in of the geometry deviating from a large-area cylinder etc. Hence, it is likely that the simplest assumptions were made. As a result, it may be assumed that the 'field' which is usually one plotting parameter is simply the applied external field

$$E_{\text{ext}} = \frac{V}{d}, \tag{5.2}$$

with voltage V and plate distance d. This interpretation is supported by the fact that the comparably new work of Schroeder from 2015 [163], also explicitly mentions equation (5.2) as the way the superimposed linear field is calculated.

In every Frenkel-Poole model, the potential landscape is described from the perspective of the charge carrier. The Coulomb potential is a result of the attractive interaction with the positively charged trap that the exiting charge carrier senses. The superimposed field acting on the charge carrier and deforming the Coulombic potential (as described in the Frenkel-Poole models) is, however, ***not*** *the externally applied field*. The electric field given in equation (5.2) would act on a particle between the large-area (non-parallel field lines at the borders can be neglected) plane-parallel plates *only in the vacuum*, that is *without the presence of matter*. Inserting a material, especially a dielectric (which most of the materials exhibiting Frenkel-Poole behaviour are) leads to a polarisation of the material and results in a decreased *internal field*

$$E_{\text{int}} = \frac{V}{\varepsilon_{\text{r}}^{(\text{stat})} \cdot d},$$

with the static permittivity $\varepsilon_{\text{r}}^{(\text{stat})}$, since the Frenkel-Poole model assumes equilibrium analysis (the given internal field is the mean field in the material, see section 5.6.3.1 for reasons why no Lorentz field contribution is expected). Poole [149] explicitly neglected the internal field calculation since only a qualitative relation should be derived, however, most of their subsequent works emphasise the *shallower slope as theoretically expected*

[48, 170, 72, 64, 81, 144] as one of the most prominent quantitative deviations of the Frenkel-Poole model from experimental observation. Surprisingly, Hartman *et al.* [61] even measured the static permittivity, but did not use it to calculate the correct internal field (the used formula is written explicitly in this case). The dynamic permittivity is the only 'free' parameter in the slope of the Frenkel-Poole model. If the consistency of the slope is checked using alternate (e. g. optical) measurements, an increased size of the dynamic permittivity is found. The problem of deviations of the slope exists until today and is even given as the motivation for the study of Schroeder in 2015 [163].

The mentioned deviation is usually not in the order of a different magnitude which makes it even more surprising, that the static superimposed field was never (correctly) calculated.[12] The permittivity at optical frequencies is typically lower than the static permittivity. The latter, however, must (due to causality [78, pp. 36-52]) not be smaller than the dynamic permittivity so that $\varepsilon_\mathrm{r}^{(\mathrm{stat})} \geq \varepsilon_\mathrm{r}^{(\mathrm{dyn})}$. Hence, in the limit, the smallest possible static permittivity is equal to the dynamic permittivity. If the static permittivity is unknown, the too large wrongly-assumed dynamic permittivity obtained using the usual external field calculation may be corrected at least by taking its square root.

In contrast to most works applying the Frenkel-Poole model, in this work bias-voltage-dependent immittance spectra were measured. Unlike for static current-voltage analysis, in addition to the (static) current-voltage behaviour itself the capacitance is contained in the measured data. Instead of fitting the capacitance separately from the parameters for the resistance model, it was tried to combine the parameters in both models: analogue to the depletion layer, where parameters like the acceptor concentration are present in both the resistance and capacitance model and, hence, fitted as a single parameter. Three models, two with different origin of the static permittivity and one without any connection between resistive and capacitive part, were compared (see section 4.2).

Indeed, the correlation between the permittivities in the Frenkel-Poole model and the corresponding capacitive bypass could be quantitatively confirmed (see section 4.2.3). It was found that the static permittivity had to be extracted as explained by Young and Frederikse in their 'Compilation of the Static Dielectric Constant of Inorganic Solids' [190]. The straightforward extraction from the constant phase element was not possible, which is not too surprising since, dependent on the cause for the constant phase element, interpretations of its values can be very different (explicitly including situations where distributions of regular-sized resistances and capacitances can lead to apparently large permittivities [65]). The inability to include the constant phase element suggests either that a Maxwell-Wagner effect was neglected in the model or that it may be caused by charging and discharging defects in some part. The latter most likely in the thin film itself, since the effect would in this case correspond to a parallel capacitance and, further, because the region of major importance for the parameters of the thin film is, naturally, greatest when the voltage drop is dominant over itself, i. e. assuming a constant number of defects (a constant capacitance), the moved charges would be maximal when the voltage

[12] This work, within the spirit of the Frenkel-Poole model, explicitly ignores the influence of the exiting electron on the surrounding polarisable material, but only considers the effect of the surrounding media on the interaction of the charge with the trap.

amplitude around the defects is highest. More details about the result can be found in subsection 4.2.3, where the residual distributions of the different models are evaluated. A more detailed analysis, why it is believed that the extraction after Young and Frederikse [190] is more likely as assuming that the permittivity is increasing towards low frequencies due to hopping conduction, is given in 5.3

5.6.3.1 Reasons for the absence of the Lorentz field

In 1916, Lorentz devised a method to calculate the local field experienced by an electron of an atom on a lattice side in an undistorted cubic crystal [105, pp. 137-139,305-308]. One might think that the local field, experienced by an electron in an atom on a lattice side, should be equal to the *mean* internal field $E_{\text{int}} = E_{\text{ext}} + E_{\text{pol}}$ which is a sum of the externally applied field E_{ext} and the field caused by the polarisation in the material $E_{\text{pol}} = -\frac{P}{\epsilon_0}$ (the minus sign causes, in conventional materials, a lower internal field E_{int} in comparison to the externally applied field). However, by removing a sphere of the material around the corresponding electron in a thought experiment and separate analysis of both pieces, the material with a spherical hole and the sphere of the material, Lorentz [105, pp. 137-139,305-308] found that the electron experiences a field additionally to the internal field. This field is called Lorentz field. Due to the high symmetry of the cubic lattice, the near field E_{near}, caused by the neighbouring atoms, is cancelled [105, p. 308]. The Lorentz field $E_{\text{Lorentz}} = \frac{P}{3\epsilon_0}$ is oriented in the direction of the applied field. Finally, the local field experienced by the electron at a point of high symmetry in the cubic solid is:

$$\begin{aligned}\mathbf{E}_{\text{local}} &= \underbrace{\mathbf{E}_{\text{ext}} + \mathbf{E}_{\text{pol}}}_{\mathbf{E}_{\text{int}}} + \mathbf{E}_{\text{Lorentz}} + \underbrace{\mathbf{E}_{\text{near}}}_{=0,\text{ for cubic lattice}} \\ &= \mathbf{E}_{\text{int}} + \mathbf{E}_{\text{Lorentz}} \\ &= \frac{\epsilon_r + 2}{3}\mathbf{E}_{\text{int}}\end{aligned}$$

In this work the Frenkel-Poole conduction was corrected by superimposing the *mean internal field* instead of the external field over the Coulombic trap potential. It is discussed below, why in this specific case of a Coulombic (hence, long-ranged in comparison to an inter-atomic distance) trap in an amorphous material, the local field without the Coulombic part is equal to the mean internal field, i. e. why there is no contribution by the Lorentz field. An explicit mathematical proof for this statement, or why the approach by Lorentz is not suited for any situation involving an impurity, i. e. a non-ideal lattice, is given by Geifman *et al.* [51]. In the following paragraphs, key arguments are presented that lead to an understanding of the reasons why the Lorentz field is negligible in the case of Frenkel-Poole conduction.

A general discrepancy between the Frenkel-Poole conductor considered here, in comparison to the material investigated by Lorentz, is that the near field contributions can no longer be omitted. Lorentz could only neglect them, since each dipole moment is assumed identical for the cubically arranged dipoles and due to the high symmetry of the

crystal [105, p. 308] [51]. The amorphous material is indeed isotropic for large distances from an arbitrary point, but locally very different potential landscapes are expected.

Another point is, that the calculation by Lorentz [105, pp. 137-139,305-308] was not intended to calculate the local field around an impurity or a trap, but in a highly symmetric *point* of an undistorted crystal. This also includes the idea, that the dipoles are small in comparison to their distance. A scenario where the distance between the opposing charges of some dipoles spans multiples of the usual length of the other dipoles (i. e. multiples of the lattice constants), as it is the case in the Coulombic potential of the traps contributing to the Frenkel-Poole conduction (see next subsection), was not intended. It is not only a result of the calculation by Geifman *et al.* [51], but also explicable to assume that a loosely bound and, hence, sufficiently delocalised electron wave function would perceive the mean internal field instead of the local field found at a lattice side. According to Geifman *et al.* , even a state radius in the order of the lattice constant would be sufficiently large to validly neglect the Lorentz field contribution.

Furthermore, as indicated by Ibach and Lüth [71, p. 375], in the limit of high dilution, the local effect of neighbouring dipoles might be omitted. Of course, the amorphous material itself is not at all diluted. However, one might apply a similar trick as Lorentz himself [105, pp. 137-139,305-308] who, in a thought experiment, separated pieces of the material, performed a distinct calculation per piece and, finally, rejoined them exploiting superposition of the fields.[13] Instead of utilising two layers (in Lorentz thought experiment, contributions of free space and the material), here, three layers are assumed: 1. free space, 2. the material without those traps contributing to Frenkel-Poole conduction and 3. a relatively diluted material consisting only of those traps. The latter material is extremely sparse and its contribution to the total polarisation may be assumed small in comparison to layer 2. Furthermore, its traps may be, due to their high distances, regarded as independent. As a consequence, the local field at a dipole of this layer is *its* external field, corresponding to the internal field of the trapless material, i. e. layer 2.

As a result, the local field perceived by an electron contributing to the Frenkel-Poole conduction is the mean internal field, dominated by the properties of the amorphous material excluding the respective traps. This simplified treatment is in accordance, with the results of Geifman *et al.* [51]. It has to be emphasised, that the electrons involved in the Frenkel-Poole conduction should be in excited states, i. e. sufficiently loosely bound, e. g. over several inter-atomic distances. In fact, the calculation by Geifman *et al.* [51] shows that already a state radius in the order of one lattice constant is sufficient to render the Lorentz field negligible. In this case, assuming the electrons to be in excited trap states is a consequence in order to validly assume that the electrons see the mean internal field. This is consistent with the result in the following subsection, where the assumption of a Coulombic potential also forces the criteria that only electrons in excited trap states may contribute to the Frenkel-Poole conduction.

[13] As in the theory of Lorentz, also this discussion assumes linearity.

5.6.4 The surprisingly good description by the Frenkel-Poole model: An endeavour to understand why it can, despite its simple theoretical basis, lead to quantitatively correct results

The novel approach presented in this work allows the joint extraction of conductive and dielectric properties of serial pieces of the sample. It is, hence, predestined to analyse models in which both, conductive and dielectric quantities, are jointly parameters. The Frenkel-Poole model falls into that category, since the dynamic permittivity is supposed to be a factor in the barrier-lowering coefficient (more precisely its square root in the denominator, confer to the beginning of this section). Up to now, there was a well-known (confer [129, 61, 80, 170, 60, 72, 81, 28, 32, 144, 163]) quantitative discrepancy between the theoretical barrier-lowering coefficient and the experimentally observed slopes in $\ln(J)$-$\sqrt{E}$ plots (mentioned in almost all publications that either enhance or discuss the Frenkel-Poole model thoroughly, see introductory remarks in section 4.2). In this work, it was suggested that the deviation of the slopes might not have been due to the value of the barrier-lowering coefficient itself, but because of the conversion of the externally applied voltage into the superimposed internal field (this is the field actually seen by a charge in a polarising media[14]). So far the superimposed linear field has been calculated ignoring the polarising character of the material itself. However, in any other case than free space, the permittivity (in the relevant frequency range) has to be used to calculate the internal field, which is the linear part of the field seen by the charge carrier escaping the trap (see subsection 5.6.3). It could be shown experimentally (see section 4.2) that the correct conversion of the voltage drop into the *internal* applied field (using the static permittivity extracted according to Young and Frederikse [190], see section 5.6.3) lead to the quantitatively correct slope. With this correction the last common deviation of the Frenkel-Poole model has been eliminated.

Probably the most interesting, maybe even surprising, fact about this finding is that the suggested correction of the Frenkel-Poole model resolves the quantitative deviations *within* the concept of this semi-classical model, *without* the demand of more sophisticated physical theory and despite all shortcomings of the local description of the potential (for a list of shortcomings see 5.6.2). In this subsection, it is speculated why the Frenkel-Poole model can lead to a quantitatively correct description of the conductive behaviour of the material despite its 'simple' concept with known shortcomings. Essential points of criticism are the, supposingly, poor description of the local environment of the trap and the restriction to a pure classical process of overcoming the barrier.

5.6.4.1 The local potential landscape

An expected point of critic is the correctness of the local potential landscape assumed by the Frenkel-Poole model. In the first part of this subsection, it is assessed for what kind of materials the Frenkel-Poole model might be relevant at all. Then the focus is on tetrahedral (amorphous) materials and possible traps in these materials. In the following

[14] Neglecting the effect of the exiting charge itself on the surrounding polarisable media.

part remaining eligible critic on the postulated potential landscape is discussed, before a possible explanation why the Coulombic potentials can, despite that critic, possibly still be assumed. Within this explanation, the structure of deep defects and how they might look like is thoroughly discussed (and literature hints for further reading, especially about the calculation, are given). Finally, an overview of important steps in the historic progress on the model for the local environment of the trap in the Frenkel-Poole model is given.

There are basically two classes of defects: shallow defects and deep defects. Shallow defects can (in certain cases) be sufficiently well approximated with the effective-mass theory [191]. Such defects have only energetically shallow levels, i. e. the distances from the states to the conductive band are low [191]. This is accompanied by a wide binding distance, e. g. hundred atomic distances, between the centre of the immobile trap and the mobile charge [191]. Shallow defects can under certain conditions (state close to a non-degenerate, isotropic band, e. g. donors in GaAs) be well described assuming a Coulombic potential and result in a behaviour similar to the binding of an electron in a, correspondingly large, hydrogen atom [191]. The shallow character is, for example, typical for some extrinsic impurities from neighbouring groups (hence, a rather unexpected type of defect in an undoped material) [41, pp. 311-320]. Another interesting point is made theoretically by Yu and Cardona [191] who find that it is possible that the excited states can be described well by a hydrogenic model although the ground state has a different form. This is also experimentally confirmed by the findings of Grimmreiss and Skarstam [55] who found that the excited states of deep centres show energy differences corresponding to a Rydberg series. Such shallow potential landscapes are actually similar to the assumptions of the Frenkel-Poole model. However, would such shallow levels exist in large-enough quantities, charges would easily overcome the barrier thermally, already at temperatures below room temperature, and the field assistance would not be necessary. Hence, systems with shallow traps would likely not show conduction based on the Frenkel-Poole model (which assumes a lack of carriers in the conductive band) at room temperature, but rather behave like doped semiconductors. Also the lack of a well-defined effective mass in non-crystalline solids makes hydrogen-type models useless for such materials [94, p. 98]. Furthermore, in amorphous materials, where the Frenkel-Poole behaviour is often observed also in the intrinsic case [85], another type of defect (subsequently discussed) is much more likely. As a consequence of all reasons above, shallow hydrogenic donors can be excluded to play a role.

The Frenkel-Poole model assumes that the conduction is limited by the number of charge carriers in the conductive band and that those charges are field-assistedly emitted from traps [46]. Hence, the relevant materials cannot be metals. Consequently, those materials exhibiting Frenkel-Poole conduction must have strongly directional and localised bonds [71, pp. 2-3]. Although ionic compounds or materials with distinct ionic character might also observe Frenkel-Poole conduction, other processes might be increasingly relevant in such materials. Consequently, the focus in this work is primarily on covalently bound materials (which might also be compounds that have bonds with negligible ionic character). The tetrahedral amorphous carbon (ta-C) thin film, investigated in this work, is a typical representative of covalently bound materials. It is, furthermore, a predestined material to analyse the Frenkel-Poole effect very purely. Its amorphous character makes

all long-range quantities isotropic resulting in a much simpler description as compared to crystalline materials with specific properties in different orientations. Another consequence is that there are no grains (and respectively no grain boundaries), dislocations or stacking faults. Due to the used method of deposition, the film can be assumed monoisotopic (only ^{12}C) and to contain only very few contaminants from other materials [101, pp. 211-213]. Since the thin film is monoatomic, it can be assumed free of typical ionic (or polaronic) effects. Furthermore, antisite defects, agglomerates of one species or other deviations from stoichiometry can be neglected.

The nature of an amorphous material is that its elements have no long range order [71, p. 21]. Especially carbon shows a high versatility with respect to its configurations: it can form thermally stable bonds with one, two and three pairs of electrons [154]. Additionally, even using MSIBD synthesis, tetrahedral (pointing to the configuration for sp^3 bonds) amorphous carbon still contains a significant content of sp^2 bonds [154]. Even without these specific properties of carbon (which makes its simulation more complicated as compared to amorphous silicon [94, p. 56]), the amorphous structure leads inevitably to geometric distortions (with respect to their respective ideal crystalline structures), like 'vacancies', other configurations or dangling bonds [94, pp. 24-25 and pp. 86-101]. This geometric diversity is assumed to lead to the expected distribution of localised states in the 'forbidden gap' [94, pp. 86-101]. The Frenkel-Poole model requires localised defect states beneath (or above) the conductive band that are neutral when occupied and charged when empty [46]. Furthermore, the long-range attraction between the mobile charge carrier and the trap should be Coulombic. Due to the lack of alternatives (see above) and in agreement with the usual assumptions about sources of traps in covalent amorphous materials [94, pp. 86-101], localised defects, like dangling bonds, are assumed the primary source for those states relevant for the Frenkel-Poole model in ta-C. Although the properties of the defect can not be straightforwardly determined, these kinds of defects are usually much deeper in the forbidden gap and highly localised, e. g. in the order of one atom distance [191, 41]. Consequently, their states, especially the state(s) of the level in the 'forbidden gap', cannot be calculated using the effective mass theory. How dangling bonds may lead to a state in the forbidden gap and which physical processes are relevant to get the actual energetic depth from the conductive band is (at least basically) explained, on the example of a vacancy in crystalline silicon, in Figure 5.4. Of course, the explanation in Figure 5.4 is purely qualitative. Even for the system in the example, crystalline silicon, more elaborate approaches are necessary for quantitatively reasonably realistic binding energies [41, pp. 285-289]. Those might be based on Green's function tight binding calculations that were introduced by Hjalmarson and co-workers [66] (this original work of Hjalmarson *et al.* still ignores important effects, including Hubbard corrections and Jahn-Teller shifts [41, pp. 309-317]). Additionally, the expected situation in tetrahedral amorphous carbon is, due to the higher stability of all three sp^n-hybridisations ($n \in \{1, 2, 3\}$), in comparison with silicon more complicated [94, p. 56]. The choice of the example should also not indicate that vacancy-like states are expected to constitute the majority of defects in tetrahedral amorphous carbon (or any other tetrahedral amorphous system for that matter). However, in a covalently bound amorphous material, like ta-C, the dangling hybrids are expected to contribute significantly to defect states (not necessarily four around a

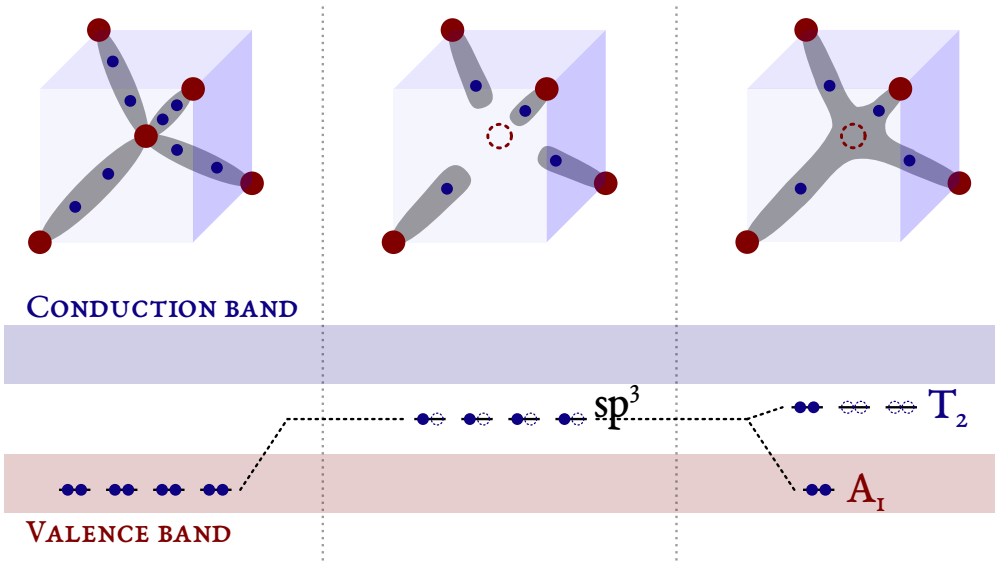

Figure 5.4: This image (and all information in this caption is after [41, pp. 285-289]) provides a qualitatively (the illustration is based on the defect molecule model which can not describe all aspects, models that are quantitatively close to measured values are given in the text) correct physical picture of the electronic structure of a vacancy in a crystalline group-IV elemental semiconductor (from now on assumed to be silicon) with a schematic representation of the four electrons of the defect molecule. From left to right: In the first part, the undistorted case is shown. As can be seen in the upper part, the silicon atom is in its place and provides its four outer electrons in the, for sp^3-hybridisation, expected tetrahedral arrangement to form σ-bonds with its second-nearest neighbours. Consequently, all eight electrons from the four bonds are valence electrons and occupy states in the valence band (electronic states are also only schematically in this figure). In the middle part of the illustration, the central silicon atom (more precisely an atom from sublattice 1 at $\mathbf{R} = 0$ in the primitive unit cell) and its electrons have been removed without regarding any reconstruction, so that the hybrid orbitals from the four outer atoms point inwards without corresponding partners. These dangling hybrids actually also influence the other hybrids of the same atoms, the nearest neighbours, atoms further away and also lead to changes in the inter-atomic distances. All these effects, except the possibility of the dangling hybrids to interact with themselves (in the next picture), are ignored within this purely qualitative picture. In the energetic picture without the interaction between themselves (and within this very limited model), the levels are in the middle of the band gap. In the last part, the dangling hybrids can interact with each other (only). This leads to a splitting of the energy into two eigenvalues for four eigenfunctions: one eigenfunction with A_1-symmetry (resembles an s-orbital of the silicon) and three eigenfunctions in the T_2-symmetry group (similar to the three p-orbitals of silicon). Within the used defect molecule model, the absolute energetic positions with respect to the band edges of the undisturbed crystal cannot be determined. From experimental observations and using more exact calculations, it can be shown that the A_1-level can be found in the valence band and the T_2-levels in the gap. Hence, the T_2-levels are the deep levels in the valence band.

vacancy, which is strictly speaking even only defined for crystalline systems). Some aspects of the crude example might, hence, still give insights to the expected form of traps in ta-C. As can be seen from the example in Figure 5.4, the localisation is on the order of an atomic distance. More accurate calculations by Bernholc *et al.* [9, 8] confirm the localised character and, furthermore, the symmetries obtained in the example (although there is also another E-symmetry state with d-like character and the symmetries are slightly distorted).[15] A typical challenge faced for these deep defects is the accurate calculation of binding energies. The potential landscape of deep centres consist of two parts: a long-range part and the short-ranged central-cell potential [66]. For deep-level traps the short-range potential alone is sufficiently strong to bind a state [66]. In consequence, the energetic position of the trap in the band gap is mostly determined by the short-range potential [66] while the long-range potential might only give corrections [41, p. 282].

In summary, distortions expected in tetrahedral-amorphous systems in sufficient quantity are dangling hybrids or other local arrangements of carbon (sp^1- or sp^2-bonded geometries). None of these are expected to lead to shallow acceptor- or donor-like states, furthermore, the effective mass theory cannot be applied since the concept of effective mass is not applicable to such amorphous systems [94, p. 98]. Since any system with a sufficient amount of shallow levels would not require field-assisted barrier lowering, anyway, only deep levels can be responsible in any material for which Frenkel-Poole conduction is relevant. Deep levels are, however, as explained, extremely localised (around one atomic distance) and their form is mainly based on the orbital geometries of the host materials [66]. To calculate their energetic states and central parts of the potential, assumption of a Coulombic potential is insufficient. For the long-range part only a (screened) Coulombic potential might be assumed (although there can be defects without any Coulombic long-range potential [41, p. 313]).

The above described properties of deep centres in the band gap are very important to calculate the energetic distances from the band gap, to understand their often not spherical symmetry and gain knowledge about their charge states. They are also important for any tunnelling process, including phonon-assisted tunnelling (already even to know the higher states in the potential), because initial and final state are needed to calculate the transition matrix element. *However*, the often criticised simplicity of the Frenkel-Poole model[80] that crudely neglects any quantum-mechanical processes in the escape of the mobile charge from the trap, might in fact be the reason why the model can actually gain quantitatively correct results (if the suggested correction is applied). The Frenkel-Poole model exclusively assumes classical thermal emission over the barrier (also in all of its extended version mentioned within this work). This basic thermal emission process alone depends *only* on the height of the barrier. The other assumption required by the Frenkel-Poole model is the field-assisted lowering of the potential. Since the result in this work was quantitatively correct assuming a Coulombic potential based on the dynamic permittivity of the bulk (the static field part is not relevant in this context), in this case,

[15] The calculated charge densities of the different eigenfunctions of a vacancy in a bulk silicon crystal can are well illustrated in Figures 4 to 8 of reference [8]. Figure 9 in the same reference places the state in the band diagram for the vicinity of the vacancy.

a long-ranged Coulombic potential over many atomic distances should be necessary. Suppose an electron is trapped in a deep level of a dangling bond. Assume further, the region is (on a large scale) neutral since the trapped electron is actually one of the four outer electrons of the atom (which has in this case no partner at one side). To leave the trap the electron has of course to leave the binding central part of the potential, but further, when it leaves the atom misses one electron. Consequently, the leaving electron perceives, after it already left the central part of the potential, an attractive force pulling it back in the direction of atom. Though the central part of the potential dominates the bound state, binding energy etc., in order to really leave the area of the trap and contribute to the current (enter an extended state), the electron must additionally overcome the attractive, possibly Coulombic, contribution. Assuming the atom with one electron missing really has an effective charge of $+e$ and the mobile charge of $-e$. Furthermore, the electron has thermally enough energy to leave the central potential and can reach large distances from this central potential. In this case, the electron could perceive a Coulombic attraction in an effective medium with the corresponding bulk dynamic permittivity. A superimposed static field would respectively lower the Coulombic barrier in the forward-hemisphere directions, while it would increase the barrier in reverse-hemisphere directions (confer discussion about three-dimensional extensions of the Frenkel-Poole model in 5.6.1). The Frenkel-Poole model, despite all its shortcomings, can describe such a situation, because it just needs the binding energy (not its complicated origin) and requires the final barrier (at long distances and at its highest point) to be Coulombic. This Coulombic potential is then lowered respectively by the applied field. The Frenkel-Poole model, in its usual form, cannot describe situations where the inner potential leads to the highest point of the barrier. For a non-Coulombic barrier, the lowering would lead to very different results, further, in the very localised (potentially asymmetric) central potential, the effect of the field would influence the bound states directly and should rather be considered in the calculation of the eigenstates and eigenfunctions of the trap as static perturbation potential (in fact, in every case the static field may affect the traps as an additional perturbation). An empiric fact supports the possible interpretation, that the inner potential is only of secondary importance and may, as approximation, be reduced to its binding energy: Frenkel-Poole behaviour is obtained for very different materials. The inner part of the potential is extremely sensitive to any changes, e. g. different types of atoms. The binding energy and the local potential landscape should for those different materials, hence, be very different. Yet, the Frenkel-Poole model can still be applied by only changing the parameters for the barrier-lowering coefficient and the initial barrier. Both must actually be barriers that can be overcome thermally, because temperature dependent measurements can be used to extract the resulting barrier per voltage as activation energy. Furthermore, an investigation of excited states at deep centres in sulphur- and selenium-doped silicon seems to confirm the suggestion in this subsection: the behaviour of their excited states seem to correspond to those predicted by a hydrogenic defect model [55]. The empirical situation described above regarding most materials displaying Frenkel-Poole conduction and the observation that extended states in deep traps may perceive a Coulombic potential, combined with the findings in this work, can be seen as a strong indication of the minor importance of the core potential for anything but the binding

energy itself.

The findings in this work also specify what kind of Frenkel-Poole model describes the experimental data correctly. The long-range potential should actually be Coulombic (the three-dimensional model by Connell *et al.* [28] was utilised, more details in the subsequent paragraph, where also opinions of other authors involved with the advancement of the Frenkel-Poole model are shown) and the distance must be large enough so that the bulk permittivity of ta-C obtained from the combined measurement of the dielectric properties is already valid. Any non-isotropic characteristics of the inner potential itself plays no role, because within this model it can be reduced to the energetic level of the trap. In an amorphous system the long-range potential should be spherically symmetric around the immobile charge centre, as assumed by using the model of Connell *et al.* as basis for the corrected model.

This section is supposed to explain the observed fact that the Frenkel-Poole model could describe the experimentally obtained data, after introducing a correction for the calculation of the internal field, using the combinedly extracted bulk permittivity (with reasonable size) without the usual deviation from the calculated barrier-lowering coefficient. This is, as already mentioned, a surprise since the Frenkel-Poole model has some known shortcomings that were often supposed to be the reasons for the observed deviations. After the introduction of the corrected calculation of the internal applied field (this did not introduce a completely new physical approach, quantum mechanics etc., this correction is within the scope of the theory), one was faced with the fact that the Frenkel-Poole model could actually describe the experimental data using the constants that were supposed to be applied. The ideas in this section are the first steps in understanding why this theory might work. They may mark the direction of the explanation. But they are probably not a final answer to that question.

Assessments of other authors about the validity of the Frenkel-Poole model With the work of Connell *et al.* [28] the realism of the assumption of a Coulombic potential undistorted by neighbouring traps seems exhausted. The influence of other traps (interestingly for this case the designation 'internal field' is often used and should not be confused with the approach introduced in this work) was investigated by Potemski and Wilamowski [151] as well as Dallacasa and Paracchini [32]. As already more thoroughly explained in section 5.6.1, it was found that for sufficiently large volumes (i. e. high numbers of considered traps) the influence of these traps can be assumed isotropic and results in a mean-field contribution (this can change if spatial and angular confinements exist). This mean internal field only influences the current-voltage curve in regions where its absolute value is higher than the one of the externally applied field and results in a flattening of the current-voltage characteristic towards low fields but no change in slope [151].

In addition to the question if the Coulombic form is influenced by nearby states, one might ask whether the basic assumption of a Coulombic potential is suited at all.

A possible explanation was given above, why the Frenkel-Poole model could lead to quantitatively correct results, though the inner (binding) parts of the potentials of deep traps are usually non-Coulombic. This question has, of course, not just emerged, it was

already discussed for a long time. Since up to now, there were deviations in the barrier-lowering coefficient, these were often mentioned as a result of the 'oversimplified'[80] assumptions, including that of a Coulombic potential. As the correction in the calculation of the applied internal field, found in this work, eliminates this discrepancy, this argumentation ceases to apply (at least for ta-C). Consequently, the above given, possible explanation was found. Below justifications of other authors are given that go beyond the oversimplification of the model. The idea of a separation into long- and short-range contributions has already been suggested [186]. Furthermore, other potential forms are analysed [125] and found to give similar results (though not similar enough to explain the quantitative compliance as found in this work using any other potential than the Coulombic potential).

Already Jonscher [80] suggested that central and outer potential form might be different, e. g. a steeper inner potential and a Coulombic form for higher distances. According to Vincent *et al.* [186], the 'same ΔE_i [barrier lowering as in the Coulombic case][16] is expected for any deep level, as soon as the edge of the potential well is Coulombic (i.e., at a large distance from the centre), whatever the central part of this potential is'. Besides investigating different forms of potential, including square wells and Dirac delta function potentials, they also consider other mechanisms of leaving the trap, apart from thermal activation, namely tunnelling and phonon-assisted tunnelling. Martin *et al.* [125] complete the investigation by Vincent *et al.* by considering even more non-Coulombic potential types, i. e. the Yukawa potential (a shielded Coulombic potential), the dipole potential and the polarisation potential. Interestingly, the obtained emission probability enhancements with respect to the applied field still have qualitatively a high resemblance with the three-dimensional Coulombic result. It is, however, important to note that the assumed base potentials (without the directional applied field) are still isotropic and do, hence, not recognise the required non-rotational symmetry by an assumed covalently bound material. Another reason, why the actual potential landscape of a deep trap in a covalently bound system might not be too important can be derived from a note by Vincent *et al.* [186]: They mention that a high doping density may lead to very high internal fields that may no longer be neglected or may even dominate the local potential environment of the trap (according to Vincent *et al.* orders of $10^8\,\mathrm{V\,m^{-1}}$ are typical at a net doping level $N_\mathrm{D} - N_\mathrm{A} = 10^{18}\,\mathrm{cm^{-3}}$ and bias voltages of -3 V). In large enough volumes of materials with very high numbers of charged defects, e. g. amorphous materials, the fields by nearby defects may in the mean be assumed equally likely distributed over all angles, like in the models of Potemski and Wilamowski [151] or Dallacasa and Paracchini [32]. Due to their large field strengths, they might dominate the local potential around the trap. However, the findings in the above mentioned sources indicate that the slope at high fields is not as much affected, but rather the low-field part. Furthermore, in amorphous systems, the directional bondings are randomly oriented with respect to the applied field. All orientations of the local geometry with respect to the applied field are equally likely and any asymmetric potential could than be described by effective symmetric potentials. Both effects might lead to the fact that in the mean, the local geometry of the undisturbed

[16] note from the author

potential plays only a minor role. However, the found permittivity that is in agreement with the bulk permittivity suggests that the potential is not effective.

Dangers of generalisation The findings of this work raise hope that the Frenkel-Poole model, with the correction introduced in this work, may indeed capture the important underlying properties responsible for current transport at height temperatures in materials with low mobilities. A temperature-dependent analysis is highly suggested as a next step to verify the corrections. It is, however, important to notice that the findings are so far only based on the analysis of ta-C. Mainly, because voltage-dependent immittance spectroscopy, which allows the connection of dielectric and electric properties (see section 2.4) and was the key piece of the puzzle in resolving the decade-old deviation in the Frenkel-Poole model, is rarely performed at all. Consequently, to determine whether Frenkel-Poole conduction may really be used as explanation for the static charge transport in a material, it is (in the opinion of the author) essential that the dielectric and electric properties obtained in an identical setup at the same sample, preferably in a single measurement, are jointly analysed sharing the relative permittivity between conductive and capacitive models. This work does not deem the use of the Frenkel-Poole model valid for any other materials. For materials, where no connections between the barrier-lowering coefficient and permittivity can be found as straightforwardly as in the presented experiments, this does not mean that the Frenkel-Poole model might be completely wrong, but other assumptions, e. g. about the symmetry of the trap potentials, might have to be considered. Without a sound explanation of the possibly effective barrier-lowering coefficient, any interpretations of the extracted parameters are, in the opinion of the author, dangerous.

6 Summary & Outlook

6.1 Summary

A novel method of interpreting immittance spectra using process-specific physical models dependent on external parameters is presented. Not only does it resolve many inherent drawbacks of conventional immittance analysis, i. e. using EECs, but it also offers advantages over the analysis with Poisson-Nernst-Planck models. Voltage-dependent immittance spectra contain the full information of the corresponding current-voltage measurement. In contrast to the latter, different serial contributions to the total resistance may be distinguished by their capacitive bypasses. Both, the resistive and the capacitive part of each serial piece, jointly lead to distinct cut-off frequencies. Furthermore, due to the knowledge of the capacitances of each serial piece, their respective permittivities may be extracted. This can be especially useful if the conduction model for the parallel resistor depends on the permittivity. This work exploited the above described feature of the analysis with immittance spectra to separate the immittance of the depletion layer (in silicon) from the thin-film immittance and to validate a proposed correction of the Frenkel-Poole model. It was found that, by using the internal field as the one superimposed to the Coulombic potential of the trap, a decades-old discrepancy in predicted and measured barrier-lowering coefficient could be resolved. Since three-dimensional modelling of the local potential landscape around the trap already solved the other major remaining discrepancy, this suggestion eliminates the last common deviation of the Frenkel-Poole model. It might seem surprising that the Frenkel-Poole model can predict the current-voltage relation in many very different materials reasonably well, despite its very simple, potentially not too realistic assumptions of the local potential environment around the trap and its restriction to a classical description. A first step to understand why this model, despite its deficiencies, may give such a successful description is ventured in section 5.6.4.

6.1.1 Benefits of this work for the analysis of immittance spectra

The most common method of analysis in immittance spectroscopy is using EECs consisting solely of idealised lumped components [110]. Such circuits are, however, ambiguous, i. e. different arrangements of components can give identical immittance spectra for all frequencies [114]. Consequently, a specific component might not represent one underlying physical process, but may instead be influenced by several processes, possibly even from different homogeneous pieces of the system. As a result, the extraction of relevant physical parameters of the processes in the system can be complicated. This may in fact

be the reason, why extraction of the relevant parameters is rarely done and why many analyses with EECs stop after resistances and capacitances have been fitted [110]. Another consequence of using EECs consisting solely of idealised lumped components, is a very large number of fit parameters when the system is investigated under varying external parameters, e. g. for different voltages and temperatures. For each condition, new values have to be fitted for every resistance and capacitive element in the system. Unlike EECs, immittance models based on the above described specific solutions Poisson-Nernst-Planck equations for immittance spectroscopy aim to extract physically reasonable parameters that are comparable between different experiments. However, these models are process-independent [119] which may result in effective parameters, e. g. independent of the actual underlying process of charge propagation a (potentially effective) mobility is assigned which might not actually exist as a mobility, in the underling system, as such. Since no dependence on external parameters is included, parallel processes cannot be distinguished and, *without indication*, effective parameters combining several parallel processes may be extracted. Another consequence of the absence of external-parameter dependence is that for each of multiple conditions a separate set of parameters has to be obtained.

One of the major goals of this work is to offer a novel approach that allows understanding the underlying physical processes in the system under investigation. This includes identification of the involved processes and extraction of their relevant parameters (i. e. doping concentrations and activation energies instead of resistances and capacitances) with minimal distortion by other contributions. In order to do that, it is necessary to reach a one-to-one assignment between physical processes and components in the circuit. Introducing process-specific physical models dependent on external parameters to replace the idealised circuit components allows fitting the relevant parameters directly in global fits over all parameters. For example, instead of fitting a resistance for each temperature, the corresponding activation energy of the process[1] is fitted which then ideally, if the model is correctly chosen, characterises the temperature dependence without the need for parameters per condition. Another effect of using those models, instead of idealised components, is that their ability to 'absorb' different contributions is, in comparison, much more restricted. This has two positive consequences: First, if a model can describe the corresponding contribution of one serial piece or, even better, if resistive and capacitive properties of one serial piece can be described with shared parameters, it is very likely that these processes are actually relevant for the serial piece, i. e. the model does usually not fit by accident. Secondly, since the dependence on external parameters is a distinct property of the model, parallel processes with different dependence on external parameters (which could in an analysis with conventional EECs only be distinguished afterwards by fitting the condition-dependent resistance with the models) may distort the parameters of the model but cannot be completely absorbed.

In the application of the novel approach to the ta-C/p-Si system in this work, the capacitance and resistance of the depletion layer in silicon is dependent on voltage. Both

[1] This is only an example, of course, a model does need more parameters, e. g. at least the pre-factor to the exponential function with the activation energy. However, ideally the corresponding set of parameters then describes the response of the model for all conditions, i. e. the set is valid independent of the external parameters and not fitted per condition.

contributions were described by the corresponding models. The parameter of acceptor concentration was shared between both models. Together, the models could describe the observed depletion-layer behaviour very well within the limits of the models. Hence, the contribution could be identified as resulting from the depletion layer in silicon. However, since the models did neither include a description for effects caused by interface defects nor charged defects in the thin film, deviations were expected and observed. This could be seen, on the one hand, because the barrier height of the capacitive and resistive part was different (the number of interface or charged defects in the insulator is calculated from this difference) and, on the other hand, from typical deviations in a plot of the residuals over the external parameters. Furthermore, the identification of the deviations was confirmed by classical capacitance-voltage analysis. Neither the models for the depletion layer nor for the thin film 'absorbed' these deviations, at least not significantly. It can, hence be deduced that the presented approach allows identifying missing processes or incomplete descriptions from the plots of residuals over the external parameter and, further, shows that the extracted relevant parameters are, at least in this case, not too distorted by such model deficiencies. The model for the thin-film immittance consists of the corrected Frenkel-Pool model, to describe the resistive properties, a constant phase element that is independent of voltage and a high-frequency limiting capacitor, also voltage-independent. The voltage independence of the capacitive parts is expected for a bulk part and can be seen as additional confirmation that the bulk thin-film properties were described. In addition to dependence on voltage, bulk permittivities are also less temperature-dependent as their resistive counterparts [37]. The permittivity extracted from the high-frequency limiting capacitor, as it is supposed to be extracted according to Young and Frederikse [190], was jointly fitted as a single parameter with the permittivity in the Frenkel-Poole model (Model 2). It could be shown, that the correction of the Frenkel-Poole model using the permittivity extracted from the capacitive part, describes the thin-film piece equally well as a model (Model 3) where both permittivities may be chosen independent from each other (since the factor in the exponent of the Frenkel-Poole model is completely free, this also includes the case where the correction introduced in this work is not correct). Furthermore, for the sample with highly-doped substrate which shows dominantly the thin-film immittance, the fit determined similar values for both permittivities when they were fitted independent of each other as two separate values.

With respect to models for the analysis of immittance spectra based on the Poisson-Nernst-Planck equations, it was suggested to combine that concept with the presented approach by including process-specific physical models for the parameters of the Poisson-Nernst-Planck models, e. g. an external-parameter-dependent model for the number of mobile ions (for example thermal activated or field-assisted). This way, effective parameters resulting from multiple parallel processes may be easier to detect and the number of parameters, which was similar to the case of conventional EECs one set of fit parameters per condition, would be greatly reduced. Furthermore, the underlying processes would be known.

In summary, evidently relevant physical parameters, like the acceptor concentration of silicon or permittivity of the thin film, can be extracted directly by global fits and describe the system under investigation for the whole parameter space. Consequently, the number

of parameters to describe the sample could be significantly reduced (to only one set of relevant model parameters) with respect to conventional EECs which determine values for each component per condition. Furthermore, it was demonstrated that the process-specific physical models with their specific dependence on external parameters are not prone to the absorption of contributions from other processes or incomplete descriptions. This allows determining the missing contributions from the residual plots and means that the extracted parameters are only weakly distorted by incomplete modelling of the system. Each relevant serial piece of the system could be described by a pair of reasonable capacitive and resistive models with shared parameters. For example, the fact that the both, voltage-dependent capacitance and voltage-dependent resistance, of the depletion layer used the same reasonable value for the acceptor concentration which was independently confirmed by conventional capacitance-voltage analysis, the same literature values for the permittivity, the effective masses, the band gap (all for silicon). This makes it virtually impossible that the described part is not a depletion layer in silicon. Similarly, the thin film could be described with the same reasonable value for the permittivity for both, resistive and capacitive part. All models together could describe the experimentally observed response of the system quite well and remaining discrepancies could be identified. As a result, the presented approach accomplishes the targeted main goal of understanding the underlying processes as well as the extraction of relevant physical parameters that are comparable between different experiments while being minimal distorted by incomplete descriptions due to missing or oversimplified models.

6.1.2 Benefits of this work for conventional current-voltage analysis

As explained above, voltage-dependent immittance spectra principally contain the full current-voltage information (see section 5.5.7). Except for the different measurement setup itself, the sample geometry may remain unchanged, since contact geometries for conventional current-voltage analysis are usually compatible with immittance spectroscopy. The possibility to separate the response of distinct serial pieces of the system allows easy removal of serial parasitic contribution. For this separation, knowledge of models to describe the parasitic pieces is not necessary. As already explained, separation of serial components is also possible for conventional EECs, however, with the mentioned drawbacks like fit parameter sets per condition. Nevertheless, if the goal is simply the removal of parasitic parts in an otherwise simple system, the parasitic parts may be modelled by idealised lumped components to get rid of their contribution and extract the intended current-voltage relation free of any disturbances. Of course, due to the ambiguity of conventional EECs, the correct arrangement has to be verified beforehand, e. g. by the presented approach. As previously mentioned, the additional information from capacitive bypasses can be used further to distinguish bulk and interface contributions (by the magnitude of capacitance and its dependence on voltage) as well as to extract the permittivity if the film thickness is known (or vice versa). The confidence in the identification of different pieces and the parameters may be further increased by using process-specific physical models dependent on external parameters not only for the resistances but also the capacitive parts. Parameters shared by both parts may than be joined to

a single parameter. This also tests the compatibility of both models. If the corresponding combined parameter(s) work equally well as single parameters an accidental association of the respective serial part is even less likely and the confidence of the relevance and correct value of the extracted parameter is higher.

6.1.3 Benefits of this work for the Frenkel-Poole model

This work suggests a correction in the Frenkel-Poole model: In it, the Coulombic barrier of a trap is lowered by a superimposed field caused by a linear voltage drop V over the sample. Up to now, the field strength at the trap was calculated as

$$E_{\text{ext}} = \frac{V}{d},$$

with film thickness d. However (as already mentioned in the paper by Poole [149] who was only interested in a qualitative description and, hence, ignored this parameter), the mean field strength *inside* a polarisable material ($\varepsilon_{\text{r}} > 1$) is not given by the external field E_{ext} but the internal field

$$E_{\text{int}} = \frac{V}{\varepsilon_{\text{r}} \cdot d}.$$

Most of the above mentioned features were utilised in this work to describe the ta-C/p-Si system. Voltage-dependent models were introduced for the resistance as well as for the capacitive part of the depletion layer. Both use the same acceptor concentration as single joined parameter and its value is verified by a separately performed conventional capacitance-voltage analysis. The depletion-layer piece is in series, and hence separated, from the thin film which is described by a Frenkel-Poole resistance that uses the permittivity, extracted from the parallel high-frequency limiting capacitor, in its barrier-lowering coefficient as well as for the calculation of the internal field (Model 2). A connection between the constant phase element and the permittivity in the resistive part (Model 1) lead to a significantly higher deviation of the description from the measured spectra. This is in agreement with the suggestion of Young and Frederikse [190] of how to extract the static permittivity from a material. They emphasise that the constant-phase behaviour at low frequencies (up to either 1 kHz or sometimes even as high as 1 GHz) is not connected to the static permittivity. The third model, where there was no connection whatsoever between any of the capacitive elements and the resistance of the thin film and each of the parameters could be varied completely independent could not lead to a significantly better result than Model 2. Indeed, even without any connection between the permittivity extracted from the high-frequency limiting capacitor and in the Frenkel-Poole model (i. e. Model 3), comparable values were fitted for both parameters in case of the sample with highly-doped silicon substrate (which is dominated by the thin-film immittance and has except a slight asymmetry no visible rectification effect). All remaining deviations could clearly be ascribed to the omission of contributions by interface traps and charged defects in the thin film. Since the properties of the (well-studied) depletion layer in silicon was not the focus of this work, it was decided against further refinement of the

used depletion-layer models. As already mentioned, the presented approach does not tend to 'absorb' contributions from other pieces. Consequently, this allowed an isolated study of the thin-film piece. The fact that the permittivity and resistive properties can be determined in a single measurement with this approach makes it the unique method to verify our hypothesis.

The suggested correction still remains within the original concept of the Frenkel-Poole model: a continuous medium approach using a simple Boltzmann factor, i. e. only the maximum of the barrier and not its actual form is relevant (within some limits, since the model of Connell *et al.* [28] is used as basis for our correction), without taking quantum-mechanical effects into account and using a simplified description of the potential landscape around the trap (see section 5.6.1, 5.6.2 and 5.6.4). It is, hence, rather surprising that this simple correction could finally explain the last remaining quantitative deviation of the Frenkel-Poole model. Possible explanations, why the Frenkel-Poole model with the suggested correction fits the experimental data well is given in section 5.6.4. It is interesting to note that despite all its deficiencies, many very different materials have (except for the factor in the barrier-lowering coefficient potentially explained and resolved in this work) a Frenkel-Poole current-voltage relation. This can be seen as an indication that the actual form of core potential, which is essential for a correct determination of the binding energy and very sensitively dependent on the involved materials [66, 41, 94], might not be as important for the current-transport process at sufficiently high temperatures, so that it may be reduced to the binding energy. Otherwise, its distinct form for the very different materials should have at least some measurable effect. Furthermore, the work of Grimmeiss [55] for sulphur and selenium in silicon shows that excited states at deep centres may well be resulting from the hydrogenic outer potential. All this may be seen as strong indication for a dominant importance of the outer potential in such cases. Which would consequently explain the successful description with generally similar and very simple assumptions for the local potential landscape, especially the Coulombic trap form (already criticised for some time [80]), for the different materials.

6.2 Outlook

6.2.1 Large-signal analysis

Already now, the calculation for the (complex) values of the fit in this work uses the non-linear character of the models to determine the resistances and capacitances at each bias voltage. Although the theoretical fundamentals for large-signal analysis, i. e. taking higher harmonic (non-sinusoidal) responses as a consequence of applying finite signal levels onto non-linear functions into account, were laid in this work: so far, the amplitude of the applied signal remains unused in the calculation of fit values. As a consequence, the performed analysis corresponds to small-signal approximation around certain points of operation: Each condition corresponds to an operation point for which external-parameter-dependent resistances and capacitive values are determined. The immittance response for the sinusoidal signal at these operation points then assumes a linear response, i. e. one that only contains the amplitude and phase of the first harmonic. This approximation is only correct for sufficiently small signals (compare 2.1.5).

Experimentally, the signal level was chosen from a plot of the absolute impedance over the amplitude. For decreasing amplitudes, the measured value approaches a constant corresponding to the small-signal impedance. From this plot for both samples at key conditions with strong impact of the non-linearity on the response, but also regarding the measurement error, an amplitude of 30 mV_{RMS} was chosen (see section 3.2.2). Utilising this procedure to select the amplitude justifies small-signal analysis for the measurements in this work. However, since process-specific physical models dependent on external parameters were introduced to understand the underlying mechanisms, it seems only logical to use their poly-harmonic response as further point of reference for the involved processes. Furthermore, higher signal amplitudes enhance the accuracy of the measurement with an auto-balancing bridge.

A possible next step towards large-signal analysis could be to obtain the resistances and capacitances of the models by determining their mean response with an integration of their respective functions over their fraction of the (oscillating) voltage drop within one amplitude. For non-linear behaviours this would give the correct offset of the response, a first order approximation (compare the offset in the large-signal response of 2.5 which is the zero-frequency contribution in the Fourier spectrum in 2.5b). Fourier transformation of a full amplitude would also contain higher harmonics. However, both calculations are only intermediate steps since charging and discharging effects of the capacitors are not taken into account. Furthermore, these intermediate approaches are not too easy to calculate, since the respective voltage drops of the serial pieces are not known beforehand. A full large-signal calculation could be performed by a simulation of the whole system in time domain, including the charge states of the capacitive elements and the voltage drops in each time step over the serial pieces. The calculation expenses are, however, expected to be rather large, particularly because the transient behaviour has to be calculated as well.

As already explained in section 2.1.5, the large-signal calculation could still be applied to conventional immittance measurements, which do not include higher harmonics, because it could correctly calculate the reduced contribution to the fundamental frequency. It

seems, however, that such expensive calculations are only justified if the measurement also includes the higher harmonics, which is not the case for the current set-up. Real large-signal analysis can, hence, only unfold its full potential if the current experimental set-up would be updated with instruments that can measure the response of higher harmonics. Furthermore, the devices should be sufficiently sensitive in order to measure responses of samples with impedances of over 1 MΩ. The higher the frequencies get, the more limited the possible range of sample impedances (typically narrowing down on 50 Ω or 75 Ω) becomes.

This investigation would be an especially interesting continuation of the experiments, since the resistive models were usually not designed for timely varied voltages. As described in section 5.4, in principle the models should be reasonable approximations for frequencies below the absorption or emission of modulation quanta, which should be at much higher frequencies than usual impedance experiments. However, this was, up to now, never experimentally verified and would, hence, be a really interesting test of the expected behaviour. The answer of this question is tight-knit with the challenge of finding a unified microscopic theory for ac and dc processes in solid materials, presented in section 6.2.4.

6.2.2 Temperature-dependence

Another important improvement regarding the measurement set-up would be the introduction of temperature dependence. All process-specific physical models with dependence on external parameters used in the current model for the system are dependent on temperature. Unfortunately, without the knowledge of the temperature behaviour some parameters could not yet be decoupled, e. g. the activation energy in the Frenkel-Poole model. Apart from the decoupling of more parameter, the novel approach in general, benefits from an increased number of varied external parameters: e. g. if the model is consistent for different voltages and temperatures, possibly even connected over joined parameters with other parallel processes, the confidence of understanding the corresponding part further increases while the accidental 'absorption' of other contribution decreases.

6.2.3 Better model for the exemplary investigated system

If one would really like to pursue the goal of understanding the ta-C/p-Si system in greater detail (which was not the goal of this work), further enhancements of the model would still be possible. Especially by a better description of interface traps and charged defects in the insulator. So far, two different barrier heights for the capacitive and resistive description of the depletion layer are used. However, it can be clearly seen that the number of interface defects and charged defect in the insulator that contribute to the interface capacitance is strongly dependent on frequency. The amount of charges through this process of charging and discharging traps is, consequently, also dispersive. Since the charges are directly connected to the shift of the flat-band voltage, the usage of only one constant shift (which is in this work represented by the two separate barrier heights for capacitive and

resistive part) cannot correctly describe the observed behaviour. Introducing a frequency-dependent flat-band voltage shift may be used to not only increase the quality of the description itself, but also to help understanding the energetic or spatial distribution of the involved states at the interface. As already mentioned in sections 2.4.1.3 and 4.1.1.3 there are yet much more elaborate and expectedly more accurate models for the interface available.

Besides the interface model, also the description of the thin film part can still be enhanced. In this case, the introduction of temperature-dependence mentioned in the last subsection should accompany this improvement. The constant phase element of the thin film might be replaced with models for hopping polarisation processes (e. g. from [40] and [104]). This might give the energetic properties of the involved traps and their corresponding concentration. These values might in the spirit of the proposed model (confer section 2.4) be combined with the resistive properties of the thin film. Although, a sound combination of microscopic models for the conducive and polarising properties of a disordered material is still a subject of research, as can be seen in the next subsection.

6.2.4 A unified microscopic theory for ac and dc properties of disordered materials

As explained in section 5.3 and in the works of Long [104], Elliott [40], Dyre [37] and Lunkenheimer [106, 108], materials with charge transport dominantly through localised states display the 'universal capacitive behaviour' discovered by Jonscher [84]. It involves an approximate [37] power-law dependence of both parts of the complex permittivity on frequency with approximately fixed ratio of dielectric loss [108]. Besides the connection of this characteristic feature of the permittivity with the charge-transport process through localised states by coincidental observation, there is also an empirical formula for the quantitative connection: The so called Barton-Nakajima-Namikawa relation connects the dc conductivity σ_{stat} to the strength of the dielectric relaxation $\Delta\varepsilon = \varepsilon'(\omega_0) - \varepsilon'(\omega_1)$ (with ω_0 a frequency before and ω_1 a frequency after the respective dielectric relaxation, e. g. the static permittivity $\varepsilon_{\text{stat}}$ and the permittivity ε_∞ extracted from the high-frequency-limiting capacitor C_∞) and the frequency of the loss peak ω_{max}, i. e.

$$\sigma_{\text{stat}} \propto \Delta\varepsilon\,\omega_{\text{max}}. \tag{6.1}$$

The proportionality constant for this relation is a temperature-independent quantity in the order of unity [36]. In particular, equation (6.1) implies that both processes, for dc conductivity and dielectric relaxation, have the same activation energy [36]. The Barton-Nakajima-Namikawa relation has been found for a wide variety of different materials: amorphous solids, ionic glasses, single crystals, polymers, micro-porous systems and proteins in hydrated state [182]. Although the above mentioned quantitative (empiric) relation exists between dc and ac properties of such (mostly) disordered materials, there is still no microscopic unified theory. It has been suggested that finding this unified theory is one of the major challenges of solid state physics [118] and Phillips saw it 1994 even as 'most important unsolved problem in physics today' [147]. Although these

assessments might be exaggerated, they make clear that researchers in this field are longing for a solution of this problem. Indeed, all empirical evidence suggests that current dc models for conductivity are missing features that become important for timely varying signals. The observation in this work that the low-frequency permittivity, extracted from the constant phase element, is larger than the conventionally, i. e. according to Young and Frederikse [190], obtained static permittivity also indicates the demand for such a unified model. The proposed method of analysis in this work should have eliminated the Maxwell-Wagner effect which is typically mentioned as argument to discard these high values of the permittivity at low frequencies. However, as it became clear in this work, although the Maxwell-Wagner effect was eliminated, the permittivities at low frequencies are still too high. As a result, the usual explanation for discarding these low-frequency values is not always justified, and other reasons have to be found.

The approach presented in this work is uniquely suited to study this 'most important unsolved problem in physics today' [147], since ac and dc properties are jointly measured, consequently compatible as well as self-consistent, and can be separately assigned to distinct pieces of the system. So far investigations in this field are limited to temperature-dependent measurements. In many materials, field-assisted barrier-lowering can be observed. It is, hence, expected that a unified theory should also include voltage dependence. Instead of fitting a resistance for each temperature (as it is done up to now for the dc contribution), models should be directly included into the circuit that derives the resistance for various conditions, including more external parameters than solely the different temperatures. With the presented approach, a convenient basis for further research towards a unified theory of ac and dc properties is now available: A connection of resistive and capacitive parts of one single piece of the system (the thin film) via the permittivity which is valid for various external conditions using a single set of model specific parameters instead of new sets of fit values at each condition has already been demonstrated in this work. Further connections between resistive and capacitive properties could be found for the interface part. Hence, it could be demonstrated that the proposed novel method of analysis allows joint extraction of consistent electric and dielectric properties simultaneously. Furthermore, the model would be directly included as a circuit component and instead of fitting resistances and capacitances the underlying microscopic properties would be determined directly.

Beside the used methods, the investigated thin-film material, ta-C, offers an exceptional opportunity for the study of a unified theory for ac and dc properties of disordered solids (as explained in greater detail in section 1.3). It is intrinsic (i. e. not doped), monoisotopic and due to the synthesis method also almost without foreign atoms. Furthermore, it has solely non-polar bonds and is, due to its amorphous structure, isotropic.

The above mentioned temperature-dependent set-up would however be an essential requirement for this research project. In a first step, parallel low-temperature dc-transport processes for the thin film have to be included as supplement to the Frenkel-Poole mechanism. Ideally, correlations are already possible between the different dc models, e. g. a specific defect level involved in both processes simultaneously, maybe in combination with the permittivity extracted from the parallel high-frequency-limiting capacitor. Latter are expected to be much less dependent on temperature and their capacitive representa-

tion, as explained in chapter 2, must be parallel to all transport mechanisms (for the fact that dielectric properties usually are less dependent on temperature in comparison to their parallel conduction processes, confer [36]). Then, the universal dielectric response behaviour would not be described by a constant phase element but more specific models, e. g. for jumps of mobile charge carriers between neighbouring traps. The temperature dependence of such a model may indicate similar activation energies as compared to the resistive models. Also hopping distances and number of involved traps may be correlated. Unified models may include the number of involved defects or probably even properties of the distribution of barriers themselves, because ac processes involve primarily probable jumps while the properties of dc processes are dominated by the barriers hard-to-overcome. Since the described frequency response is present in various different materials, finding a unified theory seems, for the beginning, most promising in a material as essential as the mass-selective ion beam deposited ta-C (i. e. only one atom species, hence non-polar bonds, even monoisotopic and with a low number of foreign atoms etc., see above) and with a measurement approach uniquely suited to combine dc and ac properties.

6.2.5 Finite-element models

Another possible direction to continue the research is the combination with finite-element methods. As a consequence of the transition from combustion to electrical engines, because of an increased amount of mobile electronic devices, but also due to an increase of renewable energy sources with their requirement of energy storage, the enhancement of battery performance has become an essential task. A better understanding of the ageing processes in the battery requires refined models that allow identification of the weak parts in a battery systems and recognition of wear processes. In such a case the combination of the main concept of the presented approach with finite-element methods may be promising. For each finite element, the locally applied field can, for example, be used to determine the conductivity, number of emitted charges or dissociation rate from field-dependent models. Using the resulting models, a spatially distributed model of a battery cell can be constructed.

6.2.6 Verifying the findings with other materials

Surprisingly, by a correction (introduced in this work, see sections 4.2 and 5.6) of the calculation for the field around the trap due to the externally applied potential difference, a valid connection between the permittivity of a material (here ta-C), extracted from dielectric properties, could be made with the permittivity in the Frenkel-Poole model, which is describing solely resistive properties. This link is not as obvious as its sounds, since the deviation between these two quantities is as old as the Frenkel-Poole model and considered *the one* remaining deviation of the Frenkel-Poole model (confer 5.6). Furthermore, the fundamental assumptions of the Frenkel-Poole model are still very simple, especially the assumptions about the local potential environment around the trap (compare 5.6.2). Although the experimental data in this work suggests that our correction

can resolve this deviation (confer 4.2), the measurements in this work are limited to one material, namely ta-C, and do not include temperature-dependence. Hence, the discovered correction might still fit only due to an accidentally similar factor which could actually have another cause. After adding temperature dependence, as mentioned above, the next important step is to verify this finding by testing also other materials that observe Frenkel-Poole behaviour. The immediately next investigated systems should be chosen carefully, i. e. without adding significantly different features that potentially lead to alternate processes: At first, a restriction to materials with covalent bonds (preferably a single species) would be preferable, since this eliminates competing processes involving polaronic transport. Also, homogeneous amorphous materials are predestined since isotropy may be assumed. As a consequence of the suggestions above, there are no dislocations, negligible impurity concentration and no volumes with one atomic species of the compound agglomerated. The system should either be restricted to intrinsic, structural localised defects or doping with a single species that solely leads to sufficiently deep, i. e. localised, traps, but not both. This way the traps involved in the Frenkel-Poole process may be identified more easily.

Furthermore, the parallel constant phase model may be more refined. The constant phase element is only an empiric description, there are, however, microscopic models that result in such a behaviour (e. g. see [104] and [40]). These models depend on microscopic properties such as trap densities and activation energies (which would again require temperature-dependence). This would possibly allow connecting properties of the constant phase part with the Frenkel-Poole model. For now, these elements are not connected.

6.2.7 Introduction of more robust regression estimators

The *robustness* of a regression estimator describes the strength of influence of outliers on the fit parameters [158, pp. 9-10]. The property may be quantified by the breakdown point [158, pp. 9-10]. Simply speaking, it is defined over the smallest fraction of outliers which can cause the estimator to take on values arbitrarily far from the regression coefficients (these were called fit parameters in this work) of untainted data points [158, pp. 9-10]. Hence, a more robust estimator is, assuming the same number of outliers, expected to result in fit parameters more closely to the 'true' ones as a less robust estimator.

For a number of reasons, a least-square estimator is used in this work. More precisely, the complex non-linear least-square estimator which was defined by J. Macdonald and Garber [121] specifically for the analysis of immittance data. It seems to be the only regression estimator used in the field of immittance spectroscopy and was, hence, for better comparability with other works also chosen here. Furthermore, least-square analysis is very common and is, consequently, expected to require no additional initial adoption for users of this novel approach of analysis. Although the least-square estimator is commonly used and there exist specific adjustments for its usage in the analysis of immittance data, with respect to robustness, it is a terrible choice and better suited estimators are available. In the case of the least-square estimator, already with one outlier the regression coefficients can be arbitrarily manipulated, i. e. its breakdown point is zero [158, pp. 9-10].

Using the method of analysing immittance spectra (with process-specific physical models dependent on external parameters) proposed in this work, deviations are much more likely as in the generic models, utilising idealised lumped components, in conventional analysis of immittance spectra with EECs. The reasons for this are: First, that the utilised model is supposed to fit not only one spectrum per condition, but jointly spectra for every condition simultaneously. Secondly, the form of the models is much more restrictive as for idealised lumped components, i. e. deviations are not easily absorbed. Thirdly, as a consequence of using potentially unfinished models during the analysis, where subsequently more and more processes are identified and their respective models added, a lot of deviations are expected to be present. Finally, even for a finished model that essentially describes all processes, certain aspects of the observed behaviour may still not be described properly, e. g. due to the (at least at first) unavoidably idealised assumptions of any model.

All the above mentioned deviations are not statistical in nature, but instead systematic deviations due to a (to a certain extent) incomplete physical theory. The occurrence of these deviations is likely also not at random positions in a residual plot over the different conditions. Instead, certain regions of (smooth) deviations may be expected. In this work, the influence of defects in the insulator or traps at the interface on the characteristics of the depletion layer has, for reasons given in sections 4.1.1.3 and 2.4.1, not been conclusively described. This lead to the pronounced deviations between the observed and the calculated immittance response (compare section 4.1.2). As can be seen in section 4.1.2 this resulted in closed regions of deviation with steady curvature (meaning there is not a strong up and down in the corresponding regions, but they rather look like a smooth hill or valley).

One of the strengths of the proposed method of analysis, in comparison to conventional analysis, is the low absorption of parasitic deviations (see section 5.1.1). Hence, this model is either less likely to, or does only in a lesser extent, change fit parameters to absorb a deviation incompatible with the model. However, with other regression estimators, this important feature (that among other things helps to identify missing processes or model deficiencies) might be further extended.

The above described deviations are *not* outliers. However, it is conceivable that a more robust regression estimator might, also in this case, result in fit parameters more closely to the values that belong to the data connected to the pure model assumptions. Of course, these more robust estimators *neither can nor should replace* improvements of the model itself, but there is no reason against *complementary* usage of more robust estimators. As a next step for a general enhancement of the proposed method of analysing immittance data, more robust regression estimators may be introduced. Potentially, one may also introduce weighting and decrease the importance for regions of deviation. Doing this manually is, however, risky since one may accidentally remove important regions falsely identified as not described within the currently applied model and, in consequence, push the fit in a direction that leads further away from the 'true' parameters. Also, some objective condition to introduce as well as select the level of weighting should be chosen to make a transparent selection of regions expected to be not explainable within the used theory.

An expected challenge in introducing more robust estimators is the uncertainty of the

influence of the specific extensions to account for complex immittance values. Due to an unavoidable generality in the research of robust estimators (which may be applied for very different purposes), the specific consequences of using the complex extension (usually used within the field immittance spectroscopy) may not be straightforwardly predictable.

6.2.8 Ion tracks

This work introduces a new method of analysis, using voltage-dependent immittance spectra that allows separating specific parts. It connects dielectric and electric properties of those parts by introducing process-specific external-parameter-dependent physical models and jointly fitting their parameters. The selection of ta-C as the investigated thin film material was not by accident. When a swift heavy ion passes through ta-C nanoscopic conductive paths are generated [127, 188]. Indeed, long-term goal is to understand the conduction properties of such conductive ion tracks in ta-C, especially also those which are interrupted by insulating materials that do not form conductive paths. In the first step, resistive and capacitive properties of the macroscopic films (ta-C and potential insulating parts) should be known separately. This step is now achieved by the current work, though temperature dependent characterisation is still pending. After irradiation of samples with swift heavy ions, in the next step, the temperature- and voltage-dependent resistive properties of the ion tracks should be measured by conductive atomic-force microscopy. The latter has also already been done (see exemplary results in Figure 6.1 which shows characteristics of ion tracks in ta-C, created by irradiation with 30 MeV C_{60}^{2+} fullerenes), but is, due to its different scope, not included in this work. Therefore, in a temperature range from 176 K to 296 K the same region of 18 ion tracks has been observed with a conductive atomic-force microscope. For nine temperatures voltage-dependent current maps (voltage ranging from −4 V to 4 V with 0.1 V steps) have been measured. In the intermediate temperatures 137 current maps at 3 V have been recorded. At least eleven identical ion tracks were recorded in every measurements. Now, the dielectric and resistive properties of the corresponding thin films are known. Furthermore, the conductive properties of the ion tracks are known. Finally, a macroscopic measurement of irradiated samples may than be performed. The results consist of the known resistive properties of the thin films and the conductive tracks (with known track density), of the known dielectric properties of the thin films and the sole unknown dielectric properties of the ion tracks (possibly intentionally interrupted by insulating films). In principle, it should hence be possible to extract the dielectric properties of the ion tracks from the observed differences.

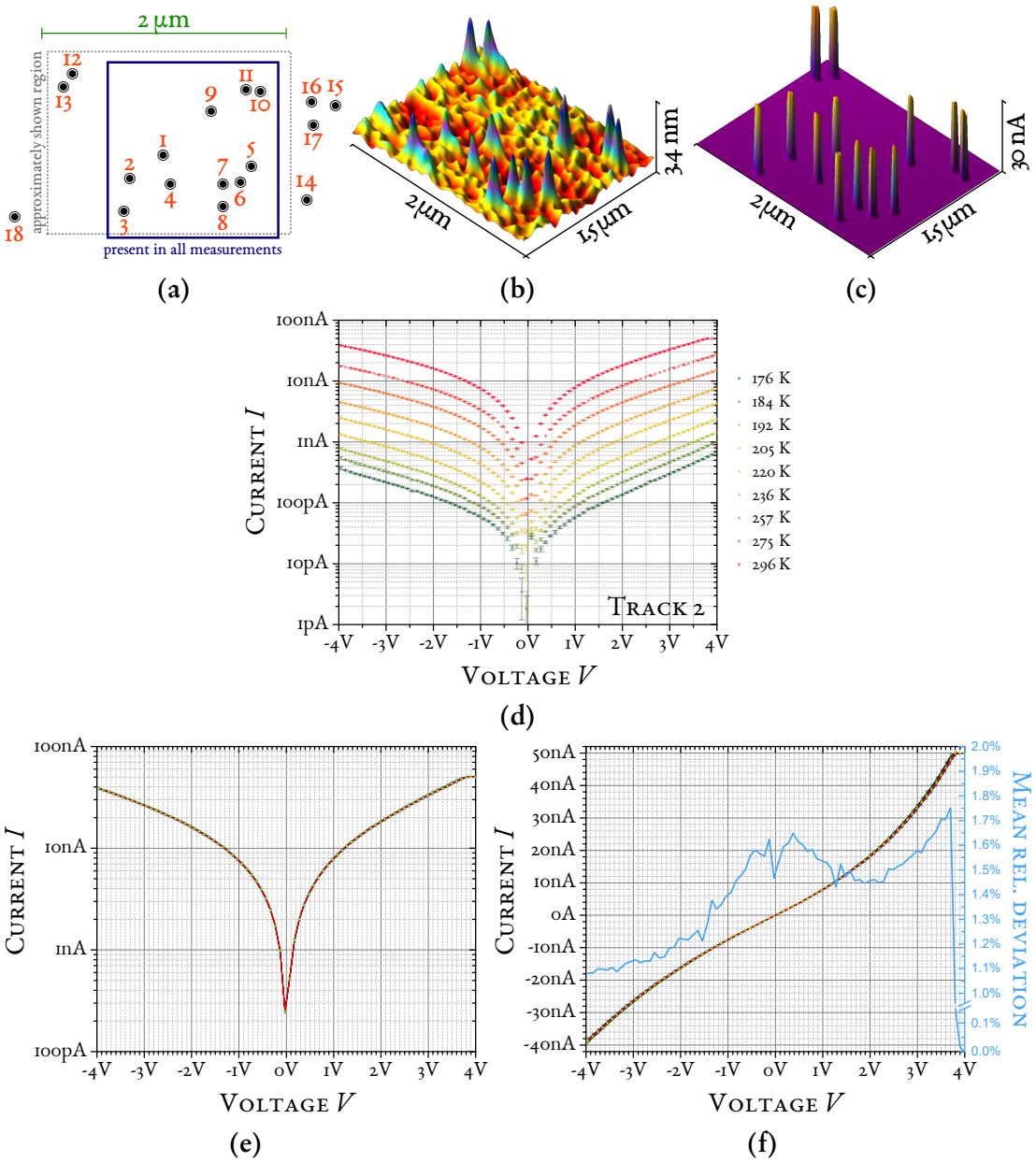

Figure 6.1: (a)-(c) show the region of the swift heavy ion irradiated sample 1339b that was measured with a conductive AFM at different temperatures and bias voltages (see section 6.2.8). While (a) illustrates the investigated area so far in the whole experiment, (b) shows an actual measurement of the topography and (c) the corresponding current map. The current-voltage characteristics for different temperatures are exemplary shown for track 2 in (d). As can be seen in (e) and (f) the response of the different traps in this region is very similar: The black area is the mean of the conductivities of track 1 to 10 (combined) enclosed by the corresponding standard deviation. The red area is the weighted arithmetic mean of these combined track conductivities with its variance. The green to blue error bars in subfigure (e) are those from tracks 1 to 10, individually at 296 K. In subfigure (f) the mean values of individual tracks are shown additionally to the errors. Furthermore, the deviation of the trap currents from the mean, normalised on the latter, are depicted.

Bibliography

[1] C. L. Alexander, B. Tribollet and M. E. Orazem. 'Contribution of Surface Distributions to Constant-Phase-Element (CPE) Behavior: 1. Influence of Roughness'. In: *Electrochimica Acta* 173 (2015), pp. 416–424. DOI: 10.1016/j.electacta.2015.05.010.

[2] J. A. Amani. 'Voltage-dependent impedance analysis of metal/ta-C/Si heterostructures'. Diplomarbeit. Georg-August-Universität Göttingen, 2012.

[3] J. A. Amani et al. 'Analysis of Immittance Spectra: Finding Unambiguous Electrical Equivalent Circuits to Represent the Underlying Physics'. In: *Physical Review Applied* 4.4 (2015), p. 044007. DOI: 10.1103/PhysRevApplied.4.044007.

[4] N. W. Ashcroft and N. D. Mermin. *Solid state physics*. 1st. Orlando, FL: Harcourt Inc., 1976. ISBN: 0-03-083993-9.

[5] K. Attenborough. 'Acoustical impedance models for outdoor ground surfaces'. In: *Journal of Sound and Vibration* 99.4 (1985), pp. 521–544. DOI: 10.1016/0022-460X(85)90538-3.

[6] A. Baca et al. 'A survey of ohmic contacts to III-V compound semiconductors'. In: *Thin Solid Films* 308 (1997), pp. 599–606. DOI: 10.1016/S0040-6090(97)00439-2.

[7] E. Barsoukov and J. R. Macdonald, eds. *Impedance Spectroscopy. Theory, Experiment, and Applications*. 2nd. Hoboken, New Jersey: John Wiley & Sons, Inc., 2005. ISBN: 0-471-64749-7.

[8] J. Bernholc, N. O. Lipari and S. T. Pantelides. 'Scattering-theoretic method for defects in semiconductors. II. Self-consistent formulation and application to the vacancy in silicon'. In: *Physical Review B* 21.8 (1980), pp. 3545–3562. DOI: 10.1103/PhysRevB.21.3545.

[9] J. Bernholc, N. O. Lipari and S. T. Pantelides. 'Self-consistent method for Point defects in semiconductors: Application to the vacancy in silicon'. In: *Physical Review Letters* 41.13 (1978), pp. 895–899. DOI: 10.1103/PhysRevLett.41.895.

[10] F. Bloch. 'Über die Quantenmechanik der Elektronen in Kristallgittern'. In: *Zeitschrift für Physik* 52.7-8 (1929), pp. 555–600. DOI: 10.1007/BF01339455.

[11] H. W. Bode. *Network analysis and feedback amplifier design*. 10th. Toronto, New York, London: D. Van Nostrand Company, Inc., 1945.

[12] B. Boukamp. 'A Nonlinear Least Squares Fit Procedure for Analysis of Immittance Data of Electrochemical Systems'. In: *Solid State Ionics* 20.1 (1986), pp. 31–44. DOI: 10.1016/0167-2738(86)90031-7.

[13] M. Brötzmann. 'Electrical characterization of Metal - Amorphous Semiconductor - Semiconductor diodes – a general conduction model'. PhD thesis. Georg-August-Universität Göttingen, 2013.

[14] M. Brötzmann, U. Vetter and H. Hofsäss. 'BN/ZnO heterojunction diodes with apparently giant ideality factors'. In: *Journal of Applied Physics* 106.6 (2009), p. 9. DOI: 10.1063/1.3212987.

[15] M. Brötzmann, U. Vetter and H. Hofsäss. 'ta-C/Si heterojunction diodes with apparently giant ideality factors'. In: *physica status solidi (c)* 7.2 (2010), pp. 256–259. DOI: 10.1002/pssc.200982415.

[16] M. Büttiker and R. Landauer. 'Traversal Time for Tunneling'. In: *Physical Review Letters* 49.23 (1982), pp. 1739–1742. DOI: 10.1103/PhysRevLett.49.1739.

[17] L. Callegaro. *Electrical Impedance. Principles, Measurement, and Applications*. Boca Raton, FL: CRC Press - Taylor & Francis Group, 2013. ISBN: 978-1-4398-4911-8.

[18] H. C. Card. 'Aluminum-Silicon Schottky barriers and ohmic contacts in integrated circuits'. In: *Electron Devices, IEEE Transactions on* 23.6 (1976), pp. 538–544. DOI: 10.1109/T-ED.1976.18449.

[19] F. Cardon and W. P. Gomes. 'On the determination of the flat-band potential of a semiconductor in contact with a metal or an electrolyte from the Mott-Schottky plot'. In: *Journal of Physics D: Applied Physics* 11.4 (1978), pp. L63–L67. DOI: 10.1088/0022-3727/11/4/003.

[20] K. S. Champlin. 'Electronic battery testing device'. US Patent 3,909,708. 1975.

[21] K. K. Chan, S. R. P. Silva and G. A. J. Amaratunga. 'Electronic properties of semiconducting diamond-like carbon-diamond'. In: *Thin Solid Films* 212.1-2 (1992), pp. 232–239. DOI: DOI:10.1016/0040-6090(92)90526-H.

[22] H.-C. Chang and G. Jaffé. 'Polarization in Electrolytic Solutions. Part I. Theory'. In: *The Journal of Chemical Physics* 20.7 (1952), p. 1071. DOI: 10.1063/1.1700669.

[23] F.-C. Chiu. 'A Review on Conduction Mechanisms in Dielectric Films'. In: *Advances in Materials Science and Engineering* 2014 (2014), pp. 1–18. DOI: 10.1155/2014/578168.

[24] K. S. Cole. 'Electric Impedance of Suspensions of Spheres'. In: *The Journal of General Physiology* 12.1 (1928), pp. 29–36. DOI: 10.1085/jgp.12.1.29.

[25] K. S. Cole. 'Electric Phase Angle of Cell Membranes.' In: *The Journal of General Physiology* 15.6 (1932), pp. 641–9.

[26] K. S. Cole. 'Dispersion and absorption in dielectrics. I. Alternating current characteristics'. In: *Current Contents / Physical, Chemical & Earth Sciences* 3 (1980), p. 61.

[27] K. S. Cole and R. H. Cole. 'Dispersion and Absorption in Dielectrics I. Alternating Current Characteristics'. In: *The Journal of Chemical Physics* 9.4 (1941), p. 341. DOI: 10.1063/1.1750906.

[28] G. A. N. Connell, D. L. Camphausen and W. Paul. 'Theory of Poole-Frenkel conduction in low-mobility semiconductors'. In: *Philosophical Magazine* 26.3 (1972), pp. 541–551. DOI: 10.1080/14786437208230103.

[29] C. D. Corcoran et al. 'Exact Inference for Categorical Data'. In: *Encyclopedia of Biostatistics*. Chichester, UK: John Wiley & Sons, Ltd, 2005. DOI: 10.1002/0470011815.b2a10019.

[30] E. Cullwick. 'Electromagnetic momentum and electron inertia in a current circuit'. In: *Proceedings of the IEE Part C: Monographs* 103.3 (1955), p. 159. DOI: 10.1049/pi-c.1956.0019.

[31] J. Curie and P. Curie. 'Développement par compression de l'électricité polaire dans les cristaux hémièdres à faces inclinées'. In: *Bulletin de la Société minéralogique de France* 3 (1880), pp. 90–93.

[32] V. Dallacasa and C. Paracchini. 'Internal Field-Assisted Thermal Ionization'. In: *IEEE Transactions on Electrical Insulation* EI-22.4 (1987), pp. 467–472. DOI: 10.1109/TEI.1987.298909.

[33] P. Debye. *Polar molecules*. New York: Dover Publications, 1929.

[34] E. Demoulin and F. van de Wiele. 'Inversion layer at the interface of Schottky diodes'. In: *Solid State Electronics* 17.8 (1974), pp. 825–833. DOI: 10.1016/0038-1101(74)90031-8.

[35] E. C. Dutoit et al. 'Investigation On Frequency-dependence of Impedance of Nearly Ideally Polarizable Semiconductor Electrodes Cdse, Cds and Tio2'. In: *Berichte der Bunsengesellschaft für physikalische Chemie* 79.12 (1975), pp. 1206–1213.

[36] J. C. Dyre. 'On the mechanism of glass ionic conductivity'. In: *Journal of Non-Crystalline Solids* 88.2-3 (1986), pp. 271–280. DOI: 10.1016/S0022-3093(86)80030-8.

[37] J. C. Dyre. 'The random free-energy barrier model for ac conduction in disordered solids'. In: *Journal of Applied Physics* 64.5 (1988), p. 2456. DOI: 10.1063/1.341681.

[38] S. Egret et al. 'Diamond-like carbon metal-semiconductor-metal switches for active matrix displays'. In: *Diamond and Related Materials* 6.5–7 (1997), pp. 879–883. DOI: 10.1016/S0925-9635(96)00676-0.

[39] G. Elert. *The Physics Hypertextbook - Dielectrics*. 2015. URL: http://physics.info/dielectrics/ (visited on 20/11/2015).

[40] S. Elliott. 'A.c. conduction in amorphous chalcogenide and pnictide semiconductors'. In: *Advances in Physics* 36.2 (1987), pp. 135–217. DOI: 10.1080/00018738700101971.

[41] R. Enderlein and N. J. Horing. *Fundamentals of Semiconductor Physics and Devices*. Singapore: World Scientific Publishing Co. Pte. Ltd., 1997. ISBN: 978-981-02-2387-8. DOI: 10.1142/9789812384690.

[42] J. M. Esteban and M. E. Orazem. 'On the Application of the Kramers-Kronig Relations to Evaluate the Consistency of Electrochemical Impedance Data'. In: *Journal of The Electrochemical Society* 138.1 (1991), pp. 67–76. DOI: 10.1149/1.2085580.

[43] R. Ferrini. 'Ricerche sulla conduttività elettrica dei carboni'. In: *Il Nuovo Cimento* 6.1 (1879), pp. 53–77. DOI: 10.1007/BF02739750.

[44] D. Fleisch. *A Student's Guide to Maxwell's Equations*. Cambridge: Cambridge University Press, 2008. ISBN: 978-0-511-39308-2.

[45] D. R. Franceschetti and J. R. Macdonald. 'Numerical analysis of electrical response'. In: *Journal of Electroanalytical Chemistry and Interfacial Electrochemistry* 100.1-2 (1979), pp. 583–605. DOI: 10.1016/S0022-0728(79)80186-2.

[46] J. Frenkel. 'On Pre-Breakdown Phenomena in Insulators and Electronic Semi-Conductors'. In: *Physical Review* 54.8 (1938), pp. 647–648. DOI: 10.1103/PhysRev.54.647.

[47] H. Fricke. 'XXXIII. The theory of electrolytic polarization'. In: *Philosophical Magazine Series 7* 14.90 (1932), pp. 310–318. DOI: 10.1080/14786443209462064.

[48] S. D. Ganichev et al. 'Distinction between the Poole-Frenkel and tunneling models of electric-field-stimulated carrier emission from deep levels in semiconductors'. In: *Physical Review B* 61.15 (2000), pp. 10361–10365. DOI: 10.1103/PhysRevB.61.10361.

[49] H. García et al. 'Electrical Characterization of Amorphous Silicon MIS-Based Structures for HIT Solar Cell Applications'. In: *Nanoscale Research Letters* 11.1 (2016), p. 335. DOI: 10.1186/s11671-016-1545-z.

[50] H.-G. Gehrke. 'Electrical characterization of conductive ion tracks in tetrahedral amorphous carbon with copper impurities'. PhD thesis. Georg-August-Universität Göttingen, 2013.

[51] I. Geifman et al. 'Local electric field in crystals'. In: *Journal of Experimental and Theoretical Physics (Zh. Eksp. Teor. Fiz.)* 74.1 (1978), pp. 84–88.

[52] W. van Gelder and E. H. Nicollian. 'Silicon Impurity Distribution as Revealed by Pulsed MOS CV Measurements'. In: *Journal of The Electrochemical Society* 118.1 (1971), pp. 138–141. DOI: 10.1149/1.2407927.

[53] C. Godet, S. Kumar and V. Chu. 'Field-enhanced electrical transport mechanisms in amorphous carbon films'. In: *Philosophical Magazine* 83.29 (2003), pp. 3351–3365. DOI: 10.1080/14786430310001605010.

[54] M. A. Green. 'Intrinsic concentration, effective densities of states, and effective mass in silicon'. In: *Journal of Applied Physics* 67.1990 (1990), pp. 2944–2954. DOI: 10.1063/1.345414.

[55] H. G. Grimmeiss and B. Skarstam. 'Excited states at deep centers in Si:S and Si:Se'. In: *Physical Review B* 23.4 (1981), pp. 1947–1960. DOI: 10.1103/PhysRevB.23.1947.

[56] S. Grimnes and Ø. G. Martinsen. *Bioimpedance and Bioelectricity Basics*. 2nd. Academic Press, Elsevier, 2008. ISBN: 9780123740045.

[57] A. S. Grove et al. 'Investigation of thermally oxidised silicon surfaces using metal-oxide-semiconductor structures'. In: *Solid-State Electronics* 8.2 (1965), pp. 145–163. DOI: DOI:10.1016/0038-1101(65)90046-8.

[58] B. Gudden and W. Schottky. 'Probleme der Ionen- und Elektronenleitung in nichtmetallischen festen Körpern'. In: *Zeitschrift für technische Physik* 16.11 (1935), pp. 323–327.

[59] K. M. Guenther et al. 'Extracting accurate capacitance voltage curves from impedance spectroscopy'. In: *Applied Physics Letters* 100.4 (2012), pp. 1–5. DOI: 10.1063/1.3679380.

[60] J. L. Hartke. 'The Three-Dimensional Poole-Frenkel Effect'. In: *Journal of Applied Physics* 39.10 (1968), p. 4871. DOI: 10.1063/1.1655871.

[61] T. E. Hartman, J. C. Blair and R. Bauer. 'Electrical Conduction through SiO Films'. In: *Journal of Applied Physics* 37.6 (1966), p. 2468. DOI: 10.1063/1.1708838.

[62] O. Heaviside. *Electrical papers - Volume II*. New York and London: Macmillan and Co., 1894.

[63] Hewlett Packard. *HP 4284A Precision LCR Meter Operation Manual*. Kōbe, 1998.

[64] R. M. Hill. 'Poole-Frenkel conduction in amorphous solids'. In: *Philosophical Magazine* 23.181 (1971), pp. 59–86. DOI: 10.1080/14786437108216365.

[65] B. Hirschorn et al. 'Constant-Phase-Element Behavior Caused by Resistivity Distributions in Films: I. Theory'. In: *Journal of The Electrochemical Society* 157.12 (2010), pp. C452–C457. DOI: 10.1149/1.3499564.

[66] H. P. Hjalmarson et al. 'Theory of Substitutional Deep Traps in Covalent Semiconductors'. In: *Physical Review Letters* 44.12 (1980), pp. 810–813. DOI: 10.1103/PhysRevLett.44.810.

[67] H. Hjelmgren. 'Numerical modeling of hot electrons in n-GaAs Schottky-barrier diodes'. In: *IEEE Transactions on Electron Devices* 37.5 (1990), pp. 1228–1234. DOI: 10.1109/16.108183.

[68] H. Hofsäss. 'Electronic Properties of Undoped and Doped Tetrahedral Amorphous Carbon'. In: *Proceedings 1st International Specialist Meeting on Amorphous Carbon*. Ed. by S. R. P. Silva et al. World Scientific, Singapore, 1998, 1998, pp. 296–311.

[69] J. Højberg et al. 'An electrochemical impedance spectroscopy investigation of the overpotentials in Li-O2 batteries'. In: *ACS Applied Materials and Interfaces* 7.7 (2015), pp. 4039–4047. DOI: 10.1021/am5083254.

[70] R. A. Huggins. *Advanced Batteries. Materials Science Aspects*. Boston, MA: Springer US, 2009. ISBN: 978-0-387-76423-8. DOI: 10.1007/978-0-387-76424-5.

[71] H. Ibach and H. Lüth. *Festkörperphysik*. 7. Springer-Lehrbuch. Berlin, Heidelberg: Springer, 2009. ISBN: 978-3-540-85794-5. DOI: 10.1007/978-3-540-85795-2.

[72] M. Ieda, G. Sawa and S. Kato. 'A Consideration of Poole-Frenkel Effect on Electric Conduction in Insulators'. en. In: *Journal of Applied Physics* 42.10 (1971), p. 3737. DOI: 10.1063/1.1659678.

[73] J. D. Jackson. *Classical Electrodynamics*. 3rd. Hoboken, New Jersey: John Wiley & Sons, Inc., 1999. ISBN: 0-471-30932-X.

[74] G. Jaffé. 'Theorie der Leitfähigkeit polarisierbarer Medien. I'. In: *Annalen der Physik* 408.2 (1933), pp. 217–248. DOI: 10.1002/andp.19334080207.

[75] G. Jaffé. 'Theorie der Leitfähigkeit polarisierbarer Medien. II'. In: *Annalen der Physik* 408.3 (1933), pp. 249–284. DOI: 10.1002/andp.19334080302.

[76] G. Jaffé and J. A. Rider. 'Polarization in Electrolytic Solutions. Part II. Measurements'. In: *The Journal of Chemical Physics* 20.7 (1952), p. 1077. DOI: 10.1063/1.1700669.

[77] E. Jones et al. *SciPy: Open source scientific tools for Python*. 2001–. URL: http://www.scipy.org/ (visited on 30/09/2016).

[78] A. K. Jonscher. *Dielectric relaxation in solids*. Chelsea Dielectrics Press Ltd., 1983.

[79] A. K. Jonscher. 'Dielectric relaxation in solids'. In: *Journal of Physics D: Applied Physics* 32.14 (1999), R57–R70. DOI: 10.1088/0022-3727/32/14/201.

[80] A. K. Jonscher. 'Electronic properties of amorphous dielectric films'. In: *Thin Solid Films* 1.3 (1967), pp. 213–234. DOI: 10.1016/0040-6090(67)90004-1.

[81] A. K. Jonscher. 'Energy losses in hopping conduction at high electric fields'. In: *Journal of Physics C: Solid State Physics* 4.11 (1971), pp. 1331–1340. DOI: 10.1088/0022-3719/4/11/008.

[82] A. K. Jonscher. 'Free-carrier Poole-Frenkel effect in crystalline solids'. In: *Journal of Physics C: Solid State Physics* 3.8 (1970), pp. L159–L162. DOI: 10.1088/0022-3719/3/8/029.

[83] A. K. Jonscher. 'Frequency-dependence of conductivity in hopping systems'. In: *Journal of Non-Crystalline Solids* 8-10 (1972), pp. 293–315. DOI: 10.1016/0022-3093(72)90151-2.

[84] A. K. Jonscher. 'The 'universal' dielectric response'. In: *Nature* 267.5613 (1977), pp. 673–679. DOI: 10.1038/267673a0.

[85] A. K. Jonscher. 'Towards the Significance of Disorder'. In: *Current Contents / Physical, Chemical & Earth Sciences* 16 (1992), p. 1992.

[86] A. K. Jonscher and C. K. Loh. 'Poole-Frenkel conduction in high alternating electric fields'. In: *Journal of Physics C: Solid State Physics* 4.11 (1971), p. 1341.

[87] J.-B. Jorcin et al. 'CPE analysis by local electrochemical impedance spectroscopy'. In: *Electrochimica Acta* 51.8–9 (2006), pp. 1473–1479. DOI: 10.1016/j.electacta.2005.02.128.

[88] Keysight Technologies. *Impedance Measurement Handbook. A guide to measurement technology and techniques*. 5th. Böblingen, 2015.

[89] A. A. Khan, J. A. Woollam and Y. Chung. 'Interfacial effects due to tunneling to insulator gap states in amorphous carbon on silicon metal-insulator-semiconductor structures'. In: *Journal of Applied Physics* 55.12 (1984), pp. 4299–4303. DOI: 10.1063/1.333040.

[90] R. U. A. Khan and S. R. P. Silva. 'Electronic Conduction in Ion Implanated Amorphous Carbon Thin Films'. In: *International Journal of Modern Physics B* 14.02n03 (2000), pp. 195–205. DOI: 10.1142/S0217979200000194.

[91] N. Konofaos and C. B. Thomas. 'Electronic transport phenomena in devices containing amorphous diamond-like films on silicon'. In: *Solid State Communications* 105.4 (1998), pp. 257–261. DOI: DOI:10.1016/S0038-1098(97)10095-3.

[92] I. O. K'Owino and O. A. Sadik. *Impedance Spectroscopy: A Powerful Tool for Rapid Biomolecular Screening and Cell Culture Monitoring*. 2005. DOI: 10.1002/elan.200503371.

[93] F. Kremer and A. Schönhals, eds. *Broadband dielectric spectroscopy*. Berlin, Heidelberg: Springer, 2003. ISBN: 3-540-43407-0.

[94] S. Kugler and K. Shimakawa. *Amorphous Semiconductors*. Cambridge: Cambridge University Press, 2015. ISBN: 978-1-107-01934-8. arXiv: arXiv:1011.1669v3.

[95] H. Lamb. 'On Electrical Motions in a Spherical Conductor'. In: *Philosophical Transactions of the Royal Society of London* 174 (1883), pp. 519–549. DOI: 10.1098/rstl.1883.0013.

[96] L. D. Landau, E. M. Lifschitz and P. P. Pitajewski. *Elektrodynamik der Kontinua*. Ed. by P. Ziesche and G. Lehmann. 4th. Berlin: Akademie-Verlag, 1985.

[97] D. V. Lang. 'Deep-level transient spectroscopy: A new method to characterize traps in semiconductors'. In: *Journal of Applied Physics* 45.7 (1974), p. 3023. DOI: 10.1063/1.1663719.

[98] S. Larfaillou et al. 'Comprehensive characterization of all-solid-state thin films commercial microbatteries by Electrochemical Impedance Spectroscopy'. In: *Journal of Power Sources* 319 (2016), pp. 139–146. DOI: 10.1016/j.jpowsour.2016.04.057.

[99] A. Lasia. *Electrochemical Impedance Spectroscopy and its Applications*. New York, NY: Springer New York, 2014. ISBN: 978-1-4614-8932-0. DOI: 10.1007/978-1-4614-8933-7.

[100] W. Leighton, R. Chaffin and J. Webb. 'RF Amplifier Design with Large-Signal S-Parameters'. In: *IEEE Transactions on Microwave Theory and Techniques* 21.12 (1973), pp. 809–814. DOI: 10.1109/TMTT.1973.1128136.

[101] Y. Lifshitz. 'Tetrahedral amorphous carbon (ta-C)'. In: *Proceedings of the International School of Physics "Enrico Fermi". Course CXXV. The Physics of Diamond*. Ed. by A. Paoletti and A. Tucciarone. Amsterdam: IOS Press, 1997, pp. 209–253. DOI: 10.3254/978-1-61499-220-2-209.

[102] B. Lindholm-Sethson et al. 'Multivariate analysis of skin impedance data in long-term type 1 diabetic patients'. In: *Chemometrics and Intelligent Laboratory Systems* 44.1-2 (1998), pp. 381–394. DOI: 10.1016/S0169-7439(98)00164-6.

[103] C. Liu et al. 'Advances in DLC coatings by hybrid PSII and PECVD as a barrier to corrosion in simulated body fluid'. In: *Journal of Materials Science* 40.21 (2005), pp. 5603–5608. DOI: 10.1007/s10853-005-1426-9.

[104] A. R. Long. 'Frequency-dependent loss in amorphous semiconductors'. In: *Advances in Physics* 31.5 (1982), pp. 553–637. DOI: 10.1080/00018738200101418.

[105] H. A. Lorentz. *The theory of electrons and its applications to the phenomena of light and radiant heat*. 2nd. Leipzig: Teubner, B. G., 1916.

[106] P. Lunkenheimer et al. 'Origin of apparent colossal dielectric constants'. In: *Physical Review B* 66.5 (2002), p. 052105. DOI: 10.1103/PhysRevB.66.052105. arXiv: 0201146 [cond-mat].

[107] P. Lunkenheimer et al. 'Apparent giant dielectric constants, dielectric relaxation, and ac-conductivity of hexagonal perovskites $La_{1.2}Sr_{2.7}BO_{7.33}$ (B=Ru, Ir)'. In: *Journal of Solid State Chemistry* 179.12 (2006), pp. 3965–3973. DOI: 10.1016/j.jssc.2006.09.005.

[108] P. Lunkenheimer et al. 'Colossal dielectric constants in transition-metal oxides'. In: *European Physical Journal: Special Topics* 180.1 (2009), pp. 61–89. DOI: 10.1140/epjst/e2010-01212-5. arXiv: 1003.4272.

[109] S. Ma, R. Hang and P. K. Chu. 'Corrosion behavior of DLC-coated NiTi alloys in the presence of serum proteins'. In: *2010 3rd International Nanoelectronics Conference (INEC)* DLC (2010), pp. 805–806. DOI: 10.1109/INEC.2010.5425198.

[110] D. D. Macdonald. 'Reflections on the history of electrochemical impedance spectroscopy'. In: *Electrochimica Acta* 51.8-9 (2006), pp. 1376–1388. DOI: 10.1016/j.electacta.2005.02.107.

[111] D. D. Macdonald and M. C. H. McKubre. 'Impedance Measurements in Electrochemical Systems'. In: *Modern Aspects of Electrochemistry No. 14*. Ed. by J. O. Bockris, B. E. Conway and R. E. White. Boston, MA: Springer US, 1982, pp. 61–150. DOI: 10.1007/978-1-4615-7458-3_2.

[112] J. R. Macdonald. 'Effects of various boundary conditions on the response of Poisson-Nernst-Planck impedance spectroscopy analysis models and comparison with a continuous-time random-walk model.' In: *The Journal of Physical Chemistry A* 115.46 (2011), pp. 13370–80. DOI: 10.1021/jp206719g.

[113] J. R. Macdonald. 'Frequency response of unified dielectric and conductive systems involving an exponential distribution of activation energies'. In: *Journal of Applied Physics* 58.5 (1985), p. 1955. DOI: 10.1063/1.336003.

[114] J. R. Macdonald. 'Impedance spectroscopy'. In: *Annals of Biomedical Engineering* 20.3 (1992), pp. 289–305. DOI: 10.1007/BF02368532.

[115] J. R. Macdonald. *LEVM / LEVMW Manual*. 2015.

[116] J. R. Macdonald. 'Theory of ac space-charge polarization effects in photoconductors, semiconductors, and electrolytes'. In: *Physical Review* 92.1 (1953), pp. 4–17. DOI: 10.1103/PhysRev.92.4.

[117] J. R. Macdonald. 'Theory of space-charge polarization and electrode-discharge effects'. In: *The Journal of Chemical Physics* 58.11 (1973), p. 4982. DOI: 10.1063/1.1679086.

[118] J. R. Macdonald. 'Universality, the Barton Nakajima Namikawa relation, and scaling for dispersive ionic materials'. In: *Physical Review B - Condensed Matter and Materials Physics* 71.18 (2005), pp. 1–12. DOI: 10.1103/PhysRevB.71.184307. arXiv: 0403118 [cond-mat].

[119] J. R. Macdonald. 'Utility and importance of Poisson-Nernst-Planck immittance-spectroscopy fitting models'. In: *Journal of Physical Chemistry C* 117.45 (2013), pp. 23433–23450. DOI: 10.1021/jp403510y.

[120] J. R. Macdonald and D. R. Franceschetti. 'Theory of small-signal ac response of solids and liquids with recombining mobile charge'. In: *The Journal of Chemical Physics* 68.4 (1978), p. 1614. DOI: 10.1063/1.435929.

[121] J. R. Macdonald and J. A. Garber. 'Analysis of Impedance and Admittance Data for Solids and Liquids'. en. In: *Journal of The Electrochemical Society* 124.7 (1977), p. 1022. DOI: 10.1149/1.2133473.

[122] J. R. Macdonald et al. 'Comparison of impedance spectroscopy expressions and responses of alternate anomalous poisson-nernst-planck diffusion equations for finite-length situations'. In: *Journal of Physical Chemistry C* 115.15 (2011), pp. 7648–7655. DOI: 10.1021/jp200737z.

[123] P. D. Maguire et al. 'Mechanical stability, corrosion performance and bioresponse of amorphous diamond-like carbon for medical stents and guidewires'. In: *Diamond and Related Materials* 14.8 (2005), pp. 1277–1288. DOI: 10.1016/j.diamond.2004.12.023.

[124] P. Marcus and F. B. Mansfeld, eds. *Analytical Methods In Corrosion Science and Engineering*. Boca Raton, FL: CRC Press - Taylor & Francis Group, 2006. ISBN: 9781420028331.

[125] P. A. Martin, B. G. Streetman and K. Hess. 'Electric field enhanced emission from non-Coulombic traps in semiconductors'. In: *Journal of Applied Physics* 52.12 (1981), p. 7409. DOI: 10.1063/1.328731.

[126] J. C. Maxwell. 'A Dynamical Theory of the Electromagnetic Field'. In: *Philosophical Transactions of the Royal Society of London* 155.January (1865), pp. 459–512. DOI: 10.1098/rstl.1865.0008.

[127] D. G. McCulloch et al. 'Ion implantation in tetrahedral amorphous carbon'. In: *Physical Review B* 52.2 (1995), pp. 850–857. DOI: 10.1103/PhysRevB.52.850.

[128] A. B. McLean, I. M. Dharmadasa and R. H. Williams. 'Schottky-barrier height determination in the presence of interfacial disorder'. In: *Semiconductor Science and Technology* 1.2 (1986), pp. 137–142. DOI: 10.1088/0268-1242/1/2/008.

[129] C. A. Mead. 'Electron Transport Mechanisms in Thin Insulating Films'. In: *Phys. Rev.* 128.5 (1962), pp. 2088–2093. DOI: 10.1103/PhysRev.128.2088.

[130] C. A. Mead and W. G. Spitzer. 'Fermi Level Position at Metal-Semiconductor Interfaces'. In: *Physical Review* 134.3A (1964), A713–A716. DOI: 10.1103/PhysRev.134.A713.

[131] W. Mendenhall and T. Sincich. *A second course in statistics. Regression analysis*. 7th. Boston, MA: Prentice Hall, 2012. ISBN: 978-0-321-69169-9.

[132] Š. Meškinis et al. 'Electrical and piezoresistive properties of ion beam deposited DLC films'. In: *Applied Surface Science* 254.16 (2008), pp. 5252–5256. DOI: 10.1016/j.apsusc.2008.02.037.

[133] M. Min and T. Paavle. 'Broadband discrete-level excitations for improved extraction of information in bioimpedance measurements.' In: *Physiological measurement* 35.6 (2014), pp. 997–1010. DOI: 10.1088/0967-3334/35/6/997.

[134] K. Misiakos and D. Tsamakis. 'Accurate measurements of the silicon intrinsic carrier density from 78 to 340 K'. In: *Journal of Applied Physics* 74.5 (1993), p. 3293. DOI: 10.1063/1.354551.

[135] N. F. Mott. 'Charge transport in non-crystalline semiconductors'. In: *Festkörperprobleme*. Vol. 9. 3. Berlin, Heidelberg: Springer, 1969, pp. 22–45. DOI: 10.1007/BFb0109150.

[136] N. F. Mott. 'Conduction in non-crystalline materials'. In: *Philosophical Magazine* 19.160 (1969), pp. 835–852. DOI: 10.1080/14786436908216338.

[137] U. Nandi, D. Jana and D. Talukdar. 'Scaling description of non-ohmic direct current conduction in disordered systems'. In: *Progress in Materials Science* 71 (2015), pp. 1–92. DOI: 10.1016/j.pmatsci.2014.12.001.

[138] E. H. Nicollian and J. R. Brews. *MOS (Metal Oxide Semiconductor) Physics and Technology*. 1st. Hoboken, New Jersey: John Wiley & Sons, 2003. ISBN: 978-0471430797.

[139] H. Nyquist. 'Regeneration Theory'. In: *Bell System Technical Journal* 11.1 (1932), pp. 126–147.

[140] I. Ohdomari and K. N. Tu. 'Parallel silicide contacts'. In: *Journal of Applied Physics* 51.7 (1980), pp. 3735–3739. DOI: 10.1063/1.328160.

[141] L. Onsager. 'Initial recombination of ions'. In: *Physical Review* 54.8 (1938), pp. 554–557. DOI: 10.1103/PhysRev.54.554.

[142] L. Onsager. 'Deviations from Ohm's Law in Weak Electrolytes'. In: *The Journal of Chemical Physics* 2.9 (1934), pp. 599–615. DOI: 10.1063/1.1749541.

[143] S. J. Orfanidis. *Electromagnetic Waves and Antennas*. Piscataway, NJ: ECE Department, Rutgers University, 2014.

[144] D. M. Pai. 'Electric-field-enhanced conductivity in solids'. In: *Journal of Applied Physics* 46.12 (1975), p. 5122. DOI: 10.1063/1.321570.

[145] R. Peterson. 'Formal Theory of Nonlinear Response'. In: *Reviews of Modern Physics* 39.1963 (1967), pp. 69–77. DOI: 10.1103/RevModPhys.39.69.

[146] D. Petrascheck and F. Schwabl. *Elektrodynamik*. Berlin, Heidelberg: Springer, 2015. ISBN: 978-3-662-43456-7. DOI: 10.1007/978-3-662-43457-4.

[147] J. Phillips. 'Microscopic theory of the Kohlrausch relaxation constant β_K'. In: *Journal of Non-Crystalline Solids* 172-174.Part 1 (1994), pp. 98–103. DOI: 10.1016/0022-3093(94)90421-9.

[148] M. Pollak and T. H. Geballe. 'Low-Frequency Conductivity Due to Hopping Processes in Silicon'. In: *Physical Review* 122.6 (1961), pp. 1742–1753. DOI: 10.1103/PhysRev.122.1742.

[149] H. Poole. 'VIII. On the dielectric constant and electrical conductivity of mica in intense fields'. In: *Philosophical Magazine Series 6* 32.187 (1916), pp. 112–129. DOI: 10.1080/14786441608635546.

[150] M. Poppe. *Die Maxwell'sche Theorie*. essentials. Berlin, Heidelberg: Springer, 2015. ISBN: 978-3-662-45592-0. DOI: 10.1007/978-3-662-45593-7.

[151] M. Potemski and Z. Wilamowski. 'High electric field transport in CdF_2:Y'. In: *Acta Physica Polonica* A67.2 (1985), pp. 479–481.

[152] B. G. Pound. 'Corrosion behavior of nitinol in blood serum and PBS containing amino acids'. In: *Journal of Biomedical Materials Research - Part B Applied Biomaterials* 94.2 (2010), pp. 287–295. DOI: 10.1002/jbm.b.31647.

[153] I. D. Raistrick. 'Application of impedance spectroscopy to materials science'. In: *Annual Review of Materials Science* 16 (1986), pp. 343–370. DOI: 10.1146/annurev.ms.16.080186.002015.

[154] J. Robertson. 'Diamond-like amorphous carbon'. In: *Materials Science and Engineering: R: Reports* 37.4–6 (2002), pp. 129–281. DOI: 10.1016/S0927-796X(02)00005-0.

[155] D. A. Robinson et al. 'A Review of Advances in Dielectric and Electrical Conductivity Measurement in Soils Using Time Domain Reflectometry'. In: *Vadose Zone Journal* 2.1996 (2003), pp. 444–475. DOI: 10.2136/vzj2003.4440.

[156] C. Ronning et al. 'Conduction processes in boron- and nitrogen-doped diamond-like carbon films prepared by mass-separated ion beam deposition'. In: *Diamond and Related Materials* 4.5-6 (1995), pp. 666–672. DOI: 10.1016/0925-9635(94)05219-0.

[157] W. Rotman. 'Plasma simulation by artificial dielectrics and parallel-plate media'. In: *IRE Transactions on Antennas and Propagation* 10.1 (1962), pp. 17–19. DOI: 10.1109/TAP.1962.1137809.

[158] P. J. Rousseeuw and A. M. Leroy. *Robust regression and outlier detection*. Hoboken, New Jersey: John Wiley & Sons, Inc., 1987. ISBN: 0-471-85233-3.

[159] L. Sang et al. 'Large signal equivalent circuit model for package ALGaN/GaN HEMT'. In: *Progress In Electromagnetics Research Letters* 20.January (2011), pp. 27–36.

[160] M. Schadt. 'Liquid Crystal Materials and Liquid Crystal Displays'. In: *Annual Review of Materials Science* 27.1 (1997), pp. 305–379. DOI: 10.1146/annurev.matsci.27.1.305.

[161] D. K. Schroder. 'Electrical Characterization of Defects in Gate Dielectrics'. In: *Defects in Microelectronic Materials and Devices*. Ed. by D. M. Fleetwood, S. T. Pantelides and R. D. Schrimpf. Boca Raton, FL: CRC Press, 2009. Chap. 5, pp. 119–162. ISBN: 1-4244-0083-X. DOI: 10.1109/ISDRS.2005.1596056.

[162] D. K. Schroder. *Semiconductor Material and Device Characterization*. 3rd. Hoboken, New Jersey: John Wiley & Sons, Inc, 2006. ISBN: 9780471739067.

[163] H. Schroeder. 'Poole-Frenkel-effect as dominating current mechanism in thin oxide films—An illusion?!' In: *Journal of Applied Physics* 117.21 (2015), p. 215103. DOI: 10.1063/1.4921949.

[164] M. Sheik-Bahae. 'Kramers-Krönig relations in nonlinear optics'. In: *Encyclopedia of Modern Optics, Vol. 3*. Ed. by Robert D. Guenther. 1st. Amsterdam et al.: Elsevier Acad. Press, 2005. Chap. Nonlinear, pp. 234–240. ISBN: 0-12-227603-5.

[165] C. C. Shih et al. 'Increased Corrosion Resistance of Stent Materials by Converting Current Surface Film of Polycrystalline Oxide into Amorphous Oxide.' In: *Journal of Biomedical Materials Research* 52.2 (2000), pp. 323–332. DOI: 10.1002/1097-4636(200011)52:2<323::AID-JBM11>3.0.CO;2-Z.

[166] D. Shmilovitz. 'On the definition of total harmonic distortion and its effect on measurement interpretation'. In: *IEEE Transactions on Power Delivery* 20.1 (2005), pp. 526–528. DOI: 10.1109/TPWRD.2004.839744.

[167] G. Sidenius. 'The high temperature hollow cathode ion source'. In: *Nuclear Instruments and Methods* 38 (1965), pp. 19–22. DOI: 10.1016/0029-554X(65)90096-0.

[168] S. R. P. Silva et al. 'The microstructural dependence of the opto-electronic properties of nitrogenated hydrogenated amorphous carbon thin films'. In: *Thin Solid Films* 332.1-2 (1998), pp. 118–123. DOI: 10.1016/S0040-6090(98)01070-0.

[169] F. E. M. Silveira and J. a. S. Lima. 'Attenuation and damping of electromagnetic fields: influence of inertia and displacement current'. In: *Journal of Physics A: Mathematical and Theoretical* 42.9 (2009), p. 095402. DOI: 10.1088/1751-8113/42/9/095402.

[170] J. Simmons. 'Poole-Frenkel Effect and Schottky Effect in Metal-Insulator-Metal Systems'. In: *Physical Review* 155.3 (1967), pp. 657–660. DOI: 10.1103/PhysRev.155.657.

[171] S. W. Smith. 'The Refractive Index of Liquids for X-Rays'. In: *Physical Review* 40.2 (1932), pp. 156–164. DOI: 10.1103/PhysRev.40.156.

[172] Y. Song et al. 'On the difference in apparent barrier height as obtained from capacitance-voltage and current-voltage-temperature measurements on Al/p-InP Schottky barriers'. In: *Solid-State Electronics* 29.6 (1986), pp. 633–638. DOI: 10.1016/0038-1101(86)90145-0.

[173] S. Srinivasan. *Fuel Cells. From Fundamentals to Applications. With 50 Figures.* New York, NY: Springer Science+Business Media, LLC, 2006. ISBN: 978-0387-25116-5.

[174] J. Sui et al. 'Corrosion behavior of NiTi alloys coated with diamond-like carbon (DLC) fabricated by plasma immersion ion implantation and deposition'. In: *Materials Science and Engineering: A* 452-453 (2007), pp. 518–523. DOI: 10.1016/j.msea.2006.10.159.

[175] S. M. Sze. 'Current Transport and Maximum Dielectric Strength of Silicon Nitride Films'. In: *Journal of Applied Physics* 38.7 (1967), pp. 2951–2956. DOI: 10.1063/1.1710030.

[176] S. M. Sze. *Physics of Semiconductor Devices*. 2nd. John Wiley & Sons, Inc., 1981.

[177] W. Thomson. 'On the Electro-Dynamic Qualities of Metals:–Effects of Magnetization on the Electric Conductivity of Nickel and of Iron'. In: *Proceedings of the Royal Society of London* 8 (1857), pp. 546–550. DOI: 10.1098/rspl.1856.0144.

[178] W. Thomson. 'The Bakerian Lecture: – On the Electro-Dynamic Properties of Metals'. In: *Proceedings of the Royal Society of London* 8 (1856), pp. 50–55. DOI: 10.1098/rspl.1856.0017.

[179] C. D. Thurmond. 'The Standard Thermodynamic Functions for the Formation of Electrons and Holes in Ge, Si, GaAs, and GaP'. In: *Journal of the Electrochemical Society* 122.8 (1975), pp. 1133–1141. DOI: 10.1149/1.2134410.

[180] A. Trellakis et al. 'The 3D nanometer device project nextnano: Concepts, methods, results'. In: *Journal of Computational Electronics* 5.4 (2007), pp. 285–289. DOI: 10.1007/s10825-006-0005-x.

[181] M. E. Troy. 'Automotive battery charging system tester'. US Patent 6,351,102. 2002.

[182] C. Tsonos et al. 'AC and DC conductivity correlation: The coefficient of Barton–Nakajima–Namikawa relation'. In: *Journal of Non-Crystalline Solids* 358.14 (2012), pp. 1638–1643. DOI: 10.1016/j.jnoncrysol.2012.04.029. arXiv: arXiv:1111.5909v2.

[183] R. Tung. 'Formation of an electric dipole at metal-semiconductor interfaces'. In: *Physical Review B* 64.20 (2001), p. 205310. DOI: 10.1103/PhysRevB.64.205310.

[184] R. Tung. 'Schottky barrier height – do we really understand what we measure?' In: *Proceedings of the 20th annual conference on the physics and chemistry of semiconductors interfaces* 11.4 (1993), pp. 1546–1552. DOI: 10.1116/1.586967.

[185] R. T. Tung. 'The physics and chemistry of the Schottky barrier height'. In: *Applied Physics Reviews* 1.1 (2014), p. 011304. DOI: 10.1063/1.4858400.

[186] G. Vincent, A. Chantre and D. Bois. 'Electric field effect on the thermal emission of traps in semiconductor junctions'. In: *Journal of Applied Physics* 50.8 (1979), pp. 5484–5487. DOI: 10.1063/1.326601.

[187] K. W. Wagner. 'Erklärung der dielektrischen Nachwirkungsvorgänge auf Grund Maxwellscher Vorstellungen'. In: *Archiv für Elektrotechnik* 2.9 (1914), pp. 371–387. DOI: 10.1007/BF01657322.

[188] M. Waiblinger et al. 'Rapid communication Electrically conducting ion tracks in diamond-like carbon films for field emission'. In: *Applied Physics A* 240.2 (1999), p. 239.

[189] J. H. Werner and H. H. Güttler. 'Barrier inhomogeneities at Schottky contacts'. In: *Journal of Applied Physics* 69.3 (1991), p. 1522. DOI: 10.1063/1.347243.

[190] K. F. Young and H. P. R. Frederikse. 'Compilation of the Static Dielectric Constant of Inorganic Solids'. In: *Journal of Physical and Chemical Reference Data* 2.2 (1973), p. 313. DOI: 10.1063/1.3253121.

[191] P. Y. Yu and M. Cardona. *Fundamentals of Semiconductors*. 3rd. Graduate Texts in Physics. Berlin, Heidelberg: Springer, 2005. Chap. 4. Pp. 159–202. ISBN: 978-3-540-25470-6. DOI: 10.1007/b137661.

[192] O. J. Zobel. 'Theory and Design of Uniform and Composite Electric Wave-filters'. In: *Bell System Technical Journal* II.1 (1923), p. 1.

Acknowledgements

First of all, I would like to thank Professor Hans Hofsäss for his continuous trust in my capabilities and, consequently, the opportunity to write my PhD thesis in his group. I would especially like to thank him for entrusting me with the degree of freedom which made this work possible.

Furthermore, I am grateful to Professor Michael Seibt for his immediate consent to examine my extensive thesis as second referee and his inspiring discussion (at the end and after my oral exam for the diploma), about the permittivity in the Frenkel-Poole model, which gave me the idea to look more closely on that parameter.

Many thanks go to Professor Ørjan G. Martinsen. Not only for accepting to act as an external referee, but especially also for the appreciation of my work on the 7th IWIS conference, despite the fact that I was really nervous during my presentation before lunch, because the projector went dark just in the beginning. The acceptance of such a notable expert in the field of immittance spectroscopy increased my motivation a lot.

I would also like to thank Professor Wolfram Kollatschny, Professor Hans-Ulrich Krebs, Professor Vasily Moshnyaga and Professor Andreas Tilgner for accepting to join my thesis committee, especially since the defence is in the pre-Christmas season.

Most sincere thanks Dr. Ulrich Vetter for many enlightening discussions, also beyond the scope of this work, and his setting me on a clear course in navigating through 'organisational difficulties'.

This thesis could not have been written without the numerous discussions with Tristan Koppe as a sparring partner and in order to carve out and pin down the important facets of ideas. Furthermore, he always helped me to focus on the bright sides.

I am grateful for the energy, time and patience Hendrik Schmidt put in the conductive AFM measurements.

Many thanks to all technical personal involved in my thesis.

Special thanks go to Dr. Lars Liebermeister, Oliver Goepfert, Patrick Peretzki and Dr. Christoph Brüsewitz for their endurance when I involved them in discussions about this work and their moral support.

Thanks also to my friends, parents and Dr. Anna Hołubowska for their encouragement, patience and moral support during this time.

Curriculum vitae

Personal information

Name	Julian Alexander Amani
Day of birth	13th of October 1985
Place of birth	Göttingen
Nationality	German

Course of education

2012 – 2016	II. Physikalisches Institut, Georg-August-Universität Göttingen *Research associate*
2012	Georg-August-Universität Göttingen *Diplom* Title: Voltage-dependent impedance analysis of metal/ta-C/Si hetero-structures
2005 – 2012	Fakultät für Physik, Georg-August-Universität Göttingen *Study of physics*
2005	Theodor-Heuss-Gymnasium Göttingen *Abitur*
1998 – 2005	Theodor-Heuss-Gymnasium Göttingen *Higher education*